Structural System Reliability with Application to Light Steel-Framed Buildings

Aritra Chatterjee

Dissertation submitted to the Faculty of the
Virginia Polytechnic Institute and State University
in partial fulfillment of the requirements for the degree of

Doctor of Philosophy
in
Civil Engineering

Cristopher D. Moen, Chair
Roberto T. Leon
Sanjay R. Arwade
Matthew R. Eatherton
Xiaowei Wu

December 5, 2016
Blacksburg, Virginia

Keywords: System reliability, Probability, Finite-Element Modeling, Cold-Formed Steel, Seismic, Incremental Dynamic Analysis, Diaphragms, Shear Walls, LRFD

Structural System Reliability with Application to Light Steel-Framed Buildings

Aritra Chatterjee

(ABSTRACT)

A general framework to design structural systems for a system-reliability goal is proposed. Component-based structural design proceeds on a member to member basis, insuring acceptable failure probabilities for every single structural member without explicitly assessing the overall system safety, whereas structural failure consequences are related to the whole system performance (the cost of a building or a bridge destroyed by an earthquake) rather than a single beam or column failure. Engineering intuition tells us that the system is safer than each individual component due to the likelihood of load redistribution and alternate load paths, however such conservatism cannot be guaranteed without an explicit system-level safety check. As a result, component-based structural designs can lead to both over-conservative components and a less-than-anticipated system reliability.

System performance depends on component properties as well as the load-sharing network, which can possess a wide range of behaviors varying from a dense redundant system with scope for load redistribution after failure initiates, to a weakest-link type network that fails as soon as the first member exceeds its capacity. The load-sharing network is characterized by its overall system reliability and the system-reliability sensitivity, which quantifies the change in system safety due to component reliability modifications. A general algorithm is proposed to calculate modified component reliabilities using the sensitivity vector for the load-sharing network. The modifications represent an improvement on the structural properties of more critical components (more capacity, better ductility), and provide savings on less important members which do not play a significant role.

The general methodology is applied to light steel-framed buildings under seismic loads. The building is modeled with non-linear spring elements representing its subsystems. The stochastic response of this model under seismic ground motions provides load-sharing, system reliability and sensitivity information, which are used to propose target diaphragm and shear wall reliability to meet a building reliability goal. Finally, diaphragm target reliability is used to propose modified component designs using stochastic simulations on geometric and materially non-linear finite-element models including every individual component.

This material is based upon work supported by the National Science Foundation under Grant Nos. 1301001 (Virginia Tech), 1301033 (University of Massachusetts, Amherst) and 1300484 (Johns Hopkins University). Any opinions, findings, and conclusions or recommendations expressed in this material are those of the author and do not necessarily reflect the views of the National Science Foundation. The author is grateful to the industry partner, the American Iron and Steel Institute, for their cooperation.

Structural System Reliability with Application to Light Steel-Framed Buildings

Aritra Chatterjee

(GENERAL AUDIENCE ABSTRACT)

This research proposes methods to design engineering networks for acceptable overall safety. Some examples of engineering networks include electrical systems, transportation systems and infrastructural systems. When any such system is designed, the properties of every individual component (size, capacity etc.) are assigned according to cost and safety requirements. However, it is typically very difficult to reliably quantify the overall safety of the entire system, which is technically known as 'system reliability'. As a result, there are limited options for engineers to adjust the individual component designs within a system to achieve a pre-specified 'targeted' system reliability . This dissertation proposes computational and statistical methods to achieve this.

The proposed methods are applied to a specific engineering system, namely a two story building subjected to ground shaking resulting from an earthquake. Computer models are developed for different scales of the building, beginning from the full building structure, then its individual floors and walls, and finally the individual components that make up each floor and wall. These models are verified with experimental results spanning all three scales. The verified models are then used to both compute the overall system reliability of the building subjected to earthquake ground shaking, as well as to modify its design component-by-component to achieve a targeted system reliability which is different from the system reliability of the original design.

The results indicate that the as-designed reliability of the building system is adequate, but this reliability results from features of the building that are not expected to provide additional safety. The research demonstrates means to obtain this additional safety by redesigning the core functional building components, without relying on the unexpected added safety from 'non-structural' components (such as partition walls inside a building). The methods developed herein can be applied to redesign the components of various engineering system networks such that a targeted overall system reliability can be satisfied, resulting in improved performance and life-safety, potentially even at reduced costs.

Dedication

This dissertation is dedicated to Babai, for saving Ma's life and being a hero when we all needed one.

Acknowledgments

(This will be long.)

I wish to thank my advisor, Prof. Cris Moen, for always pushing me ten steps beyond where I was no matter how far I had reached, for giving me sleepless nights debugging finite-element models, only to tell me the next morning he wanted another tiny component included ("they don't matter" – I would say, "you don't know that" – would be his reply), for making me question myself and every stalwart whose paper I had read or whose ideas I had imbibed, and for making me hate him and want to shout at him. (A classic example of this occurred while dancing to a live band in Baltimore, where he told me he had no interest in my example solutions and was only interested in a general algorithm for all system networks, *one month before my defense*).

I wish to thank each one of my committee members for their invaluable contributions to this work. Prof. Roberto Leon was the sole reason I reached Virginia Tech, both for admission and for being able to make ends meet financially. Three and a half years later he started questioning all of my work, and eventually pushed me to completion of the majority of chapters 2, 3 and 4, in particular deriving system load sharing factors from a computational model. Prof. Matt Eatherton started questioning all of my work at the same time that Prof. Leon did, made me think through demands and capacities for seismic loads, and practically told me my results made no sense if I used a single measurement to construct a distribution, again leading to the majority of the work in chapters 4 and 5. It was during a stochastic processes course that I took with Prof. Xiaowei Wu that I learnt about linear combinations

of random variables and the convolution method which I implemented for all my system reliability work. Later during my final defense Prof. Wu asked the trickiest questions regarding the aforementioned general system network algorithm which will hopefully guide further development of the methodology.

I wish to thank two very special mentors, firstly Prof. Sanjay Arwade who is also a committee member and who (I think) first came up with the system reliability sensitivity metric. His guidance during the first few years where I grappled with component and system reliability shaped the backbone of this work. The second mentor is Prof. Ben Schafer who was part of the same 'backbone-shaping' meetings, but more significantly who met me for half an hour at Virginia Tech six months before my defense and taught me about the discordance between seismic performance based analysis and reliability theory. In particular, he pointed me at FEMA-P695 and stated there was a system reliability function hiding in there, which I discovered soon after and used as the basis of the seismic reliability work.

I wish to thank the mentor who taught me structural mechanics, statistics and reliability, and who was the biggest motivation for me to pursue a Ph.D., my undergraduate and masters' advisor Prof. Baidurya Bhattacharya. My 'philosophy' was shaped by endless discussions with him and my two partners-in-crime Puneet and Debarshi at I.I.T. Kgp. I also wish to thank my high school teacher Mr. D. N. Bhattacharya who taught me the 'ABCD' of Physics and gave birth to my scientific philosophical musings.

I wish to thank everyone that shaped my childhood, beginning with blurry memories of wondrous stories told by my grandmother Tha, to endless relaxing and enjoyable vacations coupled with life-training from my grandparents Mammam and Dadai, my aunt and uncle Jyaji and Jyaja whose hands literally shaped my childhood, Didi and Didibhai with whom my fondest childhood memories are tied (and are now mothers to my dearly adorable niece and nephew), and a host of cousins, aunts and uncles featuring in countless fun-filled days in the past (and future).

I wish to thank my friends in Blacksburg, in particular Bhela, Ellen, Donu, Allie, Goth,

Avik and Sruthi whose support and camaraderie were invaluable cogs in the immense wheel of this Ph.D. Friends from high school that formed my support system in the USA include Darnab, Serpent and Guho – thanks to them for their support as well!

It's time now to mention my best friends and the most precious jewels of my life, the *Brodas* – Promit, Goru, Dadu, Jodu, Subri, Kihba, Kiru, Serpent, Sayo and Lamp, whom I cannot thank both because they will hurl shoes at my face as their way of saying 'you're welcome', and also because words cannot express their contribution to my life and this dissertation.

Finally and most importantly, I wish to thank the two people that mean everything to me, my parents Ma and Babai. Thank you for this life, and particularly with respect to this Ph.D., thank you for talking to me every single day and providing me with encouragement to carry on. As I fought nightmares of not being able to finish, and considered thoughts of quitting and running back to India, it was only your support that kept me going and eventually made me finish. Just as you supported me during my first semester at I.I.T. Kharagpur when I was dying to run back home, so you've supported me during my time in Blacksburg. I hope this effort makes you proud!

Letter to Grandma

(*This letter is reproduced verbatim from an assignment submitted in Spring 2016 for the 'Communicating Science' course taught by Dr. Carrie Kroehler, as part of 'Preparing the Future Professoriate' graduate certificate program at Virginia Tech. It is being presented here in the hope that it clarifies the work in plain English, avoiding much of the technical jargon which is to follow.*)

Dear Mammam,

Hope you are well wherever you are. I have never written to you since you passed away 8 years back. Since then I finished my course in Kharagpur and moved to Virginia in the USA for my Ph.D., and today I am going to tell you about my life and work here.

Having inspired both Dadai (grandpa) and Konkona (aunt) to get their Ph.D.-s in medicine and philosophy respectively, you know exactly how hard it is to get one. It requires sharp focus for extended periods of time spread over years, with frequent losses of self-belief and confidence that feel impossible to overcome when they strike. It has likewise been hard for me too, and I will give you more specific details on this towards the end of this letter, but first let me try to explain my work to you.

I say 'try' because as my core research nears completion I often find that the biggest challenge is not the work by itself, but being able to communicate it effectively to others. When I was young and naive I used to blame this on the inability of my audience to grasp the concepts I was discussing, but over time I have realized that nothing could be further from the truth.

If an idea is clear just 'in your own head' (a phrase I hear repeated over and over again in my circles) then the only place it really lives is in there and has no value to the real world. But I am beginning to ramble here on stuff you know only too well. Let me get to the point instead.

As you know, I specialized in the study of Civil Engineering during my undergrad, and that is the same broad area I'm getting my Ph.D. in. I work in the realm of structural safety. This is an important and inspiring area to work on, since structural failures take human lives. At the same time, most structures you see around yourself are standing up well enough – your house is just as sturdy even after Dadai finished your final dream by adding a third story to it. This makes it difficult to study structural safety because there are not enough failures that we can see and learn from. If you ask me what information my work can give you about the safety of your house my answer would be that if a very rare natural hazard were to occur, say a big earthquake or giant tsunami, I could tell you the survival chances of the house. As you will appreciate, this question has no bearing to our day-to-day lives, and is yet a very important one in the context of our lifetimes.

Let me now lead you on to the very specific research question I am trying to answer. If you look at the construction sequence of a structure (say your house or a bridge), there are specific elements that are designed by engineers to keep it standing. For your house these are typically the concrete and steel columns and beams, for the Howrah bridge these are the giant steel pieces that form a network, for the newer 2nd Hooghly Bridge these are the steel cables and the pillars going down from the deck to the river bed. I will now ask you to imagine that all these components from the giant to the miniature – pillars, beams, cables, nuts and bolts – play as a team to protect us from Mother Nature's hazards. My specific research question then is – what is the composition and dynamic of this team? Is every team member working equally hard? The answer to this is no, some team members are at times unnecessary but we let them stay because we cannot identify who they are, and prefer to err on the side of safety, even if it means having a bulkier team with a bigger number of beams and pillars.

I hope I haven't put you to sleep just yet because I am about to reach the exciting twist in the story! You see, a bulkier team will not always mean a better team, just as too many cooks can sometimes spoil the broth! Bulkier teams can magnify Mother Nature's wrath when an earthquake strikes because as the ground shakes heavier beams and pillars sway from side to side endangering our lives further. My job is then to identify and increase the number of important members in the structural team and throw out the useless ones. This makes structural engineering more informed and intelligent because instead of using as much material as we can to cover our lack of knowledge, we use our smart understanding of team dynamics and composition to make better (not bulkier) structures.

By this point you are probably looking at me suspiciously and warning me (wisely and correctly) that I should go slow with the big talk – what if by trying to make my team smarter I do the exact opposite and fire a team member that was essential to me? I will concede that this is a very critical point, and we are extremely wary of it. Which is why we test our ideas in a safe laboratory environment by artificially shaking buildings the way an earthquake would. I am also testing them on the computer using Math and Science principles that can predict (by calculation) if a building will stand up or fall down. In fact, the maximum amount of my time is spent doing computer work because as you well know I was always more inclined to bookish work or planning and was never too great at doing hands-on stuff!

Spending years now doing the same stuff on a computer, tackling the pressures that my advisor and other professors put on me, trying to sell my ideas to the outside world, have all been really hard. There have been multiple times when I have decided to give up and run back home, but the thoughts of all of you have given me strength to keep going. I still can't guarantee that I will succeed to the best of my ability, but I have constantly been improving and I'm in far better shape to finish than I was 3.5 years back when I first reached these shores.

Other than that, life has been good. This is a beautiful land and forests, mountains and

rivers surround me. I have made some good friends here. You will be proud to know that I have learnt to take care of myself – I cook, do my own laundry, clean my own room and so on, and Ma has finally lost the chance to put her own bad influences on me as you urged her to do all the time! I am happy despite being a bit tired. I haven't always taken the right decisions during this time but I am better off for the experiences which I have learnt from. I am ready to be finished now and move on to meet the rest of the world. Your love continues to guide and inspire me, and I promise to keep trying to make you proud.

Yours forever,

Ruku.

Contents

List of Figures

List of Tables

Chapter 1

Introduction

1.1 Research motivation

Structural systems are comprised of components attached via connections acting in a network to resist external loads, for example, bridge girder systems resisting flexural demands from gravity loads, portal frame networks resisting seismic ground motions or a linked truss roof system resisting gravity, wind and uplift loads. The performance goals for these systems are related to overall integrity and safety, and failure to meet the goal results in collapse, monetary loss, bodily injury or death.

The methodology to design these systems follows a component-by-component safety check procedure. The component failure probabilities, expressed as reliability indices, are intended to satisfy the system performance goal. This is a conservative approach because the system failure probability is intuitively known to be greater than the component reliabilities. There are several reasons that contribute to this conservatism, as listed in [36]:

1. Over-designed member sizes determined by market availability of structural sections.

2. Conservative loads and modeling assumptions.

3. Additional strength and stiffness provided by non-structural elements.
4. Several component designs are governed by a serviceability limit-state.
5. Special care is given to critical elements such as important connections, hangar rods, or columns during design and construction.
6. Several members pose no significant danger to the overall structural integrity when they fail.
7. Member limit states, especially in steel structures, are often ductile, allowing for force redistribution and alternate load paths, which are typically described as structural redundancy.
8. The design criteria for framed members are often first hinge formation or a drift limit, which do not cause structural failure and include a (typically undefined) margin against overall collapse.

At present, explicit system reliability analyses are not performed either during the actual design process or while developing component-based design standards. Due to the lack of such analyses, it is difficult to predict the actual system response, which can possess a range of behaviors – from a dense redundant network having several alternate load paths out of the system, to a weakest-link type network that collapses as soon as any one member reaches its capacity.

It is challenging to account for system effects during design due to the following reasons –

1. system level experimental results and high fidelity computational models are scarce,
2. system limit states are not well understood,
3. system reliability calculations are computationally challenging at large dimensions,
4. system reliability depends on component properties as well as the load-sharing network, which is difficult to characterize.

Particularly with relation to the fourth challenge outlined above, which is to characterize the load-sharing network, researchers have traditionally needed to identify individual component-failure events that can combine to trigger overall system collapse – a task that grows exponentially as the system gets bigger and the number of possible component failures increase.

In the proposed approach the load-sharing network is characterized by its system reliability and reliability sensitivity, defined as the derivative of system reliability with respect to component reliability. It utilizes system-level experimental results (shake-table tests on a full building) and subsystem computational models (floor-diaphragms, shear walls and roof trusses) to obtain a direct simulation-based estimate for system reliability in cases where the load-sharing network is too complex to characterize by combining all the candidate component failures.

Although some structural design standards recognize the limitations of considering only component reliabilities during design, they usually provide empirical modifications to component capacity anticipating system effects, such as system factors for highway bridge superstructures [40] or repetitive member factors used in wood design [19].

In contrast, the sensitivity methodology proposed here enables design for a specified system reliability by recommending new component reliabilities which lead to the system reliability target. These modified reliabilities are based on the individual component properties as well as the load sharing network, which is characterized by system reliability sensitivities of individual components. The proposed component reliabilities are used within the current load and resistance factor design framework to recommend component resistance factors that meet the target system reliability.

1.2 Research strategy

The research strategy begins with a pre-defined target reliability for structural systems based on engineering intuition or failure-consequence analysis. This pre-defined target reliability depends on the cost of failure of the system or the inability to meet a target performance. The targeted system reliability is set to minimize the expected value of a consequence, which is the product of the cost of the consequence times its likelihood of occurrence [11, 6]. The cost of a consequence can be envisioned as the monetary cost resulting from collapse of a residential building or damage to a critical facility. The higher the cost of failure, the lower should be its likelihood of occurrence (probability of failure), and the higher should be the targeted reliability. Target system reliability calculations thus depend on the impact of failure on society and is independent of the engineering design procedure employed to reach the target. The subject of failure-consequence analysis is beyond the scope of this dissertation, which begins from a pre-established system reliability target.

Beginning with the targeted system reliability, the system is split into a hierarchy of subsystems, which for buildings include roof trusses, shear walls, floor lateral systems and floor gravity systems. The next step is to consider each of the unfactored system load combinations listed in ASCE-7, for which the load-sharing network among the subsystems is characterized based on engineering intuition, previous research, full-scale experimental results, or in this work, a building system computational model. The system load-sharing network is used to propose target subsystem reliabilities that would meet the system reliability goal.

Taking each subsystem and its target reliability as the starting point, the next step is to define the load-sharing network among the components within each subsystem. Detailed computational models for the subsystems including every component and their connections are used at this stage. The load sharing network, characterized by its system reliability sensitivities, is used to propose component reliabilities that meet the subsystem reliability goal.

Finally, the proposed component reliabilities are used withinin a load and resistance factor design framework (chapter 2) to recommend component resistance factors. These factors satisfy the system reliability goal for each load combination and can be directly used in structural design standards. The procedure is repeated for all ASCE-7 load combinations, and the final output is a set of resistance factors that satisfy system reliability targets across all load combinations. This framework is described in Figure 1.1.

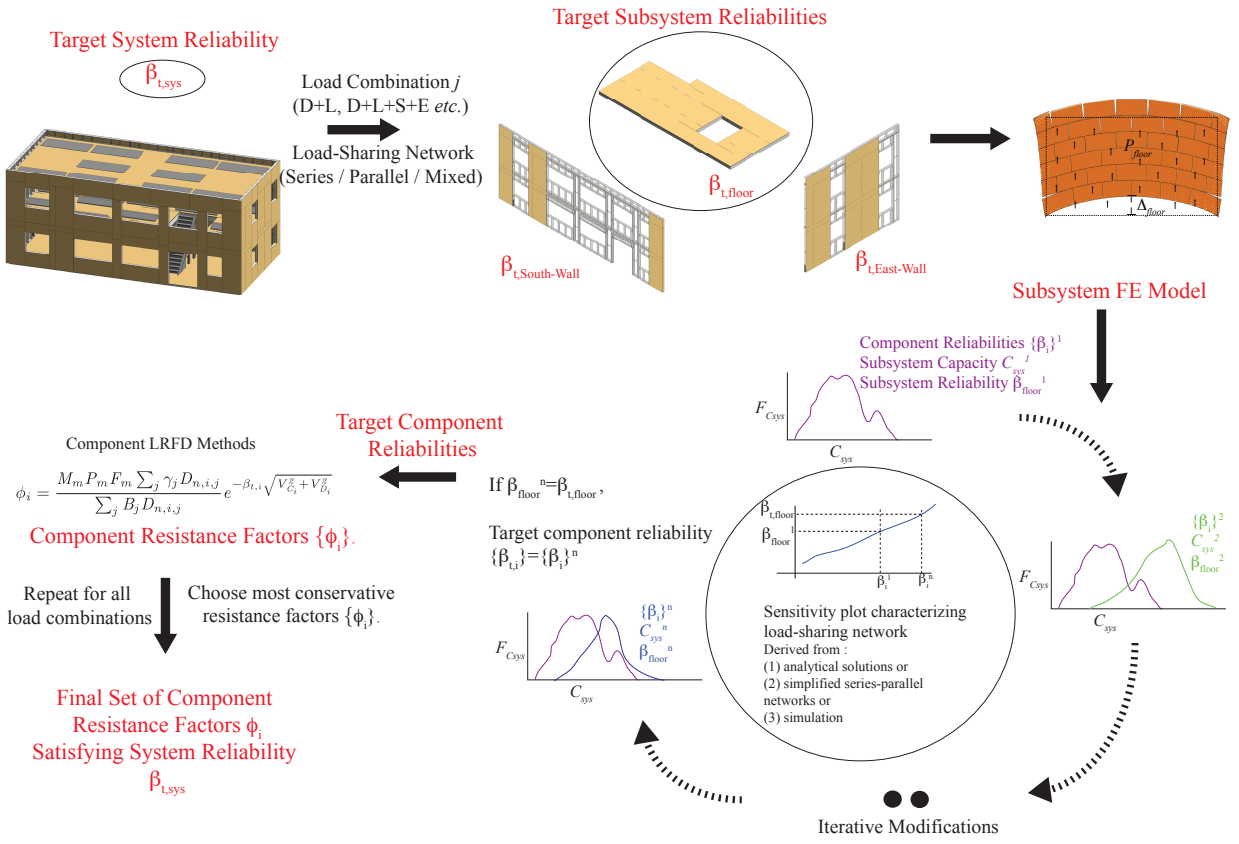

Figure 1.1: Overall research strategy to propose modified component resistance factors that meet a pre-defined target system reliability

A stochastic simulation framework is used to characterize the component load-sharing network within each structural subsystem. This begins with a baseline model derived from designing the subsystem according to current code provisions. Detailed computational mod-

els for this baseline system are developed and subjected to the specific load combination being studied. The component reliabilities for each member within the load-sharing network as well as the system reliability for the whole subsystem is computed for this load combination.

The baseline model is perturbed by modifying the properties (spacing, capacity, ductility etc.) of each individual component. As a result, the component reliabilities and the overall subsystem reliability changes. The change in subsystem reliability per unit change in component reliability quantifies the system reliability sensitivity to the component that was modified. The system reliability sensitivities are then used to recommend new component reliabilities that satisfy the reliability target for the subsystem, and the subsystem design is updated to meet the new component reliabilities.

The procedure is repeated iteratively until the subsystem reliability goal is met, and the end result is a set of component reliabilities that meet the target subsystem reliability which was chosen to satisfy the system reliability target. The component reliabilities are then used withing a load and resistance factor design framework to propose new component resistance factors.

Since the proposed component resistance factors satisfy the subsystem reliability target, which was initially chosen to meet the overall system reliability target, they result in component designs aligned to the overall system performance goals. The component designs can be met by usual load and resistance factor design approaches without necessitating full system-level simulations in the design office. Finally, the set of steps is repeated for every load combination, and the most conservative resistance factors are chosen.

The research application focuses on light-steel framed buildings, designed and tested by professional structural engineers [61] in full-scale shake table building experiments. The building is split into a hierarchical list of subsystems – shear walls, floor diaphragms and roof trusses. The target subsystem reliability is set for each of these and modified component reliabilities are recommended to satisfy them. Specifically in this dissertation, high-fidelity

finite-element modeling, system reliability and sensitivity analysis is performed for floor diaphragm subsystems under seismic loads. Parallel research efforts are focusing on applying the same methodologies to the other subsystems.

1.3 Original contributions

System-subsystem-component hierarchical enumeration provides a new approach to designing for system reliability, as outlined in Figure 1.1. The general approach is applied to light-framed building systems, which are split into a hierarchy of subsystems in chapter 4. The strategy is to first set the target system reliability for the building, which are used to recommend target subsystem reliabilities for floors, walls and trusses using assumptions on subsystem load-sharing. Rigorous finite-element analyses are performed at the subsystem level to characterize the load-sharing network, which is used to re-align component reliabilities to subsystem targets set by system reliability considerations. The new component reliabilities can be used to recommend resistance factors which satisfy the system reliability target, by following component reliability steps which are described in chapter 2.

A system-reliability sensitivity metric is proposed in section 3.2 which can be used to characterize any general load-sharing network of structural components. This characterization is demonstrated for a simple redundant network of structural components in chapter 3, highlighting its efficacy in accounting for component ductility during design. The sensitivity quantifies the dependence of system reliability on the reliability of the individual component. System reliability changes significantly if the component reliability of a critical member is modified (higher sensitivity), or remains unchanged for a relatively less-important component (lower sensitivity).

A direct-simulation based approach for system reliability estimation is proposed in section 2.2.3 as an alternative to classical failure-mode based system reliability for large systems with several possible failure paths. The methodology is inspired by hazard-fragility analysis

in earthquake engineering, and is distinct in two ways – (1) it is applicable to any hazard type, not only seismic and (2) it includes the uncertainty in structural parameters whereas seismic fragility analysis models the structure as deterministic and captures only the record-to-record variability in response. The approach is verified with failure-mode approaches for system reliability using a classical redundant system network in chapter 3.

A general approach is proposed in chapter 3 to compute target component reliabilities given the system reliability target, using the vector of sensitivities for the load-sharing network. This approach is used to compute target shear wall and diaphragm reliabilities in chapter 5 tuned to the building system reliability target, and screw-fastened connection reliabilities in chapter 7 tuned to the diaphragm reliability target.

Chapters 4 and 5 outline seismic system reliability calculation and sensitivity analysis for cold-formed steel buildings, and derive target subsystem reliabilities to meet a building system reliability goal of 2.5. Load sharing factors between different subsystems are calculated, and an interstory drift ratio based approach is recommended for system reliability calculation. A simplified reliability model is proposed that can calculate system reliabilities with lesser computational power compared to the state-of-the-art incremental dynamic analysis method used in earthquake engineering.

A high-fidelity finite element model for light-framed diaphragm subsystems is developed using the general purpose finite-element application ABAQUS (chapter 6). The model uses shell elements for all the floor diaphragm components (joists, tracks, panels, strap bracing, blocking and clip-angles) and non-linear spring elements for every single fastener connection, and matches the exact design details for a professionally-built cold-formed steel building. The critical spring elements, which are assigned quadri-linear load-deformation relationships characterized by component tests, can update their orientations during the analysis, and contact between wood panels is modeled using bearing and frictional springs. The analysis is thus both materially and geometrically non-linear. The model is used to characterize subsystem response and reliability under in-plane lateral loads.

The system reliability for floor diaphragm subsystems is calculated in chapter 7, using uncertainty quantification at the fastener level combined with finite-element simulations. Traditional failure-mode estimation approaches would be intractable for the complex model studied here due to the large number of components and candidate failure modes. Using target diaphragm reliability calculated in chapter 4, sensitivity calculations are performed to recommend final target component reliabilities and component design guidelines.

1.4 Dissertation structure

Chapter 2 provides a background on component-based load and resistance factor design, including example derivations of cold-formed steel component reliability design criteria. It also describes past research on system reliability and its application to design codes, and concludes with descriptions of hazard and fragility anaylsis in performance-based earthquake engineering which gives a more direct estimate of system reliability.

In chapter 3, the general methodology to characterize the structural load sharing network and recommend modified resistance factors is discussed. This general framework is applied to a well-known classical network, the Daniels system, which has frequently been used to study system reliability methods in previous research. A convolution-based direct simulation calculation approach for estimating system reliability is verified with example problems in the literature. A light-framed diaphragm system is modeled as a Daniels network and its members are designed to component LRFD guidelines. Component to system reliability maps are derived for perfectly ductile, brittle or quadri-linear components in the network, which are typically treated identically in component based LRFD, and modified resistance factors that account for component ductility are proposed.

Light framed building systems are introduced in chapter 4 and the framework for whole system reliability based design is described. The building is hierarchically split into subsystems and components, and the function, design and behavior of the diaphragm and shear wall sub-

systems is detailed. Load-sharing relationships between the subsystems as the building is subjected to a seismic load combination is derived using a simplified spring model subjected to non-linear time history analysis. The load-sharing relationships are used in chapter 5 to calculate building system reliability, perform sensitivity analysis to recommend subsystem reliability targets and analyze the structural implications of the sensitivity results.

In chapter 6 a high-fidelity finite element model is developed for floor diaphragm subsystems. Diaphragm force-deformation response under in-plane lateral loads is calculated along with component force distributions and reliabilities.

The deterministic modeling results are used in chapter 7 to incorporate uncertainty in component response and run stochastic (Monte-Carlo) simulations on the diaphragm model. The simulations characterize the diaphragm capacity distribution which is used to calculate subsystem reliability under seismic loads. Sensitivity analysis is performed to tune the component reliabilities calculated in chapter 6 such that the diaphragm subsystem reliability target of 2.1 may be satisfied, concluding with proposed design modifications to satisfy the component reliabilities.

Conclusions and future work are described in chapters 8 and 9 of the dissertation.

Chapter 2

Literature Review on Component-Based Load and Resistance Factor Design and Classical System Reliability

This chapter presents a review of general component reliability methods used in load and resistance factor design (LRFD), as well as previous approaches to solve the system reliability problem. A detailed derivation of the component LRFD equations is first presented including an example demonstrating the development of LRFD provisions for the design of cold-formed steel members. This is followed by a description of previous approaches to system reliability, and ends with hazard and fragility analysis approaches used in modern performance based seismic design. Specific modifications to the existing procedures described herein which define the research presented in the following chapters are highlighted.

2.1 Background on component-reliability based design

2.1.1 Derivation of component-reliability based load and resistance factors

Probability based criteria for structural design was introduced through load and resistance factors intended for routine design checks [29]. The methodology came to be known as load and resistance factor design (LRFD) which advanced the existing allowable stress design guidelines. Although the underlying theory was probabilistic, a deterministic design format was developed using proposed factors based on comprehensive statistical analysis for loads and resistances. The factors were calibrated to insure reliability levels implied in existing design recommendations against two limit states – strength (the structure withstands extreme loads) and serviceability (intended functionality is satisfied) during the design lifetime [35].

The procedure to derive load and resistance factors begins with the definition of a limit state, which is an equation demarcating structural failure from acceptable performance. It is expressed as a mathematical expression $g(X)$ for the set of basic random variables X that include structural properties (material and geometry of structural components) and component load effects (bending moment, shear or axial forces) arising from system loads (dead, live, wind, snow or earthquake).

$$\begin{gathered} g(X) < 0 \\ \text{implies failure} \end{gathered} \tag{2.1}$$

The *generalized* reliability index β is defined as the inverse standard normal distribution function Φ at the probability of failure.

$$\beta = -\Phi^{-1}(P(g(X) < 0)) \tag{2.2}$$

This is generally applicable to any form of the limit state surface unlike *simple* or *geometric* reliability indices [65]. This dissertation deals exclusively with the reliability index definition used in Equation 2.2.

The LRFD approach recommends load and resistance factors to satisfy reliability targets for each component in the structural system. Component reliability can be calculated by comparing capacities to demands on a member to member basis. If the capacity of the i^{th} component in a structural network (obtained from component testing) is denoted as C_i and its demand (evaluated from structural analysis) is D_i then the *component* limit state is

$$g_i = C_i - D_i \tag{2.3}$$

where C_i and D_i are random variables, and D_i is often described in structural reliability literature as the load effect [104]. The component reliability index is obtained by using Equation 2.3 to specialize Equation 2.2 as

$$\beta_i = -\Phi^{-1}(P(C_i - D_i < 0)) \tag{2.4}$$

The probabilistic distributions for C_i and D_i required to compute β_i are generally unknown. A convenient assumption employed in component reliability based design standards (for example, AISI design standard, highway bridge load ratings[2, 40]) prescribes that the ratio C_i/D_i is distributed lognormally [58], in which case Equation 2.4 further simplifies to

$$\beta_i = \frac{log_n \frac{\mu_{C_i}}{\mu_{D_i}}}{\sqrt{V_{C_i}^2 + V_{D_i}^2}} \tag{2.5}$$

where μ_{C_i} and V_{C_i} is the mean and coefficient of variation (COV) of C_i, and μ_{D_i} and V_{D_i} are the mean and COV of V_{D_i}.

The design criterion for a component-based LRFD procedure is to ensure that the component reliability index is always greater than or equal to the target reliability index, that is, $\beta_i \geq \beta_{t,i}$

for all i components. Target reliability indices were established from the implied reliability indices in allowable stress structural design codes in 1980 [29] and the typical values used are 2.5 for members and 3.5 for connections. This is accomplished using load factors γ and resistance factors ϕ that are calibrated to β_t. The load factors γ, provided in ASCE-7, are constant across material types and loading scenarios (that is, the relative magnitudes of dead, live, wind, snow or earthquake loads).

In general the target component reliability will be obtained using different combinations of resistance factors ϕ and load factors γ that change with the loading scenario, or conversely, the required nominal resistance C_n for a given target reliability index would vary with the relative magnitudes of individual load cases. Since it was desirable that a uniform set of load factors be used for all loading scenarios, a constrained optimization technique was employed that minimized the weighted square difference $I(\phi, \gamma)$, given by Equation 2.6, between the required nominal resistance $C_{n,i}$ given a fixed set of load and resistance factors and actual nominal resistances $C^*_{n,i}$ required for a general loading scenario, across all j possible loading scenarios [29].

$$I(\phi, \gamma) = \sum_{j \text{ loading scenarios}} p_j (C^*_{n,i} - C_{n,i})^2 \tag{2.6}$$

where $C^*_{n,i}$ is the actual nominal resistance required to reach the target component reliability $\beta_{t,i}$, and $C_{n,i}$ is the required nominal resistance obtained from the LRFD design equation using factors ϕ and γ. For example, if the load combination includes gravity and wind, $C_{n,i} = (\gamma_D D_n + \gamma_L L_n + \gamma_W W_n)/\phi$ [30], where $\gamma_D, \gamma_L, \gamma_W$ are the load factors for dead, live and wind loads, and ϕ is the resistance factor. The weighting factors p_j were assigned based on best estimates for the relative frequency of common load combinations for different construction materials, and it was noted from sensitivity studies that the factors were affected more by the range of loading scenarios considered than by the weight distributions. It was assumed that nominal wind and earthquake loads were equally likely to be 0.5, 1.0, 3.0 and 5.0 times the nominal dead load and were assigned same relative weights p_j. The relative

weights for different live to dead nominal load ratios and different construction materials are listed in Table 2.1 [30]

Table 2.1: Relative weights p_j for different live to dead nominal load ratios as provided in [29]

	Nominal Live Load / Nominal Dead Load						
Material	0.25	0.5	1.0	1.5	2.5	3.0	5.0
Steel	0	10	20	25	35	7	30
Reinforced Concrete	10	45	30	10	5	0	0
Light Gage and Aluminium	0	0	6	17	22	33	22
Masonry	36	36	20	6	2	0	0

Since the procedure outlined in Equation 2.6 would result in different load factors across different construction materials which was undesirable, it was necessary to separate the load and resistance factors, such that the set of γ factors would remain constant across different materials and limit states, and ϕ factors would account for the corresponding changes. The optimization methodology used additional constraints to obtain the final load factors. The dead load factor γ_D was assumed as 1.2 which was considered to be the minimum acceptable value in professional practice. For gravity load combinations, it was assumed that the same factor $\gamma_L = \gamma_S$ would be used for live and snow loads, and this factor should provide a resistance factor ϕ for flexure in steel and reinforced concrete in the range 0.85 to 0.9, which was satisfied by choosing $\gamma_L = \gamma_S = 1.6$.

While dead loads are expected to stay relatively unchanged over time, the quantity of interest for other load cases is the maximum expected value over a time period. The maxima of two separate load cases, for example, live and wind loads, have a low probability of occurring simultaneously, and so another quantity of interest is the point in time load value, defined as the measured load obtained when the random load process is sampled at an arbitrary

time point. For example, two separate conditions were considered for the dead + live + wind load combination – the first one included a maximum expected live load plus a point in time wind load , and the other had a maximum expected wind load and a point in time live load. Again setting ϕ factors to lie within 0.85 to 0.9 and $\gamma_D = 1.2$, the case with the point in time live load generated a wind load factor of 0.1, which was ignored to obtain a single dead + live + wind load combination given by $\gamma_D = 1.2, \gamma_L = 0.5$ and $\gamma_W = 1.3$. Similar considerations for earthquake load combinations, counteracting loads, live + snow load (important for upper story columns) and wind + snow load (important for certain roof structures) led to the following final load combinations –

$$\begin{aligned} 1.4D_n \\ 1.2D_n + 1.6L_n \\ 1.2D_n + 1.6S_n + (0.5L_n or 0.8W_n) \\ 1.2D_n + 1.3W_n + 0.5L_n \\ 1.2D_n + 1.5E_n + (0.5L_n or 0.2S_n) \\ 0.9D_n - (1.3W_n or 1.5E_n) \end{aligned} \tag{2.7}$$

where D_n, L_n, S_n, W_n and E_n are nominal dead, live, snow, wind and earthquake loads respectively. The load combinations provided in Equation 2.7 have undergone changes with new versions of ASCE-7, and the ASCE 7-10 load combinations are

$$
\begin{aligned}
1.4D_n \\
1.2D_n + 1.6L_n \\
1.2D_n + 1.6L_n + 0.5S_n \\
1.2D_n + 1.0L_n + 1.6S_n \\
1.2D_n + 1.0L_n + 1.0W_n + 0.5S_n \\
1.2D_n + L_n + 0.2S_n + E_n \\
0.9D_n - 1.0W_n \\
0.9D_n - 1.0E_n
\end{aligned}
\tag{2.8}
$$

The resistance factors ϕ are derived through the procedures outlined in [104, 58] and are summarized in this section. The overall system demand D_{sys} is a load combination of demands $D_{sys,j}$ generated from j different load cases. Component demands D_i are obtained from system demands D_{sys} using linear elastic structural analysis as $D_i = c_i D_{sys}$ where c_i is a constant that converts system loads to component load effects. Thus the mean demand μ_{D_i} used in Equation 2.5 can be expressed as [104]

$$\mu_{D_i} = c_i \sum_j B_j D_{n,sys,j} = \sum_j B_j D_{n,i,j} \tag{2.9}$$

where bias factors B_j are the ratio of code specified nominal values $D_{n,sys,j}$ to mean values for load case j. The mean capacity μ_{C_i} can be expressed as

$$\mu_{C_i} = M_m P_m F_m C_{n,i} \tag{2.10}$$

where M_m, P_m and F_m are material, professional and fabrication factors and $C_{n,i}$ is the code specified nominal capacity for component i. The reliability based design equation is

$$\phi_i C_{n,i} \geq \sum_j \gamma_j D_{n,i,j} \tag{2.11}$$

The above design check is to be performed for all ASCE-7 load combinations (Equation 2.8). The most severe case will govern, which conversely implies that the recommended resistance factor ϕ_i will be the minimum value obtained after considering all load combinations. Using Equation 2.11 in Equation 2.10, we get $\mu_{C_i} \geq \frac{M_m P_m F_m \sum_j \gamma_j D_{n,i,j}}{\phi_i}$ which can be plugged into Equation 2.5 to get the reliability expression for the lognormal case as

$$\beta_i \geq \frac{log_n \frac{M_m P_m F_m \sum_j \gamma_j D_{n,i,j}}{\phi_i \sum_j B_j D_{n,i,j}}}{\sqrt{V_{C_i}^2 + V_{D_i}^2}} = \beta_{t,i} \tag{2.12}$$

Thus, given the target component reliability indices $\beta_{t,i}$ it is possible to recommend component safety factors ϕ_i as follows [104]

$$\phi_i = \frac{M_m P_m F_m \sum_j \gamma_j D_{n,i,j}}{\sum_j B_j D_{n,i,j}} e^{-\beta_{t,i}\sqrt{V_{C_i}^2 + V_{D_i}^2}} \tag{2.13}$$

2.1.2 Example application of component-reliability design equations to cold-formed steel design standards

LRFD design provisions were developed for design loads [29], reinforced concrete [27] hot rolled steel [35, 85] and cold formed steel [58]. Out of these, the specific case of cold-formed steel is described here in detail because it is relevant to the light-framed building applications proposed later in the dissertation.

Load combinations, target reliability and resistance factor equation

Lin and Galambos first developed resistance factors for cold-formed steel structural members in [58].This research was limited to the dead plus maximum live load combination, that is

$1.2D_n + 1.6L_n$, since this was the governing case in many practical designs. Using this load combination in the design equation given by Equation 2.11 gives the required nominal component resistance as $\phi_i C_{n,i} \geq c_i(1.2D_n + 1.6L_n)$ or $C_{n,i} \geq c_i(1.2D_n/L_n + 1.6)L_n/\phi$. It was further assumed that $D_n/L_n = 1/5$, which is typical for light-steel framed structures. Thus the nominal required resistance could finally be expressed as $C_{n,i} \geq 1.84(c_i L_n/\phi)$, from which the mean component resistance can be obtained using Equation 2.10 as

$$\mu_{C_i} \geq 1.84(c_i L_n/\phi) M_m F_m P_m \tag{2.14}$$

The mean component demand was obtained from Equation 2.9, using bias factors 1.05 for dead load and 1.0 for live loads as recommended in [30], and the same assumption $D_n/L_n = 1/5$, as

$$\mu_{D,i} = c_i(1.05D_n/L_n + 1)L_n = 1.21 c_i L_n \tag{2.15}$$

The expressions for mean component capacity and demand, given by Equation 2.14 and 2.15 can be plugged into the Equation 2.5 for component reliability to get

$$\beta_i \geq \frac{(1.521/\phi) M_m F_m P_m}{\sqrt{V_{C_i}^2 + V_{D_i}^2}} \tag{2.16}$$

The load variability $V_{D_i}^2$ was obtained by combining the variabilities $V_D = 0.1$ and $V_L = 0.25$ and bias factors 1.05 and 1.0 for dead and live loads respectively, as derived in [30]. The expression for V_{D_i} is given by

$$V_{D_i} = \frac{\sqrt{(1.05D_n/L_n)^2 V_D^2 + V_L^2}}{1.05D_n/L_n + 1} \tag{2.17}$$

Again assuming $D_n/L_n = 1/5$, one can obtain $V_{D_i} = 0.21$, which is the assumed variability in demand used to derive all resistance factors.

The component capacity variability arises from variabilities in the material, fabrication and professional factors, which gives the capacity variability as

$$V_{C_i}^2 = V_M^2 + V_F^2 + V_P^2 \tag{2.18}$$

The material factor captures the variability in mechanical properties of members, and can be estimated as the mean (M_m) and variance (V_m) in the ratio of a tested mechanical property to its predicted strength. Recommended values for yield strength of stainless steel were $M_m = 1.1, V_M = 0.1$, while those for the ultimate strength were $M_m = 1.1, V_M = 0.05$. The fabrication factor captures the uncertainties due to initial imperfections, geometric properties and cross-sectional dimensions, for instance, the relatively high deviations in weld lengths. Values for F_m and V_F were provided both in the LRFD standard for cold-formed steel members as well as the AISC criteria for hot-rolled steel members [35, 85]. Finally, the professional factor reflected the uncertainty in predicting the ultimate strengths of members and can be obtained as the test to predicted member strengths, as detailed for each specific component type in the following sections.

Using the component reliability expression given by Equation 2.16 in the target reliability expression $\beta_i \geq \beta_{t,i}$, the resistance factor ϕ can be expressed as

$$\phi = \frac{1.521 M_m F_m P_m}{e^{\beta_{t,i}\sqrt{V_{C_i}^2 + V_{D_i}^2}}} \tag{2.19}$$

Target reliability indices $\beta_{t,i}$ were obtained from similar research performed for cold-formed carbon steel which indicated reliabilities of 2.5 for members and 3.5 for connections. Since the factors of safety used for allowable stress design of cold-formed stainless steel were higher than the corresponding factors for carbon steels, the proposed target reliabilities were 3.0 for members and 4.0 for connections.

Using the proposed values of $\beta_{t,i}$ in Equation 2.19, resistance factors were derived for flexural members, compression members, welded and bolted connections, as described in the following

sections. The only remaining quantities required to calculate ϕ are the mean values and coefficients of variation for the professional factors, which were obtained from the ratios of the tested ultimate capacities to predicted values for each component type.

Thus there are three essential steps to obtain resistance factors for each component:

1. Develop equations to predict the nominal member capacity.
2. Perform experiments to obtain the mean tested to predicted capacity ratio P_m and variance V_P.
3. Propose values for the material and fabrication factors M_m and F_m, their variabilities V_M and V_F and use these in Equations 2.18 and 2.19 to calculate ϕ. Use $V_{D_i} = 0.21$ throughout.

It should be noted here that the proposed modifications to the component reliability procedure discussed in this dissertation deal specifically with re-aligning the target reliabilities $\beta_{t,i}$ based on the load-sharing network and its system reliability, while the remaining steps to derive final modified resistance factors stay similar.

Resistance factors for flexural members

Two methods were proposed to obtain the nominal (predicted) strengths of flexural members. The first method used the effective beam yield moment $M_n = S_e F_y$ where S_e is the elastic section modulus and F_y the specified yield strength. The effective width method was used to calculate the section modulus S_e. The second method used the inelastic reserve strength considering partial plastification of the section, but was only applicable to members not subjected to lateral, torsional, later-torsional buckling or twisting, and only within specified slenderness ratios.

Seventeen beam experiments performed at Cornell were used to obtain the mean test-to-predicted ratio P_M and variance V_P. Since only two of these satisfied the slenderness criteria

for the inelastic reserve strength method, the effective beam yield method alone was employed to calculate predicted strengths. The mean test to predicted strength P_m was 1.189 and its variance V_P was 0.0608.

The material and fabrication factors were assumed as follows – $M_m = 1.1, V_M = 0.1, F_m = 1.0, V_F = 0.05$. The overall capacity variability calculated using Equation 2.18 was $V_{C_i} = 0.13$. Using these values in Equation 2.19, along with load variability $V_{D_i} = 0.21$, gives a value of $\phi = 0.95$, which was chosen as the resistance factor for flexural members.

Resistance factors for concentrically loaded compression members

Resistance factors were proposed for concentrically loaded stub-columns and compression members subjected to flexural or flexural-torsional buckling. Due to the unavailability of test data, resistance factors could not be derived for members that experienced torsional buckling. The capacity for stub-columns was predicted as $P_n = A_e F_{yc}$ where F_{yc} is the yield strength in longitudinal compression and A_e the effective area calculated using the effective width method. For compression members the capacity was $P_n = A_e F_n$ where F_n is the minimum among flexural, torsional and torsional-flexural buckling stresses. The flexural buckling stress, for doubly-symmetric closed cross-sections or other cross-sections not prone to torsional or torsional-flexural buckling was computed as :

$$F_n = \pi^2 E_t / (KL/r)^2 \leq F_y \tag{2.20}$$

where F_y is the 0.2% yield strength, K the effective length factor, L the unbraced length and r the radius of gyration of the full cross-section. The tangent modulus E_t corresponding to stress F_n was computed with the modified Ramberg-Osgood equation using a computer program.

The flexural-torsional buckling stress for singly-symmetric cross-sections was predicted as follows:

$$F_n = (1/2\beta)((F_{ex} + F_t) - \sqrt{((F_{ex} + F_t)^2 - 4\beta F_{ex} F_t}) \leq F_y \tag{2.21}$$

where $\beta = 1 - (x_0/r_0)^2$, x_0 being the distance between the centroid and shear center along the centroidal axis, r_0 the polar radius of gyration about shear center, F_{ex} the Euler buckling stress about the symmetry axis and F_t the torsional buckling stress.

Fourteen concentrically loaded stub column tests performed at Cornell [50, 103] yielded a mean test to predicted strength $P_m = 1.265$ and variance $V_P = 0.0608$. For members subjected to flexural buckling, tested strengths were obtained from twenty-nine column experiments [50, 102] with I-sections and box-sections and pin-ended boundary conditions , giving a mean test to predicted ratio of 1.194 with a 0.114 coefficient of variance. An experimental study on hat sections [101] provided test to predicted ratios for compression elements subjected to torsional-flexural buckling as $P_m = 1.111$ and $V_P = 0.074$.

The same material and professional factors as flexural members were chosen for compression members – $M_m = 1.1, V_M = 0.1, F_m = 1.0, V_F = 0.05$. Based on these values a ϕ factor of 0.95 resulted in a reliability index of 3.4 for stub columns, demonstrating the accuracy of the strength prediction method. For members subjected to flexural buckling, $\phi = 0.9$ gave a reliability index of 3.05, whereas in the case of members experiencing flexural-torsional buckling, $\phi = 0.85$ gave a reliability of 3.26. To maintain consistency between members prone to different buckling modes and also with the LRFD criteria for hot-rolled shapes, a uniform reliability of $\phi = 0.85$ was chosen.

The strength prediction equations for concentrically loaded columns have evolved with time. New expressions for the buckling stresses were adopted in the 1996 specifications in terms of the slenderness ratio $\lambda_c = \sqrt{(F_y/F_e)}$ similar to the column curve used in the AISC LRFD specification. This was a direct strength prediction approach since it used the gross cross-sectional area multiplied with a reduced stress for inelastic buckling to predict ultimate capacity. These were verified with 299 experiments by Pekoz and Summer [77] showing a better predictability compared to Equations 2.20 and 2.21. In the 2004 specification the

direct strength method was extended to local and distortional buckling which considered the entire cross-sectional elastic buckling stress for nominal capacity prediction, instead of combining buckling stresses of individual elements in the cross-section and their effective-widths as was the current practice at the time [88].

While the prediction equations updated with new versions of the AISI design specification, the resistance factors remained un-altered. A verification study considering results from 675 column tests including Cee sections, lipped and unlipped Z sections, angle sections, hat sections and members with perforations was carried out in [37, 38]. These studies utilized the direct strength method for capacity predictions and recommended resistance factors of 0.8 for flexural, torsional or flexural-torsional buckling, 0.9 for local-global buckling interaction and 0.95 for distortional buckling.

Resistance factors for welded connections

The nominal load for groove welds in butt joints in tension or compression was obtained as $P_n = LtF_{ua}$ where L is the welded length, t the thickness of the thinnest welded sheet, and F_{ua} the tensile strength of the annealed based metal. The nominal shear strength for longitudinally loaded fillet welds was $P_n = (0.7 - 0.009L/t)LtF_{ua}, L/t < 30$ and $P_n = 0.43LtF_{ua}$ or $P_n = 0.75Lt_wF_{xx}, L/t \geq 30$, where $t_w = 0.707t$ is the effective throat and F_{xx} the tensile strength of the weld metal. For transverse loading it equalled $P_n = 0.75LtF_{ua}$ or $P_n = LT_wF_{xx}$. The first of these was to prevent sheet failure and the second to prevent weld metal failure.

Tested strengths for groove welds were obtained from ten tests with 0.5 inch thick specimens [31] and thirty-three tests with 1 inch thick specimens [33]. The overall professional factors obtained were $P_m = 1.113$ and $V_P = 0.084$. For transverse fillet welds, ten connection tests [31] gave two sets of test to predicted ratios – $P_{m1} = 1.027$,$V_{P1} = 0.088$ for predicted capacity against sheet metal failure, and $P_{m2} = 1.207$, $V_{P2} = 0.089$ for weld metal failure. The corresponding values for longitudinal fillet welds, obtained from ten experiments conducted

in [31], were $P_{m1} = 1.083$,$V_{P1} = 0.131$ and $P_{m2} = 1.058$,$V_{P2} = 0.126$.

The material and professional factors for welded connections were different from flexural or compression members, and the values used were $M_m = 1.1, V_M = 0.05, F_m = 1.0, V_F = 0.15$. A different target reliability of 4.0 was used for these components as well. These led to resistance factors of 0.6 for groove welds, 0.55 for longitudinal fillet welds, 0.55 for transverse welds against plate metal failures and 0.65 against welds metal failures.

Resistance factors for bolted connections

Resistance factors were calculated for sheet shear failure, bearing or piling up of material in front of bolt and sheet tearing. Bolt shear or tensile failures were not included. The nominal sheet shear strength was calculated as $P_n = teF_u$, where t is the thickness of the thinnest connected part, e the minimum edge distance or center-to-center distance of two adjacent holes measured along the line of force, and F_u the tensile strength of the connected sheet. The nominal bearing strength was calculated as $P_n = F_p dt$, $F_b = 2F_u$ in single shear and $F_u = 2.75F_u$ in double shear, d the nominal bolt diameter. The tensile strength was calculated as $P_n = A_n F_t$ with A_n being the net section area and F_t the nominal tensile stress.

Tested strengths were obtained from twenty-four bolted connection tests between two 4 in. X 20 in. steel sheets with single row of fasteners in single or double shear [31]. Four of these failed in sheet shear giving test-to-predicted strength ratios $P_m = 1.055$ and $V_P = 0.054$. Thirteen tests were used for bearing resistance factors, out of which ten were pure bearing and three combined bearing, tearing and shear, for which the professional factors were $P_m = 1.018$ and $V_P = 0.078$. The remaining seven tests experienced tension failure with $P_m = 1.101$ and $V_P = 0.098$.

Material and professional factors for bolted connections were assumed as $M_m = 1.1, V_M = 0.1, F_m = 1.0, V_F = 0.05$, with a target reliability $\beta_{t,i} = 4.0$. Using these values, resistance factors of 0.7 were recommended for sheet shear, 0.65 for bearing and 0.7 for tension.

Determination of resistance factors from testing structural members

The current AISI design provisions for cold-formed steel members (AISI S100-16 chapter F) also provides recommendations for deriving resistance factors from component testing, following the same reliability procedure described in section 2.1.2 using mean and variance of test-to-predicted strengths P_m and V_P.

Test results are allowed to be used directly without a strength prediction model with $P_m = 1.0$, for which at least three identical tests are required, and if any individual test deviates from the mean result by more than 15 percent, additional tests until such deviation is eliminated have to be conducted, or at least three additional tests have to be performed. Alternately, a rational engineering model can be used for strength prediction, for which P_m is defined as the mean strength to predicted ratio. The variance of the professional factor V_P is limited to a minimum value of 0.065.

The component variability expression given by equation 2.18 is modified as $V_{C_i}^2 = V_M^2 + V_F^2 + C_P V_P^2$. The correction factor C_P depends on n, the number of tests performed, with $C_P = 5.3$ for $n = 3$ and $C_P = (1 + 1/n)m/(m - 2)$ for $n \geq 4$, where $m = n - 1$.

Target reliabilities $\beta_{t,i}$ is recommended as 2.5 for members and 3.5 for connections, and material and fabrication factors M_m, V_M, F_m and V_F are provided in table F1 of the specification, with resistance factors permitted to be derived using equation 2.19.

2.1.3 Incorporating system effects in component-reliability based design using empirical factors

It was acknowledged during the development of LRFD that although the practical recommendation was a member to member safety check insuring satisfactory component reliabilities, ideally the performance criteria should be system based [29] – a drawback that was acceptable because structural system reliability would be far greater than the most critical

component reliability. This resulted from several different factors – practical overdesign from constructability considerations, conservative member limit states (for example, first plastic hinge formation), ductile member limit states, ignoring beneficial effects from non-structural members, serviceability controlled design and the fact that the structural system may not fail when the critical member collapses due to redundancy and alternate load paths [36].

A recommended method to overcome the conservatism was the use of systems factors ϕ_s that modified component resistance factors ϕ_i depending on the system limit state, such that the final resistance factor would be $\phi_s\phi_i$ [36]. Advancing upon the general limit state $g(X)$ discussed so far which does not consider the consequence of failure upon the structural system, the following classification of limit states was recommended:

1. Serviceability limit state – Structures experience acceptable damage to system demands that are expected to be breached several times during the structure's intended lifetime. Examples include floor deflection limits due to live loads or drift limits due to wind loads.

2. Ultimate limit state – Structures respond to extreme demands that have low exceedance probabilities during the design life in a manner that major failure to the network is acceptably small, and life safety is maintained.

Based on the above limit states, the following systems factors ϕ_s were recommended for different types of component failures –

1. $\phi_s = 1.1$ for slight damage, such as first plastic hinge formation in compact members that are part of a redundant frame, yielding of tension members or simply supported non-slender beams on solid supports.

2. $\phi_s = 1.0$ for moderate damage, caused by failures of columns in statically determinate structures, slender members, beam or frame failures that lead to plastic mechanisms or connections between multiple elements acting in tension, shear or a combination.

3. $\phi_s = 0.9$ for serious damage caused by frame instability under gravity loads where side-sway is restricted by the presence of cladding.

4. $\phi_s = 0.8$ or $\phi_s = 0.7$ for complete damage cased by frame instability in the absence of structural cladding, or component failures that bring down the whole system (gross lack of redundancy).

The resistance factor modifications discussed above are similar to what is proposed in this dissertation, however as can be seen these recommendations are somewhat empirical and do not include explicit system reliability calculations.

Other examples of empirical factors that indirectly account for system effects include effective length factors in column design, nominal strength increases in repetitive light framed construction and R and C_d factors used in seismic design for response modification and deflection amplification. System factors used to account for system effects in wood construction are also based on simple modeling assumptions and engineering judgment, which lead to discrepancies between the estimated strength used in calculating 'apparent' reliabilities in design codes, and actual system strength leading to reliabilities observed in real structural system response [86].

2.2 Background on system reliability for a network of structural components

The component reliabilities β_i in a structural system network define the system reliability β_{sys} based on the component load sharing characteristics. This depends on how component failures interact and affect the network, for example, in some systems a single component failure event may trigger system collapse, whereas in other, more benign situations, several components would have to fail simultaneously for the system to fail. In this section the

methodology to failure mode and direct convolution-based approaches to estimate system reliability and their previous application to structural design methods is discussed.

2.2.1 System reliability calculation using failure mode analysis approaches

System level safety is quantified by the system reliability index β_{sys}, given by

$$\beta_{sys} = -\Phi^{-1}[P(SystemFailure)] \tag{2.22}$$

where Φ is the standard normal cumulative density function and $P(SystemFailure)$ is the system failure probability. One way to solve Equation 2.22 is to consider individual structural failure modes, any one of which can trigger system failure. Each failure mode comprises combined component failures, such that the overall system reliability is expressed as [22]

$$P(SystemFailure) = P[\cup_{k=1}^{K} \cap_{i \in C_k} (g_i(X) < 0)] \tag{2.23}$$

where K is the number of system failure modes, each triggered by simultaneous component failures for members belonging to individual cut sets C_k. The cut sets represent structural components that can fail together to trigger system failure. For example, for the Colorado State Highway bridge girder system considered in [32], two internal girders and one external girder comprise a single cut set. An n component classical series system, whose failure is triggered by any individual failing, will have n cut sets with a single component each, whereas a classical parallel system will have a single cut set of n components. Solving the system reliability problem in this form given in Equation 2.23 requires some form of non-linear structural analysis to identify component failure interactions that lead to system failure, each of which is termed a failure mode. Such procedures require the enumeration of all possible failure modes that can lead to complete structural collapse, which makes

the system reliability problem significantly challenging [70]. Various algorithms have been proposed for this – some examples include the incremental loading method [84], truncated enumeration method [66], the branch and bound method [23], hybrid analytical-simulation methods such as linear programming [16], combined enumeration and adaptive importance sampling [23],selective genetic algorithm search strategies [92], selective search for dominant failure modes [53], matrix based system reliability [96] etc.

Once the failure modes have been enumerated, the exact system reliability may be computed if the correlations between all individual failure modes are known. Since this information is not available generally, many researchers have proposed mathematical upper and lower bounds to system reliability which are practically useful if the band is narrow (upper and lower bounds are close to each other) [25, 83, 97]. From a load-sharing network viewpoint, upper and lower bound systems can be envisioned as springs arranged in series or parallel – failure occurs in series systems when the first component fails, i.e., low redundancy, and parallel systems when all components fail, i.e., high redundancy.

In general the events E_i, which imply failure of the i^{th} structural component, constituting a series or parallel system will be statistically dependent, and the exact solution to Equation 2.23 can be found only if the correlations between all modes are known. For example, the exact series system failure probability is given by the inclusion-exclusion rule –

$$P(E_{\text{series system}}) = P(\cup_{i=1}^{i=n} E_i) = \sum_i P(E_i) - \sum_{i<j} P(E_i E_j) + \sum_{i<j<k} P(E_i E_j E_K) - .... \quad (2.24)$$

Owing to the difficulty in solving Equation 2.24, there has been a great stress on developing bounds for the system failure probability [95]. Unicomponent probability bounds for the series system were first derived by Boole in 1954 [7].

$$max(P_i) \leq P(\cup_{i=1}^{i=n} E_i) \leq min(1, \sum_{i=1}^{i=n} P_i) \quad (2.25)$$

which were extended to bi-component bounds through the efforts of Kounias, Hunter and Ditlevsen [54, 43, 25, 95].

$$P_1 + \sum_{i=2}^{i=n} max(0, P_i - \sum_{j=1}^{j=i-1} P_{ij}) \leq P(\cup_{i=1}^{i=n} E_i) = P_1 + \sum_{i=2}^{i=n} (P_i - max_{j<i} P_{ij}) \tag{2.26}$$

The bounds for parallel systems can be obtained by converting to a series system using De-Morgan's rule $\overline{\cap E_i} = \cup \overline{E_i}$.

Upper and lower bound solutions for series systems have also been implemented in finite-element based system reliability treatments for geometrically non-linear elastic structures [47], with example applications to an elastic truss and suspended structures [34]. These techniques were used for system reliability evaluation of suspension bridges, with specific application to the Honshu Shikoku Bridge in Japan [48].

2.2.2 Applications of system reliability quantifications to structural design

Several studies have recommended design-code modifications based on system reliability analyses. It was demonstrated in [42] that material behavior, load and resistance statistics, load sharing relationships and damage level influence the system reliability for ductile and brittle springs arranged in parallel. This study considered redundant spring systems with linear elastic behavior until yield, following which the strength either drops to a residual (brittle springs) or stays capped at yield (ductile springs) and it was recommended that resistance factors be increased in systems with higher reserve strengths (multiple redundant components). Detailed system reliability analyses on these systems are provided in chapter 3. These studies also recommended global system factors ϕ_R similar to those proposed in [36] and discussed in section 2.1.3 which modified the component design check described in Equation 2.11 as follows :

$$\phi_R \phi_i C_{n,i} \geq \sum_j \gamma_j D_{n,i,j} \tag{2.27}$$

with ϕ_R ranging from 0.8 to 1.1 for zero to high strength reserves in the system. The strength reserve was quantified by the system performance factor $R = \beta_{sys}(intact)/(\beta_{sys}(intact) - \beta_{sys}(damaged))$ where $\beta_{sys}(intact)$ and $\beta_{sys}(damaged)$ are the system reliabilities calculated when component i is either intact or damaged.

System factors that increase or decrease nominal component resistance based on redundancy are used in highway bridge superstructure design and load ratings [40]. Four limit states were considered in this study :

1. Member failure – Component limit state described in section 2.1.1 and obtained from component reliability analysis, with a capacity LF_1, reliability β_{member}
2. Ultimate limit state – Ultimate capacity (LF_u) of the bridge system or formation of a collapse mechanism, reliability β_{ult}
3. Functionality limit state – Capacity at which the deflection of the main longitudinal member equals or exceeds the span length/1000 (LF_f), reliability β_{func}
4. Damaged condition limit state – Ultimate capacity (LF_d) after one of the main load-carrying components is removed from the bridge, reliability $\beta_{damaged}$

Using the above limit states and their capacities, system reserve ratios were defined as :

$$R_u = \frac{LF_u}{LF_1}, R_f = \frac{LF_f}{LF_1}, R_d = \frac{LF_d}{LF_1}, \tag{2.28}$$

The redundancy of the bridge system was quantified using the differences between ultimate, functionality and damaged reliability indices with the member failure reliability index, that is, $\Delta\beta_u = \beta_{ult} - \beta_{member}$, $\Delta\beta_f = \beta_{func} - \beta_{member}$ and $\Delta\beta_d = \beta_{damaged} - \beta_{member}$. Using the

lognormal form of the reliability expression given in Equation 2.5, these may be related to the system load reserve ratios as follows:

$$\Delta\beta_u = \frac{log_n R_u}{\sqrt{V_{LF}^2 + V_{LL}^2}}, \Delta\beta_f = \frac{log_n R_f}{\sqrt{V_{LF}^2 + V_{LL}^2}}, \Delta\beta_d = \frac{log_n R_d \frac{\overline{LL_{75}}}{\overline{LL_2}}}{\sqrt{V_{LF}^2 + V_{LL}^2}} \tag{2.29}$$

where V_{LF} and V_{LL} are the coefficients of variation in LF_1 and LL_{75} (the maximum 75 year live load), $\overline{LL_{75}}$ is the mean value of LL_{75} and $\overline{LL_2}$ the mean maximum 2 year live load (relevant for the damaged bridge condition).

The system factors were calibrated to target values of $\Delta\beta_u$, $\Delta\beta_f$ and $\Delta\beta_d$, which were recommended based on simple-span, steel and prestressed concrete bridge studies as :

$$\Delta\beta_u \geq 0.85, \Delta\beta_f \geq 0.25, \Delta\beta_d \geq -2.7 \tag{2.30}$$

The required reliability margins can be converted to required system reserve ratios using Equation 2.29 as :

$$R_u \geq 1.3, R_f \geq 1.1, R_d \geq 0.5 \tag{2.31}$$

Using these values, the following redundancy ratios were proposed for ultimate, functionality and damaged limit states – $r_f = R_f/1.1$, $r_u = R_u/1.3$ and $r_d = R_d/0.5$. The member reserve ratio was defined as $r_1 = (R_{provided} - D)/(R_{req} - D)$, where $R_{provided}, R_{req}$ and D are the provided member capacity, the required member capacity and the dead load respectively.

Finally, the system redundancy factor was defined as $\phi_{red} = min(r_1 r_u, r_1 r_f, r_1 r_d)$, which could be used within the component LRFD design check as $\phi_{red}\phi_i C_{n,i} \geq \gamma_d D_n + \gamma_l L_n(1+I)$, I being the impact load factor.

The system reliability methodology proposed in this dissertation follows a similar calibration methodology which quantifies the system capacity corresponding to the ultimate limit state.

However, it is distinct in the following ways – (1) the first-order lognormal assumption is relaxed and system reliability calculations are generalized for all capacity and demand distributions, (2) it is generalized for any load combination (not just dead + live) and (3) the modified resistance factors, which are recommended for all components in the system, are calibrated to an explicit system reliability target instead of the difference between first member and system limit state reliabilities.

In the next section, the first of these advancements, that is, the capability to consider general capacity and demand distributions, is described, and applied to an example problem in chapter 3. The third advancement, which is an explicit calibration to system reliability targets, is achieved by the reliability sensitivity methodology which is introduced in chapter 3.

2.2.3 Fragility and hazard analysis based system reliability for seismic performance-based design

Modern seismic performance-based structural designs recommend performance criteria (for example, immediate occupancy, life safety, collapse prevention) based on system response at specified hazard levels [17]. These approaches explicitly compute system reliabilities using multiple non-linear structural analyses [18] . The system reliability problem is broken into two separate parts – one characterizing external demand (hazard) and the other representing the probabilistic structural response (fragility). In contrast with failure mode enumeration techniques discussed above, this is a direct structural simulation approach similar to the methodologies employed in this dissertation.

The hazard level is expressed in terms of spectral acceleration which is a property of the structure's natural period and the ground-motion's frequency content. This is statistically characterized in terms of an exceedance probability over a given time period (for example, 2% in 50 years) [15]. Structural fragility is computed by probabilistically quantifying an

engineering demand parameter (such as peak inter-story drift) through multiple simulations with a ground motion set scaled to the same spectral acceleration [15]. Several examples of structural fragility assessment can be found in [10, 28, 93, 44, 98]. These studies typically quantify structural response variability to different ground motions without modeling uncertainty in the structure itself. By contrast, the work presented here focuses on quantifying the uncertainty in structural component properties to obtain fragilities for general loading scenarios not limited to seismic.

The fragility-hazard based convolution framework for calculating system reliability starts with the system failure probability definition as:

$$P(SystemFailure) = P(C_{sys} - D_{sys} \leq 0) \tag{2.32}$$

where C_{sys} and D_{sys} represent random system capacity and demand respectively. One way to solve Equation 2.32 is to carry out direct Monte Carlo simulations considering variability in structural properties as well as external demand (for example, [9]) and counting the number of simulated failures. This approach would typically require a very large number of simulations which can be prohibitive when system failure probabilities are low and structural models have high computational demand. This is circumvented by splitting the system reliability problem into two parts – fragility and hazard, the latter of which will typically be available from independent analyses (for example, Probabilistic Seismic Hazard Analysis [14]) and the former can be estimated by orders of magnitude lower number of simulations than required for direct failure probability estimation.

The system reliability expression given in Equation 2.32 can be recast as

$$P(C_{sys} - D_{sys} \leq 0) = \int_{d=0}^{d=\infty} P(C_{sys} \leq d | D_{sys} = d) dF_{D_{sys}}(d) = \int_{d=0}^{d=\infty} F_{C_{sys}}(d) dF_{D_{sys}}(d) \tag{2.33}$$

when C_{sys} and D_{sys} are independent random variables, and F_x represents the cumulative

distribution function for random variable x. The conditional probability $P(C_{sys} \leq d|D_{sys} = d)$ is known as fragility and the demand distribution $f_{D_{sys}}(d)$ is the hazard, where f_x is the probability density function for random variable x. This approach is common in probabilistic performance based seismic design, for example, where Equation 2.33 is further broken down as [15]

$$\begin{aligned} P(C_{sys} - D_{sys} \leq 0) &= \int_{d=0}^{d=\infty} P(C_{sys} \leq d|D_{sys} = d) dF_{D_{sys}}(d) \\ &= \int_{x=0}^{x=\infty} P(C_{sys} \leq d) P(D_{sys} \geq d|S_a = x) dF_{S_a}(x) \end{aligned} \tag{2.34}$$

where S_a is the random spectral acceleration at the site whose probability distribution (hazard) is usually approximated as [15]

$$P(S_a \geq x) = k_0 x^{-k} \tag{2.35}$$

with empirical factors k_0 and k depending on the site conditions. In this dissertation we assumed that the hazard distribution is known by these or other means and will typically be modeled as a lognormal random variable.

The first part of Equation 2.33, the fragility $P(C_{sys} \leq d)$ is often approximated by the deterministic expression

$$P(C_{sys} \leq d) = F_{C_{sys}}(d) = \Phi[ln(d/m_{C_{sys}})/\beta_{C_{sys}}] \tag{2.36}$$

where $m_{C_{sys}}$ is the median capacity and $\beta_{C_{sys}}$ is the logarithmic standard deviation [28, 93]. This relationship has widely been employed to obtain seismic fragilities for non-ductile reinforced concrete frames [10], building frame systems made out of steel or reinforced concrete [28], precast and prestressed bridge decks [93], highway bridge superstructures [44], nuclear power plants [52] and fire sprinkler systems [98]. The usual practice in these studies is to

determine the median demand measure at a given spectral acceleration S_a (which is random due to earthquake record to record variability) and compare it with empirically defined capacities corresponding to performance levels (example, inter story drift ratio for immediate occupancy or structural damage) to obtain the conditional failure probability given a spectral acceleration. In contrast, the fragilities obtained in this work are expressed directly in terms of demand loads at the ultimate limit state, which gives a probabilistic distribution for system capacity that can be used for system reliability estimation.

The capacity distribution $F_{C_{sys}}$ is to be obtained from a full inelastic system analysis, which is similar to failure mode enumeration discussed in section 2.2.2, however the focus is on capturing these modes within the distribution for C_{sys} from direct non-linear simulations. This is advantageous for system configurations in which some failure modes are dominant which simplifies the system analysis because the improbable modes and their correlations can be excluded.

If all uncertainty sources are modeled for a given structural system the capacity distribution may be obtained by direct Monte Carlo simulation. Every random generation of the system model including appropriate uncertainties in component behavior can be simulated to its limit (convergence loss in the solver or end of analysis), such that the failure load gives a single realization of random system capacity C_{sys}, and by multiple simulations the system capacity histogram can be constructed. It should be noted that 'failure' is intended as a general term here which can correspond to a serviceability (load at which $\Delta \geq \delta_{lim}$, where δ_{lim} is the serviceability deflection limit) or ultimate limit state, as described in section 2.1.3.

In chapter 3 the system reliability problem is solved for a representative redundant system of springs using the direct convolution approach and is verified with previous failure-mode based solutions described in the literature. The system is then designed with a modified component reliability methodology using reliability sensitivities to characterize the load-sharing network. This demonstrates the general research strategy for system reliability-based design for a simple structural system.

Chapter 3

System Reliability-Sensitivity Based Design with Example Application to a Classical Redundant Spring System

This chapter discusses the proposed methodology to derive modified resistance factors that satisfy a pre-defined target system reliability. The objective is to propose an algorithm to solve for target component reliabilities $\beta_{t,i}$ which will satisfy a system reliability goal $\beta_{t,sys}$. The methodology to convert the vector of target reliabilities $\{\beta\}$ to a vector of resistance factors $\{\phi\}$ is the component-based LRFD method described in chapter 2. The focus here is to quantify the relative importance of different components within the load-sharing network using their system reliability sensitivities, and then use that quantification to solve for $\{\beta\}$.

The chapter begins with a general discussion of the proposed methodology, and then applies it to a classical redundant structural network which is extensively used to validate system reliability methods. The system reliability and sensitivities for this network is evaluated using the convolution framework described in section 2.2.3, which is first validated with previous results presented in the literature. Finally, a light framed floor subsystem is cast as a simple parallel system model which is designed first using component-based LRFD and

then with modified component reliability targets generated from their sensitivities to satisfy a pre-defined system reliability.

3.1 Deriving functional relationships between component and system reliability

The information on system load sharing characteristics can provide system reliability estimates from failure mode analysis or system capacity distributions. For an n component system, the system reliability is a general function of the component reliabilities given by

$$\beta_{sys} = B(\beta_1, \beta_2 ... \beta_n) \tag{3.1}$$

The above functional relationship does not hold in general, because the same β_i can be achieved by different combinations of the mean and variance in component capacity $\mu_{C,i}$ and $V_{C,i}$ (see Equation 2.2). However this issue can be circumvented by constraining the component designs, for example, by assuming strength variability $V_{C,i}$ to stay constant because design changes usually cannot affect manufacturing quality control which defines $V_{C,i}$. Moreover, practical constraints in the profession may only allow for certain discrete values of $\mu_{C,i}$ and β_i to be available commercially, for example, a pre-defined set of hot-rolled steel shapes, or a small set of shear wall configurations for use in a cold-formed steel building. Thus although Equation 3.1 appears to define a continuous function that is difficult to define generally, practical constraints reduces the scope of B significantly, effectively making it a map from a finite set of the vector $\{\beta\}$ to a finite range of the scalar β_{sys}.

The function B can be estimated if the system load sharing network is defined. For a series system with independent components, the probability that the system does not fail equals the product of the probabilities that every component survives. The system failure probability is the complement of this event given by

$$P(SystemFailure) = 1 - \prod_{i=1}^{i=n}(1 - P(C_i - D_i < 0)) = 1 - \prod_{i=1}^{i=n}(1 - \Phi(-\beta_i)) \tag{3.2}$$

This can be used in Equation 2.22 to obtain the functional relationship B as

$$\beta_{sys} = -\Phi^{-1}(1 - \prod_{i=1}^{i=n}(1 - \Phi(-\beta_i))) \tag{3.3}$$

If the system load sharing network is such that the functional relationship B cannot be derived analytically, it can be constructed by numerically perturbing the component reliabilities and evaluating the system reliability at each such perturbation. This is demonstrated in this chapter for a parallel system of redundant components with general load deformation relationships.

3.2 Defining component reliability targets and resistance factors using system reliability sensitivity

While structural design codes follow a component reliability based procedure, the end goal is to insure acceptable failure probabilities for the whole system. The target system reliability index $\beta_{t,sys}$ can be connected to system failure consequences, for example, the cost of a building or a bridge being destroyed by an earthquake. This provides a more rational basis to advocate target reliabilities compared to the calibration methodologies used in the original LRFD theory development.

The pathway to make system reliability analyses usable in a structural design office is to inform changes in component reliability targets (and thereby in resistance factors). Therefore in this section the focus is on the relationship between component and system reliability which is quantified by a newly proposed metric called the system reliability sensitivity. The reliability sensitivity is used to solve for component reliability targets $\beta_{t,i}$ that lead to new

component resistance factors calibrated to the system reliability target.

The component reliabilities β_i within a structural system network determines its system reliability β_{sys} as described in Equation 3.1. Design changes influence the component β_i values which in turn impact β_{sys}. Components in a system will generally have different contributions to system reliability within a load-sharing network, and this can be quantified by the reliability sensitivity $S_{\beta,i}$ for component i calculated as $S_{\beta,i} = \partial\beta_{sys}/\partial\beta_i$. For more critical structural components, β_{sys} is expected to change more drastically with β_i, leading to higher $S_{\beta,i}$ whereas the change will be less pronounced for less important components with lower $S_{\beta,i}$.

The component sensitivities $S_{\beta,i}$ can be quantified if information on the load sharing network is available. They can also be obtained from incremental changes e_{β_i} to the component reliability using the following finite difference scheme, holding all other component reliabilities constant

$$S_{\beta,i} = \frac{B(\beta_i + e_{\beta_i}) - B(\beta_i - e_{\beta_i})}{2e_{\beta_i}} \tag{3.4}$$

Using the sensitivities $S_{\beta,i}$ a new set of component reliability targets β_i^* can be recommended to meet the system reliability target $\beta_{t,sys}$ such that

$$\beta_{t,sys} = B(\beta_1^*, \beta_2^* ... \beta_n^*) \tag{3.5}$$

The component reliability modifications $\Delta\beta_i = \beta_i^* - \beta_i$ will be chosen to effect a net system reliability change $\Delta\beta_{sys} = \beta_{t,sys} - \beta_{sys}$ based on the following equation

$$\Delta\beta_{sys} = \sum_{i=1}^{i=n} S_{\beta,i}\Delta\beta_i \tag{3.6}$$

A general approach to solve for the vector of component reliabilities $\{\beta\}$ leading to $\beta_{sys} = \beta_{t,sys}$ can be defined with the following set of steps:

1. Establish a baseline design for all components (including connections) with initial vectors $\{\beta\}$ and $\{S_\beta\}$ using allowable stress design, component-based LRFD or any other design approach.

2. Identify the most critical component m, that is, $S_{\beta,m} = max\{S_\beta\}$.

3. Reset the reliability for component m to $\beta_m^* = \beta_m + (\beta_{t,sys} - \beta_{sys})/S_{\beta,m}$.

4. Remove component m from the set and go back to step 2; repeat until all components have been considered.

5. If $\beta_{sys} = \beta_{t,sys}$ and each β_i is acceptably low (or cannot be lowered further using this methodology) then the solution has converged; use $\{\beta^*\}$ as the vector of component reliability targets.

6. If $\beta_{sys} \neq \beta_{t,sys}$ or if further reductions in some reliability targets are desired, use $\{\beta^*\}$ as the baseline and repeat from step 2.

Within the general methodology proposed above, there might be other considerations to choose $\{\beta\}$, such as preferred component limit states, for example, ductile failure mechanisms or a beam failure preferred to a column limit state in a building, although these will also be automatically captured in the system strength distribution $F_{C_{sys}}$ and the sensitivity $\{S_\beta\}$. Once a final target component reliability set $\{\beta\}$ is obtained, it may be used to propose a new set of component resistance factors using the standard component LRFD format described in chapter 2.

The above algorithm will converge quickly for systems with a small number of components or systems with a weak link (meaning that $\{S_\beta\}$ will be a vector of zeros except for the weak link which will have a high $S_{\beta,i}$). However, for redundant systems with a large number of components and connections having comparable $S_{\beta,i}$, the number of iterations to converge to $\beta_{sys} = \beta_{t,sys}$ is on the order of n, where n is the total number of components and connections in the system. The number of iterations can be reduced by treating groups of related

components together, and changing reliabilities as a group when calculating $\{S_\beta\}$ and β_{sys}. This reduced-order approach is applied to a classical parallel component network in this chapter and to floor diaphragm subsystems in chapter 7. It is also implemented by grouping all components in a building subsystem (shear wall or floor diaphragm) together in chapter 5, which is the first step of the building system reliability loop described in Figure 1.1.

3.3 Demonstration of proposed system reliability design approach with classical parallel component network

In this section the general system reliability sensitivity approach is applied to a classical system (Figure 3.1) which is often used to test and validate system reliability methods [55]. This system was solved exactly by Daniels in 1944 [20] and is commonly referred to in system reliability literature as the Daniels System [55, 97, 99, 51]. The original Daniels system was a bundle of perfectly brittle wires with independent and identically distributed strengths and the applied deterministic load was always equally distributed among the surviving wires [97]. Under these conditions the Daniels system behaves as a perfect parallel system and its solution is provided in section 3.3.1.

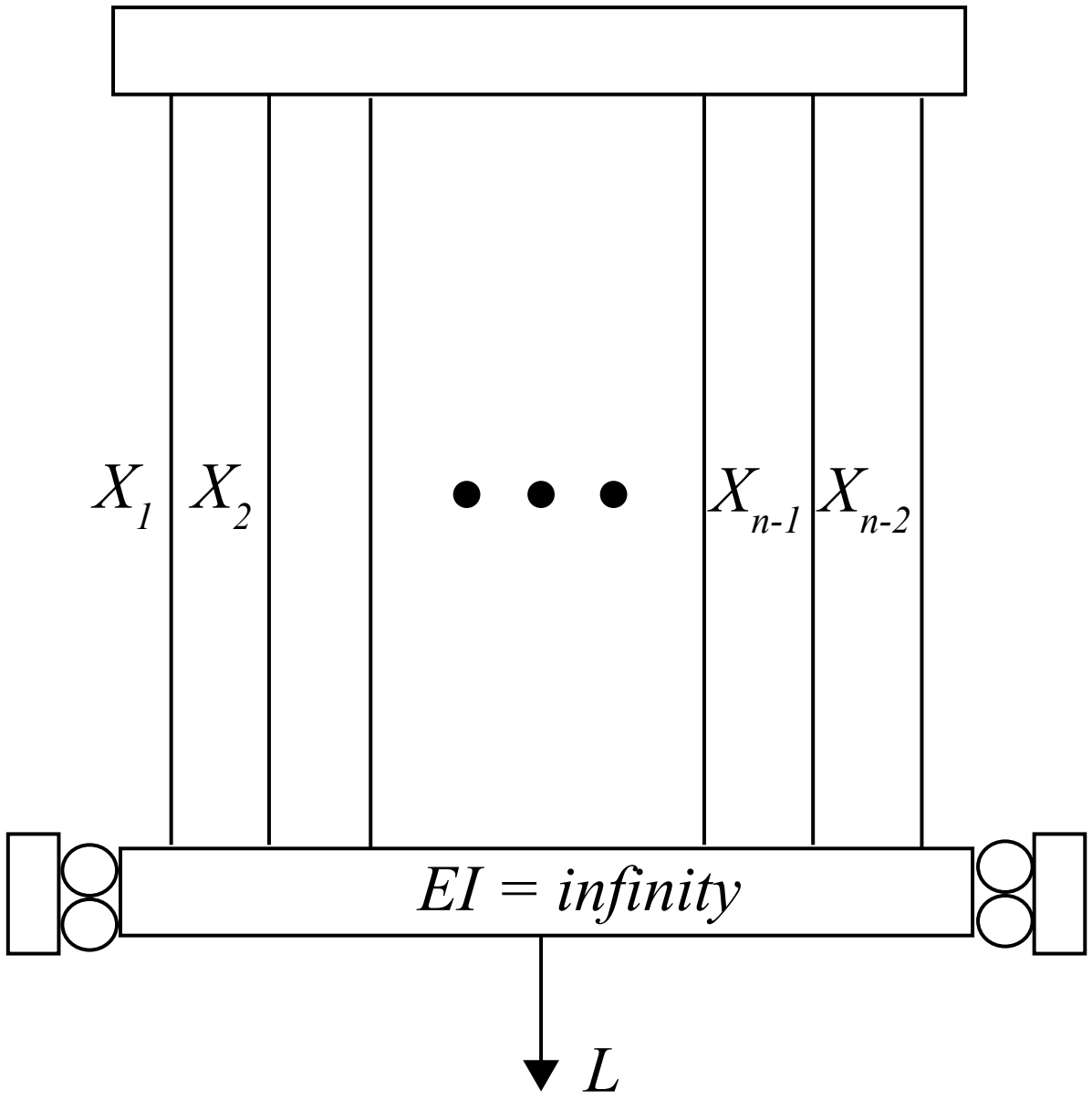

Figure 3.1: Classical Daniels system with perfectly brittle wires distributed in parallel [97]

Several variants of the Daniels system have previously been solved in the system reliability literature. Two member, three member and two tier four member systems were studied in [70], considering ductile and brittle bars. For a two member system with equal stiffnesses and resistances R_1 and R_2 subjected to a system load L, failure regions are shown by shaded

regions in Figure 3.2, with the dotted line indicating brittle and solid line ductile bars.

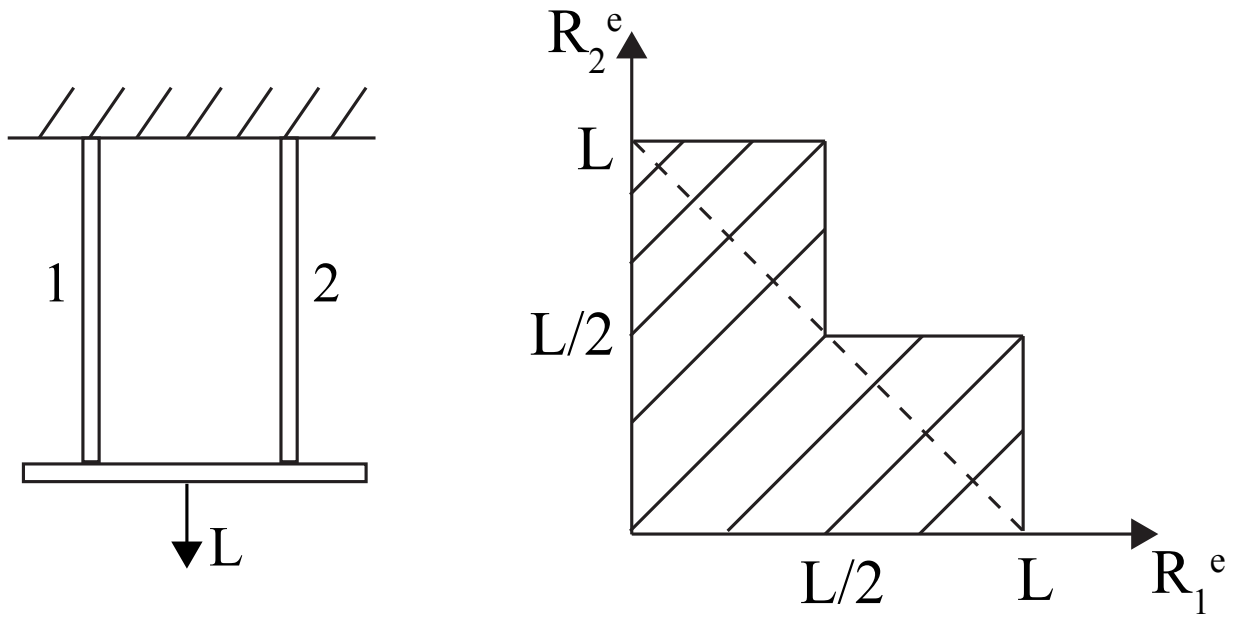

Figure 3.2: Two member Daniels system from [70] showing member resistances for system failure lying within the shaded region with dotted line for brittle bars and solid line for ductile bars

This system was extended in [84] to include semi brittle behavior, and in both cases the solutions were obtained using the incremental loading method by considering sequential component failures. The same methodology was adopted in [42] to study components with general stiffnesses, capacities and residual strengths. Two numerical examples were solved assuming ductile, brittle or semi-brittle components (Figure 3.3) – first a two member system with non-identical components for which the system reliability index was plotted against the system safety factor (defined as the sum of component resistances divided by the total applied load), and secondly a parallel system with identical components for which the variation in system reliability with number of components was obtained for different component behaviors.

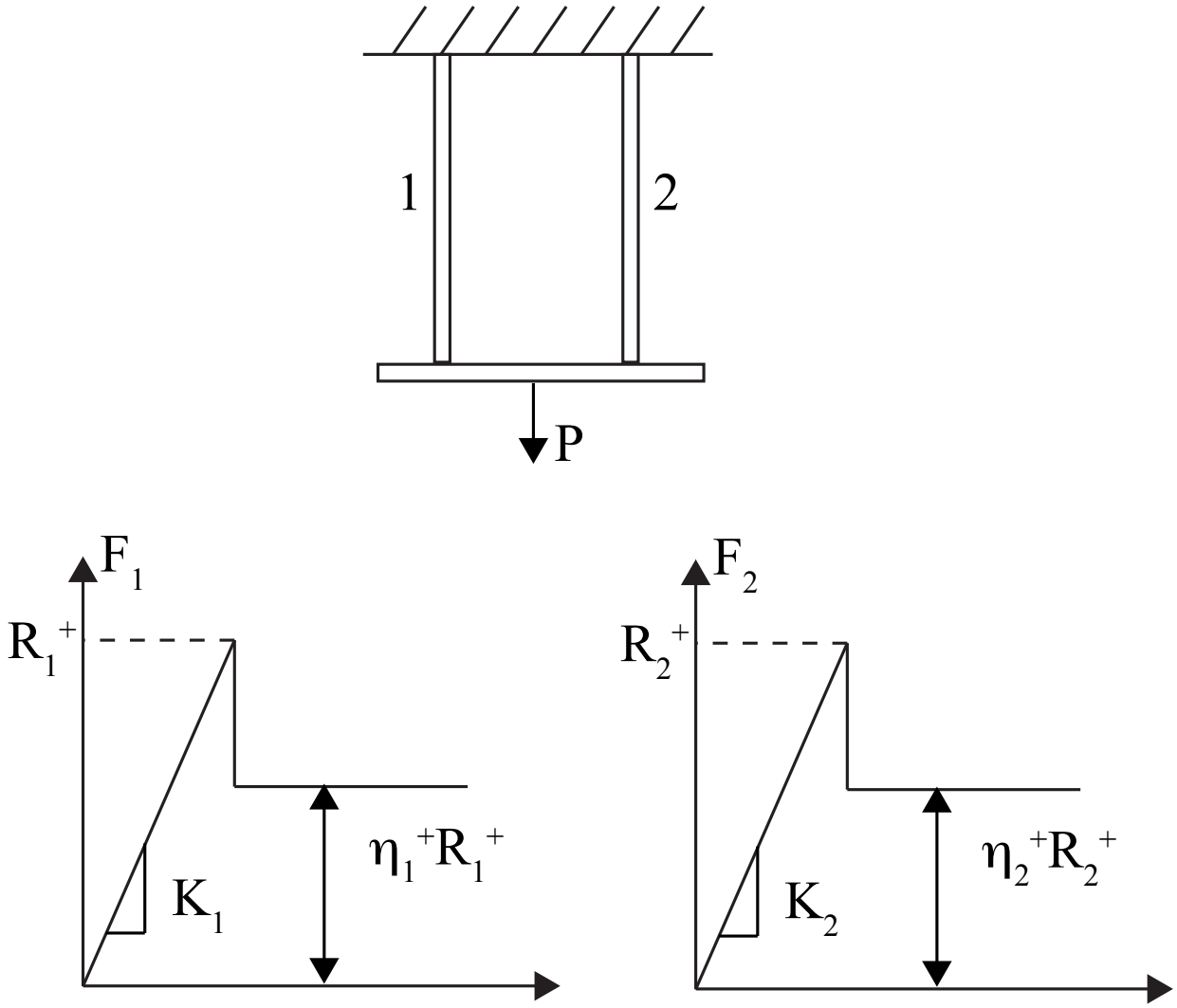

Figure 3.3: Redundant system with general post peak behavior solved in [42]

A two bar system was studied in [62] as a Bayesian network considering series (system fails when any single member fails) and parallel (all members must fail for system to fail) type behavior considering correlations between the resistances R_A and R_B and the applied load W. In the subsequent Bayesian network which was constructed, events A and B represent component failures for each bar, while event C represents system failure (Figure 3.4).

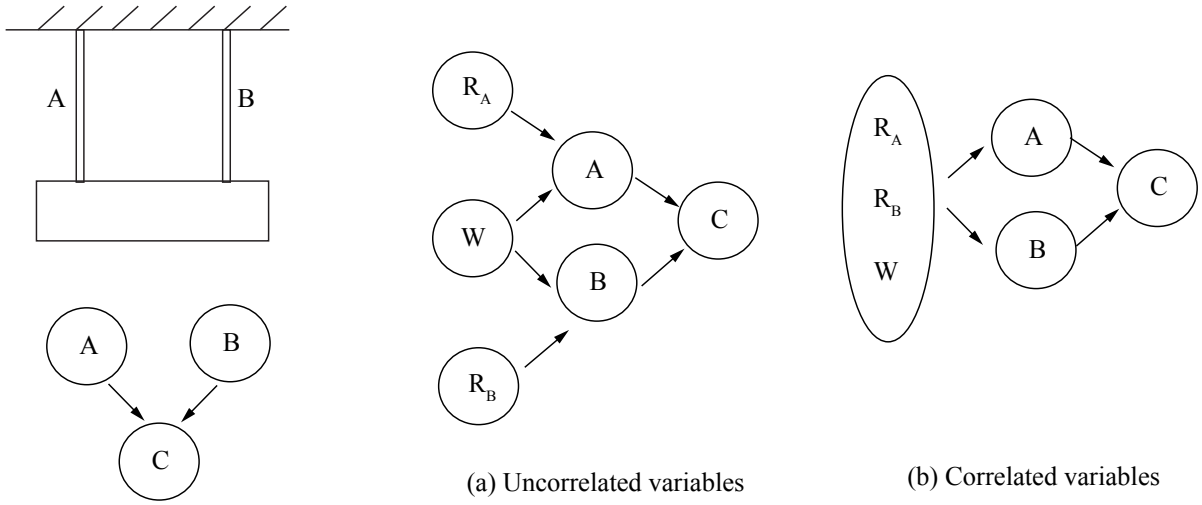

Figure 3.4: Two bar system modeled as a Bayesian network in [62] with component failure events A and B, system failure event C and correlated or uncorrelated random capacities R_A, R_B and random demand W

Similar to the studies conducted in [42], a series parallel system with general force deformation relationships as described in Figure 3.3 was solved using the failure sequence approach in [39] (Figure 3.5 a). The series parallel system was described as a general multi-layered Daniels system in [55] and solved using the branch and bound method, and a similar system was studied using finite element modeling (Figure 3.5 b) for fatigue induced sequential failures assuming perfectly brittle bars [56].

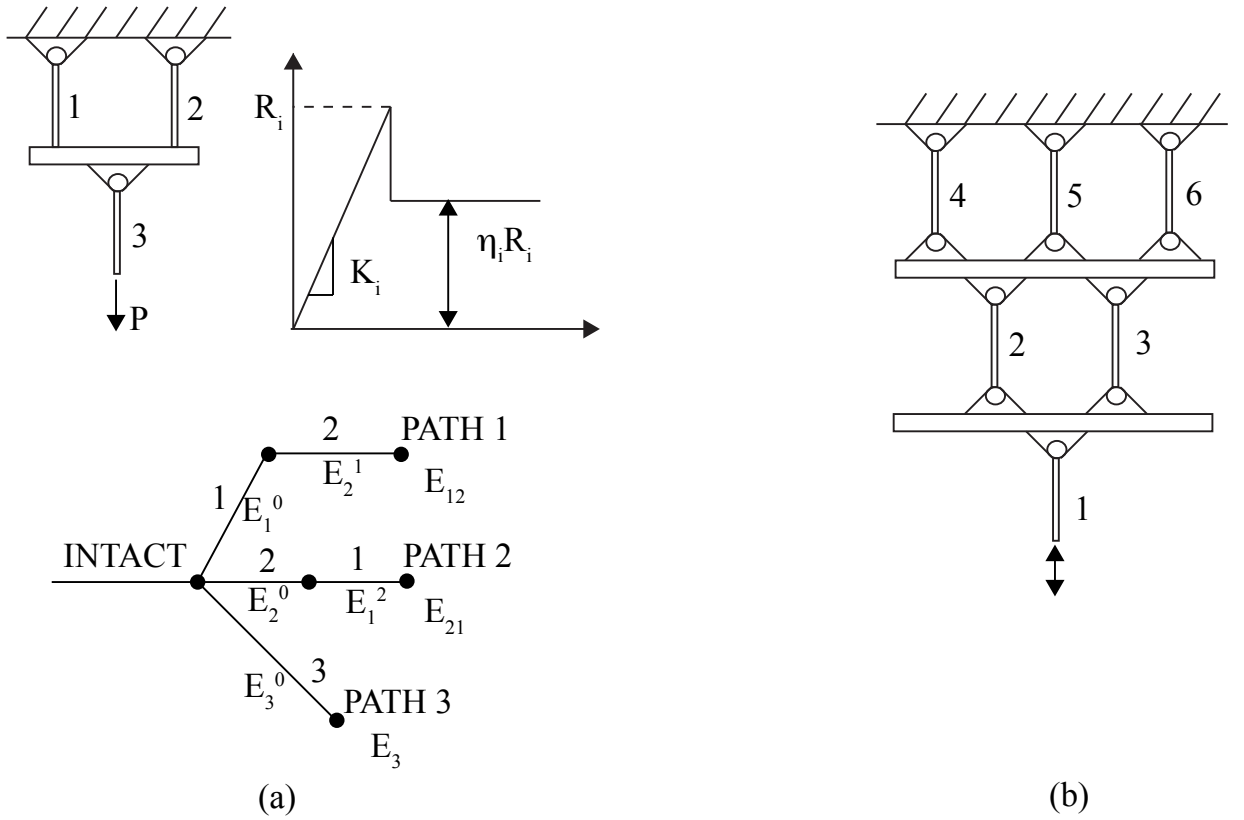

Figure 3.5: General multi-layered Daniel system or series-parallel system solved considering (a) sequential failure with semi-brittle components in [39] and (b) finite element modeling with branch and bound algorithms in [56]

Bounds on system reliability were obtained for series, parallel and general system using linear programming in [97]. The bounds were tested for the parallel scenario by considering a six component Daniels system with strengths distributed as the Weibull random variable by plotting system failure probabilities against applied load. The Daniels system was also used for validation of proposed reliability based acceptance criteria for deteriorating systems in [99].

The Daniels system is solved with the direct convolution methodology outlined in section 2.2.3 and compared to failure mode solutions. The overall system response is predicted using a simple displacement-controlled algorithm which represents a full inelastic system analyses,

simplified here owing to the inherent assumptions in the Daniels system. The system is solved by applying incremental displacements Δ at the loaded edge, and at each analysis step the force in each spring D_i is obtained from its load deformation response and summed to calculate the system force D_{sys} (see Figure 3.6). The analysis is stopped when the net system force reaches zero (all springs have failed). Monte Carlo simulations are performed by including the spring strength COV to construct the system capacity distribution $F_{C_{sys}}$. This is used in conjunction with the demand distribution $F_{D_{sys}}$ to numerically solve the convolution integral given in Equation 2.32 and obtain system reliability estimates. The advantage of using this method is that any general force-deformation relationship for the springs, including ductile, brittle and semi-brittle behaviors previously solved in the literature, can be considered with equal ease. The method can also be extended to solve Daniels systems with general non-linear response which was difficult to consider in classical failure mode analyses for system reliability.

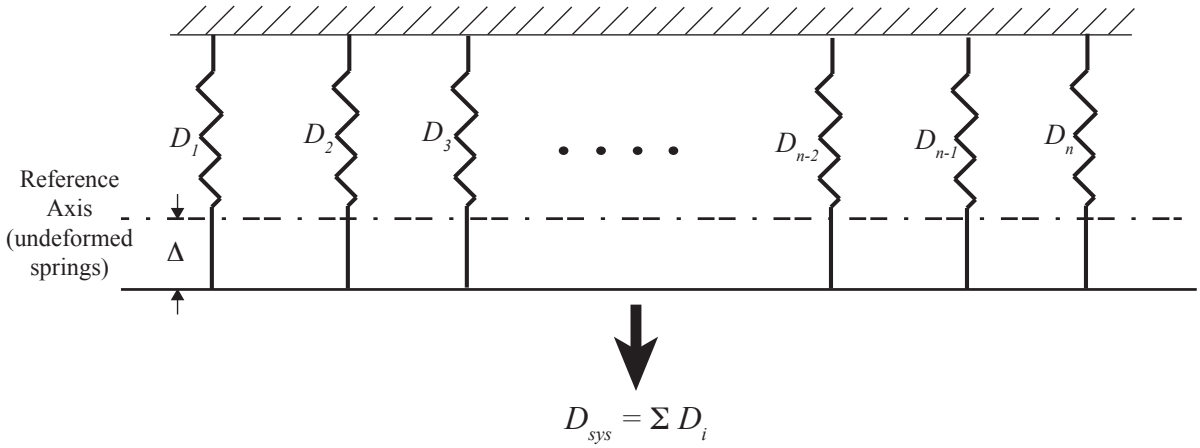

Figure 3.6: Solution algorithm for the Daniels system by applying incremental displacements Δ at the loaded edge, calculating individual spring force D_i and summing to obtain system force D_{sys}

3.3.1 Verifying the direct-convolution system reliability estimate with classical failure-mode solutions

In this section the simulation based system reliability procedure outlined in section 2.2.3 is verified using previous studies provided in the literature.

Example Problem 1 – Six-member Daniels system with brittle components

The first example is a Daniels system with six brittle wires subjected to a load L (Figure 3.1) that was used for verifying system reliability bounds in [97]. The exact solution to this was derived in [20] as a perfect parallel system whose failure event is equivalent to the intersection of all component failure events E_i, and is reproduced here in the form provided in [97]

$$P(SystemFailure) = P(\cap_{i=1}^{i=n} E_i) = (n!)det \begin{bmatrix} b_n & \frac{b_n^2}{2!} & \frac{b_n^3}{3!} & \cdots & \frac{b_n^{n-1}}{(n-1)!} & \frac{b_n^n}{(n)!} \\ 1 & b_{n-1} & \frac{b_{n-1}^2}{2!} & \cdots & \frac{b_{n-1}^{n-2}}{n-2!} & \frac{b_{n-1}^{n-1}}{(n-1)!} \\ 0 & 1 & b_{n-2} & \cdots & \frac{b_{n-2}^{n-3}}{n-3!} & \frac{b_{n-2}^{n-2}}{(n-2)!} \\ \cdots & \cdots & \cdots & \cdots & \cdots & \cdots \\ 0 & 0 & 0 & \cdots & 1 & b_1 \end{bmatrix} \tag{3.7}$$

where $det[.]$ is the determinant of matrix $[.]$, $b_i = F(L/i)$, L being the applied system load and F the cumulative distribution function (CDF) of component capacities. This system was solved in [97] for wire strengths having a Weibull distribution with CDF $F(x) = 1 - e^{-(\frac{x}{\alpha})^\beta}$ where $\alpha = 1.58$ and $\beta = 10$. System reliability bounds were obtained by Linear Programming and compared to the exact solution [20], uni-component bounds [7] and bicomponent bounds [54, 43, 25] described in chapter 2.

The system is solved here using the convolution methodology described in section 2.2.3. Uncertainty is modeled in the component strengths by independent sampling from the Weibull

distribution and 250000 simulations to failure are performed according to the displacement control mechanism given in Figure 3.6 to construct the system capacity CDF $F_{C_{sys}}$. For each applied load value L the system failure probability is computed as $n/250000$, n being the number of C_{sys} values lower than L, and the results are compared to the exact Daniels solution in Figure 3.7. The convolution based estimates are within 10% at very low failure probabilities of 10^{-4} and are overall closer at all applied load values compared to uni-component, bi-component and linear programming upper and lower bounds provided in [97].

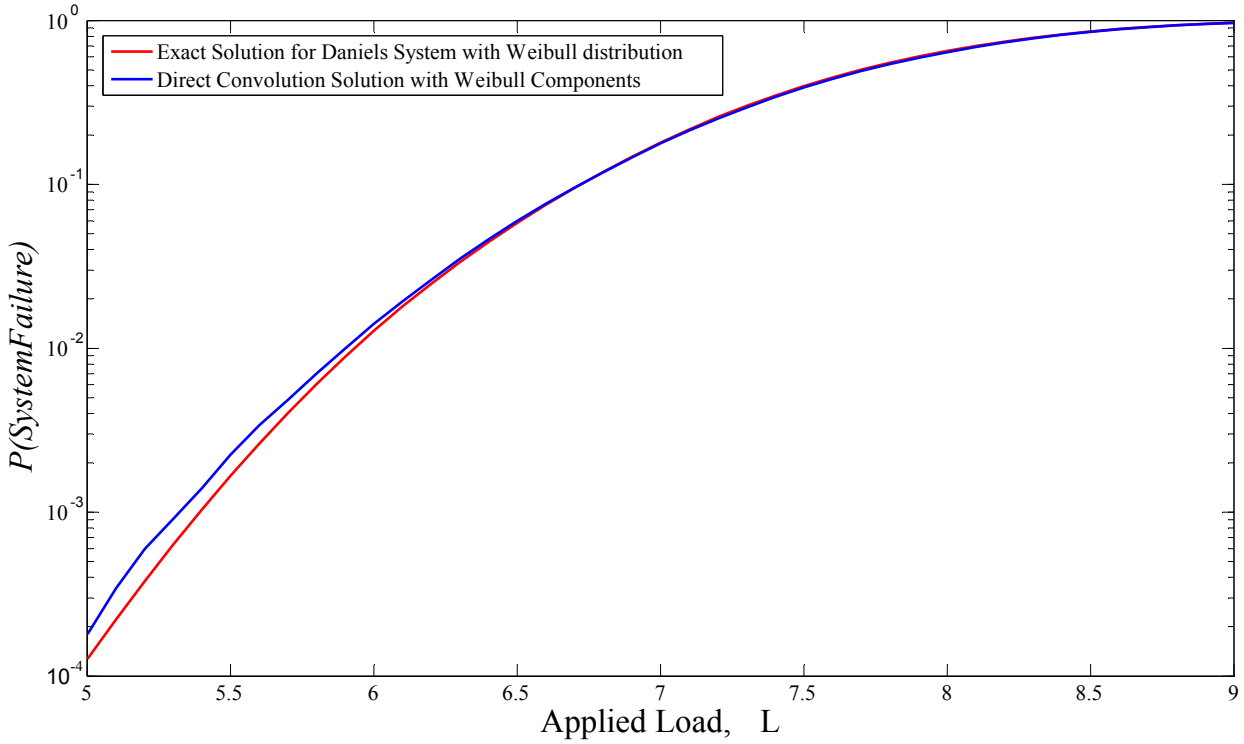

Figure 3.7: Convolution based failure probability estimates obtained for Weibull distributed Daniels system compared to exact Daniels system solution

As described in chapter 2, the system capacity CDF $F_{C_{sys}}$, which describes the structural fragility when system capacity and demand are independent, is often modeled as a lognormal random variable in the literature, and this approach will also be taken in the examples

provided later in this dissertation. The assumption is tested on a Daniels system with wire strength distributions described by the lognormal random variable having mean 1.5 and standard deviation 0.18, which are the statistical parameters for the Weibull wires solved in [97]. The same convolution methodology is used, but this time with only 5000 simulations compared to 250000 used in the previous example. The resultant C_{sys} histogram is fitted to a lognormal distribution with mean and variance as obtained from the simulations. The failure probability equals the lognormal CDF value at the applied system load. This assumes that the fragility $F_{C_{sys}}$ is lognormally distributed and provides system reliability estimates from orders of magnitude lesser simulations compared to direct Monte Carlo analysis. The results are compared to the exact Daniels solution in Figure 3.8 showing the accuracy of modeling the system capacity as lognormal when the components are lognormally distributed.

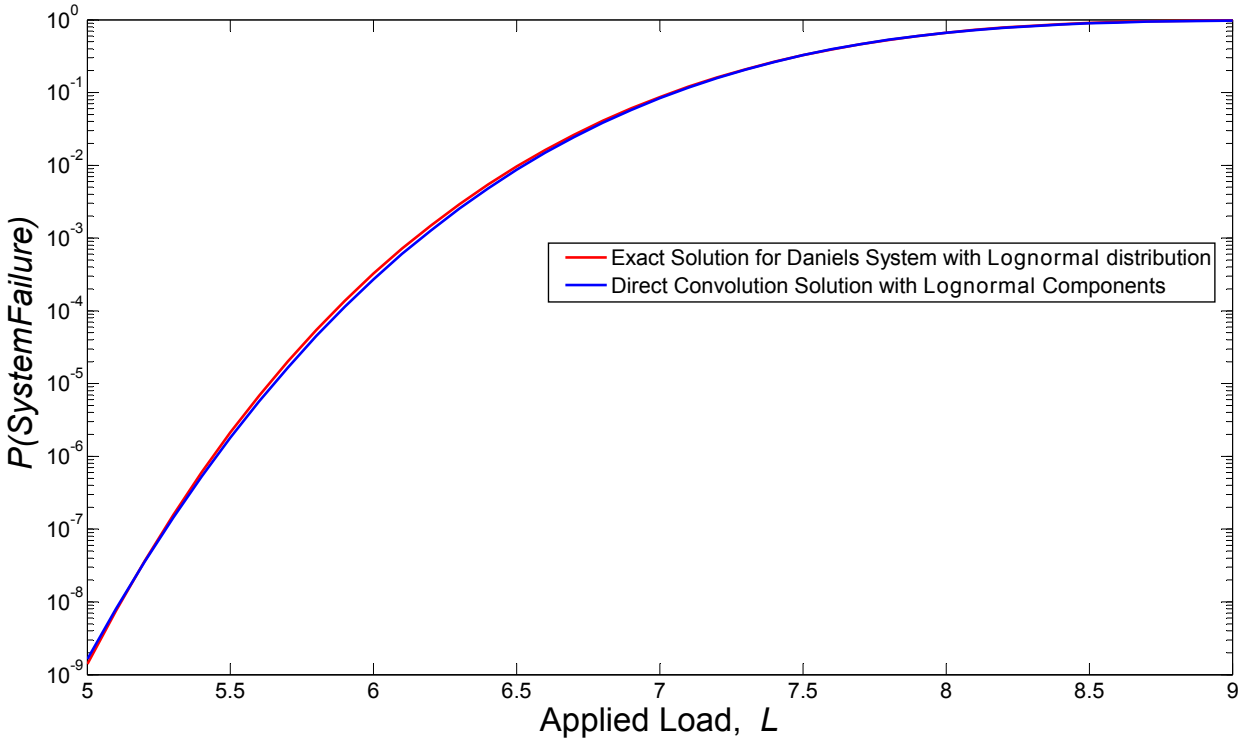

Figure 3.8: Convolution based failure estimates obtained by modeling system capacity as a lognormal random variable compared to exact Daniels system solution

Example Problem 2 – Daniels systems with ductile, brittle or semi-brittle components

The second example is a Daniels system having one to four components with semi-brittle behaviors [42]. The post failure strength factor η denotes perfectly ductile components when $\eta = 1$, perfectly brittle components when $\eta = 0$, and semi-brittle components for intermediate values (see Figure 3.3).

The system was solved in [42] by obtaining the union of cut-set events (Equation 2.23) from Monte-Carlo simulations, with sample sizes ranging from $5X10^5 - 5X10^8$. For a 4 member system, the failure probability is provided as the union of all possible cut-sets in Equation 3.8 [42].

$$\begin{aligned} P(SystemFailure) = P[&E_1^0E_2^1E_3^{12}E_4^{123} \cup E_1^0E_2^1E_4^{12}E_3^{124} \cup E_1^0E_3^1E_2^{13}E_4^{132} \cup E_1^0E_3^1E_4^{13}E_2^{134} \\ &\cup E_1^0E_4^1E_2^{14}E_3^{142} \cup E_1^0E_4^1E_3^{14}E_2^{143} \cup E_2^0E_1^2E_3^{21}E_4^{213} \cup E_2^0E_1^2E_4^{21}E_3^{214} \\ &\cup E_2^0E_3^2E_1^{23}E_4^{231} \cup E_2^0E_3^2E_4^{23}E_1^{234} \cup E_2^0E_4^2E_1^{24}E_3^{241} \cup E_2^0E_4^2E_3^{24}E_1^{243} \\ &\cup E_3^0E_1^3E_2^{31}E_4^{312} \cup E_3^0E_1^3E_4^{31}E_2^{314} \cup E_3^0E_2^3E_1^{32}E_4^{321} \cup E_3^0E_2^3E_4^{32}E_1^{324} \\ &\cup E_3^0E_4^3E_1^{34}E_2^{341} \cup E_3^0E_4^3E_2^{34}E_1^{342} \cup E_4^0E_1^4E_2^{41}E_3^{412} \cup E_4^0E_1^4E_3^{41}E_2^{413} \\ &\cup E_4^0E_2^4E_1^{34}E_3^{421} \cup E_4^0E_2^4E_3^{42}E_1^{423} \cup E_4^0E_3^4E_1^{43}E_2^{431} \cup E_4^0E_3^4E_2^{43}E_1^{432}] \end{aligned} \tag{3.8}$$

where E_i^{jkl} denotes the event that member i fails given that members j, k, l have failed.

The specific problem considered here consists of 1 to 4 member systems with $\eta = 0, 0.5, 1$ (i.e., brittle, semi-brittle and ductile), normally distributed, nominally identical and uncorrelated component resistances and deterministic system load. The system safety factor, described as the sum of the mean component resistances divided by the system load ($\sum \mu_{C_i}/\mu_{D_{sys}}$) is 1.5, and the component coefficient of variation is 10%.

The system was solved using the convolution methodology with component strengths inde-

pendently sampled from the Normal distribution with $1X10^5$ Monte Carlo simulations. The reliability index was computed as $\phi^{-1}(n/250000)$, n being the number of C_{sys} values lower than $\mu_{D_{sys}}$. The results are compared to the failure mode analysis solutions given in [42] (Figure 3.9).

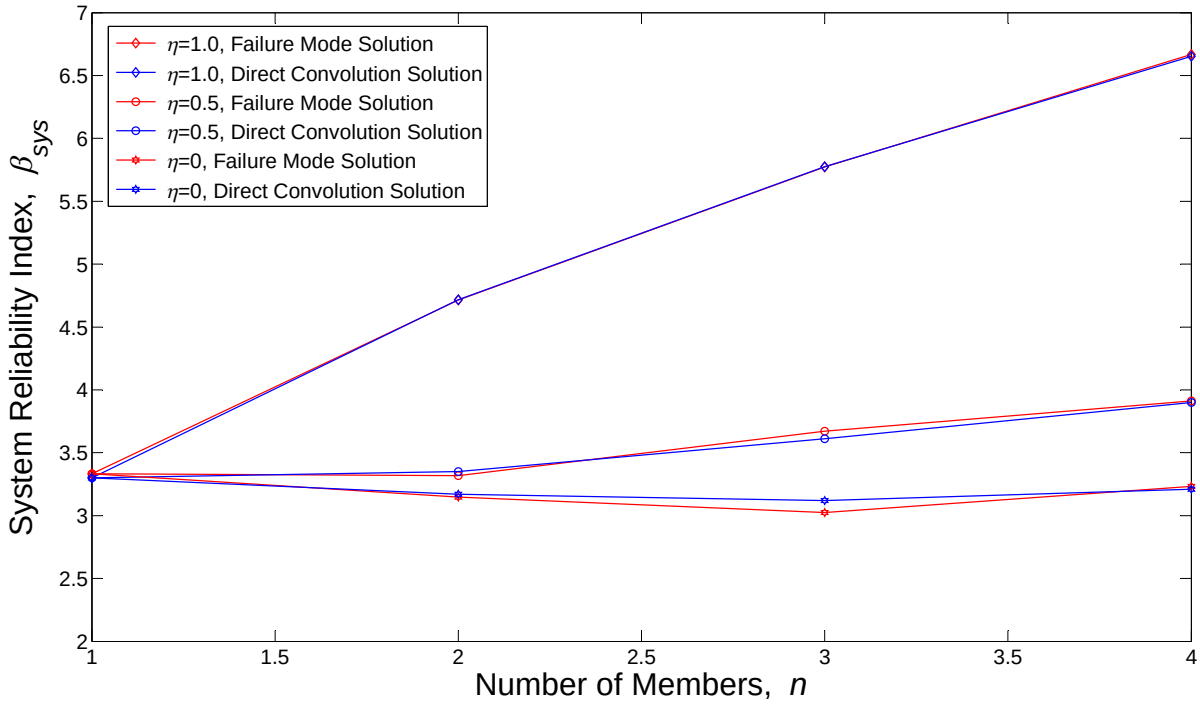

Figure 3.9: Variation in system reliability index with number of components for ductile, brittle, and semi-brittle behavior providing comparisons between convolution based results and failure mode analysis results provided in [42]

This example shows the accuracy of the proposed methodology for ductile and semi-ductile systems in addition to the brittle system verifications provided in section 3.3.1.

3.3.2 Example redundant spring system designed with LRFD

In this work we use the Daniels system to establish the general simulation based system reliability and sensitivity methodology. The system is first designed by a component based reliability approach, following which its system reliability and component to system reliability map B is established, which are then used to recommend modified component reliability targets and resistance factors. Since a direct simulation approach is used, the components are not restricted to have perfect ductile, brittle or semi-brittle behaviors. The parallel spring system can thus represent a variety of structural networks – for example, a bridge girder system under dead loads or a portal frame network under ground motions, within the bounds of a highly simplifying assumption that there is uniform load sharing among the components proportional to their stiffnesses. The rigid link connecting the springs stays rigid throughout the analysis, whereas in a real system the link will be expected to disintegrate after failure initiation leading to varying demands among the components which will cause load redistribution. The simplified model is being studied only to highlight system reliability effects in an example parallel-spring network which is comparable to other studies conducted in the literature and to demonstrate the simulation based reliability methodologies being developed in the research.

The present example represents a set of screw fastener connections comprising the load path between the lateral force resisting system (LFRS) to the floor diaphragm in a cold-formed steel building. As detailed in chapter 6, prototype floor diaphragms connect to the lateral system through hundreds of fastener elements that we model here using the highly simplified Daniels system. It is stressed that the goal is not to use this model to inform actual changes in design but simply to demonstrate the simulation based methodology using a network that is simple enough to think through and analyze, and can be verified against past research. In chapter 6, the actual floor diaphragm system is studied using high fidelity finite element models that include all components in the network without using any of the simplifying assumptions considered here.

The system is designed for the ASCE 7-10 seismic load combination $1.2D_n + L_n + 0.2S_n + E_n$. According to standard design practice, the lateral load effect on the diaphragm system arises only from the seismic load case E_n which implies that $D_{n,i,j}$ in Equation 2.13 is zero for all j load cases except seismic, and γ_j is 1.0. The nominal demand recommended by ASCE 7-10 Equation 12.8-11 for this system is 37.2 kN as derived in section 5.6.2, whereas the mean calculated demand on the diaphragm subjected to the design basis earthquake (10% probability of occurence in 50 years), obtained from non-linear dynamic simulations described in chapter 4 is 114 kN. If the mean load is then assumed to be 114 kN, with a nominal load of 37.2 kN, the bias factor is 3. Note that although the analysis is simplified here because the seismic load combination results in load effects from only a single load case, the general framework would be the same for any other load combination and could be applied using Equation 2.13.

The material factor M_m for screw connections in shear is 1.1 and the fabrication $F_m = 1.0$, as described in AISI S100 - chapter F. The professional factor P_m represents the mean test to predicted strength is the yield strength of 2 kN. Currently, prediction equations are not available for the connections considered here (wood sheathing to steel screw-fasteners), so it is assumed that the predicted strength equals the yield strength of 2.0 kN (Figure 3.10), whereas the tested ultimate strength is 3.9 kN, such that $P_m = 3.9/2.0 = 1.95$. The component strength variability is given as $V_{C_i}^2 = V_M^2 + V_F^2 + C_P V_P^2$, where $V_M = 0.1$, $V_F = 0.1$, C_P for twelve tests is 1.3, and $V_P = 0.17$ obtained from conducting twelve nominally identical experiments, as per AISI S100-12 recommendations [2] derived from [58], resulting in $V_{C_i} = 0.24$. The coefficient of variation for the seismic load case $V_{D_i} = 0.38$ as derived in [104].

If we assume that the design engineer proposes a set of nominally identical fasteners in the final design for constructability ease, Equation 2.13 can now be used to recommend component resistance factor ϕ_i for LRFD design guidelines if the target component reliability $\beta_{t,i}$ is given. As discussed in section 2.1.1, the LRFD target component reliabilities were derived from implied reliabilities in design codes that did not have a probabilistic basis, and were

typically 2.5 for members and 3.5 for connections. A component reliability procedure with $\beta_{t,i} = 2.5$ would then recommend a uniform resistance factor 0.21 for the spring set considered in this example. The extremely small value for ϕ_i results from the high seismic load bias (3.0) which results from the severe under-prediction of code recommended diaphragm nominal demand, as well as the seismic COV of 0.38 used here compared to the LRFD load effect COV of 0.21 [58]

The system can now be designed using the resistance factor $\phi_i = 0.17$ derived above. The nominal system demand $D_{n,sys}$ is 37.2 kN and the predicted nominal component capacity $\mu_{C_i} = 3.9kN$, which was observed in fastener experiments conducted at Virginia Tech for the connection configuration comprising the critical diaphragm load path (chapter 6). For a system with n fasteners the nominal component demand is $37.2/n$, and using this in Equation 2.11 gives $n = 89$ fasteners required.

Note that the design recommendation is completely silent on the nature of the load sharing network and implicitly assumes uniform load sharing between all components. The system strength, and therefore the system reliability, will vary greatly depending on the ductility and the randomness in component strengths, as demonstrated in the following section.

3.3.3 Redundant spring system structural response calculation including load-sharing

The sytem designed in section 3.3.2 is analyzed with the displacement controlled algorithm described in section 3.3.1. The force deformation response for each fastener (Figure 3.10) is obtained from quadrilinear backbones constructed from individual fastener experiments conducted at Virginia Tech and described later in this dissertation. The peak backbone force equals the component capacity μ_{C_i} used in section 2.1.1 for component reliability based design. This general backbone would be difficult to consider using classical approaches (section 2.2.2) but the convolution methodology (section 2.2.3) is easily applicable to this

case.

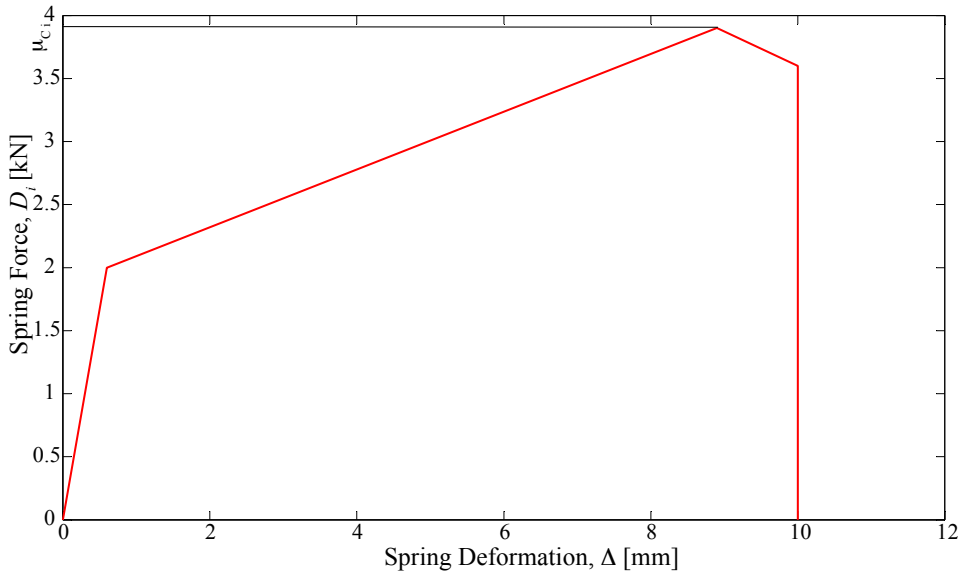

.

Figure 3.10: Force deformation relationships for each spring in redundant system, matching experimentally obtained fastener backbones for diaphragm subsystem components studied in chapter 6

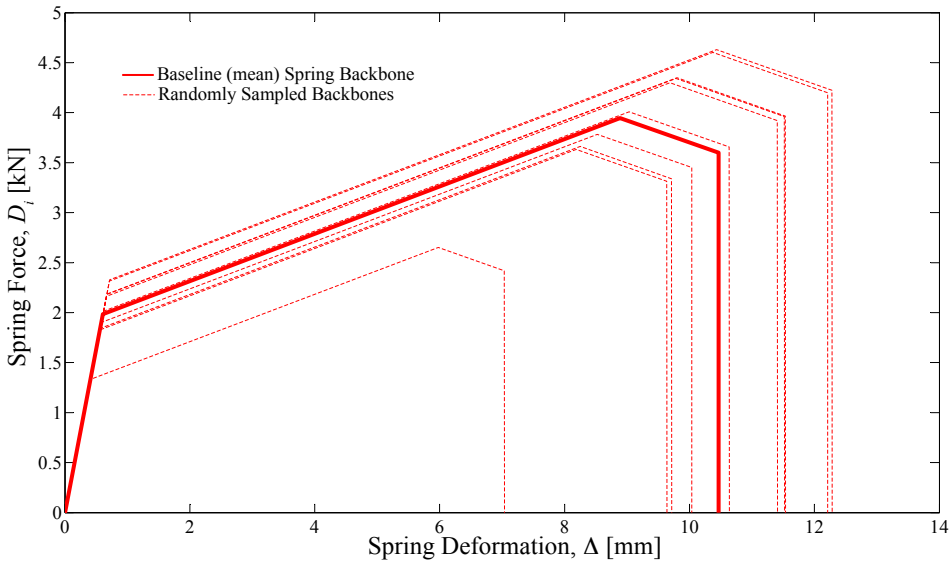

Figure 3.11: Randomly sampled spring backbones (dotted lines) obtained by independently sampling peak capacity from a lognormal distribution and keeping all secant stiffnesses constant, with the baseline or mean backbone shown in bold

The components have variable strengths characterized by their COV which affects system response. We study this by randomly sampling component peak strengths from a lognormal distribution with mean μ_{C_i} and COV V_{C_i}. The random backbones are obtained by independently sampling only the peak capacity and keeping the secant stiffnesses constant. The randomness modeling protocol is motivated from experimentally obtained force deformation relationships described in chapter 6. An example set of 10 such backbones are shown as dotted lines in Figure 3.11.

The system force deformation response for a single Monte-Carlo realization is plotted in Figure 3.12 and compared to the system load deformation response obtained when uncertainty is not modeled in the components (deterministic case). The system strength drops compared to the deterministic case because failure is triggered by the weakest link among the components.

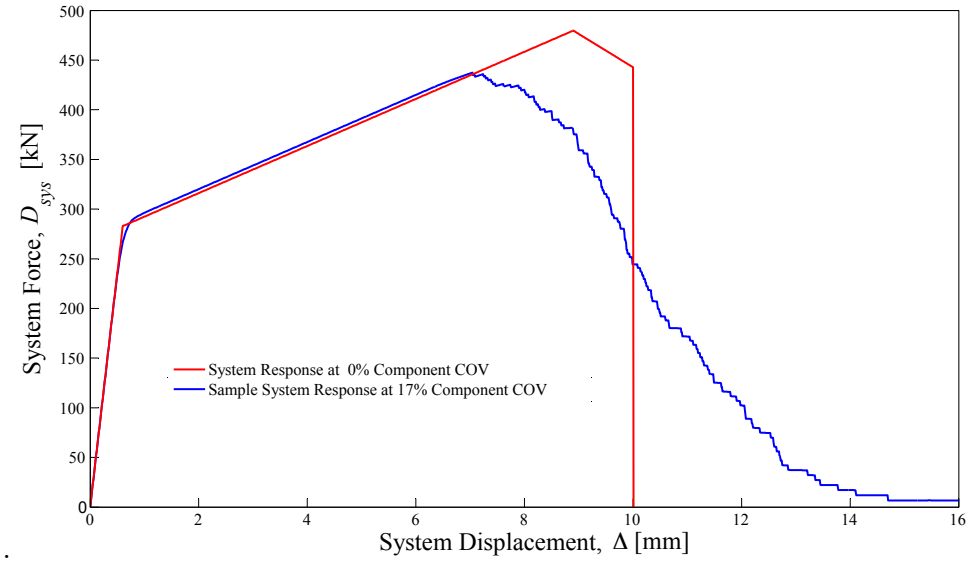

Figure 3.12: Sample system force deformation behavior when randomness in spring capacity is set to 17% (shown in blue), showing onset of system collapse caused by the weakest link causing a drop in system capacity compared to the 0 COV case (red)

The 123-spring set designed in section 3.3.2 satisfies component based LRFD guidelines. The design approach was based on a second moment procedure because it utilized only the mean and standard deviation of capacities and applied loads. No information was required on the actual component load deformation characteristics, for example, response non-linearity or ductility. We now consider two classical examples of component force deformation behavior – elastic perfectly plastic (EPP) and elastic brittle (EB) – and their effects on system load redistribution. Results from a single random simulation are plotted in Figure 3.13. For the elastic perfectly plastic system, once the weakest component reaches its capacity its load does not drop to zero, resulting in perfect load redistribution which allows the system to reach its full capacity $n\mu_{C_i}$. The elastic brittle system is characterized by essentially zero load redistribution which makes it behave as a weakest link network with no alternate load paths. These two idealizations form the upper and lower bounds to real structural response. The LRFD design method does not explicitly distinguish between these sytems on the basis of individual component behavior.

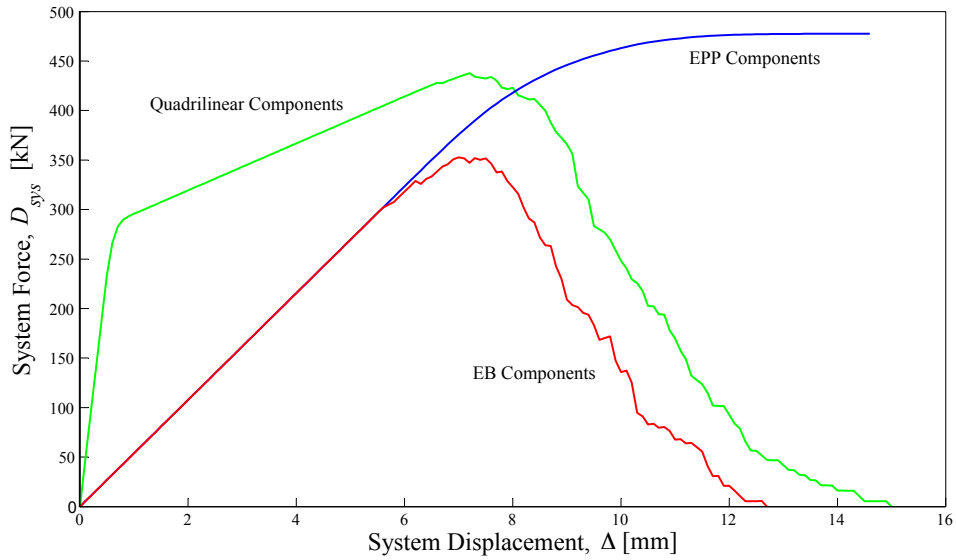

Figure 3.13: Sample system force deformation behavior for three different component models – elastic perfectly plastic, elastic brittle and quadrilinear, with randomness in spring capacity is set to 17%, showing differing load sharing behaviors leading to varying system capacities

The change in normalized mean system capacity $\frac{\mu_{C_{sys}}}{n\mu_{C_i}}$ with change in component COV V_{C_i} is plotted in Figure 3.14. At zero component variability, the EPP, EB and experimentally characterized components produce identical system capacities because the weakest link has the same strength as every other member in the system. With increasing variability the differences in system response become more pronounced as the weakest link gets weaker, resulting in lower mean capacities for the elastic brittle and quadrilinear component systems.

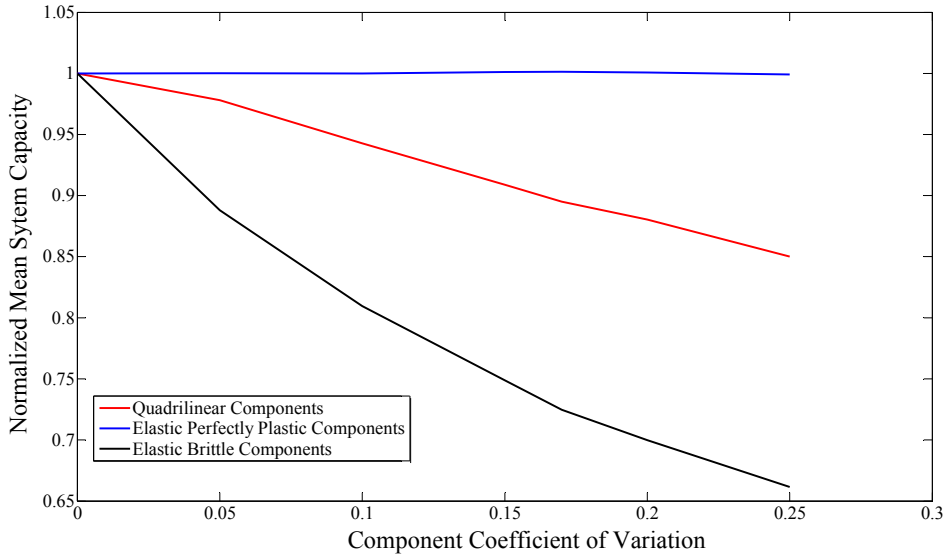

Figure 3.14: Variation in normalized mean capacity with component COV, obtained from 200 Monte Carlo runs for each system at each COV level, showing the reduction in capacity with increasing variability for EB and quadrilinear components

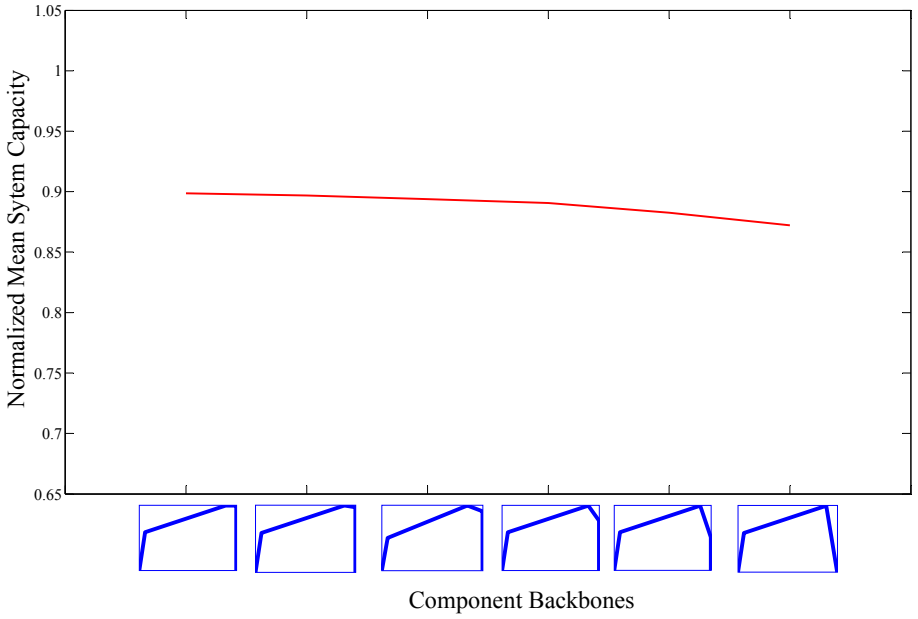

Figure 3.15: Variation in normalized mean capacity from 200 Monte Carlo runs with changes in the fastener backbone indicating that as the softening branch becomes increasingly stiff load redistribution becomes worse leading to decreasing system capacities

The variation in normalized mean system capacity $\frac{\mu_{C_{sys}}}{n\mu_{C_i}}$ with varying softening stiffnesses ($-\infty$ for EB and 0 for EPP) is plotted for component COV = 17% (Figure 3.15). As the softening branch in the component force deformation response becomes increasingly brittle, load redistribution gets weaker leading to lower system capacities.

The above results indicate that even in a simple system of identical members system response is affected strongly by member force-deformation characteristics which govern load redistribution after failure initiation. A component based LRFD procedure does not account for these effects and gives the same final design irrespective of member ductility, although a system level analysis reveals strong differences.

In a real structural network comprising interconnected members the components will not be identical and load sharing effects will dominate. This effect can be studied by including non-identical members into the system network.

3.3.4 Modified resistance factors for the redundant spring system considering system reliability sensitivity

The system reliability for the fastener network designed in section 3.3.2 can be obtained from the convolution methodology from section 2.2.3. The system capacity histogram is generated from 500 Monte Carlo simulations (Figure 3.16). Although this can directly be used to estimate the fragility $F_{C_{sys}}$ in Equation 2.33, it is approximated as a lognormal random variable with mean $\mu_{C_{sys}}$ and COV $V_{C_{sys}}$ estimated from simulations as discussed in section 3.3.1.

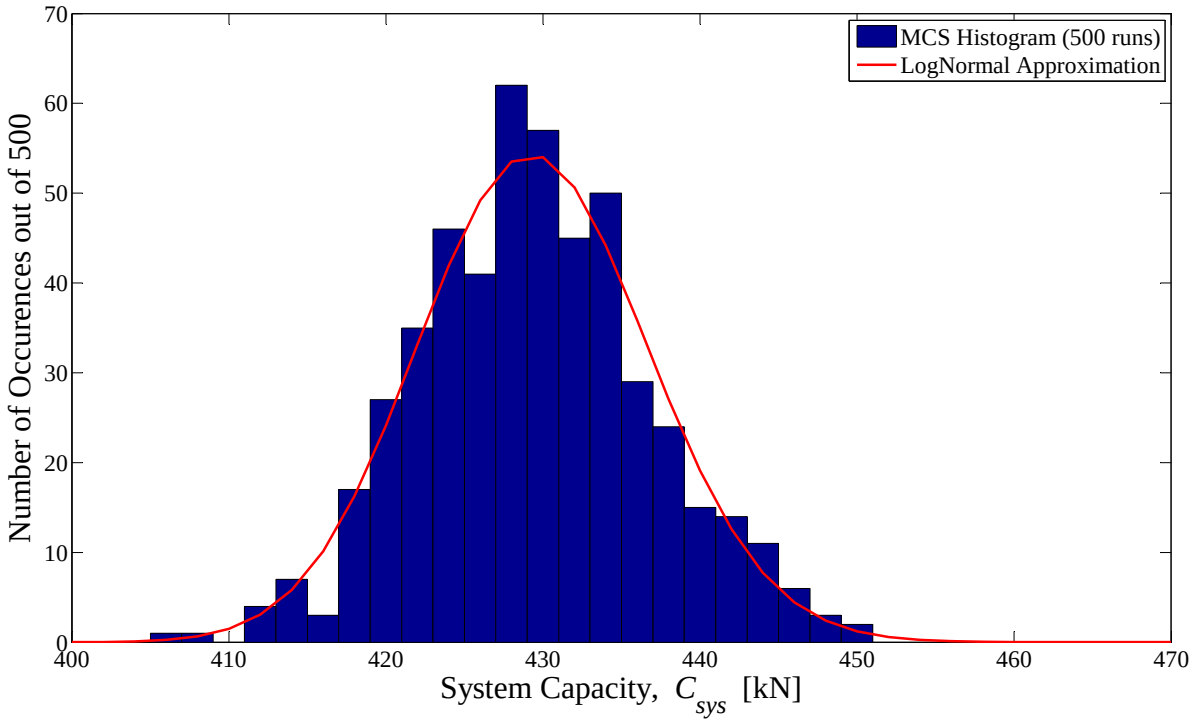

Figure 3.16: Histogram of system capacities obtained from 500 Monte Carlo simulations for the Daniels System of screw-fastened connections along with approximate lognormal probability density

The system reliability can now be obtained by using the distribution provided in Figure 3.16 in Equation 2.33. This is done by numerically evaluating the integral within limits 0 to 2000 kN at load step 1 kN. The demand distribution D_{sys} is assumed as a lognormal random variable with mean $\mu_{D_{sys}} = 114kN$ and COV $V_{C_{sys}} = 0.38$, as justified in chapter 4. The lognormal assumption is non-critical to the proposed methodology which will work just as well for other hazard distributions. The numerical convolution framework then provides a system reliability estimate of 2.7. By contrast, the minimum component reliability (in this case uniform across the nominally identical component network) is 2.5, which points to a beneficial system effect even in a system configuration characterized by unzipping or catastrophic failures.

Having obtained estimates for system reliability, the next step is to map the functional relationship B between system and component reliability, as discussed in section 3.1. For the simplified structural system considered here, all components are nominally identical and therefore the change in β_{sys} with β_i is uniform across all components. This is studied here for the three fastener definitions (elastic perfectly plastic, elastic brittle and quadri-linear) considered in section 3.3.3.

Based on the component reliability expression (Equation 2.5), β_i changes with the component capacity mean and COV μ_{C_i} and V_{C_i} as well as component demand $\mu_{D_i} = D_{sys}/n$ where n is the number of components. From a structural designer's viewpoint, if the design code were to require a higher component reliability, either μ_{C_i} or n would have to be increased as the variability V_{C_i} depends on manufacturing practices across different industries and is therefore more difficult to control. In the present case the number of components n is varied from 50 to 130 in increments of 20. Note that the baseline case for $\beta_{t,i} = 2.5$ was $n = 89$, and the limits considered here correspond to $\beta_i = 1.4$ and $\beta_i = 3.4$.

Variation in β_{sys} with β_i is plotted for EPP, Quadrilinear and EB components in Figure 3.17. This establishes the component to system reliability map B. The relationship is linear for this simple system but will be more complex in real structural networks having mixed

series/parallel combinations. For each value of n, the component reliability is calculated using the procedure outlined in chapter 2, and system reliability is evaluated using the convolution framework described in section 2.2.3. System reliability is lower than component reliability for elastic brittle components, and slightly higher for quadrilinear components. Benefits from load sharing become palpable for elastic perfectly plastic components with β_{sys} being significantly larger than β_i

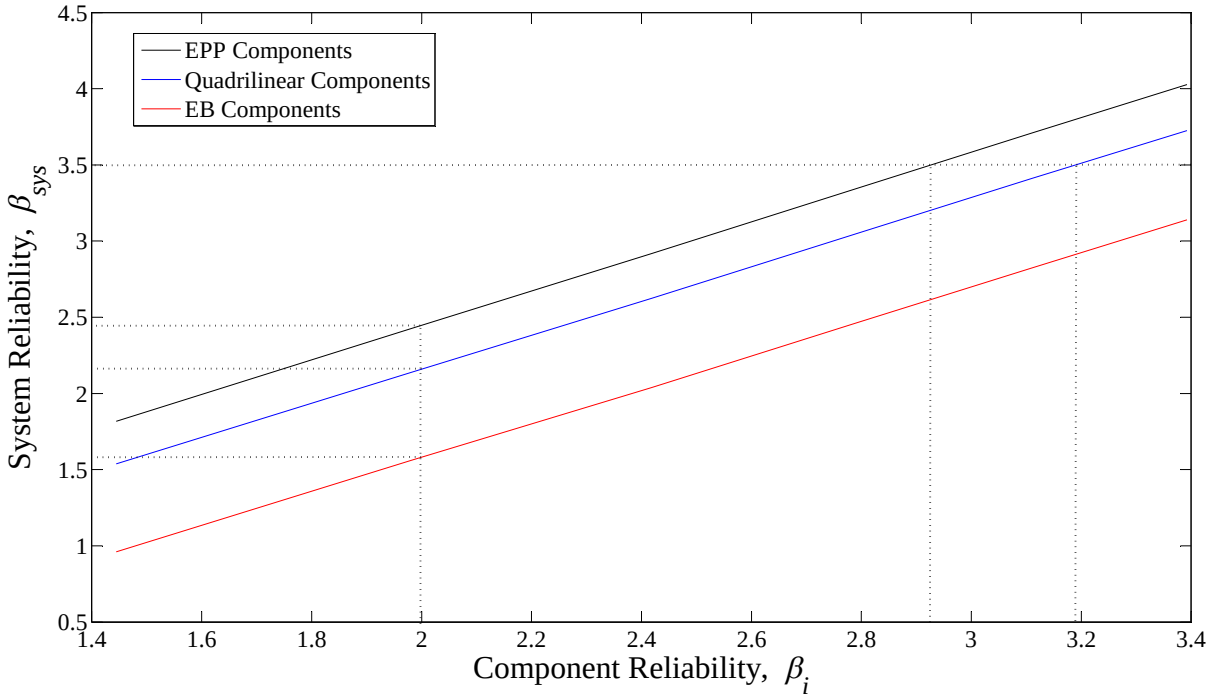

Figure 3.17: Variation in system reliability with component reliability for EPP, EB and Quadrilinear components

The linearity in the relationship between system and component reliability results from the structural topology, i.e. a set of springs in parallel, for which the mean system capacity $\mu_{C_{sys}} = gn\mu_{C_i}$, where $g \leq 1$ is the 'group effect' factor that reduces the overall system capacity based on the ductility in individual components ($g = 1$ for EPP). Assuming

that $\beta_{sys} = \frac{log_n \frac{\mu_{Csys}}{\mu_{Dsys}}}{\sqrt{V_{Csys}^2 + V_{Dsys}^2}}$, which is the lognormal assumption widely used in LRFD specifications, $V_{Csys}^2 = 1/\sqrt{n} V_{Ci}^2$, since the n fastener components are independent, such that $\beta_{sys} = \frac{log_n g + \beta_i \sqrt{V_{Ci}^2 + V_{Di}^2}}{\sqrt{1/\sqrt{n} V_{Ci}^2 + V_{Di}^2}}$, which represents a linear equation with respect to β_i.

For the system of identical components described here, the reliability sensitivity $S_{\beta,i}$ may be calculated from the β_{sys} versus β_i plots (Figure 3.17) and equals 1.1 for EPP components, EB components and quadrilinear components. The sensitivity can then be used to modify the component LRFD resistance factors obtained in section 3.3.2 using the procedure outlined in section 3.2.

Assume that the system reliability target is $\beta_{t,sys} = 3.5$, such that $\Delta\beta_{sys}$ is 0.5 for the EPP network, 0.8 for the quadrilinear network and 1.4 for the EB network. Equation 3.6 can now be used to recommend component reliability modifications $\Delta\beta_i$ for each network, which equals 0.5 for EP, 0.8 for quadrilinear and 1.3 for EB, giving new target reliabilities 3.0 for EP, 3.3 for quadrilinear and 3.8 for EB.These values can be applied to Equation 2.13 to recommend new ϕ factors 0.17 for EP, 0.15 for quadrilinear and 0.12 for EB. The higher value of ϕ_i for the EPP components rewards the system for its improved load sharing behavior, whereas it is lower for EB and quadrilinear components due to poor load sharing and unzipping system failures.

For the simplified system of identical components considered in this chapter, the system reliability methodology provides new, uniform resistance factors for all components in the system. Load sharing effects demonstrated in section 3.3.3, which were not accounted for in a component based LRFD procedure, were captured here by providing higher $\beta_{t,i}$ and lower ϕ_i for the quadrilinear components compared to EPP, which was implicitly assumed during standard component based design. In real structural systems comprising thousands of members with varying component reliabilities, the same procedure should provide spatially varying $\beta_{t,i}$ from one component to the next. The system reliability sensitivity methodology introduced here is used to complete the design loop given in Figure 1.1 in the following chapters.

Chapter 4

Defining the System-to-Subsystem Load-Sharing Network for Cold-Formed Steel Framed Buildings

4.1 Introduction to cold-formed steel building systems

In the previous chapters system reliability and sensitivity informed design was generally studied using idealized examples with lower computational demands. The end-objective is to apply the methodologies to real structural systems with application to structural design standards. The remainder of this dissertation focuses on this goal by applying the general methodologies to light framed building systems, which are constructed using cold-formed steel (CFS) with non-structural wood based cladding interconnected via screw fasteners.

Although traditionally used only in non-structural building subsystems such as curtain walls, cold-formed steel is becoming increasingly popular in the low and mid rise building industry owing to construction ease and economical viability [78]. Design methods for these systems, particularly for extreme load conditions such as earthquakes, continue to be developed [8]

and there is a relative scarcity of system level experimental / analysis data and behavior characterizations necessary for performance-based seismic design.

To overcome the above shortcomings, full scale building tests were recently performed on a prototype two story building (hereafter referred as the CFS-NEES building) by researchers at the Johns Hopkins University. The experiments applied scaled ground motions upto 100% the design basis earthquake (DBE, Canoga Park) and maximum considered earthquake (MCE, Rinaldi), with and without non-structural components. The overall conclusion from this research was that the building far exceeded code-predicted capacities with or without non-structural elements, the inclusions of which increased stiffnesses significantly. Although subsystems comprising this building were designed for response reduction factor $R = 6.5$, the actual behavior was highly elastic. Furthermore, the load was distributed to subsystems that had not been expected to attract loads, for example, the gravity and partition walls that are not detailed for seismic response.

Using the CFS-NEES building as a benchmark, this chapter discusses the overall performance of light-framed buildings, breaking it down into subsystems and components and studying the design, behavior and functionality of each. System reliability analyses are performed for this building subjected to seismic ground motions using an approximate reliability model described in chapter 5. A spring-based ABAQUS model is developed in this chapter to propose load-sharing factors and design demands calculated by non-linear dynamic analysis, which are used in chapter 5 for system reliability and sensitivity calculations.

4.2 Framework for whole building system reliability based design

The whole building system reliability based design approach (Figure 1.1) begins with a target system reliability for the building. The value for this can be derived from failure-consequence

analysis in terms of economic losses, downtime, repair costs,injuries or deaths.

The next step is to define the load-sharing network between the subsystems of the building. This is discussed in section 4.4 which uses the hierarchical classification of the buildings into its subsystems and components (section 4.3) to propose series, parallel or mixed load sharing networks for each load combination. The load sharing network can be used to compute the system reliability analytically or computationally (section 5.1) which can be used to (1) compute the system reliability given the subsystem reliabilities, or (2) compute reliability sensitivities to propose subsystem reliability targets given the system reliability target.

With the hierarchical classifications and load-sharing networks defined, a framework to calculate reliabilities and sensitivities for each individual subsystem will be required. In chapter 6 high-fidelity finite element models will be developed for cold-formed steel floor diaphragm subsystems. Uncertainty modeling will be added to the diaphragms in chapter 7, leading to its subsystem reliability calculation with a direct convolution approach and characterization of the subsystem load-sharing network using the component reliability sensitivities.

4.3 Hierarchical classification of subsystems and components in a cold-formed steel framed building

Cold-formed steel buildings are characterized by linked subsystems. These are enlisted below, and subsequently called out for the CFS-NEES building in Figure 4.1. Similar enumerations may be found in a companion paper from this project [94].

1. Diaphragm subsystem – one at each level (Figure 4.2)
   (a) Sheathing
   (b) Floor-joists
   (c) Ledger-tracks framing the floor-joists

(d) Sheathing-to-steel screw fasteners attaching floor panels to underlying framing

(e) Blocking providing lateral support between joist webs

(f) Strap bracing providing lateral support between joist bottom flanges

(g) Web-stiffeners connecting joist to blocking or ledger tracks

(h) Steel-to-steel screw fasteners attaching joist to ledger tracks, joist to wall-studs, ledger track to wall stud and web stiffeners to joist, blocking and track webs

2. Wall subsystem – four sets at each level, one along each edge of the building (north, south, east or west), each set has multiple shear and gravity walls (Figure 4.3)

(a) Sheathing

(b) Wall-studs

(c) Ledger-tracks framing wall studs at top and bottom

(d) Hold-downs at the bottom corners of shear walls (these are present only in shear walls and absent in gravity walls)

(e) Shear anchors on ledger-tracks

(f) Sheathing-to-steel and steel-to-steel screw fasteners (attachments similar to diaphragm subsystems)

3. Roof truss

(a) Top and bottom chord members

(b) Web members

(c) Ridge-plate at intersection of top chord members

(d) Heel-plates at intersections of top and bottom chords

(e) Stub-columns attaching web and chord members

(f) Deck attaching to chord members

(g) Steel-to-steel screw fasteners

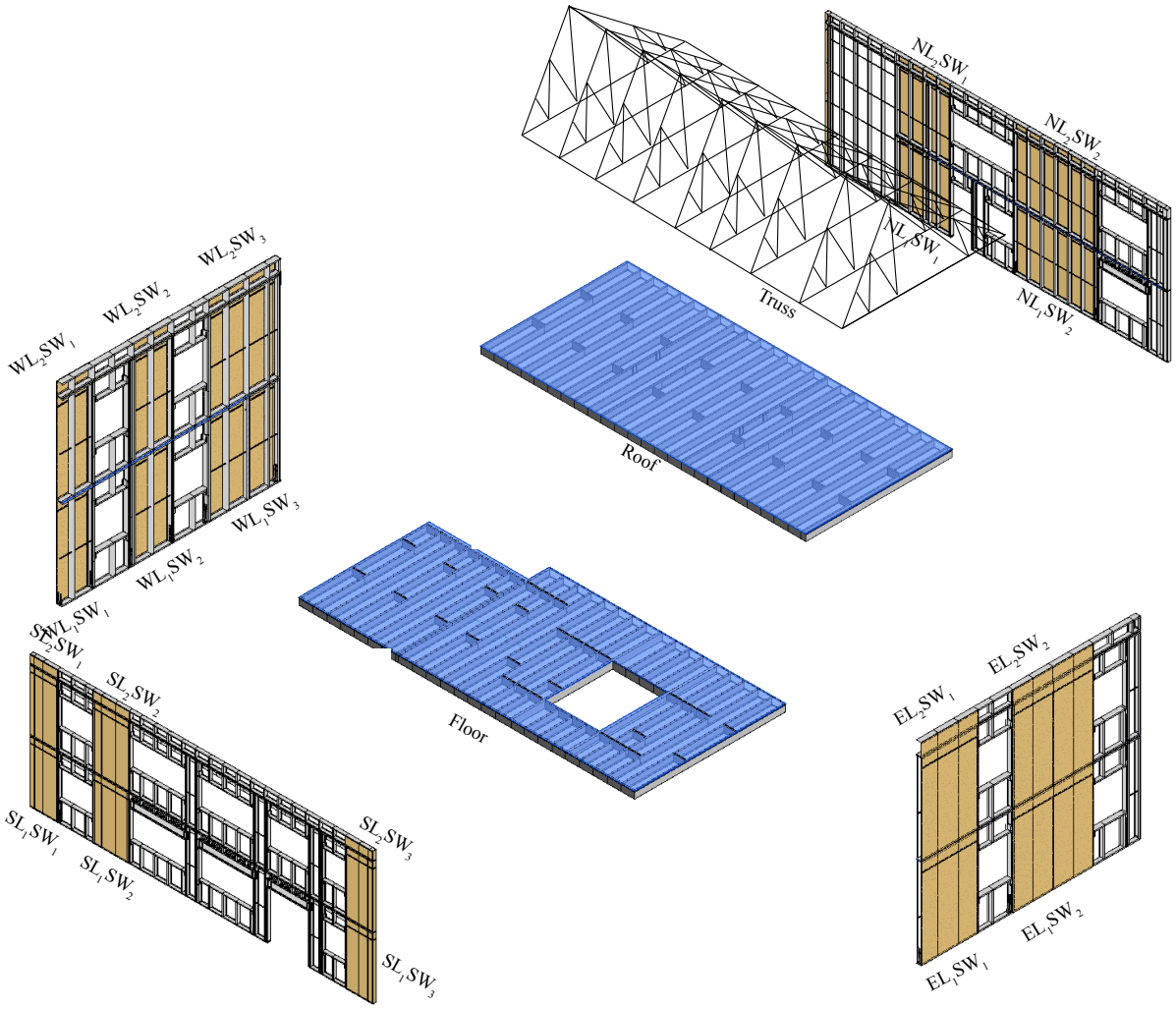

Figure 4.1: Hierarchical classification from system-to-subsystem in the NEES building with individual subsystems symbolized for system reliability calculations [61, 78]

The behavior and design of diaphragm and shear wall subsystems are detailed next to propose load-sharing networks between them as the building is subjected to seismic loads, and also to provide final reliability-based design guidelines in chapter 5. Roof trusses do no alter the load sharing relations under lateral forces and are excluded from these discussions.

4.3.1 Behavior and design of cold-formed steel floor diaphragms

Floor diaphragms with wood sheathing through-fastened to cold-formed steel joists are common in light steel framed buildings. The sheathing panels, typically 1220mm X 2440 mm, are attached to the CFS framing via minimum number 8 sized screw fasteners (4.8 mm diameter). Diaphragms connect to the lateral force resisting system (LFRS) which is detailed to provide strength and stiffness in the lateral direction. The role of the diaphragm is to resist lateral loads and transfer them to the LFRS without damage. For seismic load effects, this entails inertial load transfer occurring from floor masses (typically consisting 38% of the entire building weight in light framed construction, [78]) through cold-formed steel perimeter members as shown in Figure 2 (see inset cross-section detail) along the joist-parallel building edge . In the joist-perpendicular direction, the floor joists frame into chord members (CFS tracks). The floor and roof plates also limit building drift in extreme wind events, preventing damage to gravity walls and facades [87].

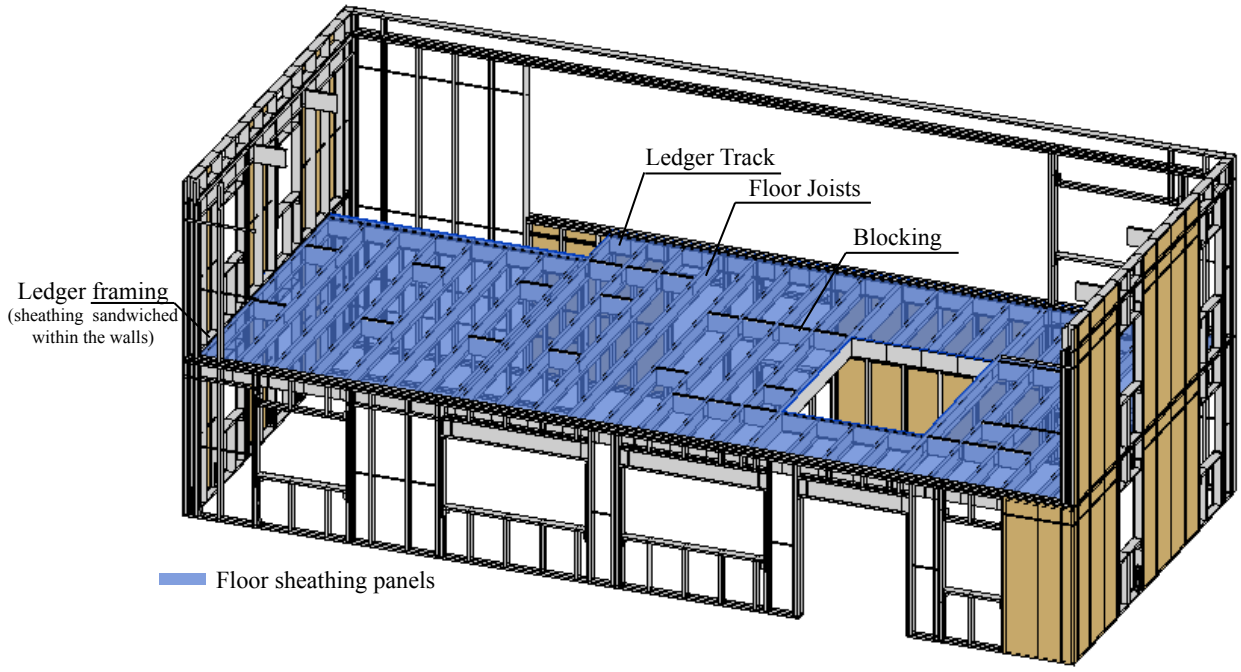

Figure 4.2: Description of the diaphragm subsystem showing joists, ledger tracks, sheathing and ledger framing [61, 78]

Since a diaphragm's function is to transfer lateral loads to the LFRS, they are designed for lateral strength and stiffness according to the provisions in AISI S400-15. Diaphragm aspect ratio (length divided by width) is limited to 4:1 for blocked diaphragms (all panel edges are attached to structural members or panel blocking) and 3:1 for unblocked. Design deflections for blocked wood structural panel diaphragms can be calculated using Equation 4.1.

$$\delta = 0.052vL^3/E_sA_cb + \omega_1\omega_2vL/\rho Gt_{sheathing} + \omega_1^{5/4}\omega_2\alpha(v/0.00579\beta)^2 + \sum_{j=1}^{n}\Delta_{ci}X_i/2b \quad (4.1)$$

where A_c is the chord member in mm^2, b is diaphragm depth parallel to load direction in mm, E_s is elasticity modulus for steel (203000 MPa), G is sheathing shear modulus in MPa, L is diaphragm length perpendicular to load direction in mm, n is number of chord splices,

s is maximum fastener spacing at panel edges in mm, $t_{sheathing}$ is nominal panel thickness is mm, t_{stud} is nominal framing thickness in mm, v is shear demand per unit width in N/mm, equalling $V/2b$ where V is total diaphragm load in N, X_i is distance between i^{th} chord splice and nearest support in mm, Δ_{ci} is deformation value associated with i^{th} chord splice, ρ is 1.85 and plywood and 1.05 for OSB, ω_1 is $s/152.4$ and ω_2 is $0.838/t_{stud}$. For unblocked diaphragms, δ is multiplied by 2.5.

Diaphragm strength checks are performed in the format $\phi R_n \geq R_u$, where ϕ, the resistance factor, equals 0.6 for seismic and 0.65 for wind loads, R_n is the nominal diaphragm capacity derived from AISI S400 and R_u is the factored diaphragm demand obtained from ASCE 7 [5].

Nominal diaphragm strengths provided in Table F2.4-1 in AISI S400-15 are derived using the following equation [57]

$$R_n = C_{pb} C_{sheathing} C_D C_{di} V_n n \tag{4.2}$$

where C_{pb} is the capacity reduction factor for wood panel buckling, which is 0.83 for 9.5 mm thick diaphragms, 0.915 for 11 mm and 1.0 for 12 mm , $C_{sheathing}$ is the reduction factor for sheathing type which is 1 for Structural 1 plywoods and 0.9 for other sheathing types like oriented strand board (OSB), C_D is the load duration factor which equals 4/3 and is increased from 1.0 typical of normal duration plywood stresses to account for the shorter duration earthquake or wind loads, C_{di} is the diaphragm factor which equals 1.1, n is the number of fasteners per ft. (or 305 mm) along the diaphragm edge. The nominal fastener strength V_n, is taken as 1.25 kN based on Lum's work in [57] which was derived from the 1991 National Design Specification methodology given in Equation (4.3). Note that Lum reported nominal strengths of 1.65 kN with a safety factor of 3.3 which gave an allowable strength of 498 N, but since the allowable strength safety factor recommended in AISI S400-15 is 2.5, the nominal fastener strengths used in Equation 4.2 to generate AISI S400-15 Table F2.4-1 is $1.65kN/3.3 * 2.5$ or 1.25 kN

$$V_n = kDt_sF_{em}/K_D/(2 + R_e) * 2.5/3.3 \tag{4.3}$$

where D is screw diameter, t_s is side member (in this case, steel) dowel bearing length, F_{em} is main member (in this case, wood) dowel bearing strength, k is a function of dowel bearing strength, ratio of main and side member strengths, diameter, dowel bending strength and side member dowel bearing length, K_D is a reduction term and R_e is the ratio of main member strength to side member strength, 2.5 is the safety factor used in AISI S400.

It should be noted here that R_n and V_n are code recommended nominal strengths and not mean strengths. Bias values (ratio of mean to nominal) are currently not provided in design specifications for either the floor diaphragm system or the screw fastener component. These considerations become important when component and system reliability analyses are performed for these subsystems in chapters 6 and 7.

The diaphragm demand R_u for seismic loads can be obtained from ASCE 7-10 [5] section 12.10-1, as $R_u = F_{px} = (\sum_{i=x}^{n} F_i / \sum_{i=x}^{n} w_i) w_{px}$, where F_i is the diaphragm design force applied at level i from an equivalent lateral force procedure, w_{px} is the weight tributary to the level x for which force F_{px} is calculated, and w_i is the weight tributary to level i. The value of R_u thus obtained must at least equal $0.2S_{DS}I_ew_{px}$ and need not exceed $0.4S_{DS}I_ew_{px}$, where S_{DS} is the short period spectral acceleration and I_e is the importance factor.

Wood-sheathed diaphragms are understood to develop resistance to lateral loads through a combination of sheathing shear stiffness and framing action (i.e., exterior cold-formed steel chords act in tension and compression like a truss) with composite interaction defined by fastener spacing and location [1]. There are limited experimental data on wood-sheathed cold-formed steel diaphragms with distributed loads applied, however the tests that do exist highlight the importance of the screw fastener connections [71]. Diaphragm load-deformation softening resulted from screws tilting and tearing through plywood sheets that translate and rotate as rectangular rigid bodies. The only tests reported in the literature were performed on a 3650 mm by 7300 mm floor subsystem by the National Association of Home Builders

(NAHB) [71]. Lateral loads were applied along one edge while the other edges running parallel to the direction of loading were held fixed to represent the stiff shear walls. Failure initiated when the fasteners along the supported edges pulled through the sheathing which is consistent with behavior observed in recent wood-sheathed diaphragm computational simulations [13]. This diaphragm edge connection limit state is the focus of system reliability calculations presented in chapter 7.

4.3.2 Behavior and design of cold-formed steel shear walls

Shear wall subsystems acting as the lateral force resisting system in cold-formed steel buildings can include wood, gypsum, fiberboard panel, or steel sheet sheathing through-fastened to cold-formed steel framing member, moment resisting frames or strap-braced walls. These systems are subdivided into Type-1 and Type-2 shear walls, with the difference lying in the fact that Type-1 walls have hold downs at the end of each segment corner (Figure 4.3) whereas Type-2 has hold downs at the very end of the entire wall segment. The focus of this dissertation is on Type-1 wood-sheathed shear walls that were used in CFS-NEES buildings.

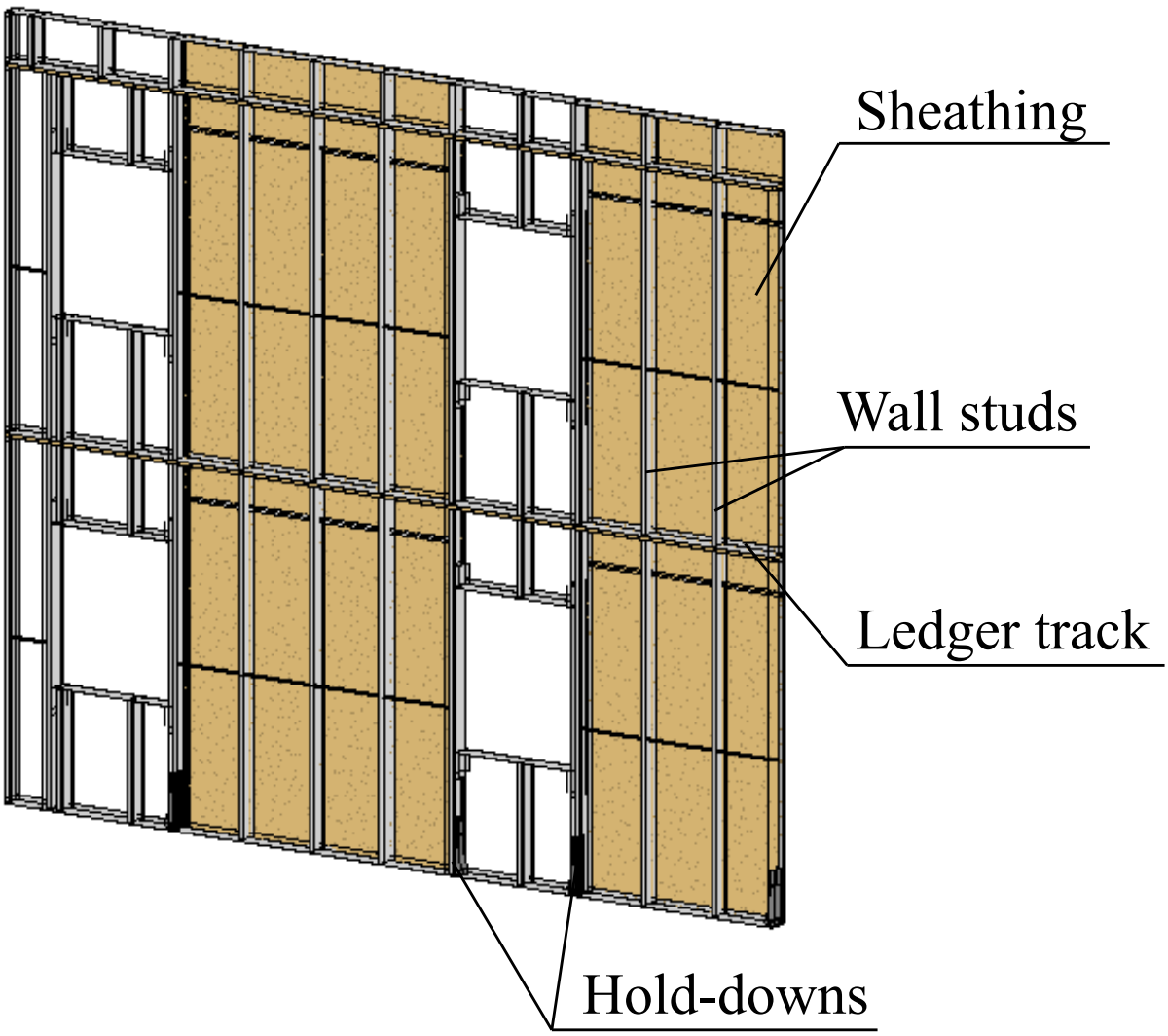

Figure 4.3: Shear wall subsystem and its essential components [61, 78]

The nominal strength of Type-1 shear walls with aspect ratio $h/w \leq 2$ is calculated as $v_n w$, where h is the shear wall height, w its width, and v_n the nominal strength per unit length given in Table B5.2.2.3-1 in the cold-formed steel structural framing standard AISI S240-15 [3], or Tables E1.3-1 and E2.3-1 for wood sheathed and steel sheathed shear walls respectively in cold-formed steel structural design standard AISI S400-15 [4]. Similar to diaphragm subsystems, the underlying assumption of the strength prediction methodology is that nominal system strength effectively equals the nominal connection strength times

number of connections. The design strength equals the nominal strength times a resistance factor which is equal to 0.6.

Design deflection of wood or steel sheet sheathed shear walls is given by:

$$\delta = 2vh^3/E_sA_cb + \omega_1\omega_2vh/\rho Gt_{sheathing} + \omega_1^{5/4}\omega_2\omega_3\omega_4(v/\beta)^2 + \frac{h}{b}\delta_v \tag{4.4}$$

where h is the wall height, $\omega_3 = \sqrt{\frac{h/b}{2}}$, b is the length of the shear wall, $\omega_4 = 1$ for wood structural panels and $\omega_4 = \sqrt{\frac{227.5}{F_y}}$, for steel sheets with F_y being the yield strength of the sheet, δ_v is the vertical deformation of the anchorage. All the other factors are the same as defined for Equation 4.1.

Shear walls act as the lateral force resisting system in cold-formed steel buildings and are designed to dissipate energy during seismic events. The designated energy dissipation mechanism in wood sheathed shear walls are the structural member to sheathing connection and the wood panel sheathing or the steel sheet sheathing, and yielding of strap bracing in cold-formed steel strap-braced shear walls. All other components and connections in the shear wall system, including chord studs, boundary members, collectors are designed for the expected capacity of the overall system, with the design force limited to the seismic load effect times the overstrength factor, that is, these are force-controlled components designed to resist the maximum capacity the shear wall can develop. The shear wall design is itself controlled by the elastic base shear divided by a reduction factor equalling 6.5 for wood-sheathed shear walls.

4.4 Load-sharing models between the subsystems in a light-framed building subjected to seismic ground motions

The remainder of this chapter will consider the load paths within the whole building as it is subjected to the seismic load combination which will be used to recommend load-sharing models for system to subsystem reliability analysis.

The load combinations to be used in the system reliability methodology are the unfactored versions of the loads enlisted in chapter 2 Equation 2.8. Here we consider the force flow path as the building is subjected to a seismic load combination $D + E$. Effects of ground motions acting along one direction of the building are assumed to be independent of the effects in the other direction, that is, the two load patterns can be considered separately in the system reliability loop. Load sharing models for seismic ground motions acting in the short building direction are discussed here for which the participating subsystems are the west and east shear walls, floor and roof diaphragms. These are based on the discussions provided in [94].

As the ground shakes, inertial forces arise from the masses sitting on the floors. Since building failure is expected to occur if any of the levels in the building collapse, it is assumed that the different building levels act in series with one another. Furthermore, at any given level, the shear wall system and the diaphragm system are assumed to be in series since the failure of either one causes failure of the entire level. Finally, within the shear wall system at each level, the east and west walls are assumed to be in series, whereas the shear walls within each of these (constituting either the east or the west shear wall system) are assumed to act in parallel. The overall building system reliability under these assumptions is given by

$$P_f(Building) = P_f[\cup(\cap WL_1SW_1, WL_1SW_2, WL_1SW_3), (\cap WL_2SW_1, WL_2SW_2, WL_2SW_3), (\cap EL_1SW_1, EL_1SW_2), (\cap EL_2SW_1, EL_2SW_2), Floor, Roof] \tag{4.5}$$

where $P_f(S)$ is the probability of failure of system, subsystem or component S. The demands on each of the subsystems are fully correlated and are a factor of the total seismic base shear. Design codes assume values for these load-sharing factors based on the elastic lateral force design method given in ASCE 7-10 and the relative stiffnesses of each subsystem, and are summarized in Table 4.2.

Table 4.1: Relative demand ratios on individual subsystems due to unit building base-shear demand, based on ASCE-7 elastic lateral force method [61, 78]

Floor	Roof	West SW (L1)			East SW (L1)		West SW (L2)			East SW (L2)	
		SW_1	SW_2	SW_3	SW_1	SW_2	SW_1	SW_2	SW_3	SW_1	SW_2
0.41	0.59	0.12	0.12	0.26	0.20	0.30	0.07	0.07	0.16	0.12	0.18

The ASCE-7 load sharing factors listed above may not reflect real building behavior under dynamic load effects and non-linear responses. The load-sharing factors are examined in this work using a structural model including shear walls, floor and roof diaphragms as non-linear springs with loading-unloading parameters modeled for dynamic loads. The development of this model and the expected load sharing factors are discussed in the following sub-sections, and inform system reliability models for the full building under seismic demands analyzed in chapter 5.

4.4.1 Full building computational model including subsystems as non-linear springs

The full-building computational model, developed in the finite element package ABAQUS, is shown in Figure 4.4. Although the model includes springs for floor and roof diaphragms, the analyses is effectively one-dimensional in the direction that lateral loads are applied, since all nodes are restrained in the two other directions (East-West, up-down). The objective is to obtain load sharing factors between the subsystems for ground motions applied in the North-South direction, and not to perform full dynamic analyses until building failure. Therefore it is assumed that $P - \Delta$ instabilities due to gravity loads, for example, are not going to affect the load-sharing results significantly.

Building seismic weight is included as lumped masses at each node. The values for the masses are assigned based on Table 1-11 in [78]. At roof level, the total mass is $11892kg$ and includes supplemental weight (achieved by placing artificial masses on the diaphragm) plus half the structural dead load (cold-formed steel framing plus wood sheathing). At each wall node at roof level a quarter of the material mass is placed ($739kg$ each). Similarly at the floor level, supplemental weight plus half material mass ($16572kg$) is applied on the floor node, and a quarter of the material mass ($1188kg$ each) at the wall nodes.

Damping is included as mass-proportional Raleigh damping using the parameter *alpha* in ABAQUS. The fundamental period of the building model is $0.45s$ (Table 4.2) or a frequency ω_n of $14rad/s$. The mass-proportional damping coefficient used in ABAQUS, assuming a $\zeta = 5\%$ of critical damped system, is $2\zeta\omega_n = 2 * 14 * 0.05 = 1.4$ [21].

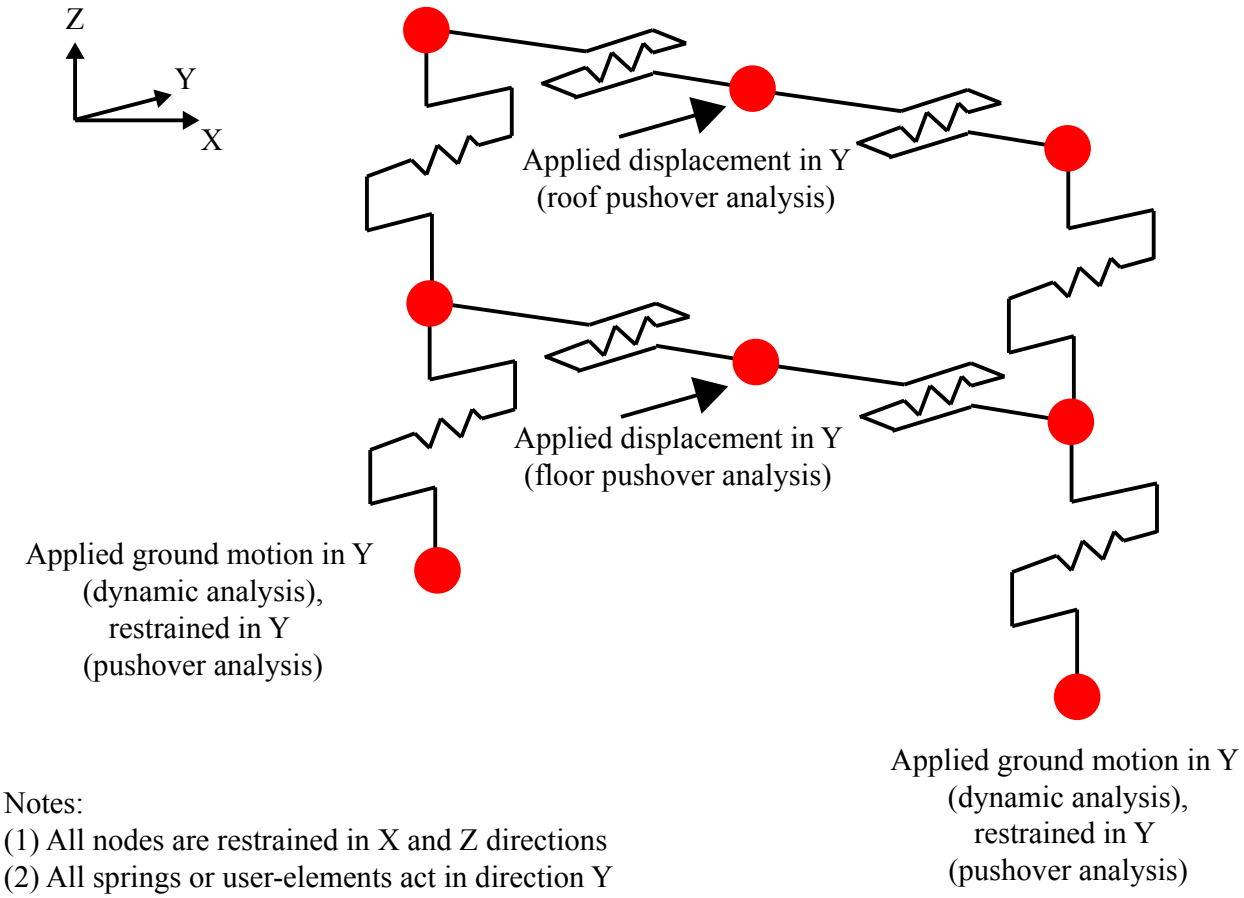

Figure 4.4: Full building model using ABAQUS nonlinear spring or user elements to represent wall and floor subsystems

The floor and roof diaphragms are modeled as non-linear *Spring2* elements acting in the East-West or short building direction, load-deformation responses for which are obtained from high-fidelity finite element models described in chapter 6. Shear-walls are modeled as *Pinching4* type [60] user-element springs (UELs) in ABAQUS [24] with cyclic backbones and unloading-reloading obtained experimentally [59]. These relationships are plotted in Figure 4.5.

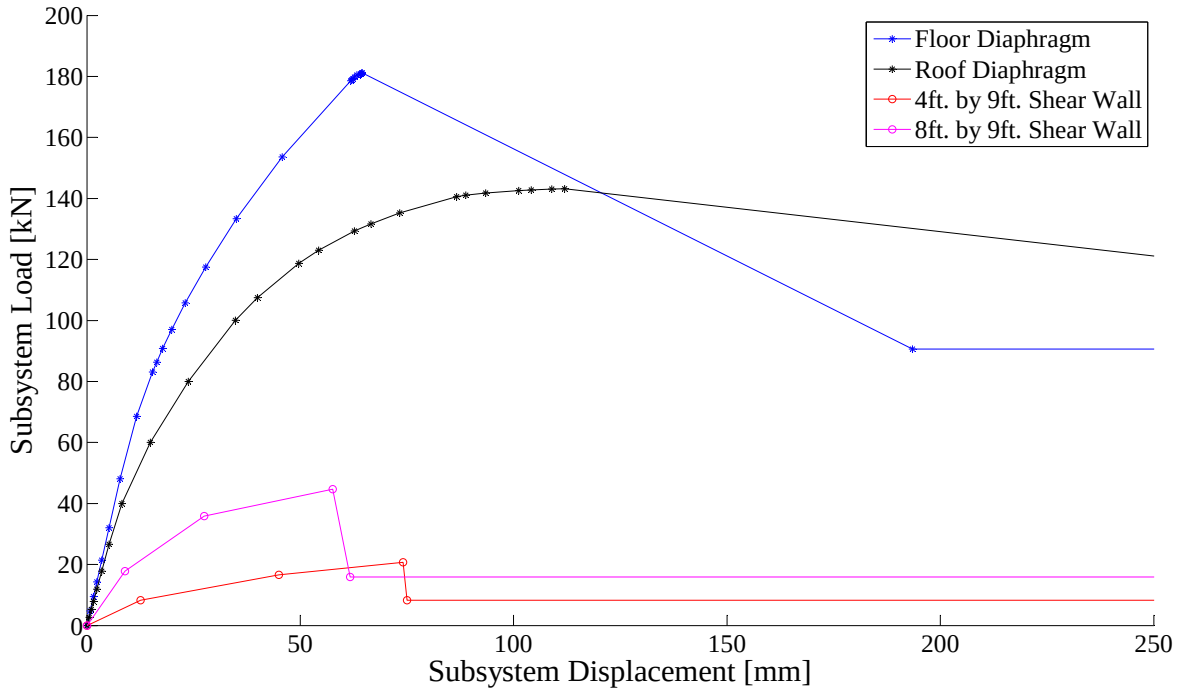

Figure 4.5: Load-deformation backbones for diaphragm and shear wall subsystems

The west wall system of the building comprises one 2.4 m by 2.7 m shear wall and two 1.2 m by 2.7 m shear walls, whereas the east wall comproses two 2.4 m by 2.7 m shear walls, as shown in Figure 4.6. The spring backbones described in figure4.5 and are assigned accordingly between the floor and roof nodes on the west and east side, for example, the west level 1 shear wall system has two 1.2 m by 2.7 m UEL's and one 2.4 m by 2.7 m UEL.

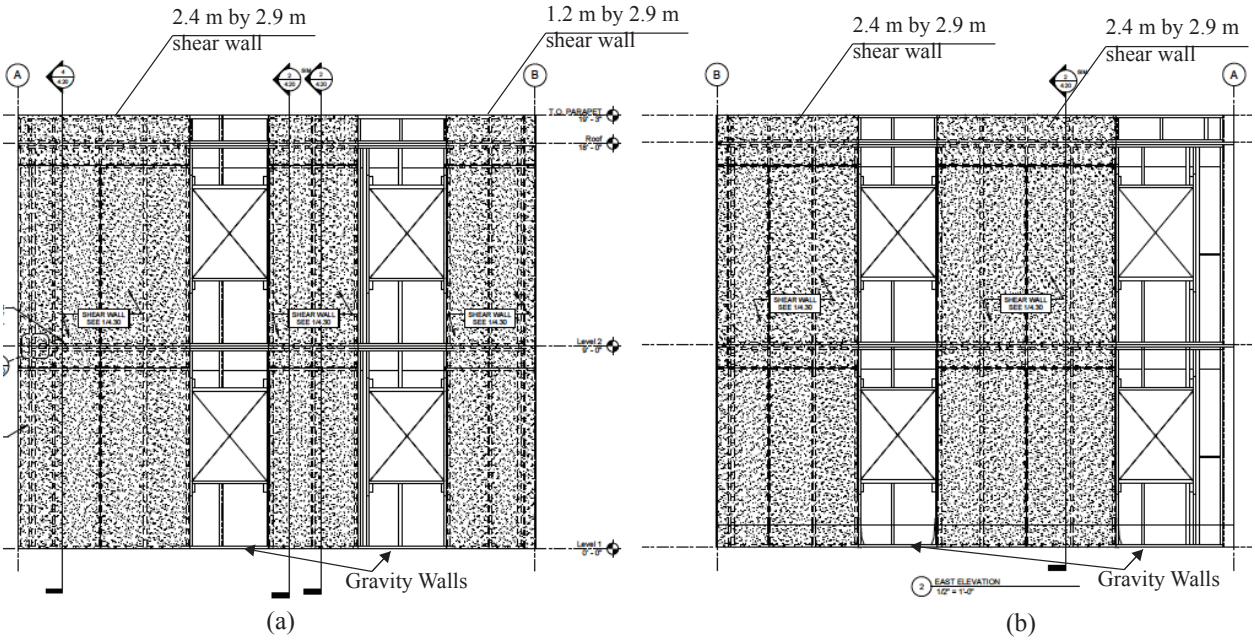

Figure 4.6: Short direction elevations for the CFS-NEES building system showing (a) the west shear wall system and (b) the east shear wall system [61]. Shaded areas represented sheathed shear walls which are part of the structural system, remainder is non-structural

It was observed during the NEES-building project that building response has a large sensitivity to gravity wall framing in the lateral load-resisting system models and on non-structural components (partition walls, interior sheathing) [90]. To include this effect in the ABAQUS model, additional springs are included in the lateral systems to simulate the gravity walls (without sheathing). The stiffnesses and strengths of these springs are modeled at the 1.2 m by 2.7 m shear wall stiffnesses, which is based on matching the modeled building fundamental period to the experimentally measured fundamental period for the NEES building including gravity framing but excluding all non-structural components, as explained in section 4.4.3. As will become apparent in the system reliability analysis presented in the chapter 5, this reduces building drift demands but increases force demands on the diaphragm subsystems. In real building structures, non-structural systems further amplify these effects.

4.4.2 Modeling protocol validation for a single degree of freedom spring-mass damper system

The non-linear dynamic analysis protocol is verified with a single degree of freedom cantilever system. The mass m assigned to this system is $0.12kN.s^2/mm$. The spring stiffness k is $20kN/mm$, which brings the system time period $2*\pi\sqrt{\frac{m}{k}}$ to $0.49s$, or a natural frequency of $12.9rad/s$. This is exactly equal to the time period calculated using an ABAQUS eigenvalue analysis. The damping coefficient for this system, using a mass proportional damping parameter $\alpha = 1.23$, is 4.76%. The relative displacement of the spring obtained using an ABAQUS implicit dynamic analysis with accelerations applied to the supported node is compared to a solution for the single degree of freedom ordinary differential equation using the MATLAB function 'ode45' [64]. The results, compared in Figure 4.7, validates the modeling protocol for dynamic analysis using applied ground accelerations.

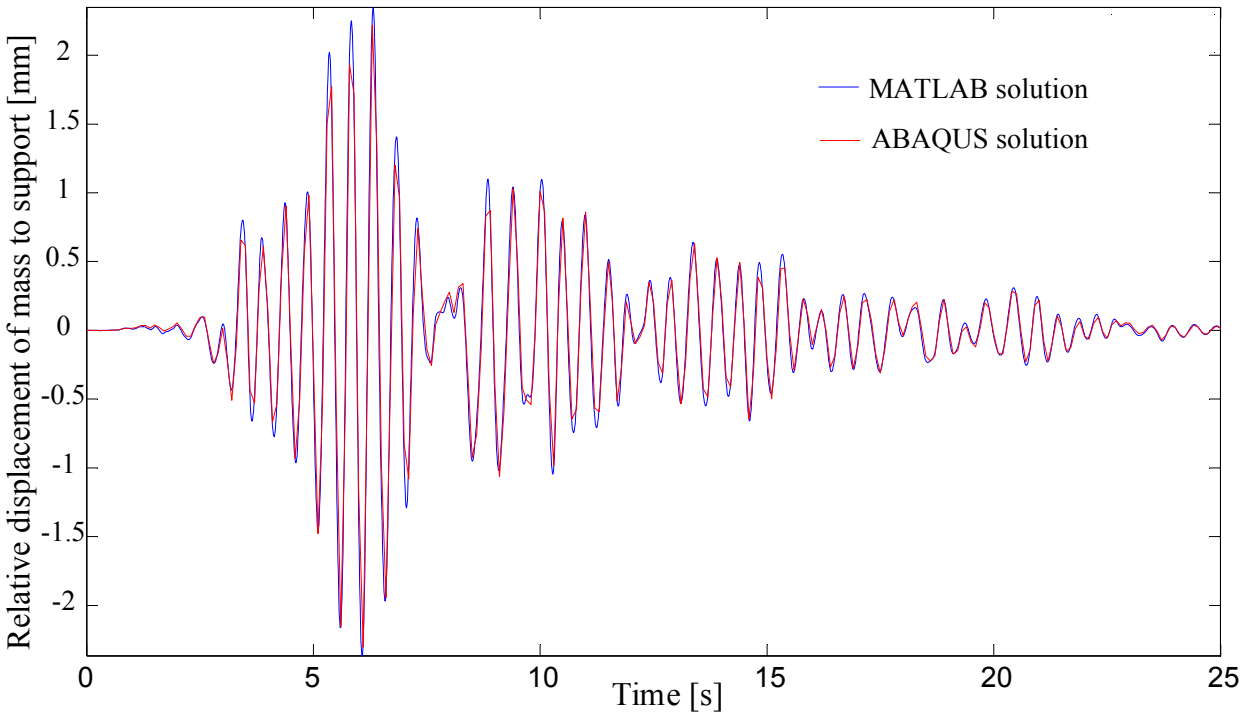

Figure 4.7: Comparison between spring displacement obtained for a single degree of freedom cantilever spring with accelerations applied at the supported node in ABAQUS, with a MATLAB solution for the ordinary damped single degree of freedom differential equation using the function 'ode45'

4.4.3 Full building model eigenvalue analyses

Natural frequencies and mode shapes for the full building models were calculated using the **Frequency* option in ABAQUS which performs a dynamic eigen-analysis. These results act as a check on the model by verifying that the computed time periods and mode shapes are reasonable, providing comparisons to previous models and experimental results that give insights on how the stiffness changes from the experiment to the modeling space, and across different modeling stages (with and without gravity framing, for example). These results can also provide estimates for the elastic base shear and drift demands, considering the entire building as a single degree of freedom mass-spring-dashpot system.

The fundamental building frequencies for each model are listed in Table 4.2 and compared to fundamental frequencies obtained at each stage of the NEES-building experiments [80] and OPENSEES model results discussed in [90]

Table 4.2: Building natural time periods in the short or north-south direction obtained from two sets of computational models and experimental white-noised testing [81, 90]

Measurement Type	Gravity Framing	First mode time period $[s]$
ABAQUS model	No	0.49
ABAQUS model	Yes, equalling shear wall stiffness per unit length	0.45
OPENSEES model	No	0.66
OPENSEES model	Yes spring-based elements	0.32
NEES building, no non-structural, undamaged	Yes	0.36
NEES building, no non-structural, after DBE	Yes	0.51
NEES building, all non-structural, undamaged	Yes	0.26
NEES building, all non-structural, after MCE	Yes	0.34

The time period for the ABAQUS model without gravity walls (only shear walls) is 0.49 s, 25% lower compared to the OPENSEES model fundamental period not including gravity framing and ledger tracks at the tops and bottoms of shear walls. When gravity walls along the short direction (Figure 4.6) are added to the model, with an assumed stiffness per unit length equaling the 1.2 m by 2.9 m (shorter) shear walls, the time period decreases to 0.45 s. The inclusion of gravity framing in the OPENSEES model reduced the first mode period to 0.32 s, effectively quadrupling the building stiffness [89]. This is comparable to the NEES building (structural only) time period of 0.36 s calculated before applying ground motions. The NEES building time period decreased to 0.26 s after non-structural components were added, and increased to 0.34 s after undergoing damage from the MCE ground motion. The ABAQUS model has a comparatively lower stiffness (higher time period) which is assumed to result from the absence of any walls along the long building direction. As will become apparent in dynamic analysis and reliability results, this increases the design inter-story drift demand on the building system, decreasing its as-design system reliability.

4.4.4 Full building model non-linear static pushover analysis

Pushover analyses on the building are performed by applying displacements at the floor and roof masses respectively. The resulting base shear versus applied displacement plots are shown in Figure 4.8.

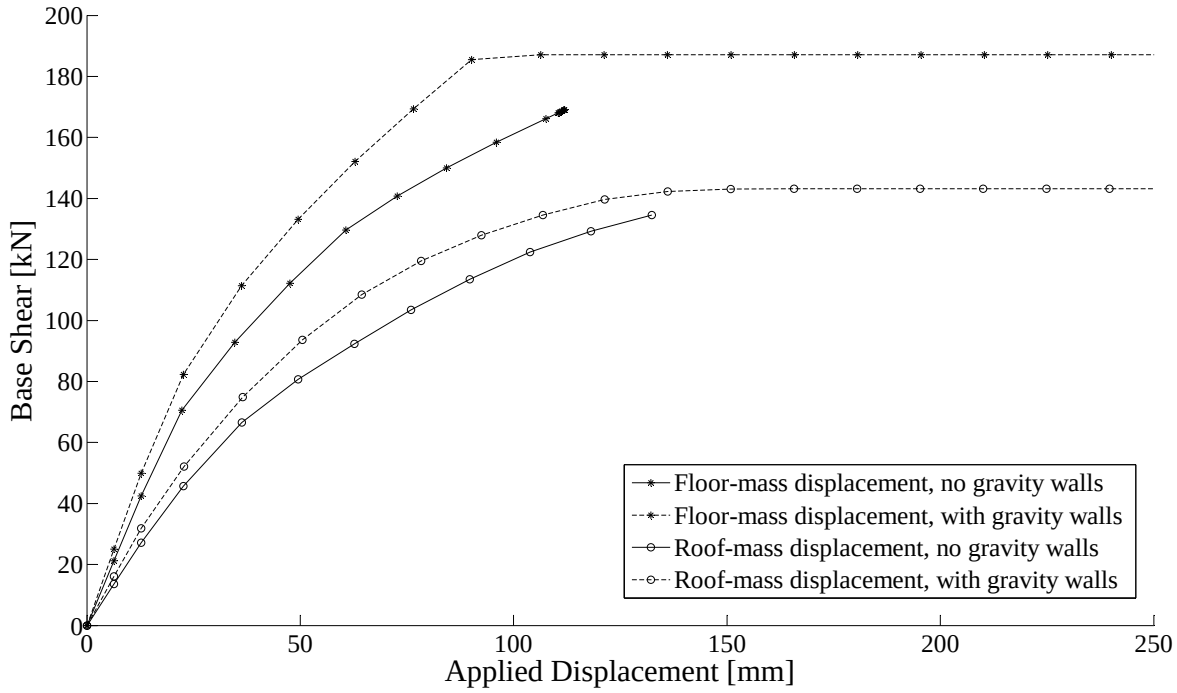

Figure 4.8: Base shear versus applied displacement plots for pushover analyses with displacement applied at floor and roof nodes

Displaced shapes (magnified 50 times) are shown in Figure 4.9. The displaced shapes at ultimate loads provide an indication of how increased stiffnesses arising from gravity walls is a non-conservative effect, because this leads to higher force demands on the diaphragm which governs the failure mode for the whole building. This is undesirable because the intended ductile failure mode is yielding of the lateral force resisting system (shear walls).

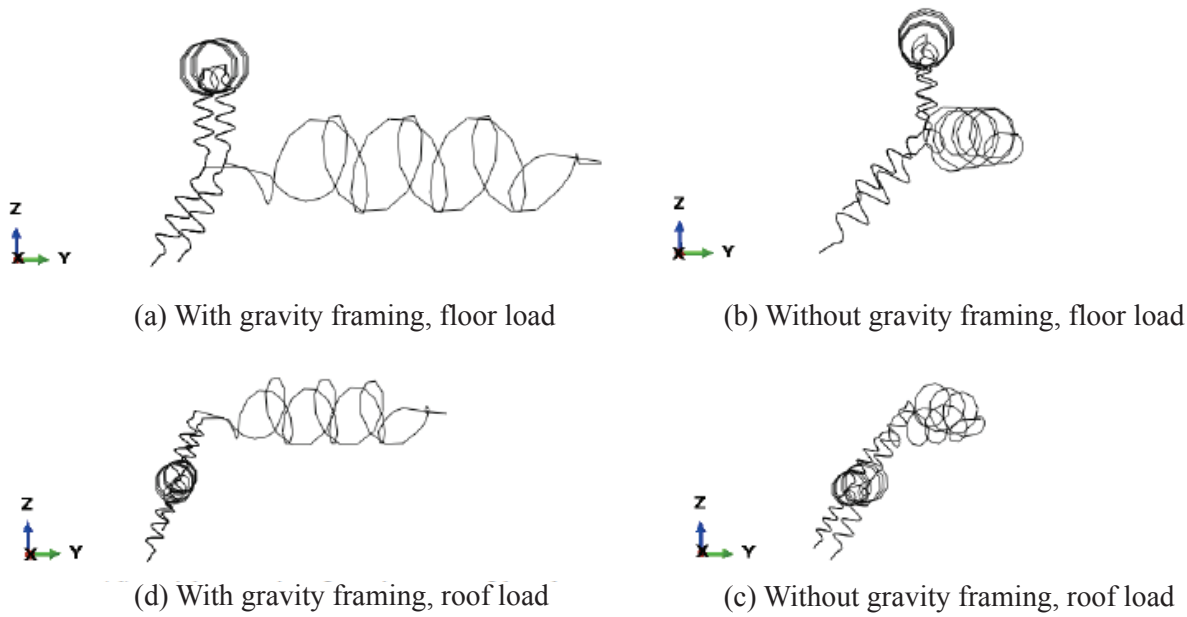

(a) With gravity framing, floor load

(b) Without gravity framing, floor load

(d) With gravity framing, roof load

(c) Without gravity framing, roof load

Figure 4.9: Displaced shape of ABAQUS model at ultimate response under pushover loads, showing the change in failure mode due to including and excluding gravity wall stiffness.

Since the pushover analysis only applies loads at one level at a time, the diaphragm failure mode could be unrealistic. In reality, the base shear is redistributed to both levels of the building, leading to a higher cumulative demand on the first-floor shear walls which are expected to trigger system failure as intended. However the analysis still demonstrates a potential undesired effect of the non-zero lateral stiffness of systems not designed to carry lateral loads, which is why this stiffness is included in the analyses presented here to include the possibility of diaphragm failure triggering system collapse.

Since the pushover analysis applies a displacement boundary condition at either the floor or roof node, it creates no force on the diaphragm to which a boundary condition is not applied. If displacement boundary conditions are applied at both floor and roof levels, the resulting forces will be dependent on the proportion of the two applied displacements, leading to artificial estimates for base shear distributions. Therefore, a pushover analysis does not provide information on base shear distribution factors between the floor and roof levels, and

non-linear dynamic analysis is employed .

4.4.5 Full building model non-linear dynamic analyses

Non-linear dynamic analyses are carried out by applying ground motion acceleration time histories at the base of the building, as indicated in Figure 4.4, using an implicit dynamic algorithm in ABAQUS implemented as **DYNAMIC, IMPLICIT*. The ground motions are scaled according to two requirements given in FEMA-P695 [18] – (1) normalization against peak ground velocity and (2) matching the spectral acceleration at the building fundamental period with the design basis earthquake spectral acceleration. The ground motions are downloaded from Haselton Structural Research Group [41] which provides values already normalized against peak ground velocities. The earthquake records used include the Northridge ground motion recorded at Canoga Park (which was employed in the NEES-building experiments) and the 44 near-field motions recommended in FEMA-P695 [18].

Base shear, floor and roof diaphragm loading time histories under the Canoga Park ground motion are plotted in Figure 4.10. Peak displacements and forces are compared to the experimental estimates in Table 4.3. The results are discussed in section 4.4.6.

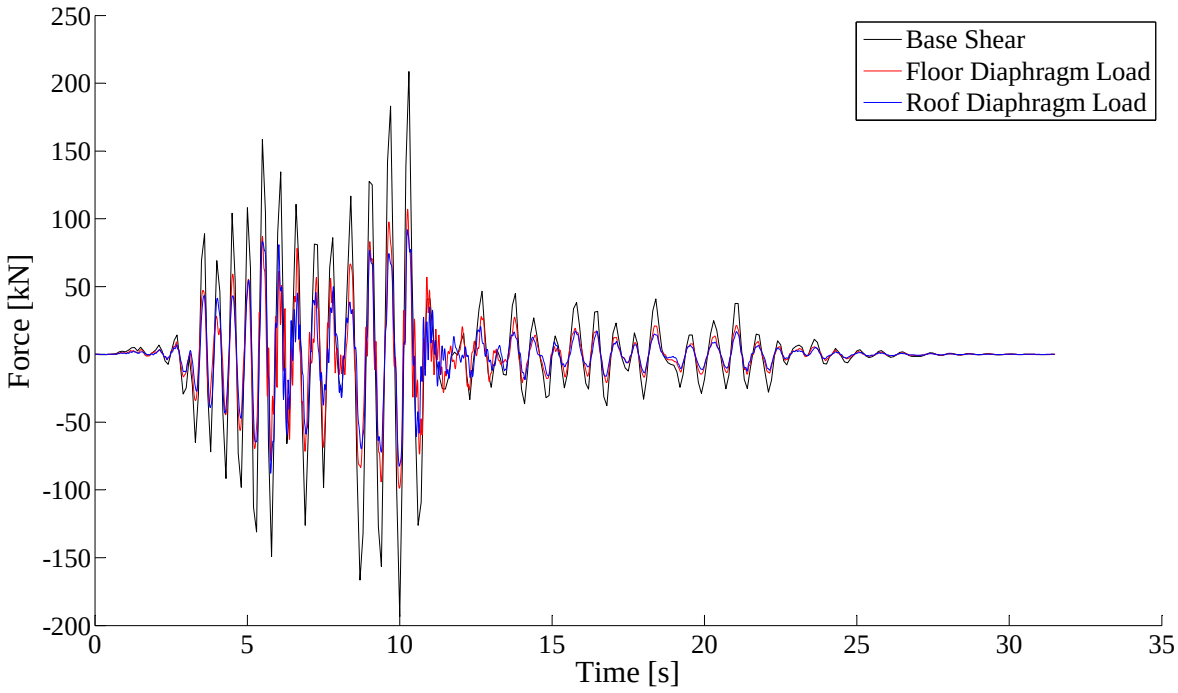

Figure 4.10: Total base shear, roof and floor force demand time histories for full building ABAQUS model under Canoga Park ground motions

Since a single set of load sharing factors will be used in reliability analyses, it is important to study the change in these factors as the system is subjected to increasingly strong ground motions, resulting in non-linear response of the subsystems. These are studied using an incremental dynamic analysis (IDA) approach [100] that applies increasing magnitudes of ground motion demand on the structure characterized by its spectral acceleration. More details on IDA and its application for seismic system reliability analysis are discussed in chapter 5. Figure 4.11 (a) shows IDA plots for the builiding model subjected to the Canoga Park earthquake record indicating spectral acceleration versus peak interstory displacement, while Figure 4.11 (c) indicates spectral acceleration versus the shear demand on the floor diaphragm relative to the total base shear demand.

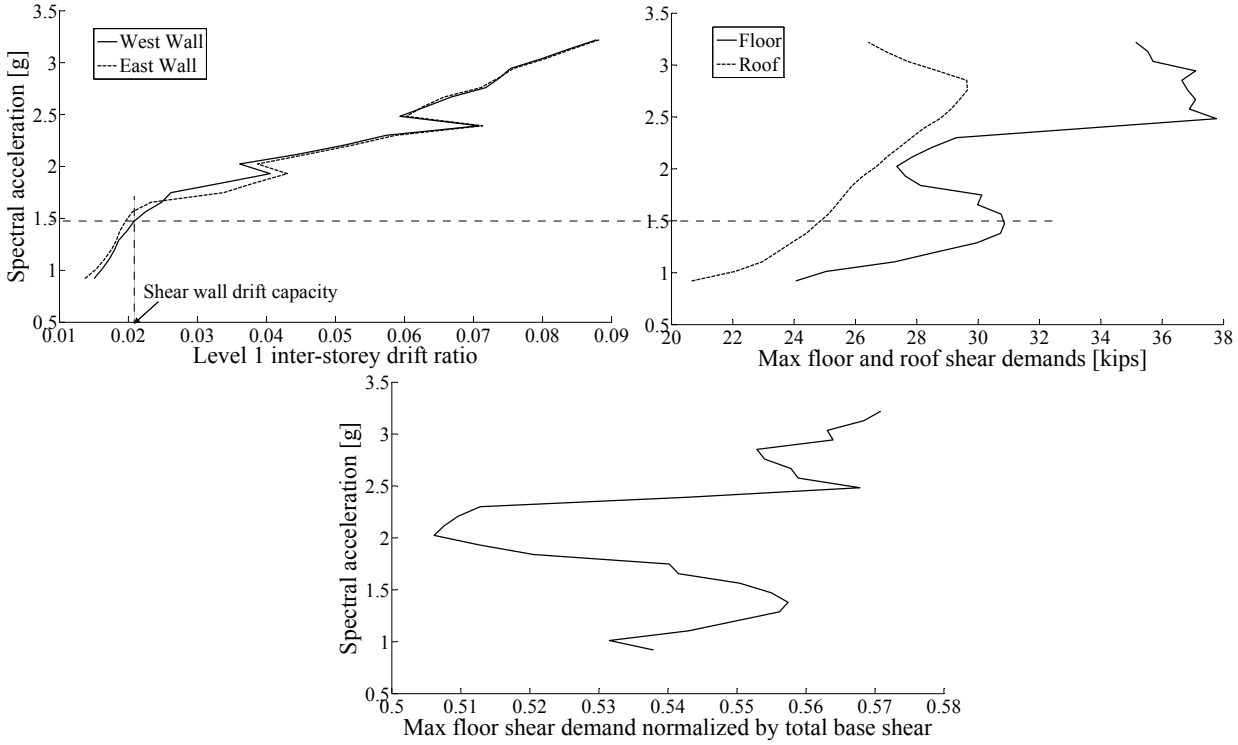

Figure 4.11: Incremental dynamic analysis for the full building model showing (a) spectral acceleration in units of acceleration due to gravity [g] versus peak interstorey drift ratio of first floor, (b) spectral acceleration versus floor and roof diaphragm shear demands and (c) relative proportion of total base shear acting at the second floor diaphragm level

As the ground motion intensity (spectral acceleration) increases, the interstory drift ratio (IDR), total base shear, and relative shear demand at the floor level increase. At 2.1% IDR, the 2.4 m X 2.7 m shear walls reach their drift capacity (Figure 4.5), as a result of which the floor shear demand begins to reduce. The results indicate that the base shear demand on the building, as well as shear demands on the diaphragms, are a function of not just the diaphragm seismic weight but also the stiffness of the lateral system. However for the scope of this dissertation, this interaction is ignored and the relative force demand ratios (load distribution factors) at the floor and roof level are assumed as constants.

The load distribution factors at the roof and floor level are calculated by taking the average

of 44 ground motions, and the resulting factors are 0.55 and 0.45 and the floor and roof levels respectively. Figure 4.12 (a) shows typical IDA plots for the builiding model subjected to each earthquake record showing spectral acceleration versus peak interstory displacement, while Figure 4.12 (c) indicates the spectral acceleration versus shear demand on the floor diaphragm relative to the total base shear demand. The results of the interstory drift plots are discussed in chapter 5. The relative base shear plots indicate that the floor shear varies from 0.48 to 0.62 of the total base shear, with a mean value of 0.55 which is used in system reliability analyses performed in chapter 5.

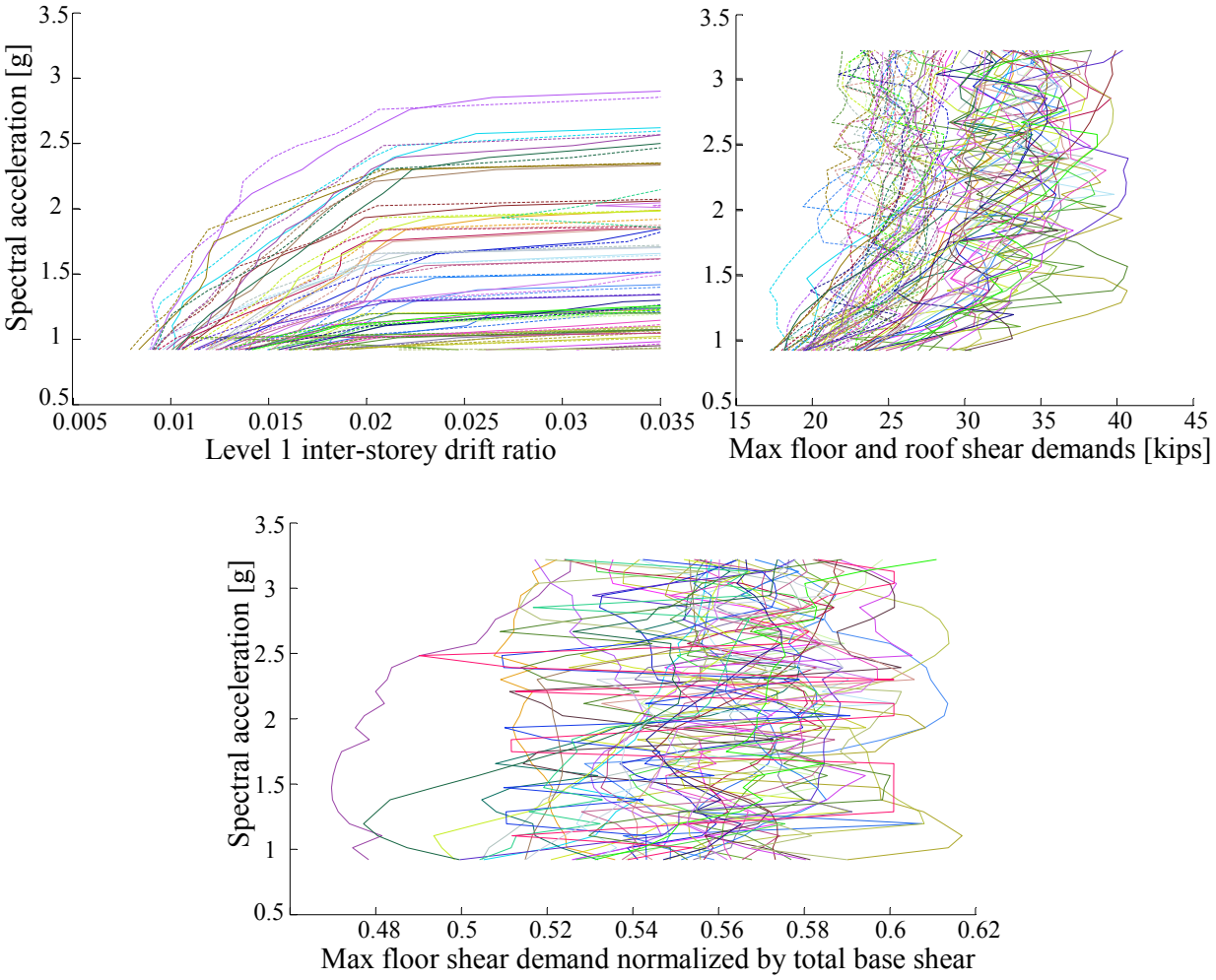

Figure 4.12: Incremental dynamic analysis for the full building model showing (a) spectral acceleration versus peak interstorey drift of first floor, (b) spectral acceleration versus floor and roof diaphragm shear demands and (c) relative proportion of total base shear acting at the second floor diaphragm level

4.4.6 Analysis of full building model responses and load-sharing factor recommendations

Table 4.3 summarizes base shear and interstory drifts demands obtained from the ABAQUS building model, the OPENSEES building model described in [90] and the NEES-building

experiment [80]. The peak level 1 story drift and floor diaphragm displacements are over-predicted in the ABAQUS model due to absence of the long-direction walls that act as diaphragm chords increasing its rigidity. The peak base shear estimate from the NEES experiment is lower than reality since it was calculated using load-cell readings at the base of the shear walls, excluding the effect of shear wall overturning and forces resulting from the gravity walls, as described in [81]. The base shear estimate from the ABAQUS model is comparable to the OPENSEES model result. Comparatively, the ASCE-7 design base shear assuming a response reduction factor $R = 6.5$ is $49kN$, and the elastic base shear (if the building stayed fully undamaged at its initial stiffness) at the actual building time period of $0.36s$ is $49kN * 6.5 = 319kN$. The results are as expected for structural systems subjected to seismic ground motions, with the mean base shear lying in between the elastic and the design base shear.

Table 4.3: Building drift, diaphragm displacements and base shear comparisons [81, 90]

Analysis Type or Experiment	Peak level 1 story drift $[mm]$	Peak floor diaphragm displacement $[mm]$	Peak base shear $[kN]$
ABAQUS model	41	23	208
NEES experiment	23	3.3	79
OPENSEES model	25	–	185

The mean interstory drift demand at level 1 from 44 near field FEMA P695 ground motions is $38mm$ (interstory drift ratio of 1.5%), with mean load sharing factors between the floor and roof diaphragms equalling 0.55 and 0.45 respectively, and a mean base shear of $208kN$, which are used in system reliability and sensitivity calculations provided in the next chapter.

Chapter 5

Building System Reliability, Sensitivity and Target Subsystem Reliabilities

The objective of this chapter is to provide subsystem and component level design guidelines tailored to a system reliability target for the CFS-NEES building subjected to an earthquake ground motion acting in the north-south direction. The target subsystem reliabilities are calculated using the reliability sensitivity algorithm introduced in chapter 3. The building system reliability is calculated by convolution of building system capacity and demand. Two different approaches are employed – firstly the incremental dynamic analysis method used in state-of-the-art earthquake engineering recommendations given in FEMA P695 [18], and a simplified alternate method to calculate seismic system reliability using interstory drift ratios. The simplified reliability method reduces the computational burden of the FEMA P695 process and directly considers the uncertainty in structural properties, and is chosen for reliability sensitivity analysis to calculate target shear wall and diaphragm subsystem reliabilities. Physical interpretations of the sensitivity results are studied using incremental dynamic analysis. The chapter concludes with overall design recommendations for CFS

buildings under seismic loads from the system to subsystem level.

5.1 System reliability calculation for a cold-formed steel building under seismic excitation

Building system reliability is evaluated with the same general treatment introduced in chapter 3, that is, by a convolution of system capacity and system demand

$$P(C_{sys} - D_{sys} \leq 0) = \int_{d=0}^{d=\infty} P(C_{sys} \leq d | D_{sys} = d) dF_{D_{sys}}(d) \tag{5.1}$$

For the seismic design case, assigning appropriate quantities for capacities and demand is a non-trivial problem, since earthquake loads act as accelerations at the base of the structure and are hard to characterize. Quantities such as moment magnitude, modified Mercalli intensity or ground motion duration are non-scalable, that is, a higher value does not necessarily indicate stronger ground motions. Some examples of scalable ground motion intensity measures are peak ground acceleration and peak ground velocity, but although suitable for hazard characterization, these quantities cannot quantify the structural capacity [100].

Two different quantities are used in this chapter to characterize structural system capacity and seismic demand. The first of these is spectral acceleration, defined as the peak displacement times square of natural frequency for a single degree of freedom spring-mass-dashpot system subjected to an acceleration history. Considering structural demand and capacity as spectral accelerations (S_a), system reliability can be estimated using the incremental dynamic analysis method (IDA), described in the next subsection [100].

Capacity and demand can also be characterized as the peak inter-story drift ratio of the structure. This approach enables an approximate system reliability calculation that does not entail the high computational resource requirements of IDA, and is described in section 5.1.2. Results from the two different approaches are compared, and the approximate method

is used to study variation in system reliability due to subsystem reliability modifications, that is, system to subsystem reliability sensitivity.

5.1.1 System reliability calculation using incremental dynamic analysis

Incremental dynamic analysis, proposed in [100], is a methodology in which the structural system is subjected to increasingly strong ground motions until collapse occures, defined by a structural mechanism or a pre-established limit to inter-story drift (such as 1.5% or 2% recommended in ASCE-7). The structural spectral acceleration capacity, denoted as S_{CT}, is the spectral acceleration at which this limit is reached.

The IDA methodology to calculate system reliability and tune designs for an acceptable target failure probability is at the basis of FEMA-P695 [18], which is currently the state-of-the-art in earthquake engineering. Table 7-3 in FEMA P695 lists the acceptable collapse margin ratios for probability of collapse of 5%, 10%, 15%, 20% and 25%, given the system collapse uncertainty. This table is derived by considering the structural capacity as S_{CT}, the spectral acceleration at collapse, and the demand as S_{MCE}, the spectral acceleration at the MCE earthquake level. The collapse margin ratio equals S_{CT}/S_{MCE}, that is, the ratio between the median capacity (assumed to equal the mean capacity) and the mean demand for an MCE level earthquake. The lognormal expression for reliability introduced in chapter 2 (Equation 2.5, $\beta_i = \frac{log_n \frac{\mu_{C_i}}{\mu_{D_i}}}{\sqrt{V_{C_i}^2 + V_{D_i}^2}}$), is then used to obtain the relationship between collapse margin ratio (CMR), collapse probability ($P_{collapse}$), and total system uncertainty (β_{TOT}), i.e., $P_{collapse} = \Phi^{-1}(-log_n CMR/\beta_{TOT})$.

The IDA methodology includes only the variability in demand (resulting from using multiple ground motions to analyze the structure) but does not consider structural uncertainties explicitly. Instead, the uncertainty parameter β is used to characterize structural capacity uncertainty, and arises from record-to-record, design methods, test data and modeling related

uncertainties, with a total value ranging from 0.275 to 0.95.

In order to find the actual system capacity distribution and its variability using IDA, multiple analyses need to be performed for each IDA curve including random perturbations in system behavior, which increases the required number of analyses by a few orders of magnitude. To circumvent these computational demands, an approximate methodology is described in the following section, which characterizes system demand and capacity in terms of the inter-storey drift ratio. However, since the structural inter-storey drift demand does depend of the capacities of the subsystems, C_{sys} and D_{sys} are not truly independent, and the distribution of D_{sys} must be re-computed at every new design point during the construction of the sensitivity plots.

IDA plots for the as-designed CFS-NEES building modeled according to the protocol shown in chapter 4 are provided below. Setting building capacity at an IDR of 2.1 % which is the displacement capacity of the shear wall with lowest ductility, the spectral acceleration capacity S_{CT} has a mean 1.6 g and variance 0.6, with the design basis earthquake spectral acceleration demand being 0.92g, when coupled with the total uncertainty 0.525 (FEMA-P695 Table 9-6 , 'good' quality test data and 'good' design requirements) provides a system reliability estimate of 1.0.

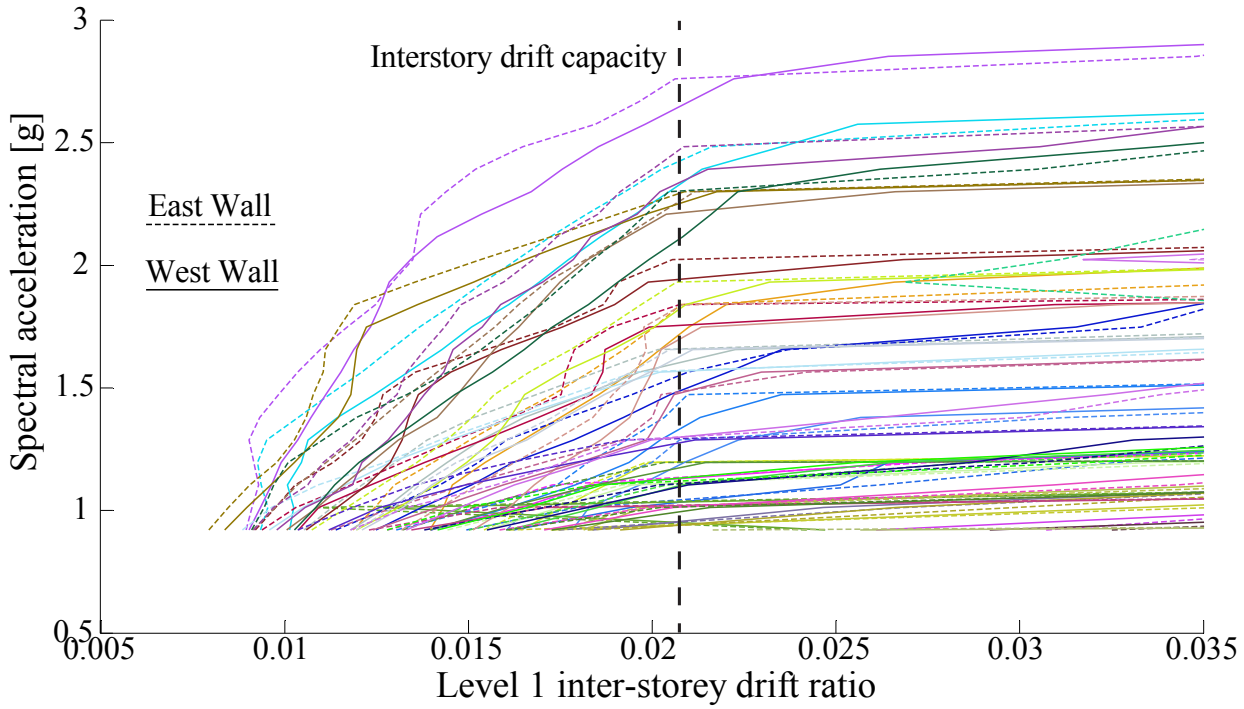

Figure 5.1: Incremental dynamic analysis results for ABAQUS spring model for full building, indicating spectral acceleration and interstory drift capacities

5.1.2 System reliability calculation assuming series-parallel relationships between subsystems

Incremental dynamic analysis is a computationally expensive process, and although it should ideally be employed throughout the design space (as diaphragms and shear wall designs are modified) to calculate system reliabilities, these analyses are time consuming. In this section system reliability calculation using load-sharing relationships described in section 4.4 is presented, which provides an alternate methodology that does not entail the computational demands of IDA. The system reliability mathematical model introduced in chapter 4 is repeated here for convenience.

$$P_f(Building) = P_f[\cup(\cap WL_1SW_1, WL_1SW_2, WL_1SW_3), (\cap WL_2SW_1, WL_2SW_2, WL_2SW_3),$$
$$(\cap EL_1SW_1, EL_1SW_2), (\cap EL_2SW_1, EL_2SW_2),$$
$$Floor, Roof] \tag{5.2}$$

The building system reliability given by Equation 5.2 can be solved using analytical expressions given for the series system in Equation 5.3 and its compliment for the parallel system.

$$P(E_{\text{series system}}) = P(\cup_{i=1}^{i=n} E_i) = \sum_i P(E_i) - \sum_{i<j} P(E_iE_j) + \sum_{i<j<k} P(E_iE_jE_K) - .... \tag{5.3}$$

where E_i denoted the failure event for the i^{th} subsystem in an n component series system. As mentioned previously in this dissertation, in general the subsystem failure events are not independent and require knowledge of the higher-order probabilities of combined failure of multiple subsystems. Methods to solve the equation can include simplified assumptions (for example, independence of subsystem failure events or assumed correlation coefficients between them) or by direct simulation (as described in chapter 3), which is the focus of the present chapter.

Building system capacity and demand in the approximate methodology used here are expressed as the inter-story drift ratio (IDR) and not spectral acceleration. This permits a simple calculation of the system capacity without needing to resort to full incremental dynamic analysis. Note that the structural demand distribution changes with a change in system capacity, since different configurations of shear walls or diaphragms lead to different IDR demands on the building. Therefore during reliability sensitivity analyses presented later in this chapter, the IDR demands are re-calculated for each new structural configuration, which increases computational demand but is still more efficient compared to full IDA curves calculated at each new design point.

The subsystem to system load sharing network can be represented as :

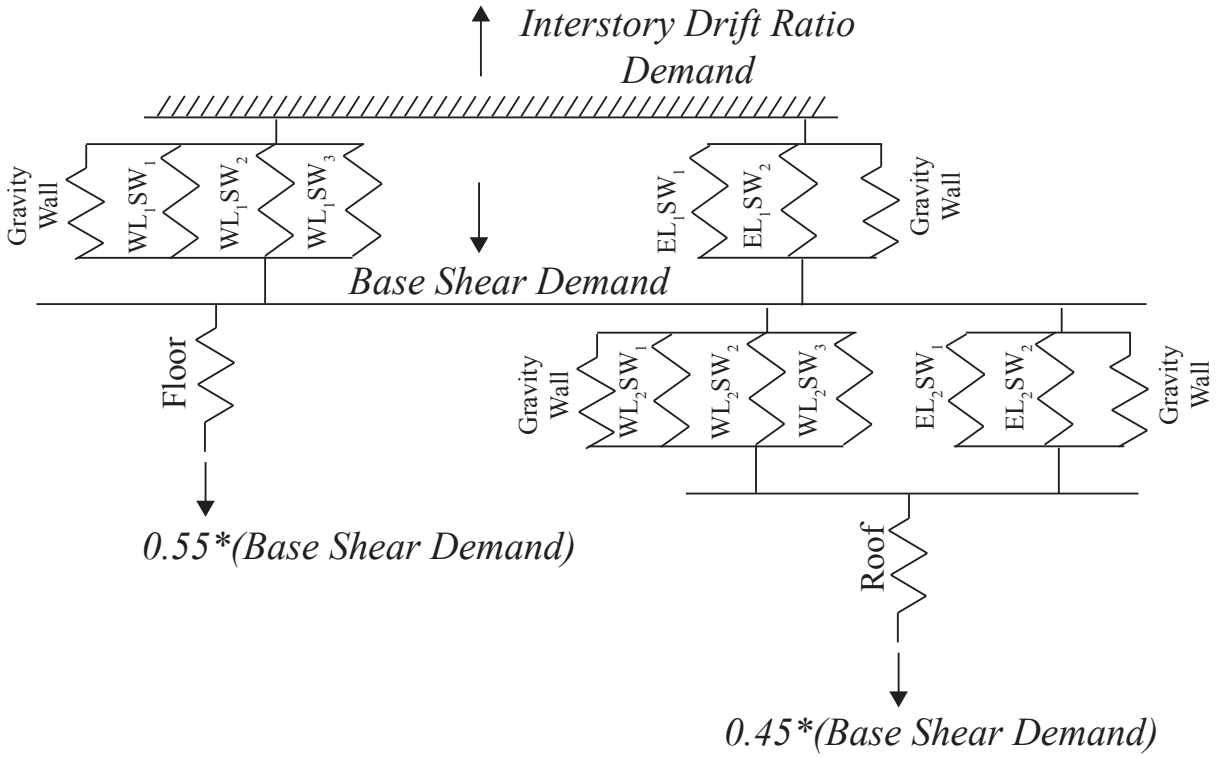

Figure 5.2: System to subsystem load-sharing network under seismic loads applied in north-south direction

Assuming that the system demand D_{sys} is known independently, the system reliability estimation problem is reduced to a capacity estimation problem. The building system capacity distribution can be calculated using a Monte-Carlo simulation procedure, given the load-deformation relationships for each subsystem, their capacities and coefficients of variation. The list of steps to calculate building system capacity for a single random simulation are provided below.

1. Generate random samples of subsystem force capacities F_{floor}, F_{roof}, $F_{WL_1SW_1}$ etc. for each subsystem listed in figure 5.2

2. Check which subsystem controls building system failure:

   (a) The total base shear when the first shear wall reaches its force capacity is the sum of forces for all shear and gravity walls at the corresponding displacement

   (b) The base shear is divided between floor and roof diaphragms according to the load-sharing proportion described in section 4.4

3. If the shear demand on the roof or floor is higher than its capacity, then the corresponding capacity controls. The IDR capacity of the building is the displacement at which the roof or floor force capacity is developed.

4. If the shear demands on the roof and floor are lower than their capacities, shear wall capacity controls. The IDR capacity of the building is taken as the third point on quadrilinear force-displacement relationships for shear walls, minimum controls.

5. Check for other IDR limits that might control system capacity, for example, a 1.5% drift limits for non-structural walls.

The final step that checks for other drift limits is meant in a general sense that can extend to any potential building collapse limit state such as out-of-plane drift capacity of walls due to diaphragm deformation, and it is anticipated that the general methodology can be tailored to these specific scenarios relatively easily. These cases will not be studied in this dissertation.

The approximate methodology assumes system failure to occur if the diaphragm capacity is reached, that is, softening and energy dissipation within the diaphragm systems are not permitted. This is a conservative estimate that can be relaxed by studying subsystem to system load-sharing behavior beyond the peak diaphragm demand in chapter 4. Alternately, the IDA-based system reliability methodology (section 5.1.1) which considers spectral accelerations as demands and capacities will directly include diaphragm energy dissipation effects.

In step 2(b) of the approximate methodology, the base shear is divided in constant proportion between the different levels of the building. The base shear proportion depends on the mode

shape that the building responds in, and thus the frequency content of the ground motion it is subjected to. These higher mode effects are automatically captured if capacities and demands are described as spectral accelerations as there are no assumptions on the base shear distribution between different levels. The proposed IDR-based methodology used here calculates the average base shear proportions at the design basis earthquake and assumes them to stay constant during reliability analysis. The limitations of this assumption could be quantified by comparing system reliability estimates using spectral acceleration demands and capacities and IDR demands and capacities. For the two story building considered here, the two methodologies provide similar estimates as described next. However, discrepancies can potentially arise for taller structures, whose analysis is beyond the scope of this dissertation.

Table 5.1 summarizes system reliability results for the as-designed CFS-NEES building, modeled with the protocol described in chapter 4. The overall uncertainty for the FEMA-P695 methodology is assumed as 0.525 for 'good' quality of test data and 'good' design requirements (Table 9-6 in FEMA-P695) – note that this includes both capacity and demand uncertainty. For the approximate IDR methodology the demand is assumed to have a 0.38 variability [104] whereas the capacity variability is obtained from simulations.

Table 5.1: Comparison of capacity and demand parameters expressed as interstory drift ratio (IDR) or spectral acceleration (S_a) obtained from approximate system reliability model and incremental dynamic analysis

Quantity	Mean	C.O.V.(%)
Design IDR demand	1.5 %	32
IDR capacity	2.1%	4.2
Design S_a demand	0.92 g	–
S_a capacity	1.6 g	60

The building system capacity distribution F_{Csys} is estimated using the algorithm discussed in

section 5.1.2. Shear wall and diaphragm system capacities are obtained from the backbones presented in chapter 4 (Figure 4.5). Shear wall system variances are obtained as 2.6% for 1.2 m by 2.9 m shear walls and 1.9% for 2.4 m by 2.9 m shear walls, from stochastic pushover simulations on OPENSEES structural models [8]. Floor and roof mean capacities and variances are obtained from the results presented in chapter 6. Combining these together using the system reliability algorithm results in a building system IDR capacity of 2.3 inches with a variance of 4.2%. As discussed in chapter 4, the building system IDR demand is 1.5 inches. Variance for the seismic load combination is assumed as 0.38 from [104]. Combining these together in the convolution methodology results in a building system reliability of 1.1. Comparatively, system reliability estimated using IDA with a 0.525 total uncertainty is 1.0.

The building system IDR capacity uncertainty of 4.2% is a result of variabilities obtained from shear wall simulations, which in turn result from fastener strength variabilities obtained from component level experiments. Additional layers of uncertainty are expected in real buildings. At the fastener level, there is added uncertainty resulting from field installation practices. At the shear wall level, variabilities are added by construction practices for the shear wall, as well as thicknesses and properties of the sheathing and steel whose screw-fastened connections govern shear wall strength. At the building level, there might be other subsystems that initiate building failure, and the assumption that failure initiates only at the shear wall with least displacement capacity may not hold. Finally, load distribution varies in a real building, both between shear walls (assumed to act as perfectly parallel springs) and at different levels of the building (assumed to be subjected to constant force ratios of 0.55 and 0.45 in this work). These additional sources of variability are neither quantified nor accounted for in this work, but could be studied at the shear wall level, for example, by performing a set of experiments on nominally identical shear wall specimens.

The calculated as-designed system reliability is low because it over-estimates displacement demands compared to the real system which has a greater stiffness resulting from gravity walls in both directions. For example, if the IDR demand is 0.8% (equalling the NEES structural-only measured IDR at the design basis earthquake), and system reliability is

still controlled by shear-wall subsystem failure, then the system capacity remains at 2.1%, resulting in a building system reliability of 2.7. The reduced IDR demand results only from the gravity systems without sheathing and without non-structural walls, which decrease the IDR demand and increase system reliability even further [80].

The system reliability results for the as-designed building are similar to findings presented in [89] which state that the building fails to satisfy FEMA-P695 requirements if the gravity walls are excluded, performs just satisfactorily when gravity walls are included, and is highly over-conservative when non-structural components are added.

5.2 Target building system reliability for seismic loads

The target building system reliability is calculated indirectly from acceptability criteria outlined in FEMA P695 [18], which checks an acceptable collapse margin ratio (ACMR), given the total system uncertainty β_{TOT}, to recommend response reduction factor R, overstrength factor Ω and deflection amplification factor C_d for the design of new seismic force resisting systems. The collapse margin ratio is defined as the ratio between the spectral acceleration causing median collapse and the spectral acceleration at MCE. This leads to an 'acceptably low probability of collapse when subjected to MCE ground motions', whose value is 0.1 (average across all archetypes) and 0.2 (for each individual archetype). The acceptable mean probability of collapse of 0.1 given the MCE ground motion equals a reliability of 1.3 under MCE demand loads.

According to Bayes theorem, the overall probability of collapse due to ground motion equals the probability of collapse given an MCE ground motion times the probability of the MCE ground motion occurring. By definition, the MCE ground motion has a 2% probability of exceedance in 50 years. Therefore, for a building with 0.1 collapse probability given an MCE ground motion, the probability of failure is 0.1*0.02=0.002 in 50 years.

In this work the DBE ground motion is used as the mean system demand to maintain

consistency with ASCE-7. Since the DBE earthquake has 10% probability of exceedance in 50 years, the building collapse uncertainty given the DBE earthquake should equal 0.002/0.1=0.02, to ensure the same overall failure probability of 0.002 in 50 years. Thus the acceptable target reliability given a DBE earthquake equals $-\Phi^{-1}(0.02)$ whose value is 2.1. Therefore, using the DBE ground motion as the mean system demand, a target reliability of 2.1 provides the overall collapse probability in 50 years which is considered acceptable in FEMA P695. However, the target in this dissertation is set as 2.5 to maintain consistency with classical LRFD which recommends a target reliability of 2.5 for structural members, and to ensure a degree of conservatism to offset potential errors in scaling the MCE probability to a DBE event.

5.3 Target subsystem reliabilities calculated with general reliability sensitivity algorithm

In this section the reliability sensitivity analysis described in chapter 2 is performed from the building system to floor diaphragm and shear walls. It begins with a computation of sensitivities for the shear wall and diaphragm subsystems, followed by subsystem reliability modifications to reach the system reliability target.

The reliabilities of shear wall and diaphragm subsystems are calculated based on their actual expected demands and capacities, which are different from what is used in codes and standards, as described in the following paragraphs. The subsystem reliabilities are calculated by the general convolution methodology given in Equation 5.1.

Subsystem capacities C_{sys} for shear walls equal their displacement capacity P_{d3} (see Figure 6.6 for convention) at the point of softening initiation, which is equivalent to a 2.25% IDR for the 2.4 m X 2.7 m shear walls (most critical subsystem). Note that this is different from current design standard procedures that consider force capacity and demand for the lateral force

resisting system and provide resistance factors for the same, whereas in reality this is part of the ductile mechanism for which a displacement capacity is more important for ensuring adequate seismic performance. Subsystem capacities for floor and roof diaphragms are taken as their ultimate strengths as obtained from finite-element models verified experimentally. Again, these are different from code-specified nominal capacities for these systems.

Both shear wall and diaphragm demands are taken as the mean values from non-linear dynamic analyses using 44 ground motions. The mean shear wall demand at the first floor of the building (the controlling case) is equal to the mean building IDR demand of 1.5%. The diaphragm mean demands are substantially different from code specified demands obtained using an ASCE-7 methodology, as discussed in chapter 6, Table 6.4. The mean demands are re-calculated for every new design point in the sensitivity analysis.

A reduced order sensitivity analysis (chapter 3) is performed by grouping all shear walls together, and the floor and roof diaphragm together, such that the system is represented as 2 main groups whose reliabilities are perturbed together, similar to what might be done during real building design. Subsystem reliabilities are modified by perturbing their force-displacement backbones as described in chapter 3. Within the shear wall group, the west level 1 2.4 m X 2.7 shear wall has the lowest reliability, as does the roof diaphragm in the second group. At each new design point (defined by modified subsystem reliabilities), the spring-based building model is analyzed under the effect of 44 far-field ground motions, which provide mean estimates of the shear wall IDR demand and diaphragm shear force demands, that can be convoluted with the corresponding subsystem capacity to obtain its subsystem reliability estimate. The table of sensitivity iterations is provided next, followed by a step-by-step description.

The reader is reminded from chapter 2 that the general set of steps in a sensitivity analysis is to identify the component m with highest reliability sensitivity $S_{\beta,m} = max\{S_\beta\}$, modify its reliability as $\beta^*_m = \beta_m + (\beta_{t,sys} - \beta_{sys})/S_{\beta,m}$, and move on to the next component, repeating until all reliabilities are as low as desired, controlling limit states are favorable and the system

reliability $\beta_{sys} = \beta_{t,sys}$.

Table 5.2: Reliability sensitivity analysis from the building system to the shear wall and diaphragm subsystems; the subsystem reliabilities are indicated as the minimum in the shear wall group ($\beta_{SW,min}$) and diaphragm group ($\beta_{diaphragms,min}$); DC indicates a discontinuity where the reliability sensitivities are indeterminate

Iteration Number	$\beta_{SW,min}$	$\beta_{diaphragms,min}$	S_{SW}	$S_{diaphragms}$	β_{sys}	$\beta_{t,sys} - \beta_{sys}$	β_m^*
1	1.3	1.3	1.3	0	1.1	1.4	2.4
2	2.5	1.3	0	1.7	1.9	0.6	1.7
3	2.5	1.6	DC	DC	2.4	0.1	–
4	2.5	2.1	1.3	0	2.4	0.1	2.6
5	2.7	2.1	–	–	2.6	-0.1	–

The algorithm begins (row 1 of Table 5.2) with subsystem reliabilities, sensitivities and system reliability for the base case design. Reliability sensitivity is 1.3 for shear walls and 0 for diaphragms because the controlling limit state is shear wall failure. The system reliability is 1.1 and the difference from the target of 2.5 is 1.4, which points to a target reliability $\beta_m^* = 2.4$ for the shear walls.

During iteration number 2, the shear wall backbone forces and displacements are increased by 40% to reach a subsystem reliability of 2.5 without modifying the diaphragms. The system reliability only increases to 1.9, and the sensitivity to shear wall reliability becomes zero, but is 1.7 for the diaphragm. The target reliability to reach the system target of 2.5 is calculated as 1.7.

In iteration number 3 the diaphragm backbones are perturbed by 10% to reach a subsystem reliability of 1.6 and a system reliability of 2.4. At this stage the system reliability sensitivity becomes discontinuous. Increasing the diaphragm reliability leads to a negligible change in β_{sys} as the limit state has shifted to the shear wall, whereas decreasing the diaphragm

reliability causes a step-decrease as the limit state shifts back to the diaphragm, followed by monotonic decrease in β_{sys}. Similarly, increasing the shear wall reliability leads to a step-decrease in system reliability as the limit state shifts to the diaphragm, and decreasing shear wall reliability causes monotonic decrease in β_{sys}. Thus this point represents a limit-state bifurcation point where the sensitivities are undefined.

In iteration number 4, the diaphragm limit state is eliminated by increasing the force-deformation backbone by 30% of its baseline, leading to a reliability of 2.1. The system reliability is 2.4, which is 0.1 less than the target of 2.5. The shear wall backbone is increased by 10% more to 150% of the base case, leading to a reliability of 2.7 and β_{sys} of 2.6. This is considered to be a converged solution and the iterations are stopped. Based on this, final reliabilities of 2.6 and 2.1 are recommended for the design of each individual shear wall and diaphragm.

5.4 Analyzing modifications to the system load-sharing network due to changes in subsystem reliability

Although the reliability sensitivity analysis converged in the above procedure, further analysis is performed to obtain physical insight into what happens within the load-sharing network. As indicated in Table 5.2, the shear wall system has highest sensitivity, but its reliability cannot be directly increased to reach the system reliability goal (row 2) because the diaphragm sensitivity increases during this modification.The shear wall reliabilities are doubled next while holding diaphragm reliabilities at their base value, and incremental dynamic analyses are performed to understand the resulting effect on the load-sharing network.

5.4.1 Effect of perturbing shear wall reliabilities holding diaphragm reliabilities constant

Since the system reliability computed in section 5.1.2 was governed by failure of the lateral system, the first sensitivity effect studied is to double the force and displacement capacities of all shear walls, keeping the stiffnesses constant at each leg of the backbone, as shown in Figure 5.3.

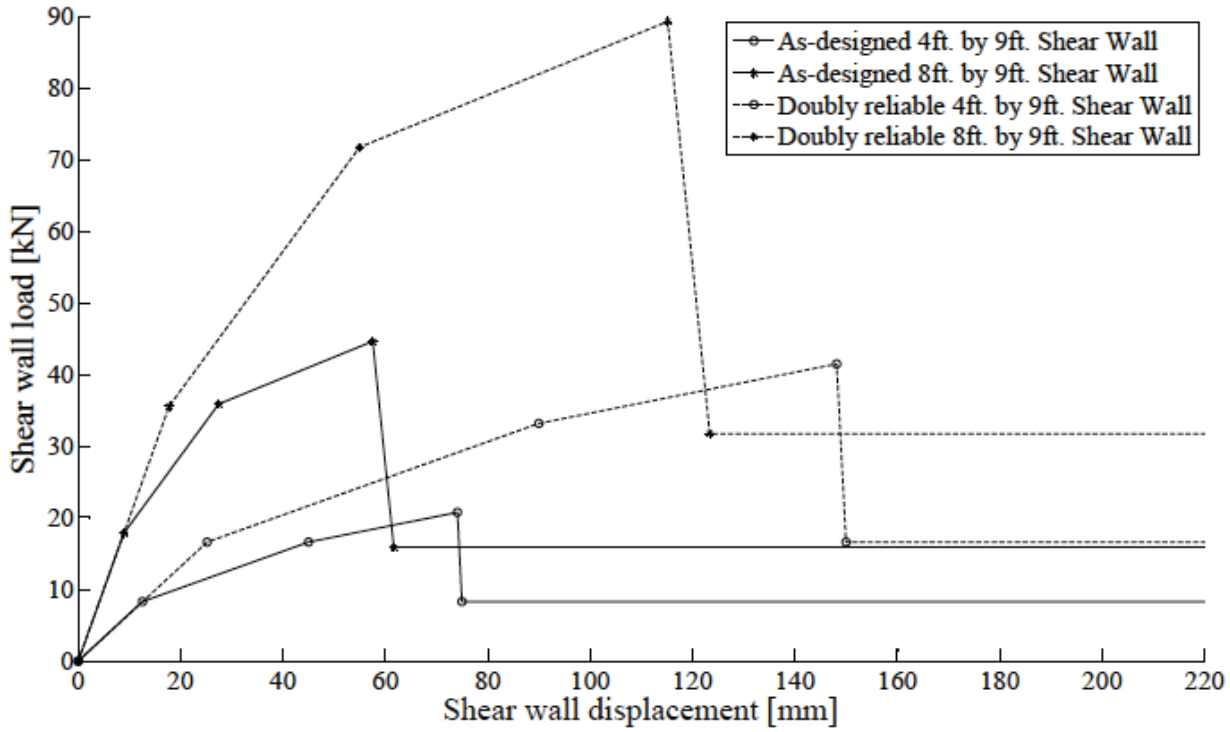

Figure 5.3: Modification of shear wall load-deformation backbone to double its subsystem reliability

The perturbation in shear wall reliability decreases the building capacity to 1.6% IDR with 3.1% C.O.V., with building capacity controlled by roof failure in every single simulation (Table 5.3). The capacity is lower compared to the base case due to increased force demands on the roof and floor diaphragms at the same level of building IDR demand (Figure 5.3).

This is also evident in the IDA curve for the Canoga Park ground motion shown in Figure 5.6.

Table 5.3: Comparison of building system capacity, demand and reliability for two different levels of shear wall reliability, holding diaphragm reliability constant at its base value 1.3

Shear wall reliability	IDR demand	IDR capacity	Building system reliability
1.3	1.5%	2.1%	1.1
3.8	1.2%	1.6%	1.0

As evident from Figure 5.6, the approximate reliability methodology assuming building failure at the onset of diaphragm failure is conservative, because the IDA plots do not indicate softening even after the shear capacities are exceeded. However for the scope of this dissertation, this additional reliability resulting from diaphragm ductility is ignored. The general methodology can be extended to include this either by directly using IDA for system reliability calculation, or by proposing load sharing relationships and failure criteria beyond diaphragm peak force capacity.

The results indicate that increasing the lateral system reliability without protecting the diaphragm lowers the overall building system reliability. One way to overcome this negative impact is to increase the force capacity of the diaphragm such that the controlling limit state remains shear wall failure. This is performed by using a blocked diaphragm configuration instead of the unblocked diaphragm, as discussed in the next section.

5.4.2 Effect of increasing diaphragm reliability by use of blocking, followed by perturbation in shear wall reliability

As described in chapter 6, the diaphragm response changes significantly from the blocked case (upper bound of perfect friction between panels) to the unblocked case (lower bound of

zero inter-panel friction). Figure 5.4 plots the load-deformation response for the floor and roof diaphragms showing its variation from the blocked to the unblocked case for each.

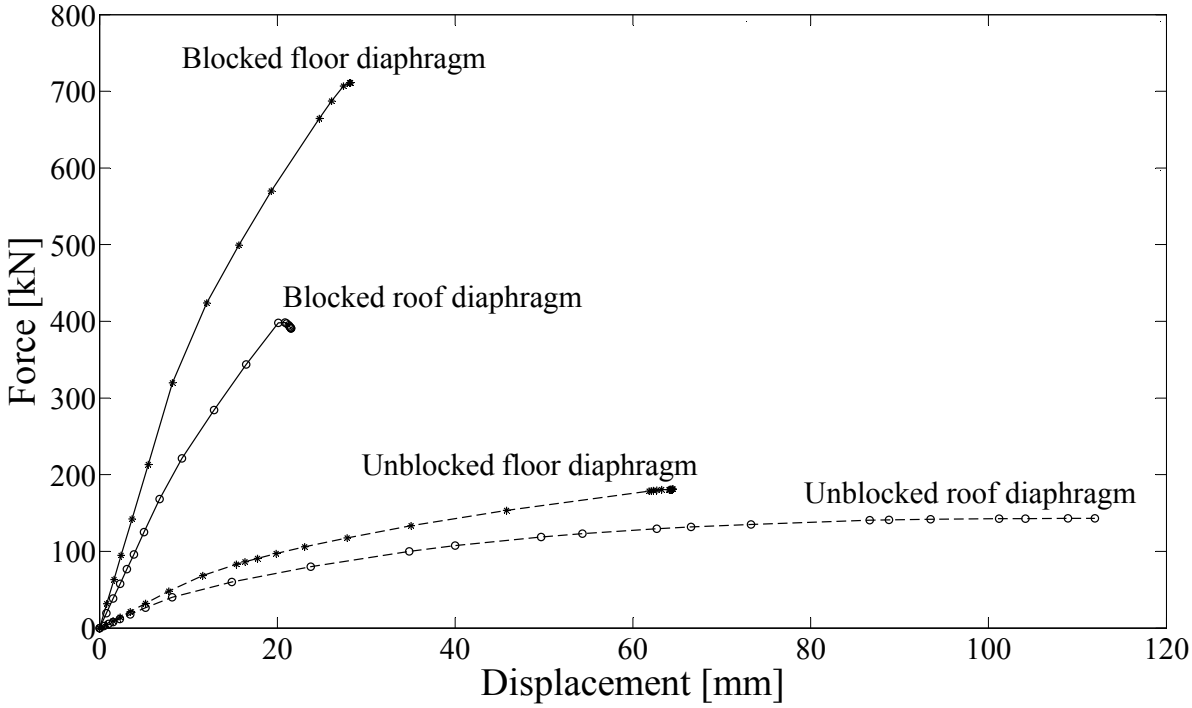

Figure 5.4: Load-deformation responses for floor and roof diaphragms with perfect inter-panel friction (similar to blocked configuration) and zero inter-panel friction (similar to unblocked configuration) showing the large increase in force capacity from the unblocked to the blocked case

The blocked diaphragm has a significantly higher force capacity for both the floor and roof, and therefore it might be used to obtain system reliability benefits using more reliable shear walls, without prematurely causing diaphragm failure before reaching shear wall deformation capacity is reached. The variation in building system reliability with shear wall reliability is plotted in Figure 5.5 for a building with blocked floor and roof diaphragms.

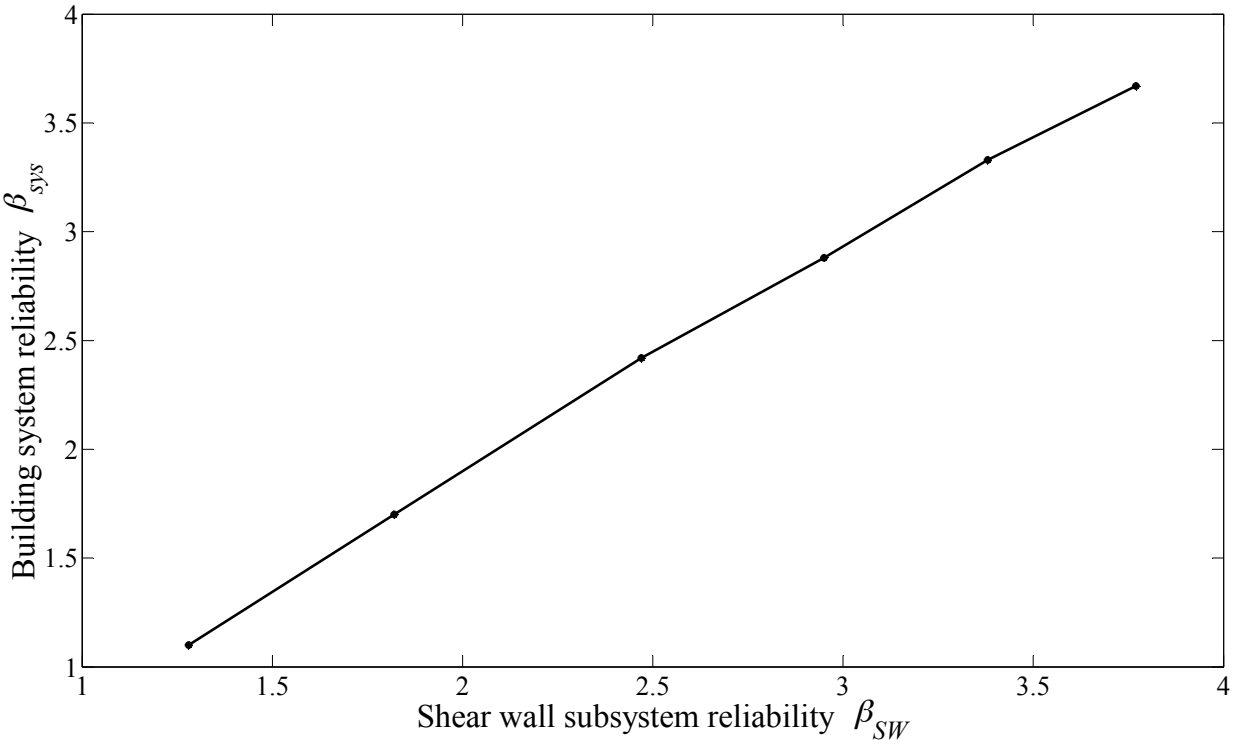

Figure 5.5: Variation in building system reliability with shear wall subsystem reliability for a building employing blocked diaphragm configurations at the floor and roof

The results indicate that reinforcing the shear wall subsystem can provide monotonic increase of building system reliability if the diaphragms have sufficient force carrying capacity (blocked configuration). Finally, incremental dynamic analysis plots are also shown in Figure 5.6 at the Canoga Park earthquake for a building with double the baseline shear wall reliability, and compared to a building system that has the same shear wall configuration but with unblocked floor and roof diaphragms. The results indicate that in the unblocked case, the roof diaphragm reaches its capacity before the full IDR capacity of shear walls can be developed, which leads to the vertical portion of the response on the left plot (see roof shear, unblocked, at the unblocked roof capacity). For the blocked diaphragm, the diaphragms continue to experience higher loads beyond this point, and the inter-storey drift ratio continues to increase.

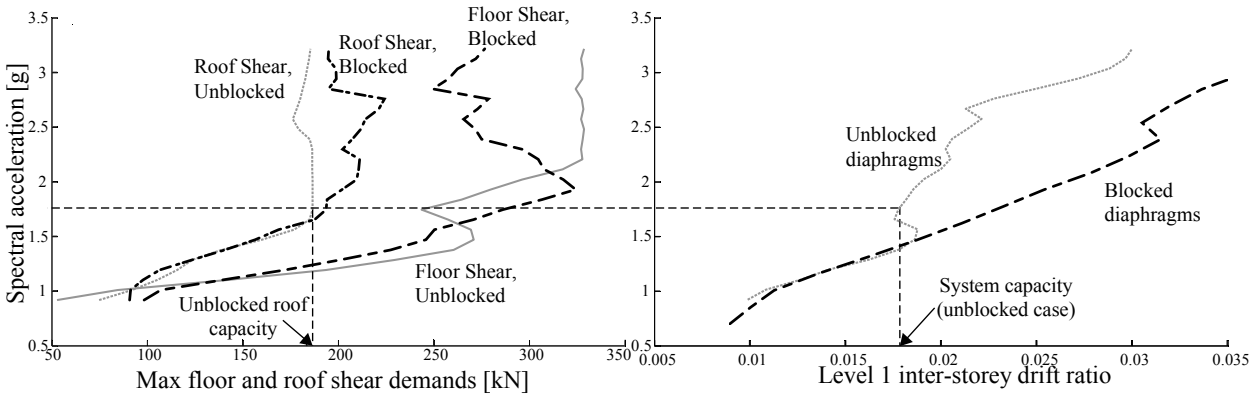

Figure 5.6: Spectral acceleration versus roof and floor shear, level 1 interstory drift, for building with doubly reinforced shear walls subjected to the Canoga Park ground motion, indicating roof diaphragm capacity reached before drift capacity of shear walls

5.5 Recommendations for cold-formed building design for seismic loads

System reliability analyses of the cold-formed steel building system subjected to seismic loads reinforced previous research findings showing that the building has a high as-designed reliability, not necessarily resulting from the design provisions (lateral force resisting system design) but due to reduction in design displacement demands by gravity and non-structural walls. The as-designed reliability (without considering the effect of non-structural elements) was found to be 1.1, whereas on considering experimentally observed demands on the building the reliability increased to 2.7, but this effect was ignored in this chapter

The building system reliability target was calculated as 2.5, conservatively chosen compared to a target of 2.1 obtained from calibration to a FEMA-P695 target recommended for the maximum considered earthquake. Reliability sensitivity analysis resulted in a shear wall reliability target of 2.6 and diaphragm reliability target of 2.1 to reach the building target reliability. It should be noted here that the sensitivity results are based on assumed subsys-

tem load-deformation changes described in Figure 5.3 which should be modified to reflect real changes in the design space (using different shear wall configurations) before being used in design standard applications.

The target reliabilities are derived here for a single prototype two story building, where the range of potential subsystems that can be used in the design of this building are covered by the reliability sensitivity perturbations. If all available subsystem modifications are considered in sensitivity iterations (different shear wall configurations, fastener sizes, other shear wall types such as strap braced shear walls, different diaphragm details), then a single prototype building is sufficient to provide recommendations for all two-story cold-formed steel buildings of similar geometry. For application to other design scenarios where such construction is employed, additional prototypes need to be considered, including different building sizes, aspect ratios, shapes and story heights. For new construction styles beyond the set of prototypes studied, a set of sensitivity analyses would first need to be performed before using subsystem reliability targets in design.

The subsystem reliability target of 2.6 is comparable to the building system reliability target of 2.5. The similar reliabilities result from the fact that the shear wall subsystems control building system failure, and the slightly higher value (2.6 vs 2.5) results from the assumed system reliability model, where the failure of the weakest shear wall is equivalent to building system failure.

5.5.1 Shear wall subsystem design using reliability sensitivity

As discussed in chapter 4, designated energy dissipation mechanisms in wood-sheathed shear wall systems are the sheathing-to-steel screw-fastened connections. The shear wall subsystem reliability target of 2.6 can be achieved by resizing the screw-fastened connection sizes and spacings such that they can provide adequate ductility, by performing a subsystem-to-component sensitivity analysis for shear walls.

Components and connections within the shear wall that are not part of the designated energy dissipating mechanism are designed to develop the force capacity of the shear wall. From a reliability sensitivity viewpoint, this would mean that the design of the system is such that all components other than the screw-fastened connections have zero reliability sensitivity within the shear wall subsystem. As the connections are made increasingly reliable and the shear wall subsystem reliability becomes greater, the force-controlled components will have non-zero sensitivity to the overall response, which should be overcome by making their component reliabilities adequately high. The final results of the shear wall subsystem sensitivity analysis will yield $\beta_{t,edm}$ and $\beta_{t,fc}$ for the energy dissipating mechanism and the force controlled component groups respectively such that the shear wall subsystem reliability $\beta_{SW} = 2.6$. Sensitivity analysis for the shear wall subsystem is beyond the scope of this dissertation.

Code specified capacities and demands are related to mean capacity and demand through bias factors B as described in chapter 2, which can be used to recommend appropriate resistance factors depending on the state-of-the-practice. For example, the strength resistance factors used on shear walls can be tuned to obtain required displacement capacity considering appropriate force-deformation models for these subsystems. As design codes change from one generation to the next, the bias and resistance factors may be updated accordingly; however, the actual subsystem and system reliabilities described here are independent of design standard assumptions.

5.5.2 Diaphragm subsystem design using reliability sensitivity

The reliability model used in this chapter (Figure 5.2) results in premature building failure at roof diaphragms when using the base-case unblocked diaphragms in conjunction with shear walls that have 4.2% IDR capacities. However IDA plots shown in Figure 5.6 indicate additional spectral acceleration capacity available after the roof diaphragm reaches its ultimate capacity. Explicit sensitivity analysis for the diaphragm-building interaction are not performed here, instead a diaphragm force-controlled reliability of 2.1 is recommended using

the approximate reliability model. This reliability is achieved by a diaphragm subsystem-to-component sensitivity analysis performed in chapter 7, using high-fidelity finite element models developed in chapter 6.

Chapter 6

Cold-Formed Steel Floor Diaphragm High-Fidelity Modeling and Component Reliability

In this chapter a high-fidelity finite element (FE) model of the as-designed 7010 mm X 15164 mm NEES building second floor diaphragm subsystem is developed using the commercial finite element software ABAQUS [21]. Several computation studies have previously been conducted for CFS building components and systems. Computational modeling that captures elastic buckling and non-linear collapse response for CFS members are discussed in [91]. Recent research has characterized CFS components and connections as non-linear hysteretic springs including cyclic strength and stiffness degradation that could be utilized in high fidelity finite element models or efficient numerical simulations [76, 24].

System level computational models have been developed for CFS shear walls at various fidelity levels. The most basic model considers a subsystem as a single hysteretic spring [8]. Some higher fidelity models utilize the fact that deformations are primarily concentrated at connection locations [8, 26, 75] and include full non-linear force deformation relationships for the fastener elements with simplified assumptions for other components – rigid panels,

beam-column elements for framing and springs for member-to-member connections and hold-downs. Non-linear finite element models have been developed for shear wall subsystems with framing members modeled as shell elements, sheathing as rigid plates, fasteners as non-linear springs and rigid couplings for hold-downs [72]. Full building finite element models have also been developed with equivalent spring elements for the panel-framing combination [63]. The finite-element models developed in this research builds on the existing modeling protocols by meshing the structural members (joists, tracks, sheathing, clip-angles, blocking and strap-bracing) into shell finite-elements, with the screw connections attaching them modeled as non-linear springs.

The model described here for cold-formed steel floor diaphragm sub-systems uses thin shell element meshing for all floor components – sheathing, joists, tracks, clip angles, blocking and strap bracing, whereas screw fasteners are modeled as non-linear spring elements. Geometrically non-linear analysis is performed with fastener elements updating their orientations as adjacent floor panels pull apart or bear against each other. The fasteners are characterized as non-linear backbones with an initial elastic branch, a second plastic branch, followed by two softening branches, based on recommendations provided in [45] using single shear experiments conducted at Virginia Tech. Boundary conditions are carefully modeled to include framing details,with the diaphragm attaching directly to ledger framing inside the shear walls. The diaphragms are loaded monotonically in their own plane with uniform body forces applied to the sheathing to simulate seismic inertia.

The FE model lateral response is compared to recent experiments performed on quarter and full-scale diaphragms [74, 73, 67]. As the diaphragm is loaded to failure the screw-fastened connection elements experience highest demands and system level non-linearity originates primarily from their non-linear response. Fastener force demand vectors are documented for all sheathing to framing springs, from which their component reliabilities are estimated. The model is used in chapter 6 for stochastic Monte-Carlo simulations and system reliability analyses.

6.1 Description of diaphragm structural system

The structural system is the 2nd floor of the NEES building introduced in chapter 4 which was studied in full scale shake table experiments at Design Basis and Maximum Considered earthquake levels [78]. The as-designed specifications for the system including joist, panel and fastener layouts, joist to track clip angles, blocking and strap bracing are adopted from design documents created by professional structural designers [61], and the diaphragm plan view is shown in Figure 6.1.

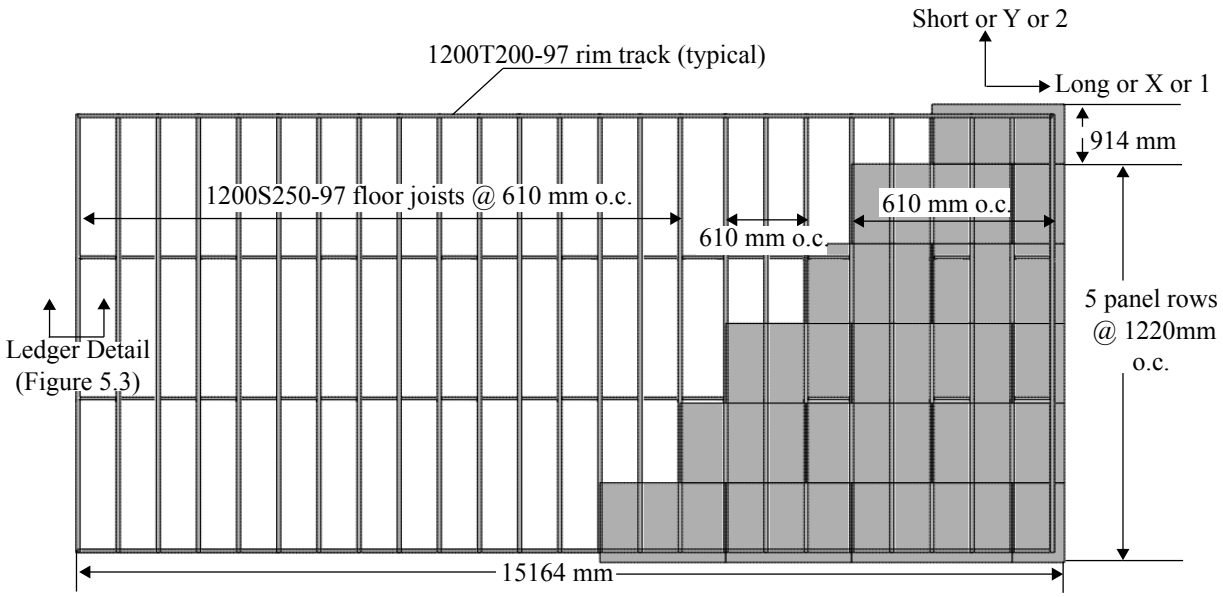

Figure 6.1: Plan view of structural system showing panel layout, floor joists, edge tracks, and edge supports that represent the lateral force resisting systems (gravity and shear walls)

The structural panels chosen were CD-CC structural oriented strand boards (OSB), each with dimensions 1200 mm by 2400 mm by 18 mm thick, arranged in a staggered configuration and fastened to supporting cold-formed steel joists (Figure 6.1). The wood sheathing connects to the underlying joists with number 10 hex head steel self-tapping and self-drilling screw fasteners (4.7 mm diameter). The fasteners are spaced at 152 mm around the diaphragm perimeter, penetrating the wood panel and rim tracks. The fastener spacing, 152 mm at

the diaphragm edges and 305 mm in the field of the diaphragm where the joists support the sheathing, is selected based on AISI-S400-15, Table F2.4-1 [9]. Cold-formed steel joists are 1200S250-97 [13] lipped Cee sections where the 1200 means a 12 inch (305 mm) out-to-out web depth, 250 means a 2.50 inch (63.5 mm) out-to-out flange width, and 97 corresponds to a base metal thickness of 2.56 mm. The joist web is through-fastened to a 1200T200-97 rim track (i.e., unlipped Cee section) with clip angles that are 1.5 inch by 1.5 inch (38 mm by 38 mm), 11 inch (279 mm) deep, 54 mil or 1.43 mm base metal thickness. Alternate sets of joists are attached to 1200S162-54 blocking (1.43 mm base metal thickness) with 1.5 inch by 4 inch (38 mm by 102 mm), 10 inch (254 mm) deep, 1.43 mm thick clip angles at approximately 1/3rd and 2/3rd distance along their lengths. Joist and blocking bottom flanges are screw-fastened to 38 mm wide continuous straps of 1.43 mm thickness. The joist and track yield stress and ultimate stress are 345 MPa and 450 MPa respectively [10]. Blocking or strapping is used to transfer shear forces across OSB panel boundaries in blocked diaphragms; in this work geometrical details corresponding to the full scale building experiments was considered (Figure 6.2), which does not satisfy code requirements for a fully blocked diaphragm.

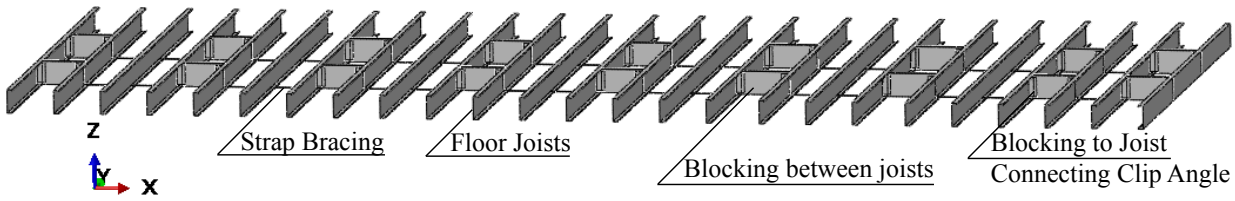

Figure 6.2: Blocking and strap bracing used to connect adjacent joists for lateral support mimicking detailing used in full scale building tests.

Typical building design practice is to carefully detail the vertical elements that comprise the lateral force resisting system (LFRS) which provide stiffness and strength against lateral loads. This gives rise to differential movement between the diaphragm and the LFRS that is resisted at the load transfer points. In the floor being studied here, the ledger framing detail (Figure 6.3) is used such that the sheathing attaches to the shear wall tracks directly. This detail plays a crucial role in determining diaphragm stiffness and load carrying capacity

because it comprises the critical load path which transfers inertial forces from the diaphragm to the lateral force resisting system, as explained in section 6.5. The critical fastener groups, called out in Figure 6.3, include number 10 screws connecting the wall track to sheathing and wall studs to edge joists that are not considered in the design code, in addition to sheathing to joist connections governing design capacities discussed in chapter 4. These connections govern the floor response to lateral loads and are characterized carefully using single component experiments.

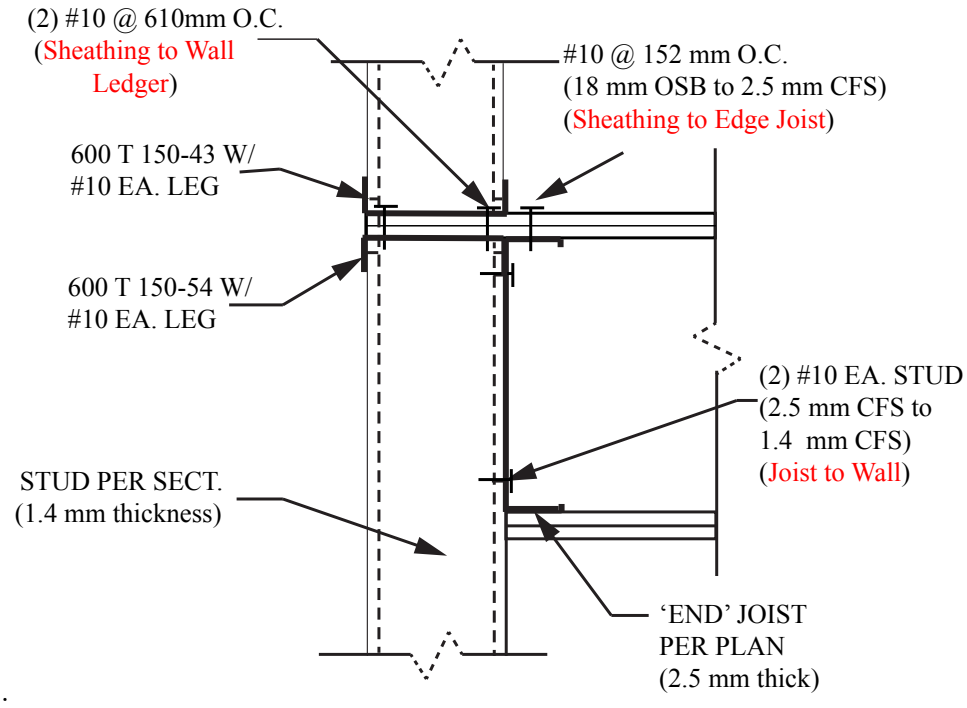

Figure 6.3: Ledger framing detail where the floor frames into the short-direction shear walls (section Ledger Detail in Figure 6.1) - note how the sheathing is sandwiched within the wall ledger providing a direct load path from the walls for ground motions

6.2 Screw-fastener shear response characterization

Nonlinearity in the diaphragm load-deformation response comes primarily from fastener behavior at the edges. These include the fastener groups described in section 1 connecting sheathing to wall, sheathing to edge joists, and joists to wall studs, according to the ledger framing details shown in Figure 6.3. Connection strength in cold formed steel construction depends on joist, sheathing and fastener properties and thicknesses [79]. Current code recommendations, (chapter 4) predict a nominal strength of 1.2 kN for diaphragm fasteners independent of sheathing and joist thicknesses which is inconsistent with engineering intuition. Therefore this section characterizes the connections as multi-linear backbones (inspired from [45]) using single-component shear experiments. The backbones have an initial elastic branch, followed by strain hardening, softening and failing branches. The multi-linear backbone parameters, described in Figure 6.4, include the peak strength F_c, the cap deformation δ_c, yield strength and deformation F_y and δ_y, failure load F_r and deformation at failure δ_r, and initial, hardening, softening and residual stiffness K_e, K_s, K_c and K_r

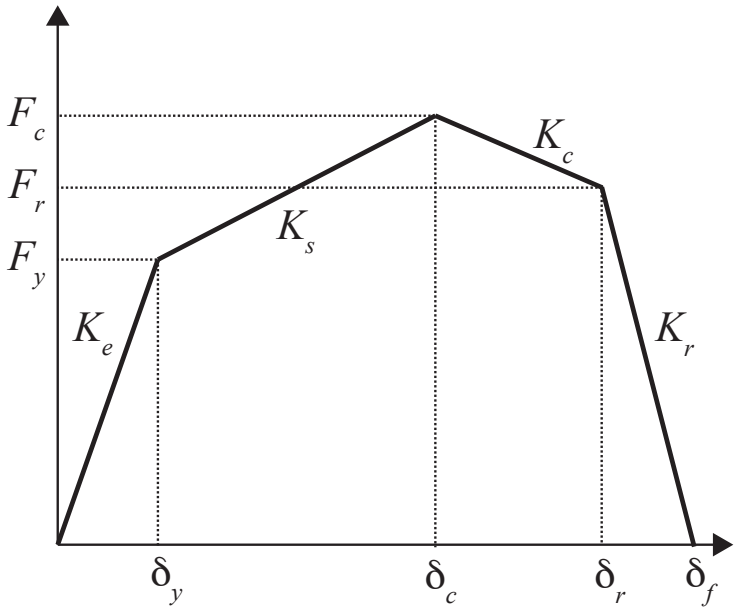

Figure 6.4: Multi-linear backbone parameters for characterizing fastener elements as quadri-linear springs in finite element models based on recommendations from [45]

6.2.1 Sheathing-to-joist connections

The 18 mm thick OSB sheathing is connected to 97 mil (2.5 mm) joists by number 10 screw fasteners. This connection configuration is tested and characterized by single shear experiments. The test configuration, shown in Figure 6.5 (inset), is described in detail in [68]. Each test specimen is a 152mm by 203 mm OSB segment attached to 152 mm by 254 mm CFS plate with a single number 10 fastener, 51 mm from the ply edge. The bottom ply is bolted to a fixed aluminum bracket and the OSB is sandwiched and bolted between two aluminum brackets to transfer load from the crosshead. The experiments were conducted with an MTS testing machine using a crosshead displacement rate of 0.025 mm/sec. Applied force to the fastener was measured by a 150 kN load cell with an accuracy of 0.1 kN. Relative displacement between the two plies was measured using a non-contact optical measuring system that was developed and validated at Virginia Tech [68]. This comprised four red

sticker targets, tracked at a rate of 30 frames per second using a Microsoft Lifecam cinema HD 720 p video camera, and MATLAB [64] image-processing custom code provided in [82]

Fastener load-deformation response for each of the 12 tests is nonlinear from the onset as shown in Figure 6.5 as the fastener cuts and tilts through the wood sheathing. In all tests, the screw failed in shear and the load dropped to zero. The primary source of connection load-deformation variability comes from the orientation and density of wood strands in the OSB sheathing surrounding the fastener.

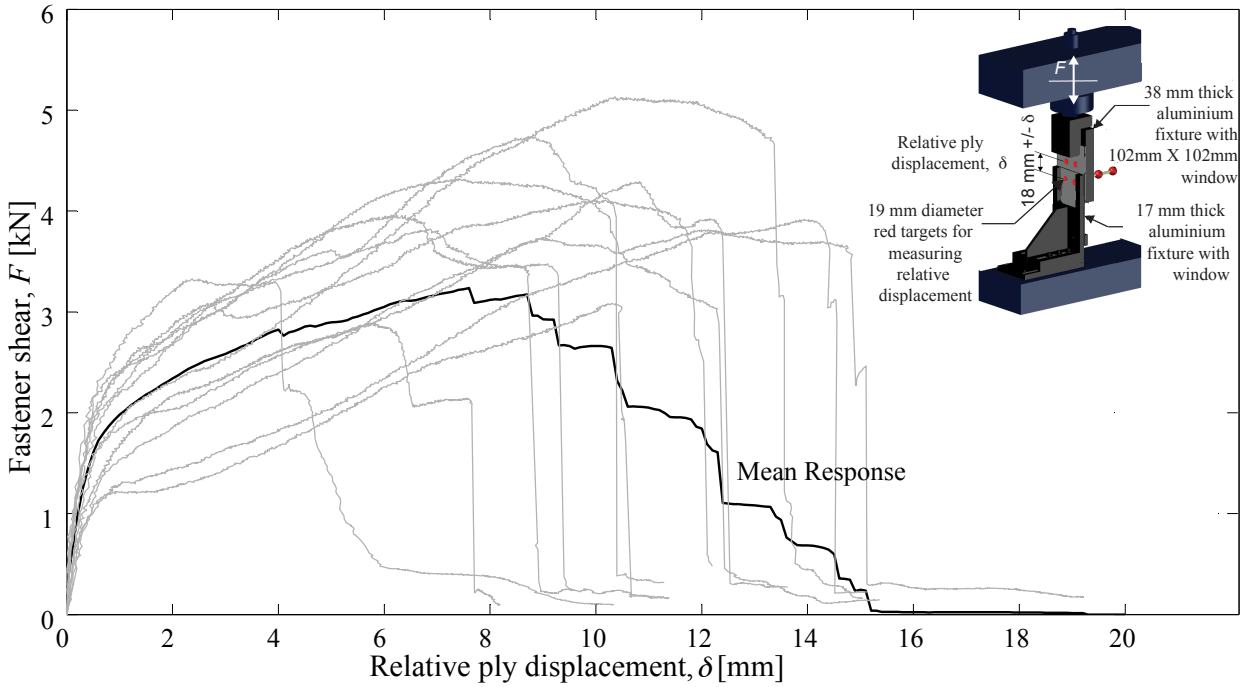

Figure 6.5: Load displacement plots for 12 monotonic single shear tests with inset detail showing test setup including OSB and CFS plates, aluminimum brackets and optical targets for measuring relative displacement

Table 1 lists results for each of the 12 tests. The mean tested strength μ_{Vtest} is 3.9 kN with a COV of 0.17. The average displacement at component failure (Δ_{test}) is 11 mm. These values are used to calibrate probabilistic fastener force-deformation models that are used in reliability analyses. Mean strength μ_{Vtest} is more than thrice the code recommended

nominal strength V_n (3.9 kN vs 1.2 kN) which highlights the inherent overstrength in the current AISI-S400-15 conservative prediction method

Table 6.1: Ultimate Capacity and Displacement at failure for twelve monotonic single shear tests plotted in Figure 4

Test Number	V_{test} (kN)	Δ_{test} (mm)
1	3.9	14
2	4.1	12
3	4.0	8.7
4	5.1	13
5	2.9	6.3
6	4.7	10
7	3.3	4.0
8	4.3	10
9	3.8	15
10	3.8	9.3
11	4.3	12
12	3.1	10

Backbone parameters for the sheathing to framing fasteners (number 10 fastener, 1200S250-97 joist, and 18 mm thick OSB) are derived from experimental force deformation relationships. Peak strength F_c is taken as the maximum force reached during the experiment, and cap deformation δ_c corresponds to force F_c in the force-deformation relationship. Residual force F_r is taken as the load at which failure first initiates indicating a sharp drop in force. Final deformation δ_r corresponds to F_r in the force-displacement plot, and it is assumed that the force drops to zero at this point in the model corresponding to brittle failures observed experimentally (Figure 6.5). Yield force and deformation F_y and δ_y are obtained using the optimization routine *fminsearch* in MATLAB. The objective function to be minimized is set

as the total squared difference in force between the fitted bi-linear curve and the experimental results until peak force F_c is reached. The initial estimates for F_y and δ_y are set as $0.55F_c$, and deformation at $0.55F_c$ respectively. Maximum allowed evaluations and iterations for the *fminsearch* routine are both set at 5e9.

6.2.2 Joist-to-stud connections

Joist-to-stud and track-to-stud fastener backbones (number 10 fastener, 2.5 mm steel to 1.4 mm steel) are obtained from recommendations provided in [68], using general expressions for force and stiffness that model the two plies as springs in series, $F = \alpha\psi^{\beta}P_{ss} \leq P_{ss}$ and $K = \alpha\psi^{\beta}(\frac{1}{E_1t_1} + \frac{1}{E_1t_1})^{-1}$, where $\psi = (\frac{P_{ss}}{t_1f_{u1}d})(\frac{P_{ss}}{t_2f_{u2}d})$, P_{ss} is the manufacturer reported fastener shear strength (8.16 kN for number 10 hex head fasteners), f_{u1} and f_{u2} are the ultimate tensile strengths of ply 1 and ply 2 obtained from tensile coupon tests (505 MPa and 493 MPa), d is the fastener diameter (4.75 mm), E_1 and E_2 are the elasticity moduli of ply 1 and ply 2 (203.4 GPa), and t_1 and t_2 are the thicknesses of ply 1 and ply 2 (2.56 mm and 1.43 mm). The parameters α and β are obtained using MATLAB function *fminsearch* by minimizing the error between model predicted and tested [68], and are provided for the different backbone parameters in Table 6.2. Final backbones are plotted in Figure 6.6 and parameters provided in Table 6.3

Table 6.2: Fastener backbone trendline parameters for strength and stiffness, number 10 fastener, 2.5 mm steel to 1.4 mm steel [68]

Backbone Parameter	α	β
F_y	1.37	-0.52
F_c	1.76	-0.46
F_r	1.52	-0.59
K_e	0.32	-0.80
K_s	0.013	-0.68
K_c	-0.035	-0.87
K_r	-0.52	-1.58

6.2.3 Track-to-sheathing-to-track double shear connections

The sheathing-to-wall connections act in double shear between 43 mil (1.1 mm) steel, 18mm OSB and 54 mil (1.4mm) steel with number 10 fasteners. Dedicated double shear experiments were not conducted for these connections. Design recommendations provided in AISI S100 chapter E [2] predicts connection strengths for both 43 mil CFS - 18 mm OSB and 18 mm OSB – 54 mil CFS as P_{ss} indicating that the governing limit state is screw shear failure. The connection backbones are therefore approximated with double the stiffness and strength of the OSB to Steel single shear backbones based on their two planes of resistance (Figure 6.6).

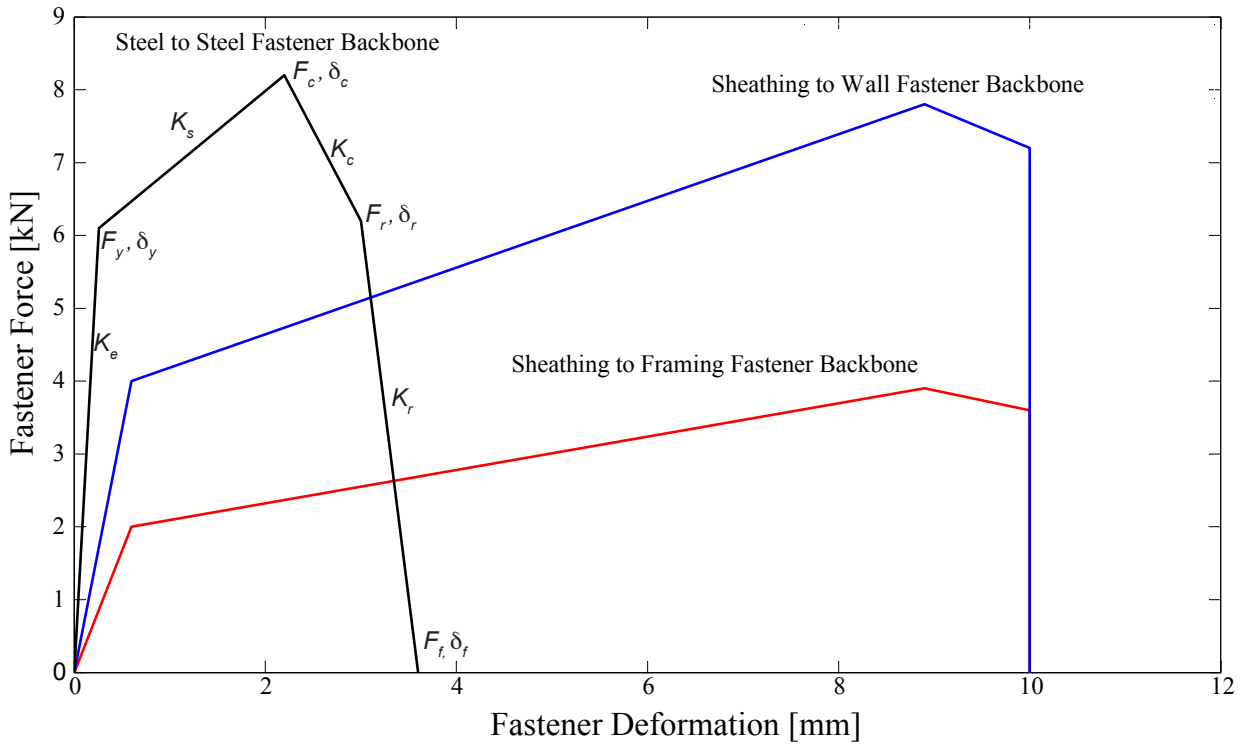

Figure 6.6: Final hysteretical backbones for critical fastener connections used as quadrilinear spring force deformation relations in FEM

Table 6.3: Hysteretic backbone parameters for critical diaphragm fastener connections used to characterize them as quadrilinear springs during FEM (forces in kN and stiffnesses in kN/mm)

	F_y	F_c	F_r	F_f	k_e	k_s	k_c	k_r
Sheathing to Wall	4.0	7.8	7.2	0	6.7	0.46	-0.55	$-\infty$
Sheathing to Edge Joist	2.0	3.9	3.6	0	3.3	0.23	-0.27	$-\infty$
Framing to Wall	6.1	8.2	6.2	0	23	1.1	-2.4	-12

6.3 Finite-element modeling protocol for cold-formed steel floor diaphragms

This section describes the finite element modeling protocol employed in ABAQUS [21] including mesh descriptions, material models, contact modeling and spring modeling.

6.3.1 Model geometry and material properties

Joists, tracks, panels, clip angles, blocking and strap bracing are modeled as ABAQUS S4R elements – a 4 node linear shell element where R stands for reduced integration, meaning that the number of Gaussian integration points used to calculate the element stiffness matrix is decreased to improve computational efficiency and avoid shear locking. The S4R element converges to plate buckling solutions at lesser elements per half-wavelength than the S4 element, which uses more Gaussian integration points (stiffer element, better accuracy) and experiences membrane locking at less than 2 elements per half-wavelength [69]. ABAQUS also provides the option to use quadratic shell elements (S8R, S9R5) that capture buckling deformations more accurately with a coarser mesh compared to linear elements [69, 91]. However, these elements ignore changes in thickness with deformation and are inaccurate at finite strains [21]

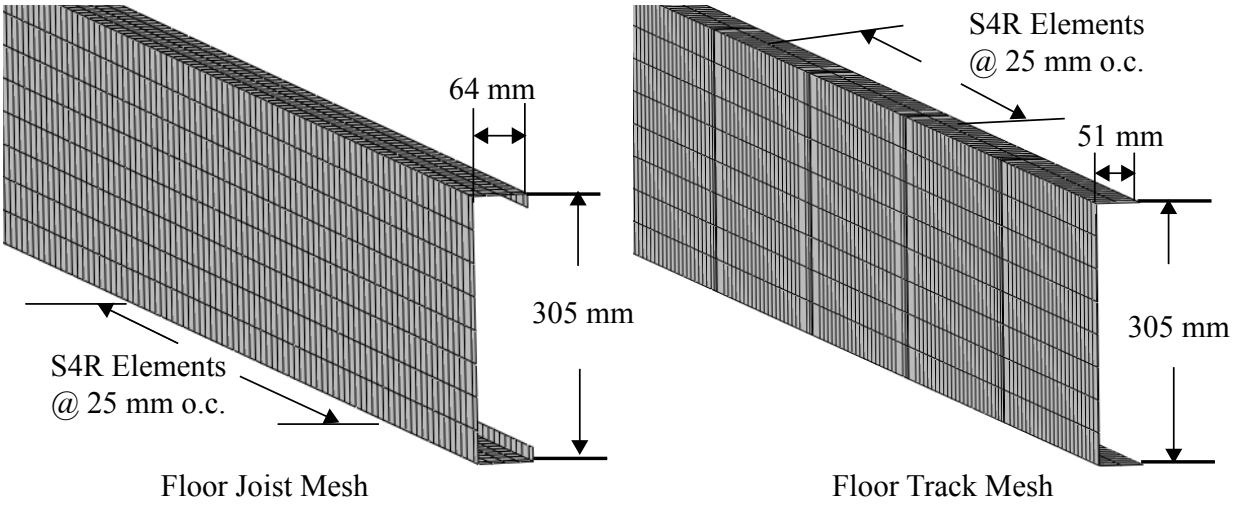

Figure 6.7: CFS joist and track finite element meshing with selective refinement for clip angle attachment locations

Mesh densities for joist and tracks are described in Figure 6.7. Rounded corners at flange-web and web-lip intersections are not modeled. The mesh is selectively refined depending on the floor layout to provide attachment points for fasteners. Initial geometrical imperfections are not modeled because loading imperfections are adequate to trigger inelastic buckling. The element size is 1in. (25 mm) along the length of the member, a sinusoidal buckled half-wavelength of 12in. (305 mm) will be linearly interpolated across 12 nodes, which is typically adequate for global, local distortional buckling modes. Except where the mesh is selectively refined to provide fastener-attachment points, the unstiffened elements at joist flange edges (lips) have the highest aspect ratio (4.8:1), which is well within the recommended limit of 8:1 [6]. This limit was proposed for S9R5 elements and is used here for S4R elements since both elements perform comparably at this range at least for stiffened elements [6].

Panels are meshed as S4R elements with typical aspect ratio 1:1, except where the mesh is selectively refined to provide attachment points to underlying framing. Mesh densities for joist to track and joist to blocking clip angles, block sections and strap bracing are selectively refined depending on fastener attachment points.

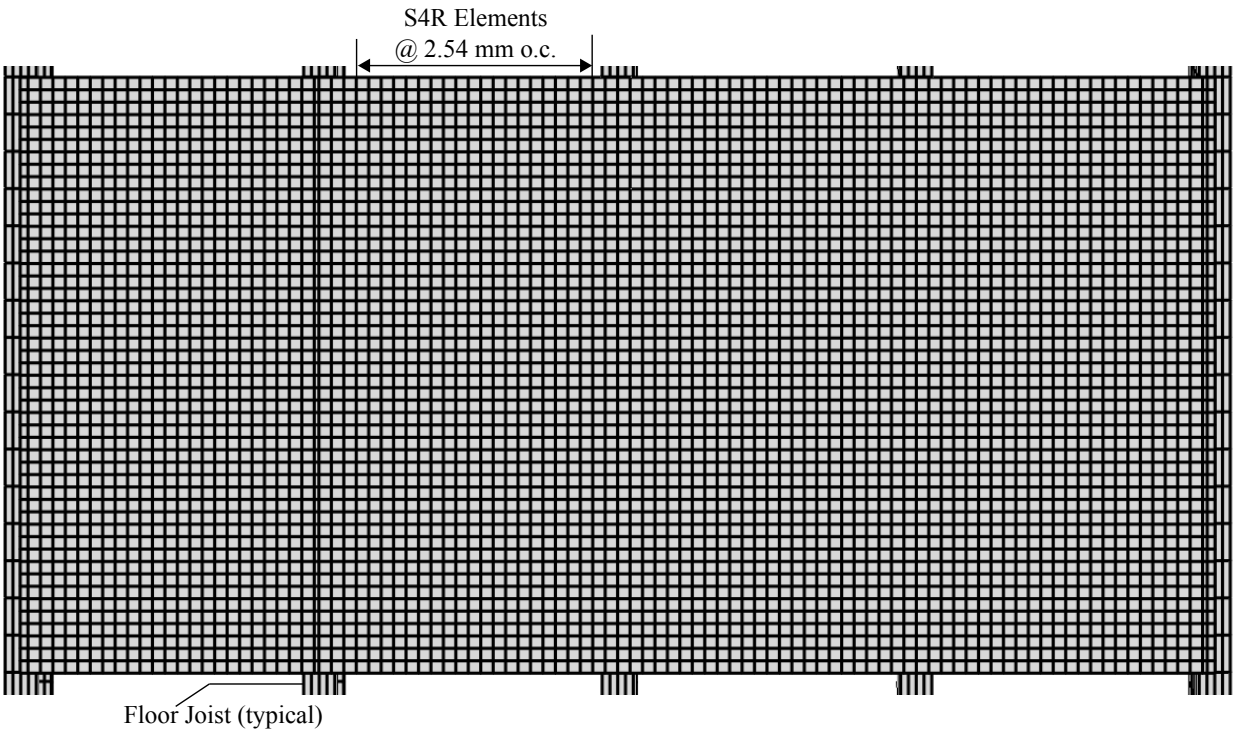

Figure 6.8: Typical finite element meshing for floor panel with selective refinement for fastened connections to underlying framing (floor joists and ledger track)

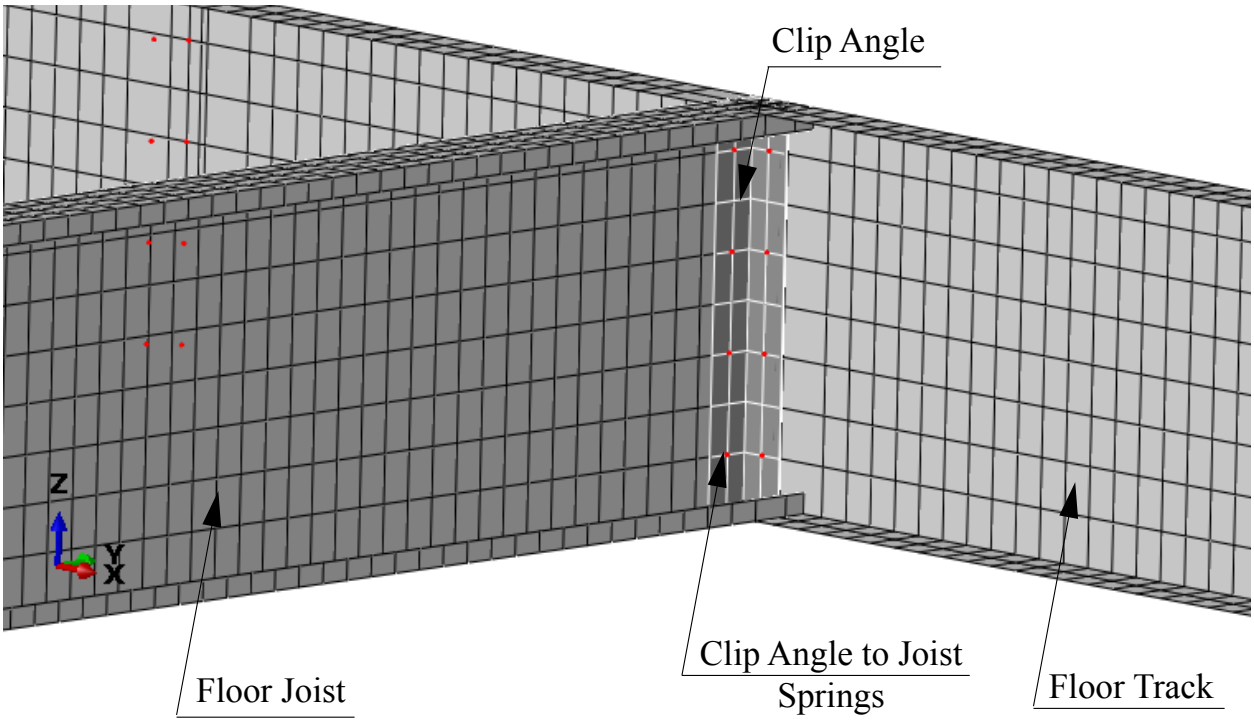

Figure 6.9: Finite element mesh for joist to track clip angles with attachment points for screw fasteners (spring element locations) shown in red

Blocking is used in the floor system at approximately 1/3rd and 2/3rd the joist length to restrict lateral deflection between joists in the arrangement shown in Figure 6.2. Strap bracing is used to provide a continuous connection between the bottom flanges of all the joists. The joists connect to the blocking through clip angles, as shown in Figure 6.10. Contact is modeled between the clip angle and the block as well as discussed in section 6.3.3.

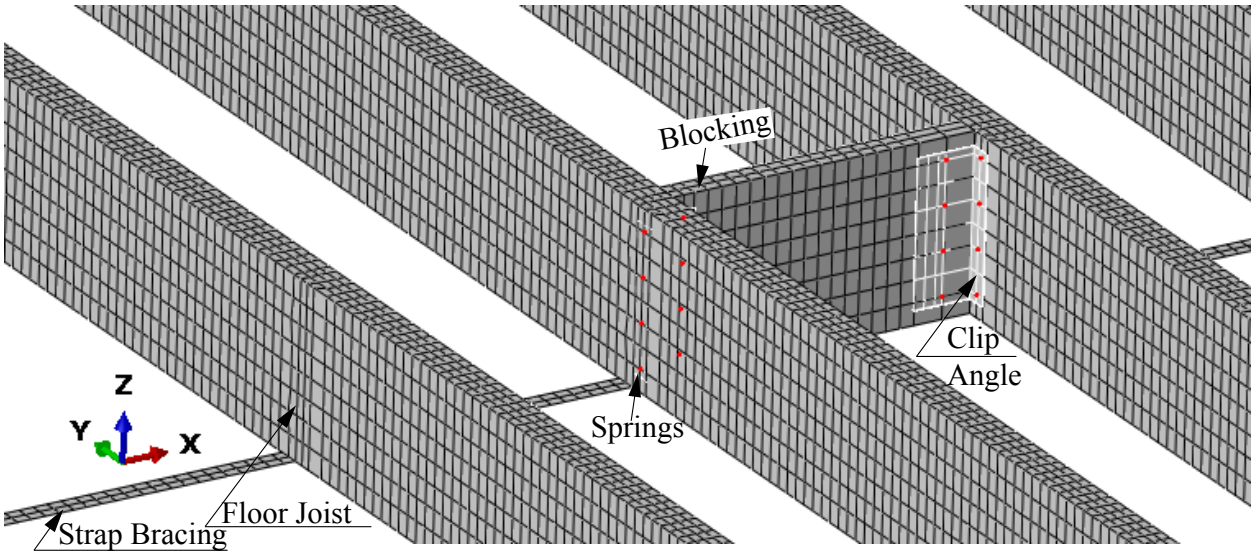

Figure 6.10: Finite element mesh for blocking, strap bracing and blocking to joist clip angles, with attachment points for screw fasteners (spring element locations) shown in red

The material elasticity modulus for CFS is assumed as 203 GPa. Plasticity is modeled using the *Plastic command in ABAQUS, assuming the yield stress to be 400 MPa and the plasticity curve as provided in [69]. The OSB is modeled as isotropic with an elastic modulus of 2.4 GPa and Poisson's ratio of 0.30. This is based on shear modulus recommendations provided in the International Building Code [46] Table 2305.2.2 for rated OSB sheathing. The fastener connections are modeled as a combination of shear springs and axial couplings as discussed in the next section.

6.3.2 Screw-fastened connection modeling for monotonic response

Sheathing-to-track and sheathing-to-edge-joist screw connections are modeled as ABAQUS materially non-linear SpringA elements for in-plane (shear) response and coupling constraints for out-of-plane (axial) response. In geometrically non-linear analyses, SpringA elements develop internal forces as a function of the difference between their deformed and initial (undeformed) lengths. Owing to the fact that the spring is capable of rotating, the initial

length of the spring must be negligibly small so that the difference between original and deformed lengths equals the shear deformation. This is shown in Figure 6.11

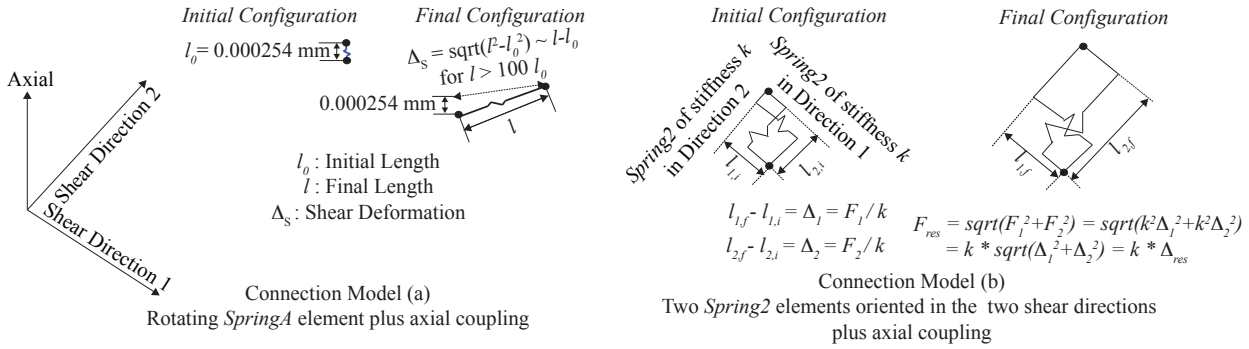

Figure 6.11: Modeling of screw fasteners in the floor as a combination of axial couplings and SpringA elements or two Spring2 elements

While the SpringA element is capable of updating its orientation during the course of the solution akin to screw fastener behavior in a real structural system, it poses a geometrically nonlinear problem to the finite element solver, and in the case of the floor diaphragm subsystem which has more than 2000 fastener elements, convergence problems can easily arise. An alternate to using the SpringA element is to use two mutually perpendicular Spring2 elements as shown in Figure 6.12. The two elements respond independently and can accommodate different forces without needing to update their line of action, such that the resultant force acts along the line of action of the rotated fastener.

The following study demonstrates results of modeling a connection between two nodes as either a single SpringA element of varying initial lengths, or as a pair of mutually perpendicular Spring2 elements.

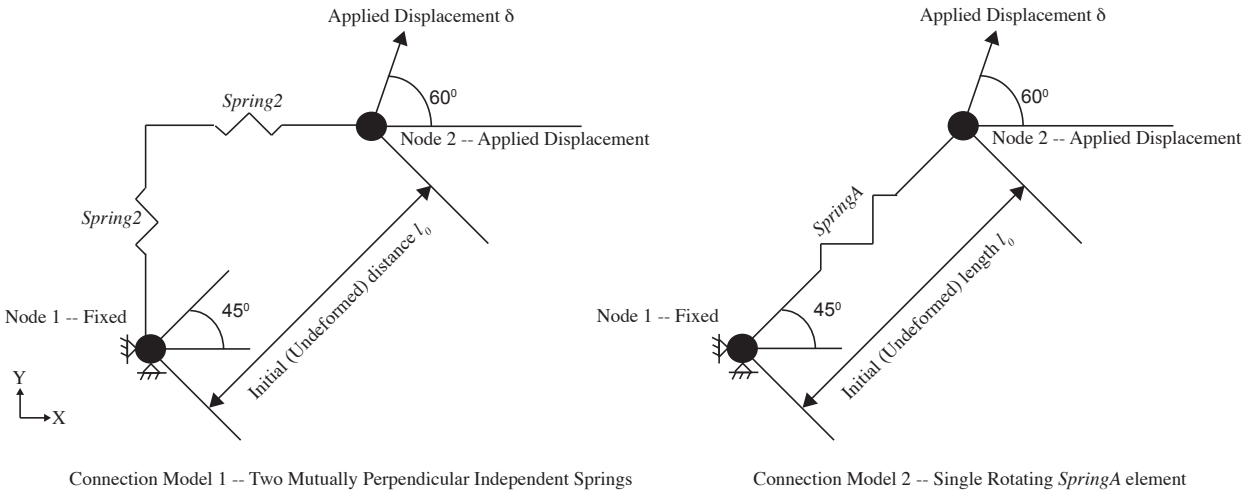

Figure 6.12: Modeling of screw fasteners in the floor as a combination of axial couplings and SpringA elements or two Spring2 elements

Force deformation relationships are plotted for the various springs as a function of spring length and compared with the input backbone parameter. The coupled Spring2 pair acts independent of the initial length, matches the initial response until the first change in stiffness and then overpredicts the response. This element is thus appropriate only in cases where the spring acts within the first leg of the response. The SpringA pair captures the actual response well when the initial length is lower than 0.0254 mm which is approximately the displacement at which the first stiffness change takes place.

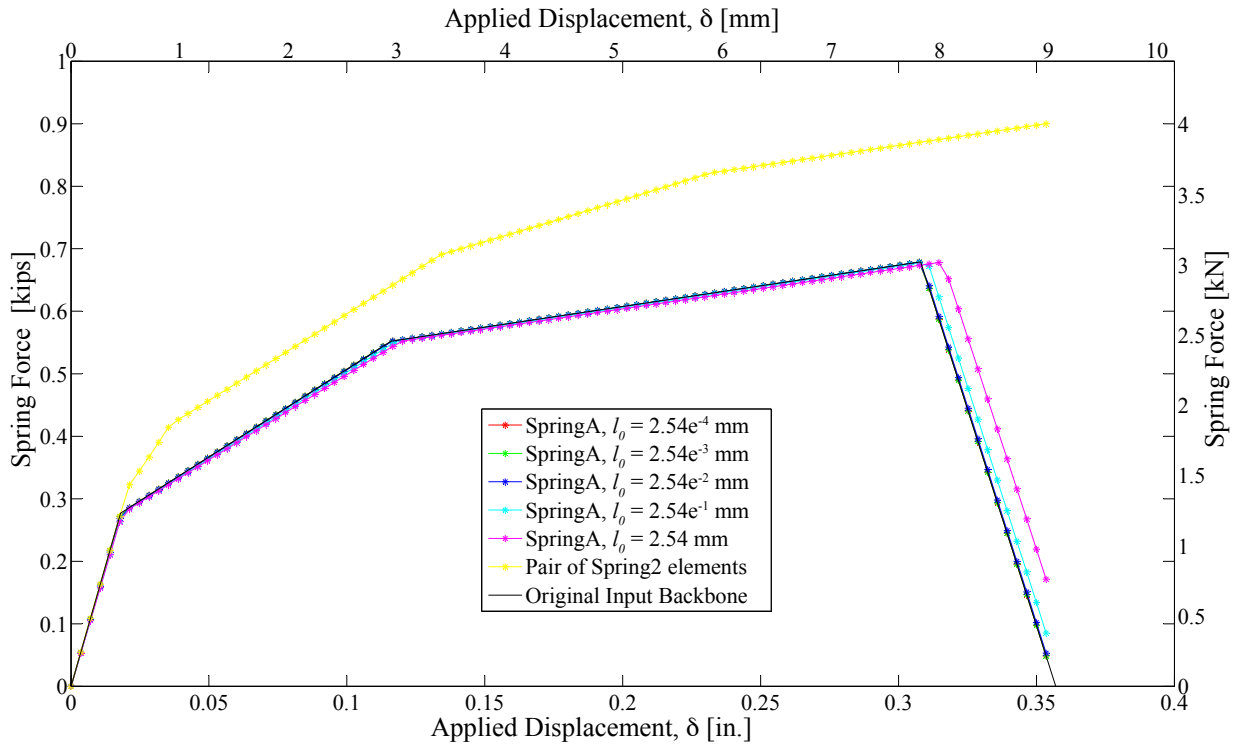

Figure 6.13: Force deformation relationships for Figure 6.12 case study in SpringA elements with varying initial lengths and a pair of Spring2 elements

ABAQUS has difficulty converging when only SpringA elements are used in this floor model. This is overcome by running an elastic analysis with Spring2 elements, setting the initial orientations of all springs on that basis and then running a new analysis with SpringA elements. Since the initial orientations match the first trial solution, the program is then able to converge.

Screw fasteners connecting clip angles and straps to structural elements (joists, tracks or blocking) are modeled as elastic Spring2 elements in ABAQUS with a spring stiffness 18 kN/mm because they do not experience sufficient demands to trigger non-linear response. All other fasteners, i.e., sheathing to joist, sheathing to track, sheathing to wall, joist to wall stud and track to wall stud connections are modeled as nonlinear ABAQUS SpringA elements in the fastener shear plane and axial couplings in the out-of-plane direction. The

SpringA elements are assigned quadrilinear force deformation relationships as described in Figure 6.6 and Table 6.3.

6.3.3 Wood sheathing panel-to-panel contact modeling

Contact is modeled along all panel edges (seams) to prevent adjacent panels from penetrating into or sliding against each other. This is achieved using 2 sets of springs running parallel (frictional) and perpendicular (penetration) to seam boundaries. Contact spring locations are shown in Figure 6.14. Frictional springs are rigid while penetration springs are bi-linear with infinite stiffness in compression and zero stiffness in tension. Contact is also modeled between clip angles and blocking sections (Figure 6.10) using the same protocol (compression and frictional springs).

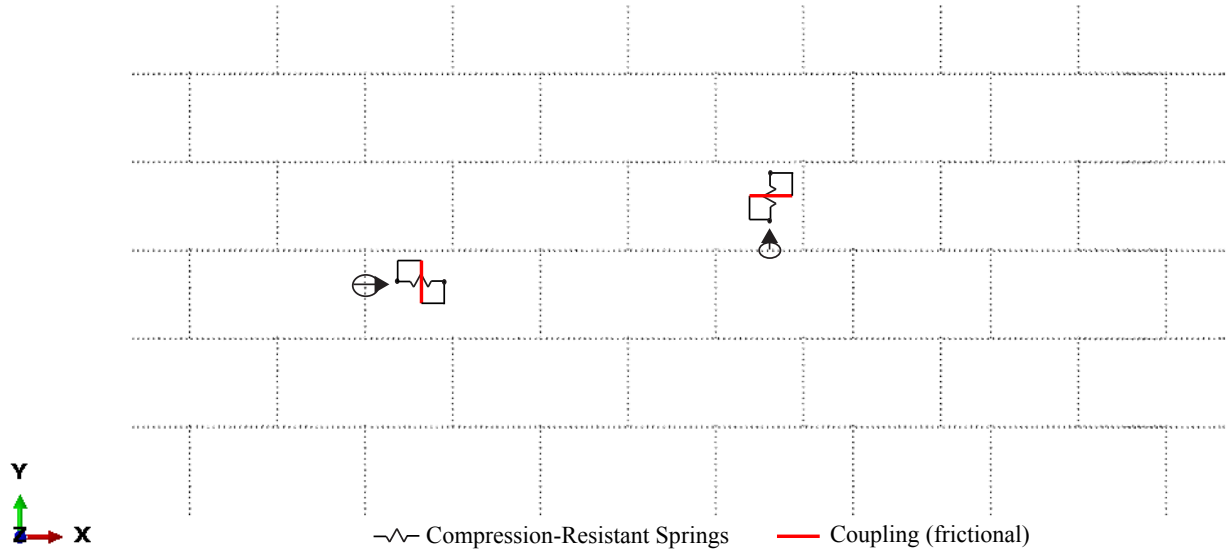

Figure 6.14: Springs that model panel-to-panel contact along all seam edges

Recent experimental results [73, 67, 74] indicate that frictional coupling between panel seams is high in blocked diaphragms due to support from underlying steel blocking through fastened to the panels. However in unblocked diaphragms where panel seams are unsupported, the

frictional coupling is minimal, allowing the panels to slide relative to one another. Therefore an unblocked diaphragm configuration was also modeled using ABAQUS, and the comparative model-to-predicted responses described below will further elucidate the role played by these frictional springs at panel seams.

6.3.4 Model solution algorithm and boundary conditions

The Riks solution algorithm (*STATIC, Riks in ABAQUS) was used for diaphragm pushover analyses with point loads distributed across the diaphragm to simulate inertial forces in the short (weak) direction (DOF 2 or Y, see Figure 6.1). Boundary conditions are defined on a set of nodes (highlighted in Figure 6.15) to which boundary conditions are applied via the *BOUNDARY keyword in ABAQUS.

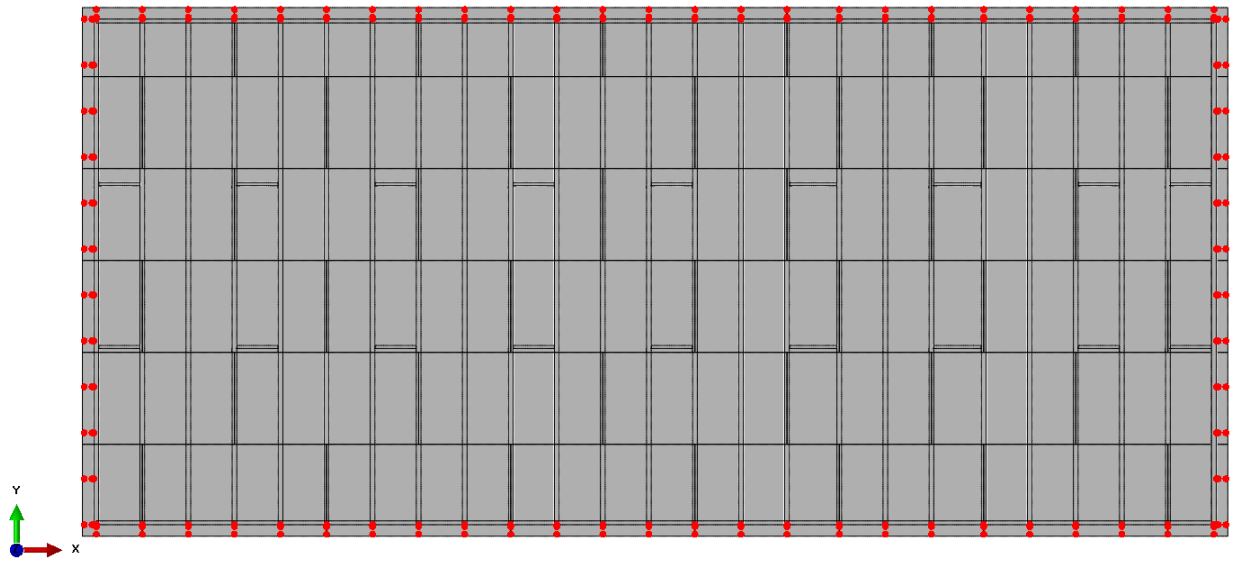

Figure 6.15: Diaphragm FEM model plan view with highlighted points representing boundary nodes indicating regions where boundary conditions are applied via ABAQUS keyword *BOUNDARY

The long-direction boundary nodes are restrained in the long direction (DOF 1 or X) while

the short-direction boundary nodes are restrained in the short direction (DOF 2 or Y) representing a case where the shear walls have infinite in-plane stiffness and negligible out-of-plane stiffness. All boundary nodes are also restrained in the vertical direction (DOF 3 or Z). The edge joists, tracks and sheathing connect to the boundary nodes via SpringA elements and axially rigid links as shown in Figures 6.16 and 6.17.

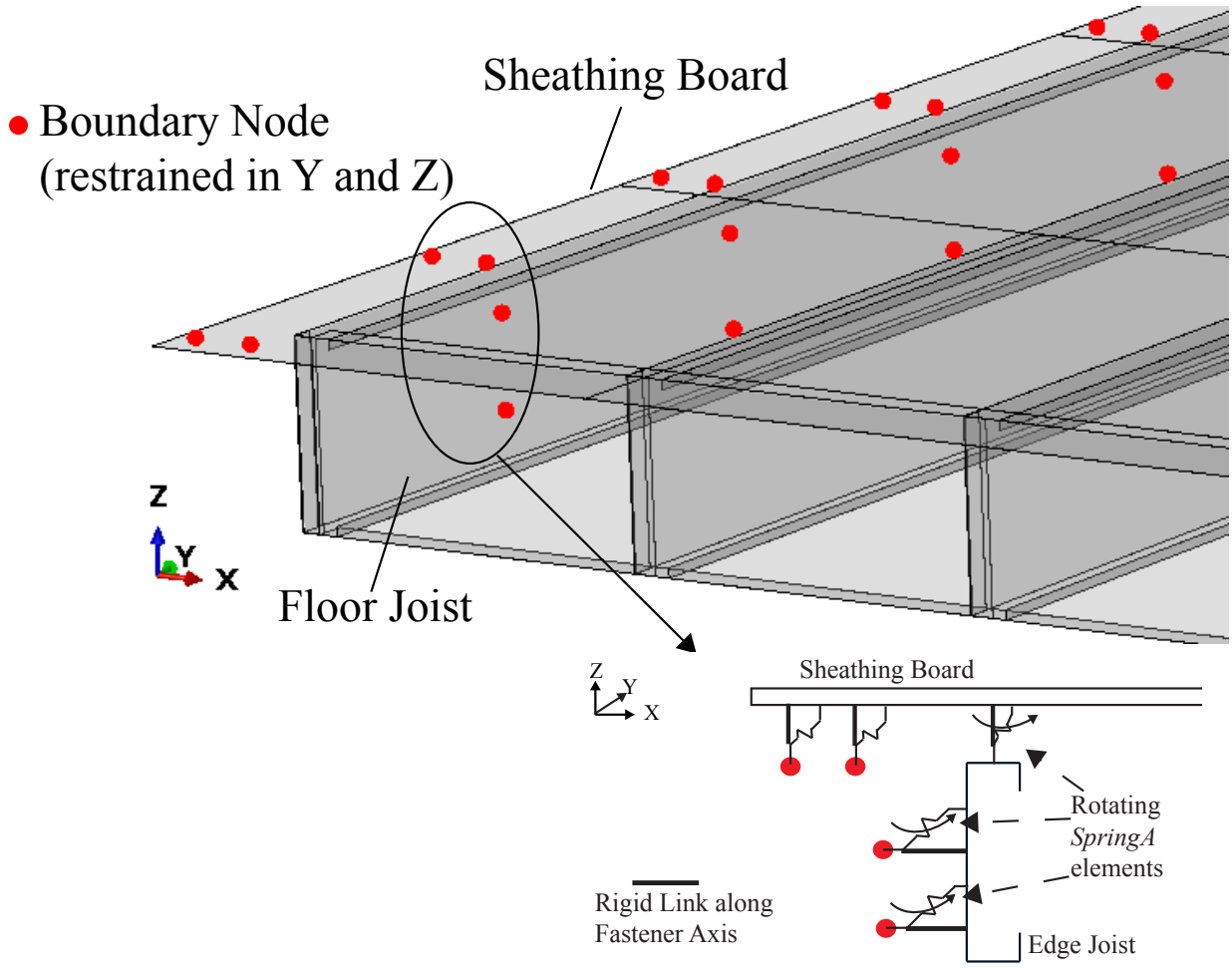

Figure 6.16: Short boundary conditions for the diaphragm with sheathing and edge joists connected to boundary nodes restrained in the short (Y) and vertically upward (Z) directions through axially rigid links and ABAQUS SpringA elements that update their orientations during the analysis

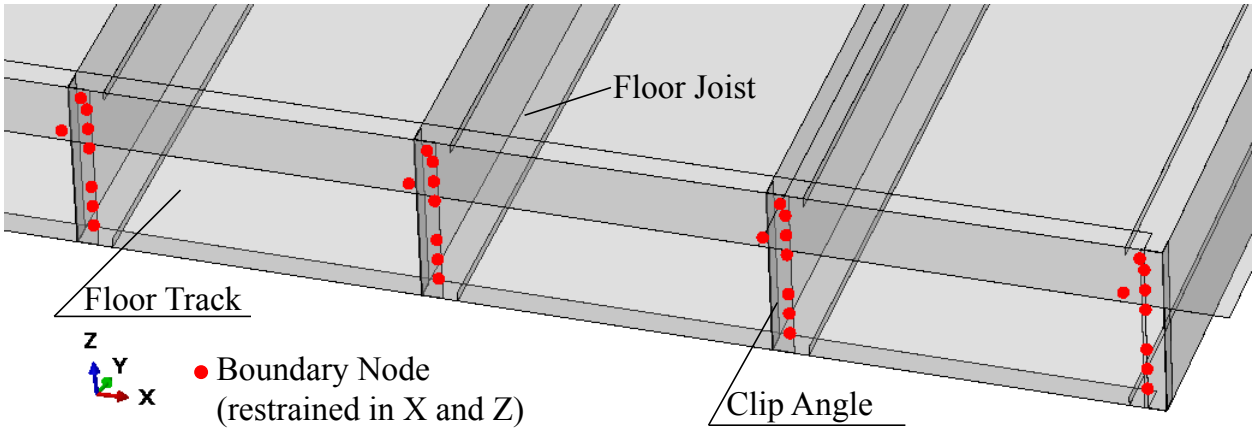

Figure 6.17: Long boundary conditions for the diaphragm with sheathing and ledger track connected to boundary nodes restrained in the long (X) and vertically upward (Z) directions (connection modeling same as short boundary)

6.4 Verification of finite-element modeling protocol with scaled experiments

The finite-element modeling protocol was verified against quarter-scale diaphragm experiments recently conducted at McGill University [73, 74, 12]. The diaphragm configurations for the experiments matched roof and floor diaphragms in the CFS-NEES building, with the specimen configuration described in Figure 6.18.

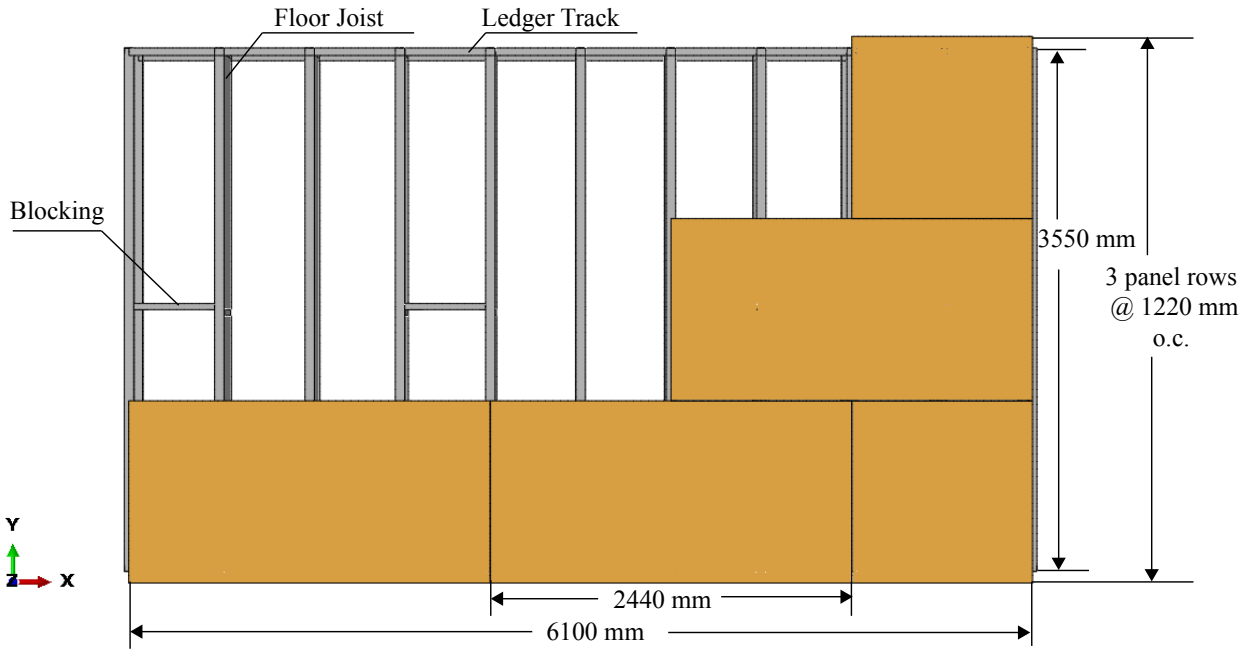

Figure 6.18: Quarter-scale CFS-NEES building diaphragm experimental configuration for tests performed at McGill University [73, 74, 12]

The diaphragm was tested under monotonic and cyclic displacement protocols applied to one edge whereas the other edge was held fixed. The corresponding FE model, developed using the same general principles discussed in section 6.3, is shown in Figure 6.19 with appropriate boundary conditions.

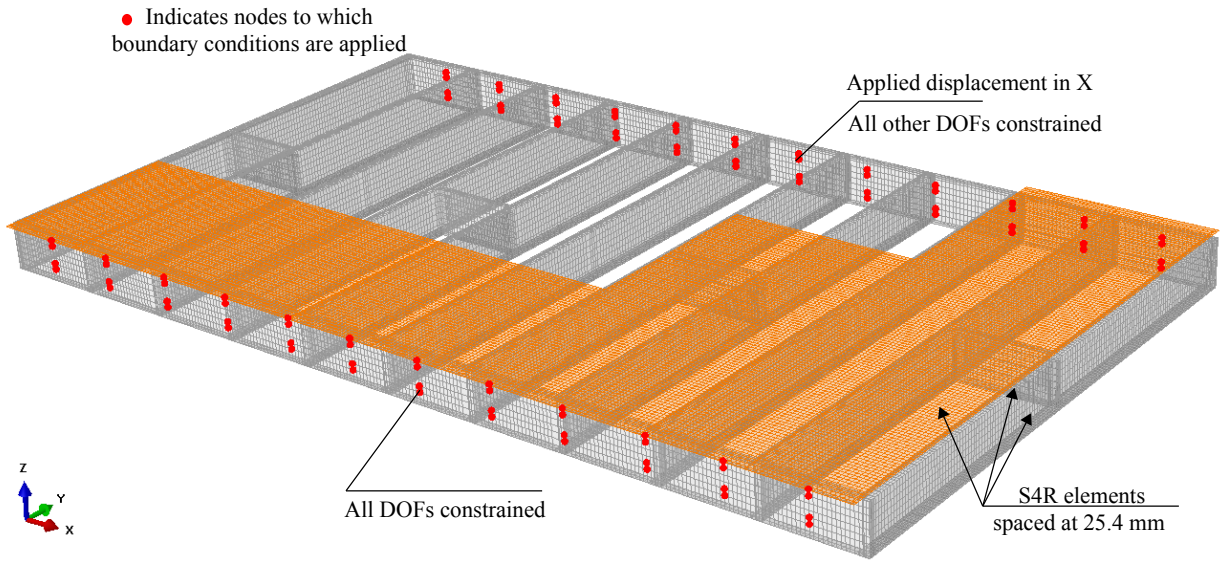

Figure 6.19: Finite element model boundary conditions for McGill diaphragm experiments [73, 74, 12]

The cyclic response of this model was captured using custom user-elements for screw-fastened connections that are capable of including unloading-reloading response [24], whereas the monotonic response was simulated using ABAQUS SpringA elements. The screw-fastened connection backbone and cyclic parameters were measured with the experimental protocol described in section 6.2.1.

The unblocked diaphragm experimental results were found to be bounded in between computational models with perfect and zero friction between panel seams. This was due to the fact that even in the absence of blocking, there is a non-zero inherent friction acting in between the panel edges. The monotonic experimental response was matched by the finite-element model (see Figure 6.20) by using spring elements spaced at 76 mm between panel edges. These 'friction' spring were characterized with non-linear force deformation relationships that increased as a step function as the inter-panel relative displacement exceeded zero (model for static friction). The spring forces were capped at 0.07 kN for the CFS-NEES building roof configuration, and 0.20 kN for the floor configuration. Friction was higher at

the floor level than the roof level due to the use of thicker OSB panels which also had a tongue-in-groove configuration that created a mechanical interlock. Interestingly, the same frictional coefficient when used for the full-scale diaphragm model was found to match tested results accurately (Figure 6.22).

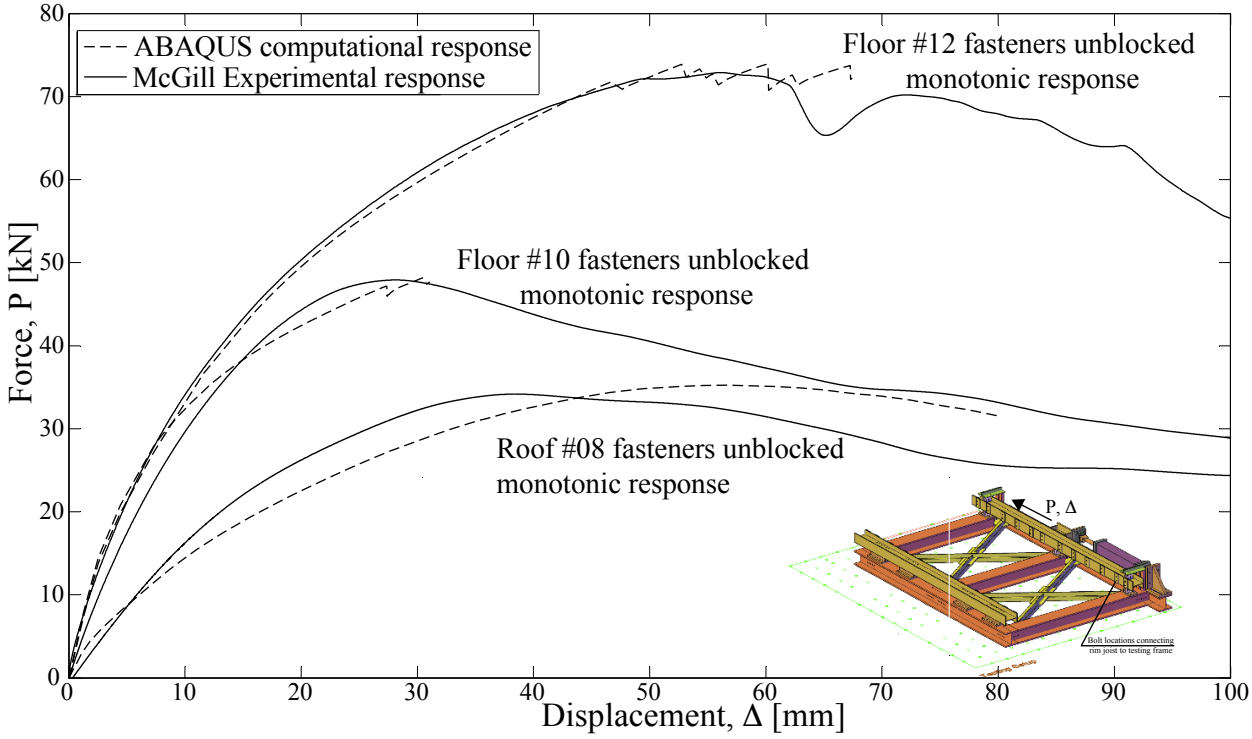

Figure 6.20: Comparison of monotonic responses obtained experimentally and with finite-element model for CFS-NEES floor and roof configurations built with #8, #10 and #12 sheathing-to-framing screw fasteners [73, 74, 12]

The diaphragm model was also subjected to cyclic displacement protocols to compare its predictions to the McGill experiments. However, the force-deformation relationship used for frictional springs did not converge under cyclic loads due to the step-function assumption for static friction, which is also an incorrect material model under load reversals. However, the first few cycles for which the model converged under full-friction and no-friction scenarios reiterated that these represented upper and lower bounds to the real response (Figure 6.21).

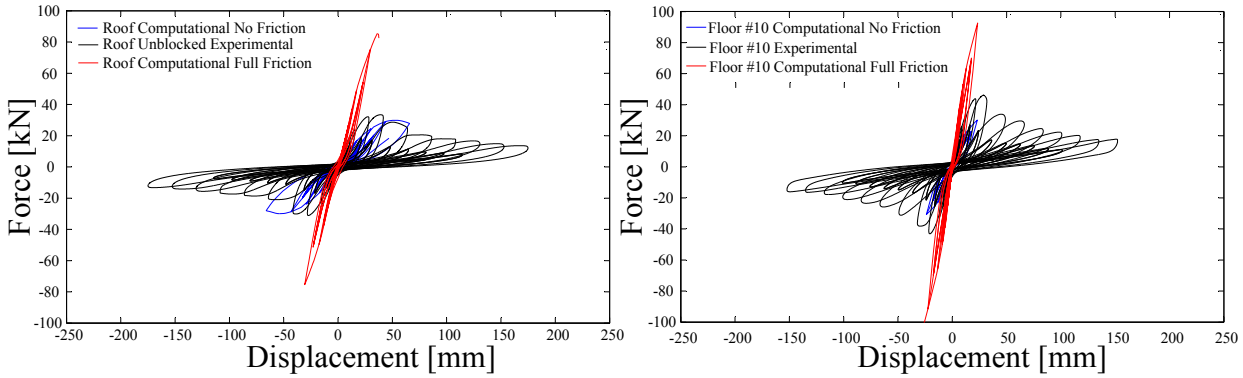

Figure 6.21: Comparison of cyclic response obtained experimentally to full-friction and zero-friction computational model responses that act as upper and lower bounds to the real behavior [73, 74, 12]

The monotonic and cyclic responses of the finite-element model compare well to the experiments which verifies the overall modeling protocol. The response of the full-scale model developed using the same protocol is studied next under the influence of in-plane distributed lateral loads.

6.5 Simulated full-scale diaphragm response under uniformly distributed lateral loads

Floor diaphragm response for the full-scale model under lateral loads is studied by applying a uniform body force on the sheathing material using the option **Dload* in ABAQUS. The floor diaphragm midspan deflection, Δ_{floor}, resulting from the distributed force, P_{floor} is plotted in Figure 6.22. The load-deformation response is nonlinear because of the fastener connection until its capacity is reached when the sheathing to wall fasteners on the short edges fail suddenly and the diaphragm loses the ability to carry more loads.

The diaphragm system load-deformation response for the unblocked case (where friction at

the OSB panel seams is assumed as zero) in Fig. 7 shows an initial stiffness reduction of 85% when compared to the blocked diaphragm because in-plane shear stiffness continuity is lost (39 kN/mm to 6.2 kN/mm tangent or secant stiffness from 0 to 8 mm), requiring the underlying framing to carry the in-plane loads from OSB panel to panel until it flows in the lateral system. The system failure mode also changes, shifting from the diaphragm-shear wall interface to the field fasteners along the panel seams as they slide relative to one another, resulting in an 80% decrease in diaphragm system capacity (compare 711 kN to 181 kN in Fig. 7).

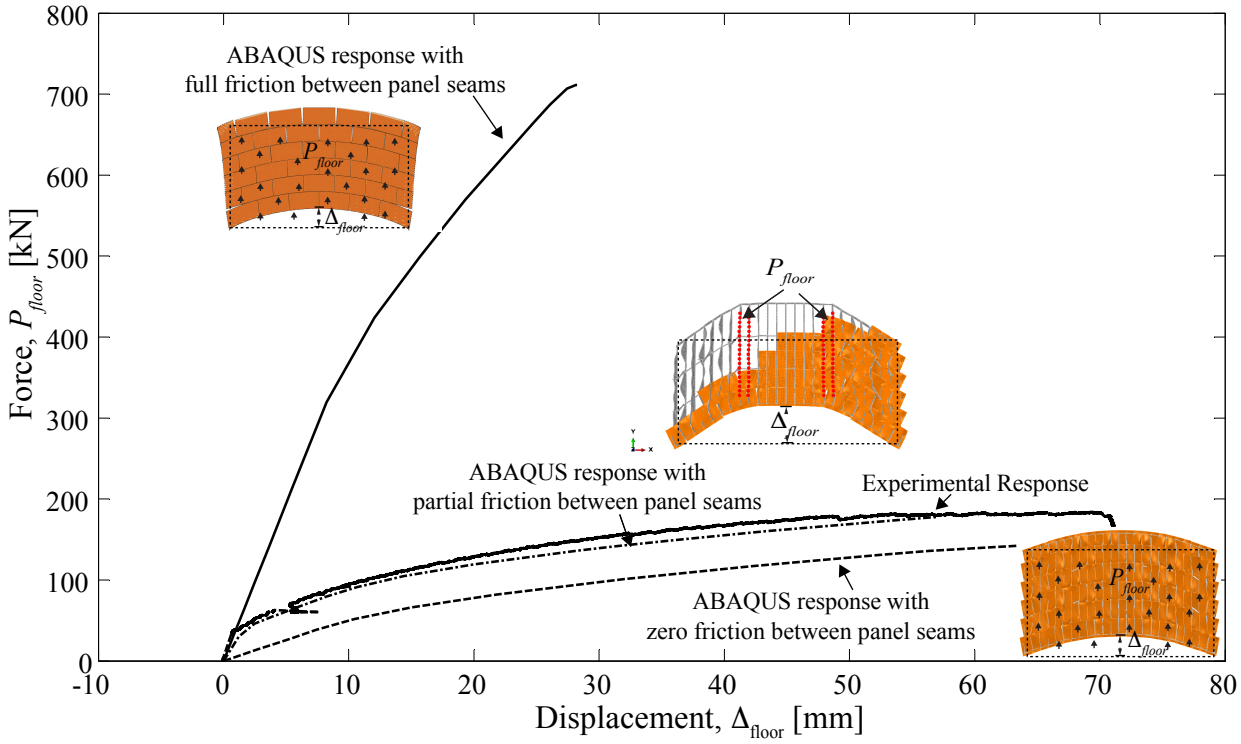

Figure 6.22: Simulated wood-sheathed cold-formed steel floor diaphragm load-deformation response under a distributed inertial force until failure initiation and convergence loss, showing 85% higher stiffness and 80% higher strength when considering perfect inter-panel friction (blocked) versus frictionless panel boundaries (unblocked)

Aside from verification with scaled diaphragm tests as discussed in section 6.4, a full-scale

experiment was also recently completed on the same wood-sheathed cold-formed steel framed diaphragm configuration considered herein [67]. The diaphragm test was conducted with a geometry and fastener pattern consistent with the simulations, however the load was applied with a drag strut connected between two joists at the diaphragm quarter points. As described in section 6.4, a frictional coupling spring between all long edge panel tongue-and-groove seams is incorporated in the simulation, where the spring stiffness of 0.003 kN/mm was calculated from panel relative edge slip measurements taken during and after the scaled diaphragm test [12]. The responses, compared in Figure 6.22 again confirm the accuracy of the finite-element model.

The dependence of floor force-deformation relationship on the modeled coupling between the panels (section 6.3.3) is further demonstrated by considering deformed shapes of the floor in either case. The contact modeling which includes perfect frictional coupling is similar to a 'blocked' diaphragm configuration which uses supporting steel framing along the panel boundaries (seams) to transfer shear loads from one panel row to the next. For 'unblocked' diaphragms, this shear is not transferred through inter-panel friction and the panels slide relative to one another instead. As a result, the diaphragm no longer deflects flexurally as one whole unit, but the individual panels slide and rotate relative to one another. This is evident from the final deflected shapes of the diaphragm model shown in Figure 6.23.

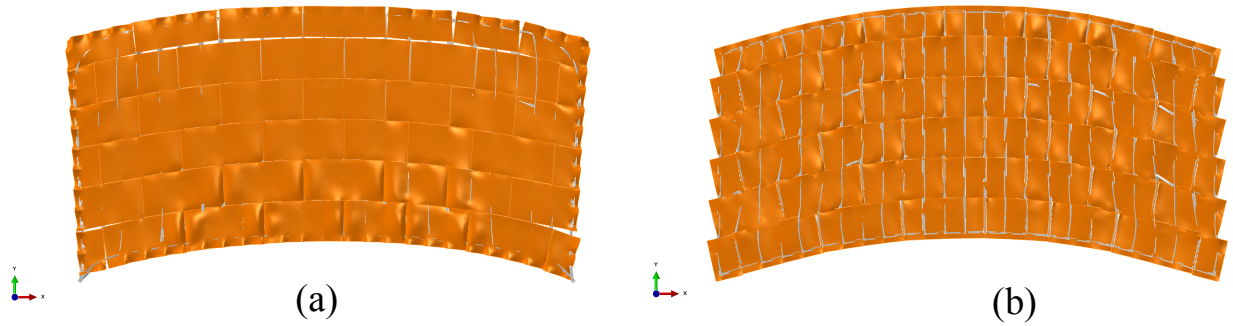

Figure 6.23: Diaphragm deformed shapes at ultimate loads for (a) full coupling between panel edges so that diaphragm responds flexurally as one unit or as a blocked diaphragm and (b) no friction between panel edges with panels sliding individually relative to one another or as a completely unblocked diaphragm

6.6 Load-path mapping for floor diaphragms under in-plane lateral loads

The high-fidelity finite element model provides the capability to track force demands in individual screw-fastened connection components within the floor, with the use of custom MATLAB [64] code to read ABAQUS [21] **.dat* output files, post process and plot force demand vectors. Example output can be seen in Figure 6.24 which shows the load distribution among fasteners in the critical load path for the blocked diaphragm at the failure load of 711 kN. There are two primary load paths transferring inertial forces from the blocked diaphragm to the lateral force resisting system – sheathing to wall ledger (50.3%) and edge joist to wall joist connections (49.7%). In other words, approximately half the diaphragm load is transferred directly through the diaphragm panels and the other half through the framing. The 49.7% transferred through the edge joists (framing) originate primarily from sheathing to edge joist connections (47.2%) with some contribution from the field fasteners (2.5%). This force distribution is characteristic of the blocked diaphragm case where perfect

friction is modeled in between the panel boundaries.

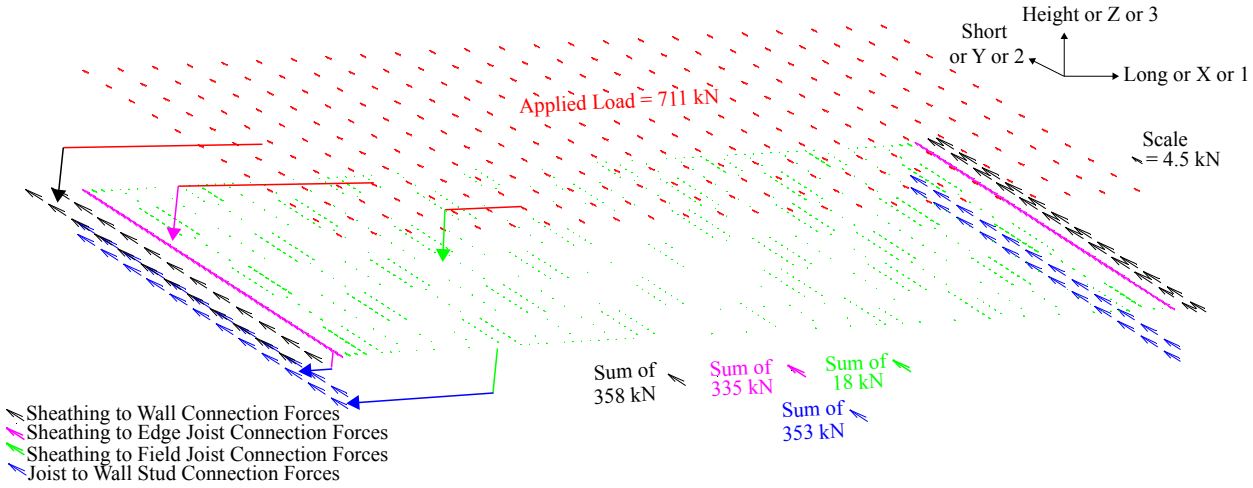

Figure 6.24: Fastener forces in the applied load direction (short or Y or 2) showing load transfer from diaphragm forces (red arrows, 711 kN) to (1) sheathing to ledger connections (black arrows, 358 kN), (2) edge joists (magenta arrows, 335 kN) and (3) field joists (green arrows, 18 kN), where (2) and (3) add up and get transferred through the joist to stud connections (blue arrows, 353 kN)

For purposes of component reliability analysis described in section 6.7 and system reliability analysis discussed in chapter 6, the flow of in-plane forces from the sheathing to the underlying framing is needed. The force distributions in all sheathing to framing fasteners for blocked and unblocked diaphragms are plotted in Figure 6.25. For the blocked diaphragm case, the in-plane diaphragm forces are carried in the OSB as a shear element to the OSB-to-wall connections, and the field fastener forces are minimal as shown in Figure 6.25 (a). Similar to shear stress distributions in a deep beam, these increase progressively towards the supported edges. The top ledger track is in a state of tension (fastener vectors point away from each other) whereas the bottom ledger track is compression (fastener vectors point towards each other). The corner fasteners experience a combination of shear and flexural demands. Structural components experiencing highest demands include sheathing to wall and joist to wall fasteners, with the former subjected to higher demand to capacity ratios

due to lower peak strengths (see Figure 6.6). Failure initiates at the ultimate load in the sheathing to wall connections, and once a single fastener fails, the load sheds to the adjacent fasteners and the diaphragm connectivity 'unzips' resulting in convergence loss in the finite element solver.

For the unblocked diaphragm case, the OSB sheathing is less effective and the field fasteners experience up to 100% higher demands as they transfer in-plane forces from OSB panel to panel, see Figure 6.25 (b). As described in [67], the individual panels in the unblocked diaphragm rotate as rigid bodies, resulting in a displacement incompatibility relative to the underlying framing. This relative displacement leads to high fastener shear demands at the panel seams. This effect is also considered in cold-formed steel diaphragm design standards [3, 4] which recommend lower diaphragm strengths in the unblocked case for loads applied parallel to panel seams. As a result of this effect, the field fasteners are the first to fail in the unblocked diaphragm in-plane response. Similar to the blocked diaphragm case, fasteners towards the center of the diaphragm experience least force demands. The force vectors obtained from the finite-element model agree well with fastener failure locations observed in the full scale experiment [67], where fastener failures were not observed near the center of the diaphragm.

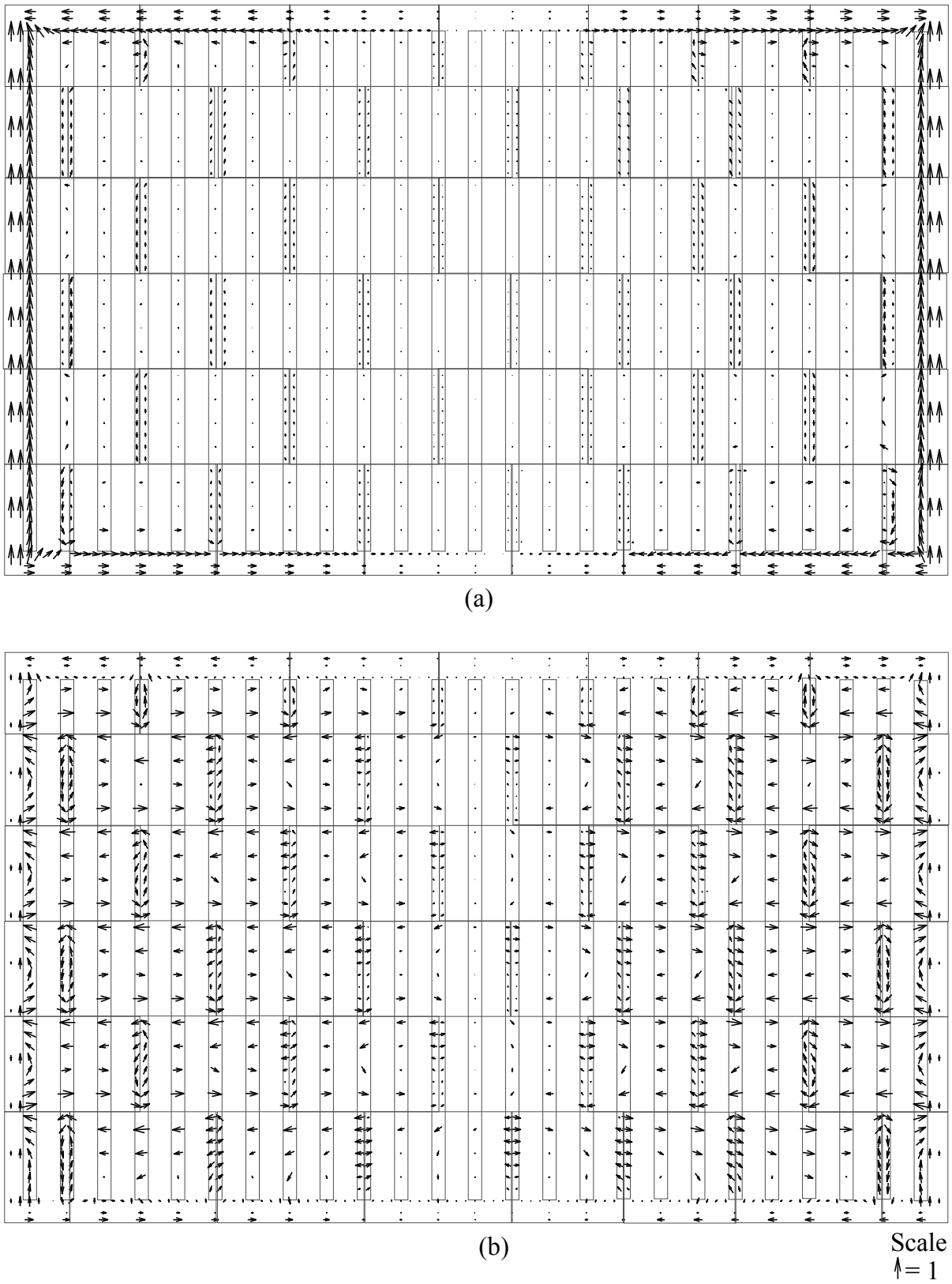

Figure 6.25: Normalized screw fastener to shear capacity vectors (D_i/C_i) at diaphragm system failure considering (a) blocked and (b) unblocked panel edges

6.7 Floor diaphragm fastener reliability calculation

With the floor diaphragm structural system and its simulation protocol defined, reliabilities can be calculated for the floor diaphragm components. As discussed above, critical components governing system response are the sheathing to framing and edge joist to wall stud fasteners connections which are the focus of this work.

6.7.1 Variability in the fastener strengths

Fastener ultimate strength F_c is used as component capacity in reliability calculations. The mean strengths for sheathing to joist, sheathing to wall and joist to stud connections are taken as F_c values defined in Figure 6.6 and Table 6.3. Sheathing to framing connection strength coefficient of variation (COV) obtained experimentally is 0.165, which is also taken as the COV for sheathing to wall fasteners. Joist to stud connection strength COV is taken as 0.048 which is the average COV for steel to steel connections with number 10 fasteners [68].

6.7.2 Variability in the seismic demand loads

The design standard recommended equivalent lateral force (ELF) on the floor diaphragm can be calculated using ASCE 7-10, Equation 12.8-1 (ASCE 2010) for total base shear $V = C_s W$, where $C_s = S_{DS}/(R/I)$. The design spectral response acceleration parameter in the short period range, $S_{DS} = 0.93$, is determined for a design basis earthquake (10% probability of occurrence in 50 years) assuming the building is located in Orange County, CA. The total base shear $V = 49.2kN$ using a response modification factor $R = 6.5$ for the cold-formed steel framed lateral system considered, an importance factor $I = 1.0$, and $W = 345kN$ as the effective building seismic weight, 41% of which acts at the floor level according to the first mode building response, resulting in a diaphragm design load of 20.2 kN.

The building loads standard ASCE 7-10 also has special provisions for diaphragm design loads $F_{px} = \frac{\sum_{i=x}^{n} F_i}{\sum_{i=x}^{n} w_i} w_{px}$, where F_i is the ELF load at level i, with a minimum set at $0.2 S_{DS} I w_{px}$ and maximum $0.4 S_{DS} I w_{px}$, where w_{px} is the seismic weight tributary to level x, which for the NEES 2nd floor diaphragm is 200 kN.

Mean diaphragm loads, which are the actual loads expected to act on a diaphragm during a seismic event (different from design loads) can be estimated from the CFS-NEES building shake table test for the DBE (Northridge ground motion recorded at Canoga Park). Instrumentation for the experiment included load cells attached to the ties and hold-downs at shear wall locations, whose forces were resolved to estimate a total of 79 kN base shear for the building excluding non-structural components subjected to the DBE [81]. Assuming the same load factor of 0.41 for first mode building response, this results in a 32.4 kN load at the floor diaphragm, which is an under-estimate since it does not include the shears at the bases of gravity walls.

The peak horizontal floor diaphragm acceleration in the CFS-NEES building shake table test for the DBE Canoga Park earthquake record was measured as 0.92g with an average of four accelerometers at the four corners measuring in the short building direction [78]. Multiplying the acceleration by the floor seismic mass of 186 kN results in an inertial force of 171 kN. This includes the sum of internal and damping forces in the system and therefore is higher than the actual force demand on the diaphragm.

The seismic demand estimates show a wide variability since they depend on the inelasticity in building response (assumed as a response reduction factor R=6.5 in ASCE 7-10), the effect of non-structural components [78] and the energy dissipated due to damping. The demand estimates are summarized in Table 4, and out of these the mean diaphragm demand of 114 kN obtained from ABAQUS full building simulations at the design basis earthquake is used in this work. In Table 6.4, the mean load is compared to design force levels used in ASCE-7, indicating a bias (mean demand to code specified design demand ratio) of 3.1 for the floor diaphragm. The 3 times difference between the mean and design demand is not unexpected,

since the design demand for earthquake loads is typically significantly lower than the mean demand. From a reliability standpoint, this if usually offset by the mean ultimate capacity being higher than the code-specified design capacity.

Table 6.4: Design forces at floor and roof diaphragm levels considering elastic lateral forces (ELF), diaphragm design forces and simulation results

Level x	Weight w_x [kN]	ELF F_x [kN]	Diaphragm Load F_{px} [kN]	F_{px} minimum $0.2S_{DS}Iw_{px}$ [kN]	F_{px} maximum $0.4S_{DS}Iw_{px}$ [kN]	Mean demand from simulations [kN]
Roof	144	29	29	27	54	94
Floor	200	20	28	37	74	114

Variability in the diaphragm seismic demand is represented using the COV for load effects, $V_Q = 0.38$. It should be noted that a wide range of estimates are available for the uncertainty associated with seismic loads. Values for the COV as low as 0.21 [58] and as high as 1.24 [104] are reported or recommended in the literature. A value of 0.38 has been selected here to correspond to the ASCE 7-10 load combination $1.2D + 1.0L + 0.2S + 1.0E$ where D is dead load, L is live load, S is snow load, and E is earthquake load, for California [104]. The seismic load effect COV is obtained from a first order second moment reliability parameter study employing Monte Carlo simulation that demonstrated V_Q is as much as 75% higher for load combinations including earthquakes than a typical $D + L$ combination.

6.7.3 Screw-fastened connection reliabilities in floor diaphragms under seismic loads

The screw fasteners connecting the wood sheathing to the floor joists define the diaphragm behavior, and the reliability of fastener component i can be estimated as per Equation 2.5:

$$\beta_i = \frac{log_n \frac{\mu_{C_i}}{\mu_{D_i}}}{\sqrt{V_{C_i}^2 + V_{D_i}^2}} \tag{6.1}$$

where $\mu_{C,i}$ and $V_{C,i}$ are the mean and coefficient of variation (COV) of the fastener capacity, and $\mu_{D,i}$ and $V_{D,i}$ are the mean and COV of the component demand [58].

The distribution of fastener component reliability, calculated with Equation 6.1, is shown in Figure 6.26, where $\mu_{C,i}$ and $V_{C,i}$ are the mean and COV of ultimate fastener strengths as described in section 6.7.1. The mean fastener component demand, $\mu_{D,i}$, is obtained from the elastic distribution of fastener forces for the mean seismic demand 114 kN calculated from simulations. The COV of the applied seismic load, $V_{D,i} = V_D = 0.38$ is calculated in recent studies characterizing variability in ASCE 7-10 earthquake load combinations [104].

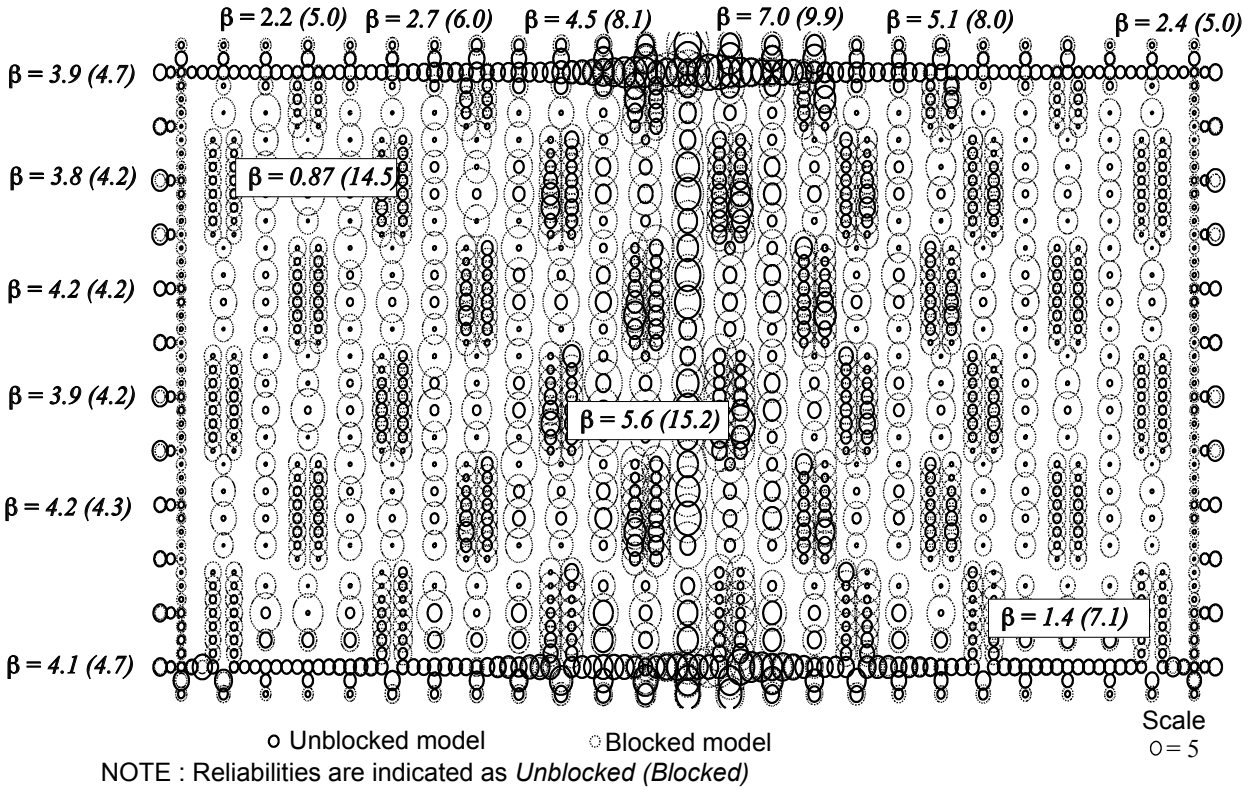

Figure 6.26: Fastener reliabilities at mean system demand of 114 kN for unblocked and blocked floor diaphragms.

In the blocked diaphragm, fastener reliability β_i is lowest at the sheathing-to-wall connections where the demand loads collect ($\beta_{edge,min} = 4.1$), and increases in the field of the diaphragm ($\beta_{field,min} = 7.1$). In the unblocked diaphragm, fastener reliabilities are lowest in the diaphragm field ($\beta_{field,min} = 0.87$), with higher edge fastener reliabilities ($\beta_{edge,min} = 1.1$) because the underlying steel framing carries 93% more of the demand load to the lateral system.

The reliabilities obtained using the mean diaphragm seismic demands are relatively high for the blocked diaphragm, but are quite low in the unblocked case. In the CFS-NEES building there were additional non-structural components attached to the diaphragm which potentially increased its reliability under seismic loads. Also, as discussed in the previous

sections, the no-friction assumption between panels is conservative. However, just from the diaphragm structural system viewpoint and its expected demands, system reliability improvements are desirable for the unblocked diaphragm case.

In conclusion, the component reliability β_i for each screw-fastened connection element in the floor diaphragm subsystem was calculated in this chapter, using load-path mapping obtained from high-fidelity finite-element models. The computer model was characterized by component scale tests and its predictions were verified by subsystem scale experiments. The next chapter studies the diaphragm capacity distribution and system reliability, and tunes the set of component reliabilities obtained here to reach the diaphragm subsystem reliability target of 2.1 which was calculated in chapter 5.

Chapter 7

Cold-Formed Steel Floor Diaphragm Sensitivity Analysis and Component Design

System reliability for the NEES building second floor diaphragm subsystem is estimated in this chapter using the convolution framework discussed in chapter 2. Subsystem capacity (C_{sys}) distribution or fragility is computed using Monte-Carlo simulations on the high-fidelity finite-element model described in chapter 6. Based on the component reliability trends, a subset of structural parameters are selected for probabilistic modeling which, when combined with variability in the system demand D_{sys}, in this case mean inertial shear force resulting from seismic ground motions, leads to a direct system reliability calculation for the floor diaphragm. The reliability sensitivity algorithm described in chapter 3 is then applied to the component reliability vector β calculated in chapter 6 (Figure 6.26) to calculate the sensitivity vector S_β. The vector of sensitivities is utilized to reach a set of component reliabilities for the screw fasteners that satisfy the subsystem reliability target $\beta_{t,sys} = 2.1$ for floor diaphragms. As discussed in chapter 5, this subsystem reliability target is chosen to meet the building system reliability target under seismic loads.

The chapter begins with a description of the uncertainty modeling and fragility evaluation framework, followed by system capacity distributions for the floor subsystem and system reliability estimation using convolution.

7.1 Convolution based system-reliability assessment framework

The finite-element model developed in chapter 6 is treated as a tool or black-box which takes diaphragm structural parameters and load pattern as input and outputs the subsystem capacity. Structural properties include all subsystem characteristics – floor geometry and layout, cold-formed steel framing and OSB panel material and geometric properties, fastener spacing and load-deformation response. The load pattern is the expected system demand description, which in general could include any combination of the basic load cases. The capacity is obtained by scaling the base load pattern until system failure occurs (in this case characterized by loss of convergence in the solver). This procedure is detailed in Figure 7.1.

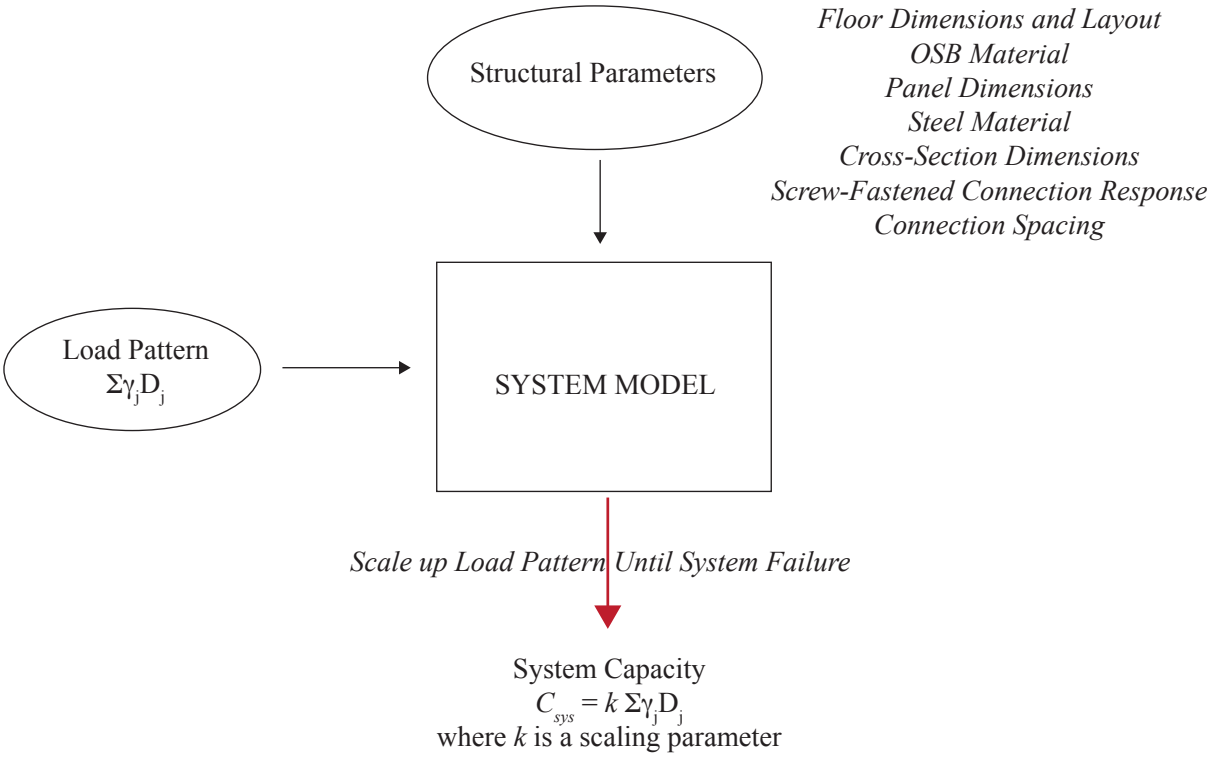

Figure 7.1: Finite-element model represented as a black-box which accepts structural parameters and applied load pattern as input, scales the load until failure occurs and provides the scaled load at failure as the system capacity output

In general, the procedure outlined in Figure 7.1 can be extended to any external hazard based on the analysis requirements for the specific application. For example, if the design procedure stimulates a non-linear time-history analysis, the load pattern would be provided as ground motion excitations at the support. The capacity would then be obtained by scaling up the ground motions until failure occurs, and would be expressed in terms of a spectral acceleration, in which case the stochastic methodology becomes equivalent to an incremental dynamic analysis. A detailed description of this approach is provided in section 5.1.1.

The next step is to incorporate uncertainty in the structural parameters which converts the analysis into a stochastic problem because the model and its capacity are both random. The uncertainty is modeled by sampling from the statistical distributions for the structural

parameters which provides a random generation for the structural model for each Monte-Carlo simulation. Running an individual sample model to failure gives a single capacity estimate (Figure 7.1) such that multiple simulations can be used to construct a histogram of capacities as described in Figure 7.2

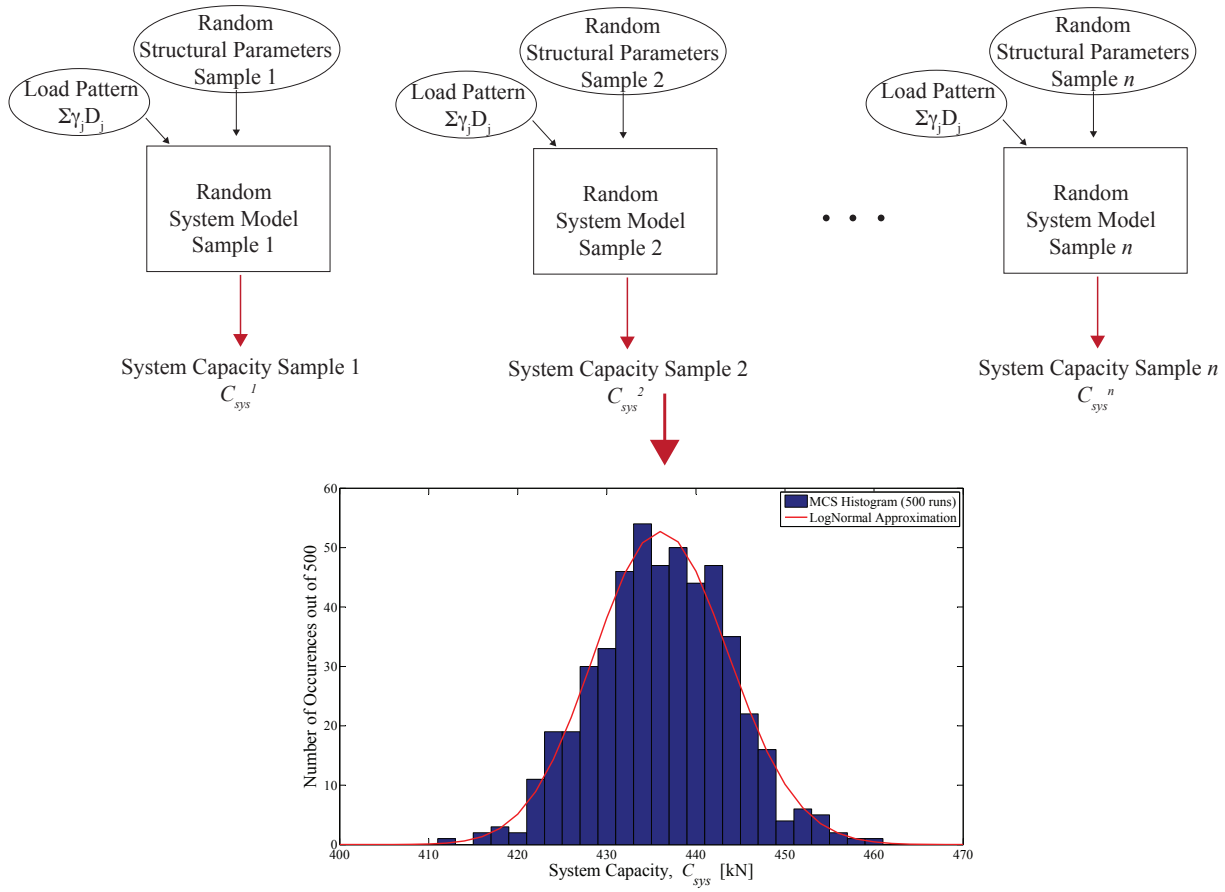

Figure 7.2: Stochastic simulation protocol incorporating randomness in structural parameters to generate n random system models from which the system capacity distribution $F_{C_{sys}}$ may be constructed for system reliability estimation

It should be noted that uncertainty is not modeled in the load pattern. Instead, the demand distribution is convoluted with the subsystem capacity distribution obtained above to estimate the subsystem reliability as described in chapter 2.

7.2 Incorporating uncertainty in floor diaphragm subsystem finite-element model

Uncertainty in floor diaphragm structural response can arise from variabilities in any of its component properties, including joist and track cross-sections, cold-formed steel stress-strain response, OSB strengths and panel dimensions or even variabilities from construction practices. As discussed in chapter 6, the diaphragm capacity under lateral loads is governed by the sheathing-to-steel screw-fastened connection properties. Although there will be significant variability in the other components as well, the baseline simulations indicate that these stay well within their elastic limits as the system reaches its ultimate strength. This is supported by previous observations in similar diaphragm and shear wall systems whose responses were governed entirely by the fastener behavior. Therefore it is assumed that randomness in all components other than screw-fastened connections do not affect system capacity which is why they are modeled as deterministic variables. The only components that are treated as random are sheathing to cold-formed steel framing connections and joist to wall stud connections along short edges.

Fastener ultimate strength F_c is treated as a lognormal distribution with mean and COV as described in section 6.7.1. The fasteners backbones are sampled randomly such that ultimate strength F_c is lognormally distributed, that is, the i^{th} random generation F_{ci} is obtained by independent sampling from a lognormal distribution [58]. Stiffnesses are assumed to stay constant in the four multi-linear backbone branches such that the remaining quadri-linear parameters scale linearly with F_c, i.e. $F_y^i = F_c^i F_y/F_c, F_r^i = F_c^i F_r/F_c, \delta_y^i = F_c^i \delta_y/F_c, \delta_c^i = F_c^i \delta_c/F_c, \delta_r^i = F_c^i \delta_r/F_c, \delta_f^i = F_c^i \delta_f/F_c$. Figure 7.3 shows example sets of 10 randomly generated backbones (dotted lines) obtained using this protocol. Other than these fastener connections all other diaphragm components are treated as deterministic because they do not affect system response significantly.

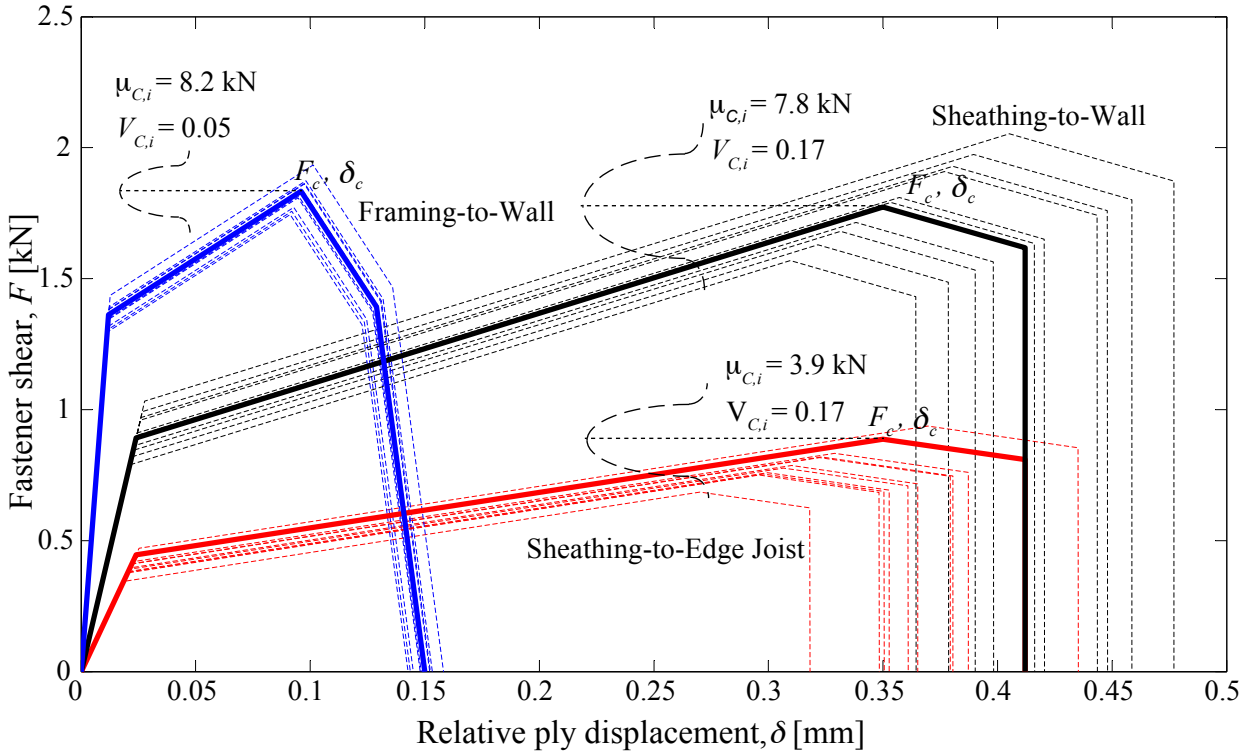

Figure 7.3: Example random backbones sets for sheathing to wall, sheathing to edge joist and joist to wall stud connections with baseline (deterministic) shown in bold and random realizations shown as dotted lines

7.3 Floor diaphragm subsystem capacity distribution

With the floor diaphragm baseline finite-element model described in chapter 5 and the structural uncertainty modeling protocol from section 7.2 defined, the next step is to choose a load pattern for which the system capacity distribution may be estimated. For LRFD design-code applications, each of the existing ASCE-7 load combinations would have to be considered for system reliability analysis. We focus here on the ASCE 7-10 seismic load combination $1.2D_n + L_n + 0.2S_n + E_n$. The lateral load effect on the diaphragm subsystem arises only from the seismic load case E_n which is simulated as a uniformly distributed body force on the sheathing as described in chapter 6. The gravity forces arising from dead, live and snow

loads are not applied to the model under the assumption that they do not create a lateral demand on the floor components.

Each Monte Carlo realization for the floor diaphragm model includes randomly sampled fasteners distributed across the floor and is simulated until loss of convergence at the onset of cascading system failure. The fastener resistances are sampled as independent and identically distributed random variables and the total lateral load is treated as independent of the fastener resistances. Brute force Monte Carlo simulation is used throughout. That is, no specialized sampling techniques such as Latin Hypercube, Importance Sampling, etc. are used. Figure 7.4 shows the histogram of system capacities obtained from 100 Monte Carlo runs for the blocked and unblocked floor diaphragms, the capacities obtained from the deterministic simulation (Figure 6.22) and the assumed distribution of system demand D_{sys}

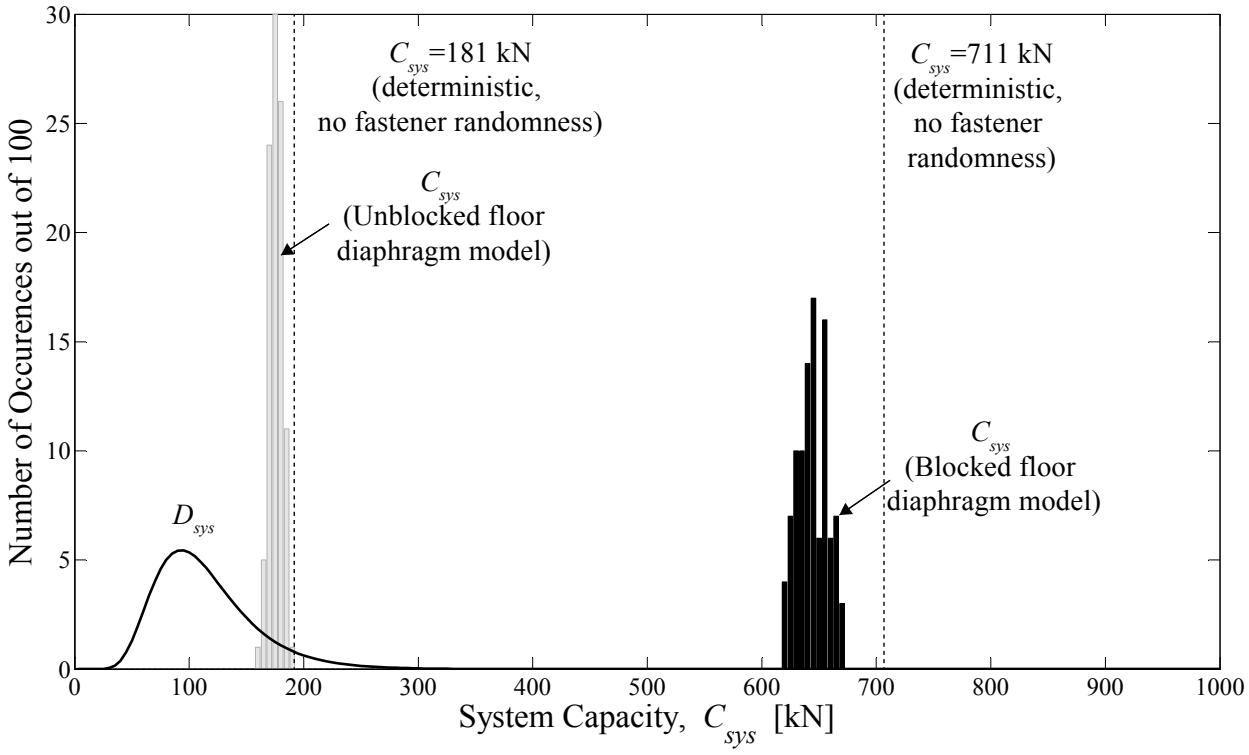

Figure 7.4: Diaphragm system capacity (C_{sys}) distributions for the blocked and unblocked cases, showing random samples and baseline (deterministic) capacity; diaphragm system demand (D_{sys}) distribution for the design basis earthquake

The mean system capacity is 644 kN with a COV of 2% for the blocked diaphragm, and 176 kN with a COV of 3.3% for the unblocked diaphragm. The mean capacity in each case is lower than the deterministically obtained capacity, which results from the fact that the weakest component is driving system failure, as discussed in chapter 2.

7.4 Diaphragm system reliability calculation using convolution

The system strength distribution obtained above from Monte Carlo simulations can be used in conjunction with an assumed distribution for the system demand to obtain a system reliability estimate. The system reliability index β_{sys} is

$$\beta_{sys} = -\Phi^{-1}[P(C_{sys} - D_{sys} \leq 0)] \tag{7.1}$$

where Φ is the standard normal cumulative density function, C_{sys} and D_{sys} are random variables for the system capacity and system demand, respectively. This can be approximated if the distributions of independent random variables C_{sys} and D_{sys} are known by numerically solving the convolution integral

$$P(C_{sys} - D_{sys} \leq 0) = \int_{d=0}^{d=\infty} P(C_{sys} \leq d | D_{sys} = d) dF_{D_{sys}}(d) \tag{7.2}$$

and substituting the result into Equation 7.1. Typically, the demand distribution D_{sys} is available from independent studies, for example, probabilistic seismic hazard analysis [14] and is assumed here as lognormal with mean 114 kN and COV 38% as provided in section 6.7.2. System capacity C_{sys} is assumed to follow a lognormal distribution with mean and COV 644 kN and 2% for the blocked diaphragm, and 176 kN and 3.3% for the unblocked diaphragm, as obtained in section 7.3. Numerically evaluating Equation 7.2 between the

limits 0 kN and 1200 kN in 1kN increments and substituting the result in Equation 7.1 gives a floor subsystem reliability β_{floor} of 4.9 for the blocked diaphragm and 1.4 for the unblocked diaphragm.

The subsystem reliability is higher in both cases than the minimum component reliabilities $\beta_{i,min}$ which is 4.1 for the blocked diaphragm and 0.87 for the unblocked diaphragm. The higher system reliabilities compared to minimum component reliability represents the system effect in the floor diaphragm. Based on this analyses, diaphragm design can now be geared towards a target system reliability $\beta_{t,sys} = 2.1$, derived for a building system reliability of 2.5 in chapter 5, as described in the following sections.

7.5 Identifying fastener groups which are most critical to system performance

The stochastic simulations carried out above can characterize the load-sharing network by identifying which components affect the system response more significantly and which ones are less critical. One way to do this is to study the correlation between the random system capacity and the fastener capacities. An example is shown here for the blocked diaphragm configurations by choosing four fastener groups – sheathing-to-ledger track along the short direction (short wall shear tabs), sheathing-to-ledger track along the long direction (long wall shear tabs), sheathing-to-edge joist fasteners, and sheathing-to-ledger-track fasteners. The random system capacities are plotted against the minimum fastener strength for each of these fastener groups in figure 7.5.

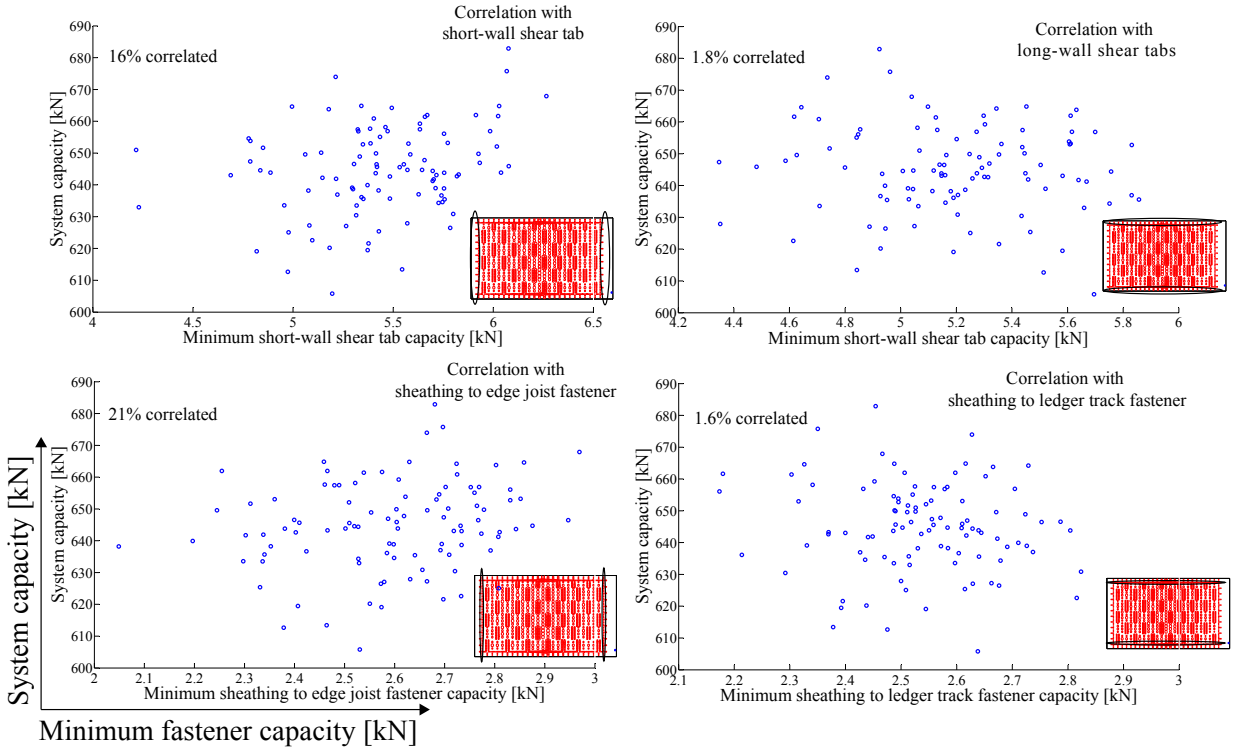

Figure 7.5: Scatter plots between random blocked diaphragm system capacity and minimum fastener capacity among four different groups of fasteners modeled as random variables

The results indicate high positive correlations between the system capacity and the minimum fastener capacities within the short wall shear tab and sheathing-to-edge-joist fasteners, and low correlations with the fasteners along the longer edge of the building. This is expected because the load which is applied parallel to the short direction of the building is resisted primarily by the edge-fasteners at these locations. In other words, for the load pattern being studied here, the system reliability sensitivity is higher for edge-fasteners along the short diaphragm edges, and lower for the fasteners along the long diaphragm edges.

Although the correlation plots help identify fastener groups that critically affect the system performance, they do not quantify the system reliability sensitivity. In the next section component reliability modifications are performed for the screw-fastened connection components to calculate system reliability sensitivities and solve for target component reliabilities that

satisfy a system reliability goal.

7.6 Floor diaphragm sensitivity analysis and target component reliabilities

The system reliability sensitivity plot for the floor diaphragm model with perfect friction is shown in Figure 7.6. As the short-edge fastener reliability increases, the system reliability increases linearly at first, similar to the redundant parallel system described in chapter 3. After the fastener reliability reaches 4.9, the weakest link in the floor shifts from the short-edge fasteners to the joist-to-wall stud connections. After this point, the floor system reliability no longer changes with the edge-fastener component reliability and remains constant at 5.1. In order to increase system reliability beyond this point, the joist-to-wall stud connections need to be strengthened.

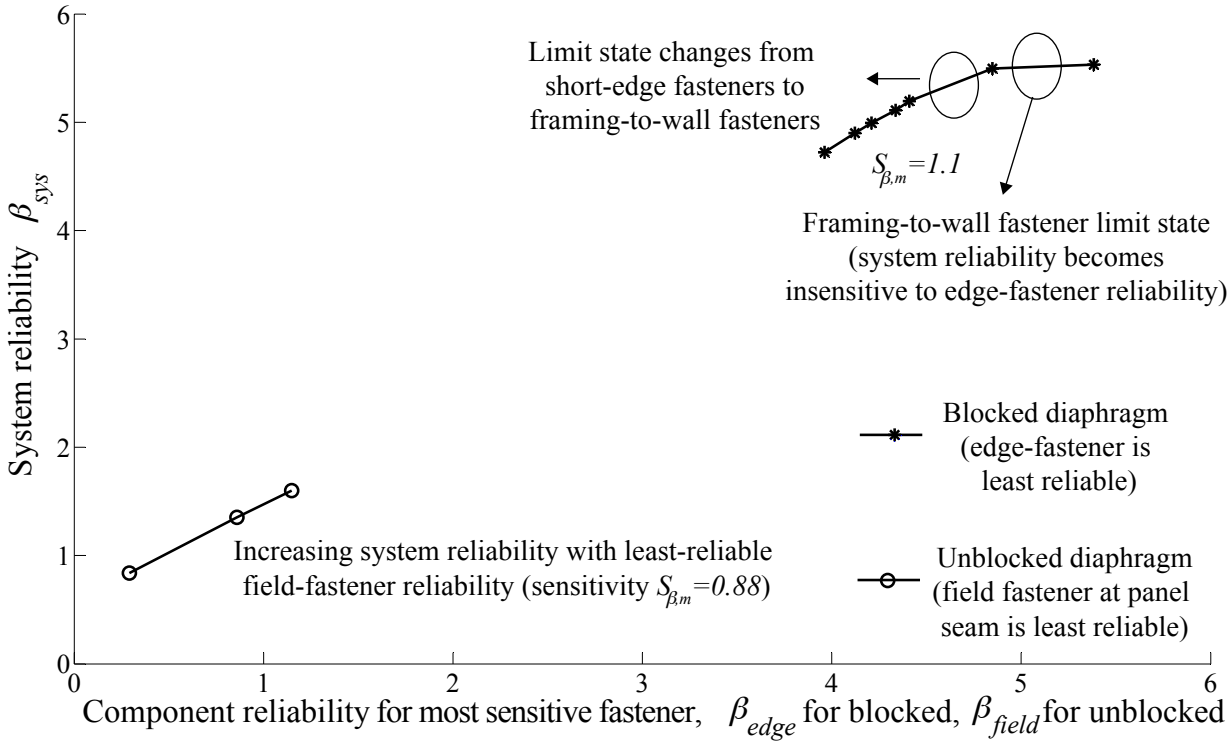

Figure 7.6: System reliability sensitivity plot showing increase in floor reliability with edge-fastener reliability until the system limit state changes (blocked diaphragm) and field fastener reliability (unblocked diaphragm)

The target component reliabilities for edge and field fasteners can be calculated by the sensitivity analysis algorithm from chapter 3, which was used to derive the diaphragm target reliability of 2.1 in chapter 5. The steps in the analysis are described in table 7.1 for unblocked diaphragms.

Table 7.1: Reliability sensitivity analysis from the unblocked diaphragm subsystem to edge and field fastener components.

Iteration Number	$\beta_{edge,min}$	$\beta_{field,min}$	S_{edge}	S_{field}	C_{sys} [kN]	β_{sys}
1	1.1	0.9	0.20	0.88	176	1.4
2	1.1	1.8	0.38	–	229	2.1

The sensitivity analysis for the unblocked diaphragm begins with the baseline minimum edge and field fastener reliabilities of 1.1 and 0.9, and a system reliability of 1.4. The sensitivities are 0.20 and 0.88, and the component with the highest sensitivity, the field fastener, is chosen to be modified to reach the target reliability of 2.1. This is carried out in the second step by increasing its reliability to 1.8, at which stage the floor system reliability converges to its target value of 2.1. The reliability sensitivity for the next component, the edge fastener, is computed next. This has a non-zero value of 0.38, which means that its reliability cannot be reduced for savings without adversely affecting β_{sys}. The values of $\beta_{edge} = 1.1$ and $\beta_{field} = 1.8$ are thus the minimum component reliabilities allowable for the unblocked floor diaphragm, and the reliability sensitivity algorithm has converged in two steps.

7.7 Floor diaphragm component design recommendations

Based on recommended edge and field fastener reliabilities 1.1 and 1.8 for the unblocked diaphragms component design resistance factors can be recommended using equation 2.13, repeated here for convenience:

$$\phi_i = \frac{M_m P_m F_m \sum_j \gamma_j D_{n,i,j}}{\sum_j B_j D_{n,i,j}} e^{-\beta_{t,i}\sqrt{V_{C_i}^2 + V_{D_i}^2}} \tag{7.3}$$

where material, professional and fabrication factors M_m, P_m and F_m convert the code-specified nominal capacity to mean capacity, $\sum_j \gamma_j D_{n,i,j}$ represents the load combination (in this case $1.0E$, the earthquake load case), B_j is the bias factor on load case j, $\beta_{t,i}$ is the target component reliability (1.1 for edge fasteners and 1.8 for field fasteners), V_{C_i} is the component capacity variability (0.17) and V_{D_i} is the component demand variability (0.38).

There are certain hindrances against performing this exercise at present. The diaphragm design demand is 37.2 kN whereas the mean seismic load is 114 kN (Table 6.4). Thus the

bias factor B_j (ratio of mean value to code-recommended nominal value) on seismic demand is 3.1, and the demand load variability is 0.38. Combined together, these would lead to resistance factors of the order of 0.1 as derived in chapter 3. Such a value will not be acceptable to the engineering community, but it is not incorrect. If the design procedure predicts component demands which are 3 times less than reality, the reliability method will penalize it with appropriately low resistance factors. There is no mechanics-based pathway to predict fastener demand loads D_i such as the ones plotted in Figure 6.25 for cold-formed steel floor diaphragms, and no prediction equations in design codes to calculate sheathing-to-steel screw-fastened connection strengths, such that even if ϕ factors were derived, they could not be applied in an actual component design scenario. Therefore it is recommended that accurate methodologies to predict capacity and demand be developed first before new resistance factors are proposed.

On the other hand, the LRFD resistance factor methodology and the current discrepancies in load bias and variability can be circumvented to directly predict fastener capacities leading to the diaphragm reliability target of 2.1, which in turn is calibrated to a building-system reliability of 2.5. In the unblocked diaphragm case, this was achieved with the baseline (#10) screw-fasteners along the diaphragm edge, and with a mean fastener strength of 5.8 kN in the field, which is 1.5 times the baseline strength of 3.9 kN. This design target can be reached by reducing the fastener spacing along panel edges from 152 mm to 102 mm, which will ensure that the diaphragm force capacity is not exceeded before the shear walls reach peak load, allowing energy dissipation as intended and ensuring a building system reliability of 2.5 under the design basis earthquake. This closes the system reliability loop proposed in Figure 1.1.

Chapter 8

Conclusions

This chapter summarizes the work presented in the dissertation and discusses its major conclusions, starting with general theoretical ideas and moving gradually to more specific topics that were studied in greater detail.

8.1 General methodology to design for target system reliability using system reliability sensitivity

8.1.1 System reliability calculation approach

A general system reliability methodology was proposed in chapter 2 which considers distribution of system capacity (C_{sys}) conditioned on system demand (D_{sys}) and evaluates a convolution integral to calculate probability of system failure. This approach relies on the estimation of a probabilistic distribution for system capacity using multiple stochastic simulations on physics-based computer models, and assumes that the demand distribution can be obtained from separate hazard analysis studies.

Physical quantities representing capacity and demand change from system to system. In

classical force-based structural design, such as the redundant system network studied in chapter 3, or the floor diaphragm system studied in chapter 6, the physical quantities of interest are structural forces. In displacement-based structural design, such as the approximate reliability method described in chapter 5, displacement capacity and demand distributions are required. For the earthquake engineering state-of-the-art incremental dynamic analysis method, capacities and demands are expressed as spectral accelerations, defined as peak displacement times square of natural frequency for a single degree of freedom system subjected to a seismic ground acceleration. These examples show how the random variables (C_{sys}) and (D_{sys}) can encapsulate both relatively straightforward and more complicated physical quantities.

Examples of the capacity-demand convolution approach for system reliability can also be envisioned for non-structural applications. In a transportation network the physical quantity in question would be the number of vehicles, in an electrical network it would be energy in $kW - hr$, in an infrastructure network comprising n number of hospitals this would be number of patients expecting treatment and so on.

The convolution approach provides more accurate estimates for system reliability compared to traditional methods such as fault or event-tree analysis and Bayesian networks. This was demonstrated in chapter 3 by comparing results of a classical redundant system using both approaches. Furthermore, since the convolution methodology uses physics-based models, it can capture more realistic system response, for example, actual load-deformation behavior, softening, energy-dissipation, strength and stiffness degradation in structural components. Comparatively, classical reliability methods or Bayesian networks are generally two-state systems represented as 'fail / safe' or '0 / 1' which cannot capture load-redistribution within the network. The proposed method can lead to detailed recommendations for the design of such systems as discussed in the next subsection.

8.1.2 System reliability sensitivity based design approach

A design approach to recommend component designs that satisfy a system reliability goal was proposed in chapter 3 using system reliability sensitivity S_β, defined as the vector of partial derivatives $\partial\beta_{sys}/\partial\beta_i$ of system reliability with respect to component reliability. The sensitivity vector S_β, which may be calculated analytically if closed-form solutions for system reliability are available, or can be estimated by a finite-difference scheme, quantifies individual elements' contributions to the load sharing network

The design application of S_β is to reinforce components with high sensitivity and reduce reliabilities for less sensitive components for savings. A general sensitivity-based design algorithm was proposed which explores the space of alternate designs and converges to a solution vector of component reliabilities resulting in a pre-defined reliability target set for the system.

Although in general the sensitivity algorithm is a computationally demanding process in a design space continuum with infinite alternate component reliability solutions, practical constraints reduce these demands significantly. For instance in the structural domain, only a few potential sizes of beams, columns or connections available in the market constitute the design space that can be explored efficiently to propose a solution vector of component reliabilities.

The sensitivity methodology was used in chapter 3 to obtain system reliability benefits on ductile components compared to brittle components in a redundant load-sharing network, in chapter 5 to recommend target subsystem reliabilities for lateral force resisting systems and diaphragms in a building subjected to seismic ground motions and in chapter 7 to define different resistance factors and design capacities for field and edge fasteners in blocked and unblocked diaphragms.

8.2 System-reliability based load and resistance factors for structural design

The system reliability and sensitivity methodology can be utilized to recommend load and resistance factors for structural design standards. Currently, resistance factors are calibrated to a pre-defined component reliability target for different classes of structural components through the load and resistance factor design (LRFD) methodology described in chapter 3. The objective of the proposed sensitivity approach is to calculate new target component reliabilities that can be used in an LRFD framework to calculate resistance factors for structural components.

The sensitivity-LRFD framework was demonstrated for a network of redundant components in chapter 3 resulting in higher resistance factors for ductile members and lower resistance factors for brittle members, which results from considering the system reliability and its sensitivity. This is an improvement over standard component LRFD which only considers member capacities and not their force-deformation relationships, resulting in identical resistance factors for ductile and brittle components.

The general framework also considers all possible load combinations acting upon the structural system, providing different component reliability targets for each. This is an improvement over current AISI design standards that use resistance factors derived for a single load combination $1.2D + 1.6L$ in all structural design scenarios. In the example problem studied in this dissertation, an assumed load combination $1.0E$ or just the seismic load case is considered since it provides load-sharing information for perhaps the least understood load case in structural engineering. Since the proposed methodology is not restricted to just considering force capacities and demands on structural systems, it provides a pathway for accurately considering seismic ground motions for which a displacement demand is usually more significant than a force demand.

8.3 Target design criteria for cold-formed steel building subsystems under seismic loads

The reliability methodology was applied to the analysis and design of cold-formed steel buildings under seismic excitations. The end goal was to calculate system reliability for the building and its sensitivity to subsystem reliabilities to propose subsystem reliability targets aligned to the target system reliability.

To obtain system reliability and sensitivity estimates, a spring-based model for a two-story building previously tested in shake table experiments (NEES building) was built using ABAQUS (chapter 4). The model had a lower stiffness compared to estimates obtained experimentally on the real building, indicating that non-structural components and gravity walls along the direction perpendicular to applied seismic ground motions had a significant impact on the overall lateral stiffness of the building.

The ABAQUS building model was subjected to 44 ground motions selected based on recommendations provided in state-of-the-art earthquake engineering standard FEMA-P695, and the non-linear dynamic analysis results were used to calculate inter-story drift demand, base shear, and vertical force distribution statistics due to design basis earthquakes. The drift demands on both the lateral system and the diaphragms were found to be high compared to experimental observations, once again underlining the lower model stiffness compared to reality.

System reliability analysis using the convolution approach on the full building under seismic loads was discussed in chapter 5. Two approaches were presented, the first using spectral acceleration demands and capacities as used in incremental dynamic analysis [100] and FEMA-P695, and the other considering interstory drift demands and capacities using a proposed approximate system reliability model. The latter approach is limited to considering a lateral system drift limit as the building capacity and is incapable of considering additional capacity due to diaphragm energy dissipation (as was demonstrated using example analyses)

but entails far less computational resources, which is why it was chosen for system reliability and sensitivity analysis. It was verified that the two methods provided comparable system reliability estimates for the as-designed building under the design basis earthquake.

The sensitivity methodology was applied to two design scenarios, one using unblocked diaphragms at the roof and floor level, and the other with blocked diaphragms whose capacities are several times higher compared to the unblocked case (Figure 5.4). The reliability of the shear wall subsystem was modified in each case, and it was observed that system reliability increases due to this modification only if a blocked diaphragm configuration is used; for unblocked diaphragms the shear wall displacement capacity isn't fully utilized due to premature failure of the diaphragm. It should be noted that this is partly due to a conservative reliability assumption that reaching a diaphragm ultimate force capacity results in system failure. Incremental dynamic analysis results (Figure 5.6) indicated that this might not necessarily be true as there is reserve spectral acceleration capacity within the system beyond diaphragm ultimate force capacity.

The sensitivity results were used to recommend design criteria for shear wall and diaphragm systems within the modeling and reliability assumptions considered. These design criteria were used within a sensitivity methodology for the subsystems to recommend component reliability criteria as discussed for floor diaphragm subsystems in the next section. The reliability sensitivity methodology is similar to a FEMA-P695 approach but can provide design recommendations down to the component level instead of only recommending strength reduction, displacement amplification and overstrength factors currently used in earthquake engineering.

8.4 Resistance factors for components in a cold-formed steel floor diaphragm system under lateral loads

The reliability sensitivity approach was used to provide design recommendations for cold-formed steel floor diaphragm subsystems in chapter 7. The sensitivity algorithm was implemented on a high-fidelity finite-element model for the floor diaphragm developed in chapter 6, including shell and spring finite-elements for floor joists, ledger tracks, sheathing panels, blocking, bracing, clip angles and screw-fastened connections. The model was validated using experimental results from quarter-scale and full-scale diaphragm experiments, and provided valuable information on the connection load paths and component reliabilities.

The diaphragm system reliability was calculated as 4.9 and 1.4 at two limiting cases with perfect frictional coupling between panel seams (blocked diaphragms) and zero coupling between panel seams (unblocked diaphragms). The reliabilities were modified to their target value of 2.1 by changing the edge and field fastener reliabilities, culminating in a design recommendation of reducing field fastener spacing in unblocked diaphragms from 152 mm to 102 mm along panel seams. This demonstrated the potential of the reliability sensitivity approach to convert a system level reliability target (building reliability of 2.5 under design basis earthquake) to a component design change (reduced fastener spacing at panel edges). The approach can be applied to other systems in the cold-formed steel building to eventually provide design-standard recommendations for each individual component.

Chapter 9

Future Work

This chapter discusses future research applications of the work presented in this dissertation, beginning with specific application to diaphragms and cold-formed steel building systems, and then moving gradually to general applications in structural engineering, other engineering problems and the system reliability sensitivity theoretical framework.

9.1 Cold-formed steel diaphragm analysis and design

The finite element models for cold-formed steel diaphragm systems could be further developed by calculating friction between panel seams, by characterizing the fastener backbones better to capture the unloading portion of the response and by improving the cyclic models to capture more cycles and match experimental results. These models could then be used to characterize the unloading-reloading response parameters for diaphragm subsystems for full building dynamic analysis. The models could also be used to perform multiple non-linear analyses and recommend seismic response reduction, deflection amplification and overstrength factors.

As discussed in chapter 7, the current design methodology for sheathed-cold formed steel

diaphragms (AISI S400, AISI S240) does not include a pathway to calculate component demands and capacities. This could be overcome by using a mechanics-based method to calculate fastener force vectors, such as the one used in the Steel Deck Institute design manual [49]. Screw-fastened connection capacity prediction may be carried out using recently proposed general force-deformation trendlines developed at Virginia Tech [68]. These could then be used in conjunction with the resistance factors recommended in chapter 7, or new factors derived by a similar methodology, to perform LRFD component design for diaphragm connections aligned to a building system reliability target.

9.2 Building system modeling, analysis and design

A full-scale high-fidelity model for cold-formed steel buildings can be developed. In the present work, a reduced-order spring model was used to represent the building. Previous work [90] has developed full building models primarily using truss elements in OPENSEES. A full-scale high-fidelity shell, spring and user element based model for diaphragms was developed in this dissertation. Similar models are available for shear walls [72] and could be conjoined to create a finite-element building model which can be used for analysis under any general loads to study the structural response and interaction of subsystems.

System reliability and sensitivity analysis can be performed using incremental dynamic analysis considering spectral acceleration capacities and demands instead of the simplified reliability model used in this work. This will provide further insight into system response and include load-redistribution after failure initiation in the weakest subsystem. Currently, the reliability model is designed such that the first subsystem failure is considered to be equivalent to building failure. However in reality the load can redistribute after the diaphragm or the first shear wall reaches its capacity. These effects can be captured by a spectral acceleration based system reliability sensitivity analysis.

Reliability sensitivity analysis should be performed using actual force-deformation backbones

for shear wall, diaphragm and screw-fastened connection configurations available commercially. In this work perturbations in the backbones were assumed based on an equivalent stiffness assumption as a design example. In reality, the backbones at each perturbed value of shear wall reliability (for example) should be available from tests, and can be used to conduct a more realistic sensitivity analysis.

Sensitivity analysis and component design recommendations for shear wall subsystems can be carried out in the same general manner as performed here for buildings and diaphragms. As was discussed in chapter 5, these will eventually result in target reliabilities for the energy dissipative members and force controlled components within the shear wall system.

In the seismic design domain, the methodology should be improved by predicting the effect of gravity and non-structural walls more accurately, as these can have a significant impact on the reliability calculations. The sensitivity method should still result in comparable target reliabilities for the subsystems, but this can only be verified after studying such examples. Displacement-design criteria can be developed for lateral force resisting systems using the resistance factors proposed here. Overall, this can potentially provide pathways to obtain more rational design criteria and resistance factors down to the component level under seismic demands, as compared to the current FEMA-P695 methodology of calibrating seismic design factors (which can have conceptual inconsistencies) to results from non-linear dynamic analyses.

9.3 Application to other structural and non-structural engineering systems

The general system reliability sensitivity approach can be applied to other structural systems. System reliability analysis has previously found wide application in bridge redundancy recommendations, and the new method can add valuable new information to previous research

results. It can also be applied to structural design standards in concrete or hot-rolled steel similar to the proposed applications to cold-formed steel presented here. Another potential application to the structural engineering community is to consider performance-based or serviceability limit states that are easily included in this methodology by modifying capacity values that relate to those limit states, for example, a floor deflection demand and capacity in buildings under occupancy live loads.

Since the system reliability and sensitivity algorithms are formulated in general terms for capacity and demand, they can also be applied to other non-structural engineering systems, as discussed in chapter 3. Applications can be envisioned for transportations, electrical or infrastructure networks. The key to the methodology is to develop physics-based models that can capture capacity distributions, load sharing and load redistributions. These models compare and contrast to statistical models such as Bayesian Networks or Markov Chains that could potentially be too simplistic for the actual engineering network. Physics-based models, on the other hand, would include the real response of the system, such as an interstate highway with 5 lanes and the effect of an accident on one of the lanes, time to remove the vehicle and the resulting traffic build-up. Realistic simulations can then be performed on such systems to characterize their capacities under different loading scenarios, say office-hour traffic at 5 pm, or Saturday afternoon traffic.

9.4 General system reliability sensitivity theory

The general approach for system reliability sensitivity based design proposed in chapter 3 was applied to building and diaphragm structural systems. More examples should be considered to broaden and understand the approach better, for example, studying small sized systems (2-5 components) that include one weak link, systems with several different element groups (this disseration focused on a maximum of 2 groups), competing limit states and sensitivity bifurcation (as observed for shear walls and diaphragms in chapter 5), simplified redundant

spring systems with unloading-reloading response under dynamic loads and so on. These examples will help to develop a more robust and elegant algorithm that can generally be applied to different load-sharing networks in the real world.

Bibliography

[1] AISI. S213-07: North american standard for cold-formed steel framing - lateral design, 2007.

[2] AISI. North american specification for the design of cold-formed steel structural members, 2012.

[3] AISI. North american standard for cold-formed steel structural framing. Technical report, American Iron and Steel Institute, 2015.

[4] AISI. North american standard for seismic design of cold-formed steel structural systems. Technical report, American Iron and Steel Institute, 2015.

[5] ASCE. Asce 7-10: Minimum design loads for buildings and other structures, 2010.

[6] B. Bhattacharya, R. Basu, and Kai-tung Ma. Developing target reliability for novel structures: the case of the mobile offshore base. *Marine Structures*, 2001.

[7] G. Boole. Laws of thought. *American Reprit of 1854*, 1854.

[8] S. G. Buonopane, G. Bian, T. H. Tun, and B. W. Schafer. Computationally efficient fastener-based models of cold-formed steel shear walls with wood sheathing. *Journal of Constructional Steel Research*, 2015.

[9] S. G. Buonopane and B. W. Schafer. Reliability of steel frames designed with advanced analysis. *Journal of Structural Engineering*, 2006.

[10] O. C. Celik and B. R. Ellingwood. Seismic fragilities for non-ductile reinforced concrete frames – role of aleatoric and epistemic uncertainties. *Structural Safety*, 2010.

[11] E. J. Cha and B. R. Ellingwood. Quantification of risk aversion in decisions related to safety of nuclear power plants. *Safety, Reliability, Risk and Life-Cycle Performance of Structures Infrastructures*, 2013.

[12] A. Chatterjee, C. A. Rogers, and C. D. Moen. High fidelity monotonic and cyclic simulation of a wood-sheathed cold-formed steel framed floor diaphragm. In *16th World Conference on Earthquake Engineering, 16WCEE 2017*, 2017.

[13] A. Chatterjee, Y. Xiang, C. D. Moen, S. R. Arwade, and B. W. Schafer. Towards quantifying beneficial system effects in cold-formed steel wood-sheathed floor diaphragms. In *22nd international specialty conference on cold-formed steel design and construction*, September 10-12 2014.

[14] C. A. Cornell. Engineering seismic risk analysis. *Bulleting of the Seismological Society of America*, 1978.

[15] C. A. Cornell, F. Jalayer, R. O. Hamburger, and D. A. Foutch. Probabilistic basis for 2000 sac federal emergency management agency steel moment frame guideline. *Journal of Structural Engineering*, 2002.

[16] Ross B. Corotis and Avinash M. Nafday. Structural system reliability using linear programming and simulation. *Journal of Structural Engineering*, 115:2435–2447, 1989.

[17] APPLIED TECHNOLOGY COUNCIL. Nehrp guidelines for the seismic rehabilitation of buildings. Technical report, BUILDING SEISMIC SAFETY COUNCIL, 1997.

[18] APPLIED TECHNOLOGY COUNCIL. Fema p695 quantification of building seismic performance factors. Technical report, 2009.

[19] American Wood Coundil. National design specification for wood construction. Technical report, ANSI/AWC, 2015.

[20] H. E. Daniels. The statistical theory of the strength of bundles of threads. 1. *Proceedings of the Royal Society of London. Series A, Mathematical and Physical Sciences*, 1944.

[21] Dassault-Systems. Abaqus 6.13 documentation, 2013.

[22] A. Der Kiureghian, T. Haukaas, and K. Fujimura. Structural reliability software at the university of california, berkeley. *Structural Safety*, 2006.

[23] Animesh Dey and Sankaran Mahadevan. Ductile structural system reliability analysis using adaptive importance sampling. *Structural Safety*, 20:137–154, 1998.

[24] C. Ding. Monotonic and cyclic simulation of screw-fastened connections for cold-formed steel framing. Master's thesis, Virginia Tech, 2015.

[25] Ove Ditlevsen. Narrow reliability bounds for structural systems. *Journal of Structural Mechanics*, 7(4):453–472, 1979.

[26] D. Dubina. Behavior and performance of cold-formed steel-framed houses under seismic action. *Journal of Constructional Steel Research*, 2008.

[27] B. R. Ellingwood. Reliability based criteria for reinforced concrete designs. *Journal of the Structural Division, ASCE*, 105, 1979.

[28] B. R. Ellingwood, O. C. Celik, and K. Kinali. Fragility assessment of building structural systems in mid-america. *EARTHQUAKE ENGINEERING AND STRUCTURAL DYNAMICS*, 2007.

[29] B. R. Ellingwood and T. V. Galambos. Probability-based criteria for structural design. *Structural Safety*, 1, 1982.

[30] B. R. Ellingwood, T. V. Galambos, J. G. MacGregor, and C. A. Cornell. Development of a probability based load criterion for american national standard a58. Technical report, National Bureau of Standard, 1980.

[31] S. J. Errera, B. M. Tang, and D. W. Popowich. Strength of bolted and welded connections in stainless steel. Technical report, Cornell University, 1970.

[32] A. C. Estes and Dan M. Frangopol. Repair optimization of highway bridges using system reliability approach. *Journal of Structural Engineering*, 1999.

[33] J. W. Flannery. Tests justify higher design stress for welded quarter-hard 301 stainless. *Welding Engineer*, 1968.

[34] Dan M. Frangopol and Kiyohiro Imai. Geometrically nonlinear finite element reliability analysis of structural systems. ii: applications. *Computers and Structures*, 77:693–709, 2000.

[35] Theodore V. Galambos. Proposed criteria for load and resistance factor design of steel building structures. Technical report, American Iron and Steel Institute, 1976.

[36] Theodore V. Galambos. Systems reliability and structural design. *Structural Safety*, 7:101–108, 1990.

[37] K. Ganesan and C. D. Moen. Lrfd and lsd resistance factors for cold-formed steel compression members. Technical report, Virginia Polytechnic Institute and State University, 2010.

[38] K. Ganesan and C. D. Moen. Lrfd resistance factor for cold-formed steel compression members. *Journal of Constructional Steel Research*, 2012.

[39] E. S. Gharaibeh, Dan M. Frangopol, and T. Onoufriou. Reliability-based importance assessment of structural members with applications to complex structures. *Computers and Structures*, 2002.

[40] Michel Ghosn and Fred Moses. Redundancy in highway bridge superstructures. Report, Transportation Research Board, 1998.

[41] Haselton Research Group. http://www.csuchico.edu/structural/researchdatabases.

[42] Samer Hendawi and Dan M. Frangopol. System reliability and redundancy in structural design and evaluation. *Structural Safety*, 16:47–71, 1994.

[43] D. Hunter. An upper bound for the probability of a union. *Applied Probability*, 1976.

[44] H. Hwang, J. B. Liu, and Yi-Huei Chiu. Seismic fragility analysis of highway bridges. Technical report, Mid-America Earthquake Center, 2001.

[45] L. F. Ibarra, R. A. Medina, and H. Krawinkler. Hysteretic models that incorporate strength and stiffness deterioration. *EARTHQUAKE ENGINEERING AND STRUCTURAL DYNAMICS*, 34, 2005.

[46] ICC. International building code, 2012.

[47] Kiyohiro Imai and Dan M. Frangopol. Geometrically nonlinear finite element reliability analysis of structural systems. i: theory. *Computers and Structures*, 77:677–691, 2000.

[48] Kiyohiro Imai and Dan M. Frangopol. System reliability of suspension bridges. *Structural Safety*, 24:219–259, 2002.

[49] Steel Deck Institute. Diaphragm design manual - no. ddm04. Technical report, SDI, 2016.

[50] A. L. Johnson. *The Structural Performance of Austenitic Stainless Steel Members*. PhD thesis, Cornell University, 1969s.

[51] Won-Hee Kang, Y-J Lee, Junho Song, and Bora Gencturck. Further development of matrix-based system reliability method and applications to structural systems. *Structure and Infrastructure Engineering*, 2012.

[52] R. P. Kennedy and M. K. Ravindra. Seismic fragilities for nuclear power plant risk studies. *Nuclear Engineering and Design*, 1984.

[53] D.S. Kim, S.Y. Ok, Junho Song, and H.M. Koh. System reliability analysis using dominant failure modes identified by selective searching technique. *Reliability Engineering and System Safety*, 2013.

[54] E. G. Kounias. Bounds for the probability of a union, with applications. *Annals of Mathematics and Statistics*, 1968.

[55] Y-J Lee and Junho Song. Risk analysis of fatigue-induced sequential failures by branch-and-bound method employing system reliability bounds. *Journal of Engineering Mechanics*, 2011.

[56] Y-J Lee and Junho Song. Finite-element-based system reliability analysis of fatigue-induced sequential failures. *Reliability Engineering and System Safety*, 2012.

[57] LGSEA. Lateral load resisting elements: Diaphragm design values, tech note 558b-1. Report, Light Gauge Steel Engineers Association, 1998.

[58] S. H. Lin, W. W. Yu, and T. V. Galambos. Fourth progress report: Load and resistance factor design of cold-formed stainless steel – statistical analysis of material properties and development of the lrfd provisions. Report, American Iron and Steel Institute, 1988.

[59] P. Liu, K. D. Peterman, and B. W. Schafer. Impact of construction details on osb-sheathed cold-formed steel framed shear walls. *Journal of Constructional Steel Research*, 2014.

[60] Laura Lowes, Nilanjan Mitra, and Arash Altoontash. A beam-column joint model for simulating the earthquake response of reinforced concrete frames. Report, Pacific Earthquake Engineering Research Center, 2004.

[61] R. L. Madsen, N. Nakata, and B. W. Schafer. Cfs-nees building structural design narrative. Report, 2011.

[62] Sankaran Mahadevan, Ruoxue Zhang, and Natasha Smith. Bayesian networks for system reliability reassessment. *Structural Safety*, 2001.

[63] J. Martinez-Martinez and L. Xu. Simplified nonlinear finite element analysis of buildings with cfs shear wall panels. *Journal of Constructional Steel Research*, 2011.

[64] MathWorks. Matlab r2014b, http://www.mathworks.com/products/matlab/, 2014.

[65] R. E. Melchers. *Structural Reliability Analysis and Prediction*. John Wiley and Sons, 1999.

[66] R. E. Melchers and L. K. Tang. Dominant failure modes in stochastic structural systems. *Structural Safety*, 1984.

[67] C. D. Moen, S. Florig, and A. Chatterjee. Tested in-plane response of a wood-sheathed cold-formed steel-framed floor diaphragm. *Journal of Structural Engineering*, (In Preparation).

[68] C. D. Moen, F. Tao, and R. Cole. Monotonic and cyclic backbone response of single shear cold-formed steel screw-fastened connections. In *The International Colloquium on Stability and Ductility of Steel Structures, Timisoara, Romania*, 2016.

[69] Cristopher Dennis Moen. *Direct Strength Design of Cold-Formed Steel Members with Perforations*. Thesis, Johns Hopkins University, 2008.

[70] F. Moses. System reliability developments in structural engineering. *Structural Safety*, 1:3–13, 1982.

[71] NAHBRC. Innovative residential floor construction: Horizontal diaphragm values for cold formed steel framing. Report, NAHB, 1999.

[72] Hung Harry Ngo. *Numerical and Experimental Studies of Wood Sheathed Cold-Formed Steel Framed Shear Walls*. Thesis, Johns Hopkins University, 2014.

[73] V. Nikolaidou, P. Latreille, and C. A. Rogers. Characterization of cfs framed diaphragm behaviour ; experimental program summer 2015. Technical report, Research Report prepared for the American Iron and Steel Institute Seismic Code Team, AISI Project Number CM - 432., 2015.

[74] V. Nikolaidou, P. Latreille, C.A. Rogers, and D Lignos. Characterization of cold-formed steel framed / wood-sheathed floor and roof diaphragm structures. In *16th World Conference on Earthquake Engineering. Santiago, Chile*, 2017.

[75] M. Nithyadharan and V. Kalyanaraman. Modelling hysteretic behaviour of cold-formed steel wall panels. *Engineering Structures*, 2013.

[76] D. A. Padilla-Llano. *A Framework for Cyclic Simulation of Thin-Walled Cold-Formed Steel Members in Structural Systems*. PhD thesis, Virginia Tech, 2015.

[77] T. Pekoz and O. Sumer. Design provisions for cold-formed steel columns and beam columns. Technical report, American Iron and Steel Institute, 1992.

[78] K. D. Peterman. *Behavior of full-scale cold-formed steel buildings under seismic excitations*. Thesis, Johns Hopkins University, 2014.

[79] K. D. Peterman and B. W. Schafer. Hysteretic shear response of fasteners connecting sheathing to cold-formed steel studs. Report, American Iron and Steel Institute, 2013.

[80] K. D. Peterman, M. J. J. Stehman, R. L. Madsen, S. G. Buonopane, N. Nakata, and B. W. Schafer. Experimental seismic response of a full-scale cold-formed steel-framed building. i: System-level response. *Journal of Structural Engineering*, 2016.

[81] K. D. Peterman, M. J. J. Stehman, R. L. Madsen, S. G. Buonopane, N. Nakata, and B. W. Schafer. Experimental seismic response of a full-scale cold-formed steel-framed building. ii: Subsystem-level response. *Journal of Structural Engineering*, 2016.

[82] H. Pham and C. D. Moen. Stiffness and strength of single shear cold-formed steel screw-fastened connections. Technical report, Virginia Tech Research Report No. CE/VPI-ST-15/07, Blacksburg, VA, 2015.

[83] K. Ramachandran. System bounds: a critical study. *Civil Engineering Systems*, 1984.

[84] Reza Rashedi and Fred Moses. Identification of failure modes in system reliability. *Journal of Structural Engineering*, 114(2):292–313, 1988.

[85] M. K. Ravindra and T. V. Galambos. Load and resistance factor design for steel. *Journal of the Structural Division*, 1978.

[86] D. V. Rosowsky and B. R. Ellingwood. Performance-based engineering of wood frame housing: Fragility analysis methodology. *Journal of Structural Engineering*, 2002.

[87] Rafael Sabelli, Thomas A. Sabol, and W. Samuel Easterling. Seismic design of composite steel deck and concrete-fillled diaphragms – a guide for practicing engineers. Report, NEHRP, 2011.

[88] B. W. Schafer. Local, distortional, and euler buckling of thin-walled columns. *Journal of Structural Engineering*, 2002.

[89] B. W. Schafer. Seismic response and engineering of cold-formed steel framed buildings. In *Geotechnical and Structural Engineering Congress*, 2016.

[90] B. W. Schafer, D. Ayhan, J. Leng, P. Liu, D. A. Padilla-Llano, K. D. Peterman, M. Stehman, S. G. Buonopane, M. Eatherton, R. L. Madsen, B. Manley, C. D. Moen, N. Nakata, C. Rogers, and Yu. C. Seismic response and engineering of cold-formed steel framed buildings. *Structures*, 2016.

[91] B. W. Schafer, Z. Li, and C. D. Moen. Computational modeling of cold-formed steel. *Contents lists available at ScienceDirect Thin-Walled Structures*, Thin-Walled Structures(48):752–762, 2010.

[92] Shaowen Shao and Yoshisada Murutsu. Approach to failure mode analysis of large structures. *Probabilistic Engineering Mechanics*, 14:169–177, 1999.

[93] M. Shinozuka, M. Q. Feng, J. Lee, and T. Naganuma. Statistical analysis of fragility curves. *Journal of Engineering Mechanics*, 2000.

[94] B. H. Smith, S. R. Arwade, B. W. Schafer, and C. D. Moen. Design capacity, component and system reliability in cold formed steel framed buildings. *Engineering Structures*, (Submitted).

[95] Junho Song and A. Der Kiureghian. Bounds on system reliability by linear programming. *Journal of Engineering Mechanics*, 2003.

[96] Junho Song and Won-Hee Kang. System reliability and sensitivity under statistical dependence by matrix-based system reliability method. *Structural Safety*, 31:148–156, 2009.

[97] Junho Song and Armen Der Kiureghian. Bounds on system reliability by linear programming. *Journal of Engineering Mechanics*, 129:627–636, 2003.

[98] S. Soroushian, A. E. Zaghi, E. Maragakis, A. Echevarria, Y. Tian, and A. Filiatrault. Seismic fragility study of fire sprinkler piping systems with grooved fit joints. *Journal of Structural Engineering*, 2015.

[99] D. Straub and A. Der Kiureghian. Reliability acceptance criteria for deteriorating elements of structural systems. *Journal of Structural Engineering*, 2011.

[100] D. Vamvatsikos and C. A. Cornell. Incremental dynamic analysis. *EARTHQUAKE ENGINEERING AND STRUCTURAL DYNAMICS*, 2002.

[101] G. J. Van der Berg and P. Van der Merwe. The torsional flexural buckling strength of cold-formed stainless steel columns. In *Proceedings of the Ninth International Specialty Conference on Cold-Formed Steel Structures, University of Missouri-Rolla*, 1988.

[102] P. Van der Merwe and G. J. Van der Berg. The advantage of using cr-mn steels instead of cr-ni steels in cold-formed steel design. Technical report, Rand Afrikaans University, Johannesburg, South Africa, 1987.

[103] S. T. Wang. Cold-rolled austenitic stainless steel: Material properties and structural performance. Technical report, Cornell University, 1969.

[104] V. M. Zeinoddini and B. W. Schafer. Impact of load combinations on structural reliability determined from testing cold-formed steel components. *Structural Safety*, 2014.